EFFECT OF STRUCTURAL WALL AREA TO FLOOR AREA RATIO ON THE SEISMIC PERFORMANCE OF MID TO HIGH RISE REINFORCED CONCRETE BUILDINGS

A THESIS SUBMITTED TO
THE GRADUATE SCHOOL OF NATURAL AND APPLIED SCIENCES
OF
MIDDLE EAST TECHNICAL UNIVERSITY

BY

GÖKSU GÜLER

IN PARTIAL FULFILLMENT OF THE REQUIREMENTS
FOR
THE DEGREE OF MASTER OF SCIENCE
IN
CIVIL ENGINEERING

NOVEMBER 2025

Approval of the thesis:

EFFECT OF STRUCTURAL WALL AREA TO FLOOR AREA RATIO ON THE SEISMIC PERFORMANCE OF MID TO HIGH RISE REINFORCED CONCRETE BUILDINGS

submitted by **GOKSU GULER** in partial fulfillment of the requirements for the degree of **Master of Science** i**n Civil Engineering, Middle East Technical University** by,

Prof. Dr. Naci Emre Altun
Dean, **Graduate School of Natural and Applied Sciences** _____

Prof. Dr. Erdem Canbay
Head of the Department, **Civil Engineering** _____

Assoc. Prof. Dr. Burcu Burak Bakır
Supervisor, **Civil Engineering, METU** _____

Examining Committee Members:

Prof. Dr. Erdem Canbay
Civil Engineering, METU _____

Assoc. Prof. Dr. Burcu Burak Bakır
Civil Engineering, METU _____

Prof. Dr. Murat Altuğ Erberik
Civil Engineering, METU _____

Prof. Dr. Afşin Sarıtaş
Civil Engineering, METU _____

Prof. Dr. Alper Aldemir
Civil Engineering, Hacettepe University _____

Date: 28.11.2025

I hereby declare that all information in this document has been obtained and presented in accordance with academic rules and ethical conduct. I also declare that, as required by these rules and conduct, I have fully cited and referenced all material and results that are not original to this work.

Name Last name : Göksu Güler

Signature :

ABSTRACT

EFFECT OF STRUCTURAL WALL AREA TO FLOOR AREA RATIO ON THE SEISMIC PERFORMANCE OF MID TO HIGH RISE REINFORCED CONCRETE BUILDINGS

Güler, Göksu
Master of Science, Civil Engineering
Supervisor : Assoc. Prof. Dr. Burcu Burak Bakır

November 2025, 210 pages

This study investigates the effect of increasing structural wall area to floor area ratio, referred to as the structural wall ratio, on the seismic performance of mid to high rise reinforced concrete buildings. A total of 35 building models are developed by combining five different number of stories (5, 7, 10, 20, and 30) with seven structural wall ratios (0.0%, 0.5%, 1.0%, 1.5%, 2.0%, 2.5%, and 3.0%). Nonlinear time history analyses are conducted in ETABS v22.4.0 using a suite of 11 ground motion records for each model. Seismic performance is assessed based on several key parameters including roof drift, maximum interstory drift, distribution of interstory drifts, base and story shear forces, base shear vs. roof drift response and the percentage of structural members with reinforcement yielding. The results reveal that increasing the structural wall ratio significantly improves seismic performance, primarily by reducing interstory drifts, and plastic deformations. The structural wall ratio of 1.0% significantly reduces the interstory drifts for all buildings. 5, 7 and 10 story buildings

require approximately 1.0% structural wall ratio to shift the structural response from frame-dominated to cantilever wall-dominated behavior, while the same behavioral transition for 20 and 30 story buildings requires 1.5-2.0% structural wall ratio.

Keywords: Structural Wall Ratio, Seismic Performance, Reinforced Concrete Buildings, Nonlinear Time History Analysis, Drift.

ÖZ

PERDE DUVAR ALANININ KAT ALANINA ORANININ ORTA VE YÜKSEK KATLI BETONARME BİNALARIN DEPREM PERFORMANSINA ETKİSİ

Güler, Göksu
Yüksek Lisans, İnşaat Mühendisliği
Tez Yöneticisi: Doç. Dr. Burcu Burak Bakır

Kasım 2025, 210 sayfa

Bu çalışmada, yapıların kat alanına göre betonarme perde duvar alanı oranının, diğer adıyla perde oranının, orta ve yüksek katlı betonarme binaların deprem performansı üzerindeki etkisi incelenmiştir. Beş farklı kat sayısı (5, 7, 10, 20 ve 30 kat) ve yedi farklı perde oranı (%0.0, %0.5, %1.0, %1.5, %2.0, %2.5 ve %3.0) düşünülerek toplam 35 bina modeli oluşturulmuştur. Her model için 11 adet yer hareketi kaydından oluşan bir set kullanılarak ETABS v22.4.0'da doğrusal olmayan zaman tanım alanı analizleri gerçekleştirilmiştir. Yapıların sismik performansı; çatı ötelenmesi, maksimum katlar arası göreli öteleme, göreli ötelemelerin bina yüksekliği boyunca dağılımı, taban ve kat kesme kuvvetleri, taban kesme-çatı ötelenmesi ilişkisi ve donatı akması gerçekleşen eleman yüzdesi gibi temel parametreler üzerinden değerlendirilmiştir. Sonuçlar, perde oranının artırılmasının özellikle katlar arası göreli ötelemeleri ve plastik şekil değiştirmeleri azaltarak sismik performansı belirgin şekilde iyileştirdiğini göstermektedir. Yaklaşık %1.0 perde oranı, tüm binalarda katlar arası ötelemeleri önemli ölçüde azaltmaktadır. 5, 7

ve 10 katlı binalar yaklaşık %1.0 perde oranıyla çerçeve davranışından konsol perde davranışına geçerken, 20 ve 30 katlı binalarda benzer davranış değişimi için yaklaşık %1.5-2.0 perde oranı gerekmektedir.

Anahtar Kelimeler: Perde Oranı, Deprem Performansı, Betonarme Yapılar, Doğrusal Olmayan Zaman Tanım Alanında Analiz, Öteleme

To those whose belief in me never wavered

ACKNOWLEDGMENTS

First and foremost, I would like to express my sincere gratitude to my advisor, Assoc. Prof. Dr. Burcu Burak Bakır, for her continuous support, guidance, and encouragement throughout the course of this study. Her insightful feedback and expertise greatly contributed to the quality of this thesis.

Special thanks go to my friends and colleagues for their constant support and motivation, particularly during the most challenging moments of this process.

Lastly, I am deeply grateful to my family for their unwavering belief in me, their patience, and their endless encouragement. This accomplishment would not have been possible without them.

TABLE OF CONTENTS

ABSTRACT v

ÖZ vii

ACKNOWLEDGMENTS x

TABLE OF CONTENTS xi

LIST OF TABLES xiv

LIST OF FIGURES xv

CHAPTERS

1 INTRODUCTION 1

1.1 General 1

1.2 Objective and Scope 3

1.3 Thesis Outline 4

2 LITERATURE REVIEW 5

2.1 General Characteristics and Categorization of Structural Walls 5

2.2 Nonlinear Modeling of Structural Walls 8

2.2.1 Macroscopic Modeling of Structural Walls 9

2.2.2 Microscopic Modeling of Structural Walls 21

2.3 Structural Wall Ratio 22

3 VALIDATION OF NONLINEAR MODELING 35

3.1 RW2 Structural Wall Specimen 35

3.1.1 Fiber Hinge Model of RW2 Structural Wall Specimen 39

3.1.2 Layered Shell Model of RW2 Structural Wall Specimen 48

3.2 Seven Story Full Scale Building 53

3.2.1 Fiber Hinge Model of the Seven Story Full Scale Building 57

3.2.2 Layered Shell Model of the Seven Story Full Scale Building..... 73
3.3 Results of the Validation of Nonlinear Modeling 77
4 ANALYTICAL MODELING AND BUILDING GENERATION 79
4.1 Introduction 79
4.2 Seismic Design of Model S05_R00 80
4.2.1 Material Properties of Model S05_R00..... 82
4.2.2 Member Dimensions and Reinforcement Detailing of Model S05_R00 87
4.3 Building Generation 91
4.4 Selection of Ground Motion Records..... 95
4.5 Scaling of Time History Records 98
4.6 Modeling of Nonlinear Behavior..... 100
4.6.1 Plastic Hinge Definition of Beams 100
4.6.2 Plastic Hinge Definition of Columns 104
4.6.3 Plastic Hinge Definition of Structural Walls..... 105
5 ANALYTICAL RESULTS..... 107
5.1 Modal Period 107
5.2 Percentage of Base Shear Carried by Structural Walls 108
5.3 Distribution of Story Shear..... 109
5.4 Maximum Roof Drift Ratio 112
5.5 Roof Drift vs. Time Response 115
5.6 Maximum Interstory Drift 124
5.7 Distribution of Maximum Interstory Drifts..... 129
5.8 Roof Drift vs. Base Shear Response..... 134

5.9 Percentage of Members with Reinforcement Yielding 142
6 SUMMARY AND CONCLUSIONS 147
6.1 Summary 147
6.2 Conclusions 148
6.3 Future Research Recommendations 151
REFERENCES 153
APPENDICES
A. Material Hysteresis Models 163
B. Reinforcement Detailing of Seven Story Test Building 170
C. Spectral Matching of Time History Records 171
D. Percentage of Members with Reinforcement Yielding 182

LIST OF TABLES

TABLES

Table 3.1 Steel stress-strain curve parameters used for modeling RW2 specimen. 39
Table 3.2 Effective stiffness modifiers 45
Table 3.3 Brief description of the seven story building test series 56
Table 3.4 Mechanical properties of the reinforcing bars in the seven story building 58
Table 4.1 Stress-strain parameters for unconfined concrete and reinforcing steel materials 86
Table 4.2 Selected ground motion records 97
Table 5.1 Statistical parameters for maximum interstory drift 128
Table 5.2 Percentage of members with reinforcement yielding-5 story buildings 144
Table D.1 Percentage of members with reinforcement yielding-7 story buildings 182
Table D.2 Percentage of members with reinforcement yielding-10 story buildings 186
Table D.3 Percentage of members with reinforcement yielding-20 story buildings 190
Table D.4 Percentage of members with reinforcement yielding-30 story buildings 197

LIST OF FIGURES

FIGURES

Figure 2.1 Types of cantilever structural walls (Aejaz and Wight, 1990) 7
Figure 2.2 Structural wall systems (Aejaz and Wight, 1990) 8
Figure 2.3 Typical representation of One-Vertical-Line-Element Model 10
Figure 2.4 Types of OVLEMs 11
Figure 2.5 Three-Vertical-Line-Element Model (Kabeyasawa et al., 1983) 12
Figure 2.6 Two-Axial-Element-in-Series Model (Vulcano and Bertero, 1986) 13
Figure 2.7 Modified TVLEM (Linde and Bachmann, 1994) 14
Figure 2.8 Multiple-Vertical-Line-Element Model (Vulcano et al., 1988) 14
Figure 2.9 Modified AESM 15
Figure 2.10 Uncoupling mode of deflection in MVLEM 16
Figure 2.11 Stress state of shear panel element 17
Figure 2.12 2D nonlinear panel element model (Chen et al., 2000) 17
Figure 2.13 Two types of wall web elements (Chen et al., 2000) 18
Figure 2.14 Equivalent Truss Models 19
Figure 2.15 SFI-MVLEM (Kolozvari et al., 2015) 21
Figure 2.16 Roof drift vs. structural wall ratio (Wallace, 1994) 23
Figure 2.17 Extreme fiber strain vs. structural wall ratio (Wallace, 1994) 24
Figure 2.18 Proposed evaluation method (Hassan and Sozen, 1997) 26
Figure 2.19 Roof Drift vs. Wall Ratio (Gulkan and Utkutug, 2003) 29
Figure 2.20 Maximum interstory drift vs. structural wall ratio (Soydas, 2009) 30
Figure 3.1 Geometry of RW2 specimen (Thomsen, 1995) 36
Figure 3.2 Test setup of RW2 specimen (Thomsen, 1995) 36
Figure 3.3 Cross section view of RW2 specimen (Thomsen, 1995) 37
Figure 3.4 Elevation view of RW2 specimen (Thomsen, 1995) 37
Figure 3.5 Hognestad model for concrete (Hognestad, 1955) 38
Figure 3.6 Steel stress-strain curve used for modeling RW2 specimen 38
Figure 3.7 Elevation view of RW2 specimen with fiber hinge model 40

Figure 3.8 Displacement vs. time history of RW2 41
Figure 3.9 Load pattern of RW2 specimen 41
Figure 3.10 RW2 specimen model fiber hinge definition 43
Figure 3.11 Base Shear vs. Top Displacement of RW2 with fiber hinge model (ASCE 41-23) 44
Figure 3.12 Base Shear vs. Top Displacement of RW2 with fiber hinge model (TBEC-2018) 46
Figure 3.13 Base Shear vs. Top Displacement of RW2 with fiber hinge model (ACI 318-19) 47
Figure 3.14 Comparison of Base Shear vs. Top Displacement of RW2 with different ESM 48
Figure 3.15 Elevation view of RW2 specimen with layered shell model 49
Figure 3.16 Definition of the layered shell element for the confinement zone of RW2 specimen 51
Figure 3.17 Definition of the layered shell element for the web of RW2 specimen 51
Figure 3.18 Comparison of Base Shear vs. Top Displacement Response of RW2 specimen with layered shell model 52
Figure 3.19 Comparison of Base Shear vs. Top Displacement Response of RW2 specimen with both layered shell and fiber hinge models 53
Figure 3.20 Plan view of the seven story validation building 54
Figure 3.21 Elevation view of the seven story validation building 55
Figure 3.22 Plan view of the fiber hinge model of the seven story building 57
Figure 3.23 Elevation view of the fiber hinge model of the seven story building 57
Figure 3.24 Acceleration vs. time history of SPD-2 test 59
Figure 3.25 Acceleration vs. time history of SPD-3 test 59
Figure 3.26 Representative M3 moment-rotation hinge 60
Figure 3.27 Representative P-M3 fiber hinge 61
Figure 3.28 Representative P-M2-M3 fiber hinge 62
Figure 3.29 Location of frame hinges 64

Figure 3.30 Location of shell hinges 65
Figure 3.31 Roof displacement vs. time (ESM-ALA) 66
Figure 3.32 Base shear vs. time (ESM-ALA) 67
Figure 3.33 Roof displacement vs. time (ESM-ANA) 67
Figure 3.34 Base shear vs. time (ESM-ANA) 68
Figure 3.35 Roof displacement vs. time (ESM-ACI 318-19) 68
Figure 3.36 Base shear vs. time (ESM-ACI 318-19) 69
Figure 3.37 Roof displacement vs. time (ESM-TBEC-2018) 69
Figure 3.38 Base shear vs. time (ESM-TBEC-2018) 70
Figure 3.39 Roof displacement vs. time (no ESM) 70
Figure 3.40 Base shear vs. time (no ESM) 71
Figure 3.41 Pushover curves of models with different ESM superimposed on experimental the base shear vs. roof displacement hysteresis 73
Figure 3.42 Elevation view of the layered shell model of the seven story full scale building 74
Figure 3.43 Definition of the layered shell element for the confinement zone 74
Figure 3.44 Definition of the layered shell element for the web 75
Figure 3.45 Comparison of the top displacement vs. time responses of seven story full scale building for the layered shell model and fiber hinge model 76
Figure 3.46 Comparison of the base shear vs. time responses of the seven story full scale building for the layered shell model and fiber hinge model 76
Figure 4.1 Preliminary floor layout 81
Figure 4.2 Two types of design spectra 82
Figure 4.3 Unconfined concrete stress-strain relationship 83
Figure 4.4 Reinforcing steel stress-strain relationship 84
Figure 4.5 Confined concrete stress-strain relationship (columns) 84
Figure 4.6 Confined concrete stress-strain relationship (wall boundaries) 85
Figure 4.7 Reinforcement detailing of 600 × 600 mm columns 88
Figure 4.8 Reinforcement detailing of 500 × 700 mm columns 89
Figure 4.9 Reinforcement detailing of 300 × 600 mm beams 90

Figure 4.10 Reinforcement detailing of 300 × 5000 mm structural walls.....91
Figure 4.11 Plan configuration of the generated buildings with 0.0% structural wall ratio.....92
Figure 4.12 Plan configuration of the generated buildings with 0.5% structural wall ratio.....92
Figure 4.13 Plan configuration of the generated buildings with 1.0% structural wall ratio.....93
Figure 4.14 Plan configuration of the generated buildings with 1.5% structural wall ratio.....93
Figure 4.15 Plan configuration of the generated buildings with 2.0% structural wall ratio.....94
Figure 4.16 Plan configuration of the generated buildings with 2.5% structural wall ratio.....94
Figure 4.17 Plan configuration of the generated buildings with 3.0% structural wall ratio.....95
Figure 4.18 MCE_R response spectrum.....99
Figure 4.19 Average of scaled spectrum compared with MCE_R design spectrum 100
Figure 4.20 Beam section in SAP2000 Section Designer tool.....102
Figure 4.21 Moment vs. curvature relationship of beams.....103
Figure 4.22 Definition of M3 moment-curvature beam hinges.....103
Figure 4.23 Fiber hinge definition of 500 x 700 mm columns.....104
Figure 4.24 Fiber hinge definition of 600 x 600 mm columns.....105
Figure 4.25 Fiber hinge definition of structural walls.....106
Figure 5.1 First modal period vs. structural wall ratio.....108
Figure 5.2 Base shear contribution of structural walls vs. structural wall ratio....109
Figure 5.3 Distribution of story shear under the Christchurch Earthquake.....111
Figure 5.4 Distribution of story shear under the Erzincan Earthquake.....112
Figure 5.5 Maximum roof drift vs. structural wall ratio.....115
Figure 5.6 Roof drift vs. time response of Northridge Earthquake for buildings with 0.0% structural wall ratio.....116

Figure 5.7 Roof drift vs. time response for Northridge Earthquake for S05_R00, S07_R00 and S10_R00 117
Figure 5.8 Roof drift vs. time response for Northridge Earthquake for S20_R00 and S30_R00 117
Figure 5.9 Roof drift vs. time response for Northridge Earthquake for S05_R05, S07_R05 and S10_R05 118
Figure 5.10 Roof drift vs. time response for Northridge Earthquake for S20_R05 and S30_R05 118
Figure 5.11 Roof drift vs. time response for Northridge Earthquake for S05_R10, S07_R10 and S10_R10 119
Figure 5.12 Roof drift vs. time response for Northridge Earthquake for S20_R10 and S30_R10 119
Figure 5.13 Roof drift vs. time response for Northridge Earthquake for S05_R15, S07_R15 and S10_R15 120
Figure 5.14 Roof drift vs. time response for Northridge Earthquake for S20_R15 and S30_R15 120
Figure 5.15 Roof drift vs. time response for Northridge Earthquake for S05_R20, S07_R20 and S10_R20 121
Figure 5.16 Roof drift vs. time response for Northridge Earthquake for S20_R20 and S30_R20 121
Figure 5.17 Roof drift vs. time response for Northridge Earthquake for S05_R25, S07_R25 and S10_R25 122
Figure 5.18 Roof drift vs. time response for Northridge Earthquake for S20_R25 and S30_R25 122
Figure 5.19 Roof drift vs. time response for Northridge Earthquake for S05_R30, S07_R30 and S10_R30 123
Figure 5.20 Roof drift vs. time response for Northridge Earthquake for S20_R30 and S30_R30 123
Figure 5.21 Maximum interstory drift vs. structural wall ratio 126
Figure 5.22 Coefficient of variation vs. structural wall ratio 129

Figure 5.23 Distribution of maximum interstory drift for S30_R00 130
Figure 5.24 Distribution of maximum interstory drift for S30_R20 130
Figure 5.25 Distribution of maximum interstory drift of buildings under the Christchurch Earthquake 132
Figure 5.26 Distribution of maximum interstory drift of buildings under the Erzincan Earthquake 133
Figure 5.27 Roof drift vs. base shear under the Erzincan Earthquake for 30 story buildings 136
Figure 5.28 Roof drift vs. base shear under the Erzincan Earthquake for 10 story buildings 137
Figure 5.29 Roof drift vs. base shear under the Erzincan Earthquake for 5 story buildings 138
Figure 5.30 Roof drift vs. base shear under the Christchurch Earthquake for 30 story buildings 139
Figure 5.31 Roof drift vs. base shear under the Christchurch Earthquake for 10 story buildings 140
Figure 5.32 Roof drift vs. base shear under the Christchurch Earthquake for 5 story buildings 141
Figure A.1 Concrete Hysteresis Model (CSI, 2024) 164
Figure A.2 Degrading Hysteresis Model (CSI, 2024) 166
Figure A.3 Parameters for Degrading Stiffness Hysteresis 166
Figure A.4 Pivot Hysteresis parameters (CSI, 2024) 168
Figure A.5 Pivot Hysteresis Model (CSI, 2024) 168
Figure A.6 Pivot Hysteresis parameters 169
Figure B.1 Frame B reinforcement detailing of 7 story test building (Wight et al., 1995) 170
Figure C.1 Spectral matching of Imperial Valley Earthquake 171
Figure C.2 Spectral matching of Loma Prieta Earthquake 172
Figure C.3 Spectral matching of Erzincan Earthquake 173
Figure C.4 Spectral matching of Landers Earthquake 174

Figure C.5 Spectral matching of Northridge Earthquake 175
Figure C.6 Spectral matching of Kobe Earthquake 176
Figure C.7 Spectral matching of Kocaeli Earthquake..... 177
Figure C.8 Spectral matching of Chi Chi Earthquake 178
Figure C.9 Spectral matching of Duzce Earthquake..... 179
Figure C.10 Spectral matching of Sierramex Earthquake..... 180
Figure C.11 Spectral matching of Christchurch Earthquake 181

CHAPTER 1

INTRODUCTION

1.1 General

Approximately 70% of the countries worldwide are exposed to varying degrees of seismic hazard, while around 25% are located in active tectonic regions with a documented history of destructive earthquakes (Johnson et al., 2023). Turkey belongs to this latter group and is considered as a country with high seismicity. As reported by the TMMOB Chamber of Civil Engineers (2010), nearly 92% of Turkey's territory lies within zones of seismic hazard. According to the Emergency Events Database (EM-DAT, 2023), a total of 110 earthquake related disasters occurred in Turkey between 1900 and 2022, resulting in 89,532 fatalities and 99,874 injuries. Following this period, the devastating Kahramanmaras earthquakes that struck southeastern Turkey on February 6, 2023, led to an additional 53,537 deaths and over 107,000 injuries, as reported by the Disaster and Emergency Management Authority (AFAD, 2023). These quantities highlight the severe and ongoing impact of seismic activity in the region. Therefore, seismic safety must be prioritized in construction practices in Turkey, as well as in other countries facing seismic risks.

Post earthquake assessments following the February 2023 Kahramanmaras earthquakes indicated that approximately 97% of the collapsed buildings had been constructed before the year 2000. Whereas, more than 5000 buildings constructed after 2000 either collapsed or required immediate demolition. Although the Turkish Building Earthquake Code (TBEC) was updated in 1995, 2007, and 2018, several studies demonstrate that recorded earthquakes have still exceeded the design spectra prescribed by these codes (Binici et al., 2023). Therefore, strengthening existing structures becomes as important as designing new ones in accordance with the

seismic codes, as demolishing and reconstructing would involve significant time and economic costs.

Structures are required to resist seismic loads, which can be achieved by ensuring adequate stiffness and lateral load carrying capacity. One of the most effective ways to provide these requirements is through the utilization of structural walls. In both newly designed and existing buildings that lack sufficient stiffness and strength, the addition of structural walls plays a crucial role in enhancing seismic performance and is among the most widely adopted strengthening techniques worldwide.

Observations made by Fintel (1995), spanning from the Chilean earthquake in May 1960 to the Armenian earthquake in December 1988, indicate that reinforced concrete buildings with structural walls demonstrated very satisfactory seismic performance. Specifically, regarding the period from the Skopje earthquake of 1963 through the Armenian earthquake of 1988, Fintel reported that not a single concrete building containing structural walls collapsed. While instances of cracking with varying degrees of severity were noted, no lives were lost in these buildings. In contrast, the collapse of hundreds of frame structures was attributed to excessive interstory distortions, which precipitated shear failures in columns.

Following the 1985 Mexico City earthquake, observations reported by the Institution of Structural Engineers (2019) highlight the critical role of reinforced concrete shear walls in enhancing seismic performance. The reconnaissance findings indicated that among the heavily damaged buildings examined, only one building employed shear walls as the principal lateral force resisting system, and this structure, originally a moment frame later strengthened with external shear walls after the 1981 earthquake, exhibited notably good performance during the 1985 event. Additional buildings that incorporated shear wall cores or isolated shear walls within predominantly moment frame systems showed significant cracking in the wall elements; however, none experienced collapse, suggesting that even damaged shear walls significantly contributed to structural stability (Institution of Structural Engineers, 2019, Report No. EEFIT/2019/0809).

1.2 Objective and Scope

In this study, the influence of increasing structural wall area to floor area ratio—also referred to as the structural wall ratio—on buildings with varying number of stories, ranging from 5 to 30, is investigated. A total of five building heights (5, 7, 10, 20, and 30 stories) and seven different structural wall ratios (0.0%, 0.5%, 1.0%, 1.5%, 2.0%, 2.5%, and 3.0%) are considered. From the combination of these parameters, a total of 35 building models are generated. All buildings have a square floor plan measuring 25 meters in each direction, resulting in a floor area of 625 m². Each structure consists of 5 bays in both directions and is designed to avoid torsional irregularity. The five story frame building with 0.0% structural wall ratio is designed in accordance with the requirements of TBEC-2018 (Turkish Ministry of Environment and Urbanization, 2018) and ACI 318-19 (American Concrete Institute, 2019) design provisions. After determining the structural member dimensions to satisfy the design provisions, the amount of transverse reinforcement in the columns is increased to prevent compressive failure in the columns of the 30 story frame building with 0.0% structural wall ratio. The column and beam dimensions, along with the reinforcement detailing, are kept constant across all building models in the study. To generate the remaining models, additional stories are replicated vertically, and 30 cm thick structural walls are incorporated. The reinforcement detailing of the structural walls is designed to meet the minimum requirements specified in TBEC-2018 and ACI 318-19. Each of the 35 building models is subjected to 11 time history records and their seismic performance is evaluated based on the roof and interstory drifts, base and story shear characteristics, base shear versus roof drift hysteresis behavior, and the percentage of yielded structural members. The software program ETABS 22.4.0 (Computers and Structures [CSI], 2024) is utilized for the nonlinear time history analyses.

1.3 Thesis Outline

To evaluate the influence of structural wall ratio on the seismic performance of mid to high rise reinforced concrete buildings, a total of 35 structures with varying wall ratios and number of stories are analyzed. Chapter 1 introduces the research objectives and provides an overview of this analytical study. A detailed literature review is presented in Chapter 2, covering structural wall characteristics, modeling strategies, the role of wall ratio in structural systems, and its effect on seismic performance. In Chapter 3, the selected nonlinear modeling approach is validated, and the accuracy of the results is examined. Chapter 4 outlines the structural properties of the modeled buildings and the ground motion records used in the analyses. Chapter 5 presents the analytical findings and includes the key outcomes. The study concludes in Chapter 6, which summarizes the main results, acknowledges the limitations, and offers recommendations for future research.

CHAPTER 2

LITERATURE REVIEW

2.1 General Characteristics and Categorization of Structural Walls

Structural systems are primarily designed to resist gravity loads, while also being required to withstand lateral loads such as wind pressure and seismic excitations. When subjected to lateral loads, structures may experience significant stresses and deformations, which can lead to partial or total collapse if adequate strength and stiffness are not provided. Structural walls, also referred to as shear walls, play a crucial role in enhancing both the lateral load carrying capacity and the overall stiffness of the structure.

Structural walls are defined by Turkish Building Earthquake Code (TBEC, 2018) as vertical load bearing elements for which the aspect ratio, defined as the length to thickness ratio in plan, is equal to or greater than six. According to ACI 318-19 (American Concrete Institute, 2019), a wall is described as a vertical component intended to carry axial forces, lateral forces, or a combination of both, with its horizontal length being at least three times its thickness. These members are commonly used to divide spaces or provide enclosure, and when designed to resist in plane axial, shear, and bending effects, they are referred to as structural walls.

In multistory buildings, especially in highly seismic zones, structural walls contribute significantly to overall structural stability. When reinforced concrete (RC) buildings were evaluated after the 2023 Kahramanmaras Earthquakes, it was observed that those with a certain amount of RC walls performed significantly better. Buildings lacking sufficient wall content experienced severe damage, highlighting the importance of adequate RC wall design for seismic safety (Sonmez et al., 2025).

Most residential buildings in Turkey are reinforced concrete structures with insufficient lateral strength, making them vulnerable to earthquakes. Adding external structural walls, even with window openings, significantly improve both base shear capacity and structural stiffness (Dere, 2017).

The performance of structural walls relies on various factors, such as their location, geometry and interaction with surrounding structural components. Numerous studies have demonstrated that L-shaped structural walls placed at the corners, as well as box shaped structural walls positioned centrally, are particularly effective in reducing the fundamental period, interstory drift, and roof displacement (Aniket et al., 2018; Khelaifia et al., 2024).

Structural walls have traditionally been classified into two categories based on their overall aspect ratio, defined as the width to horizontal length ratio: (i) squat walls, with aspect ratios less than 1.5, which are typically governed by shear failure; and (ii) slender walls, with aspect ratios greater than 3.0, which generally exhibit flexural failure. In contrast, ASCE 41-23 (American Society of Civil Engineers, 2023) employs a performance based approach by categorizing walls as either flexure controlled or shear controlled, based on the comparison of actual shear and flexural demands with their respective capacities. Recent analysis of a structural wall test database (Abdullah, 2019) has demonstrated that failure mechanisms are more closely associated with demand to capacity ratios than with aspect ratio alone. Representative elevation views of squat and slender walls are shown in Figure 2.1.

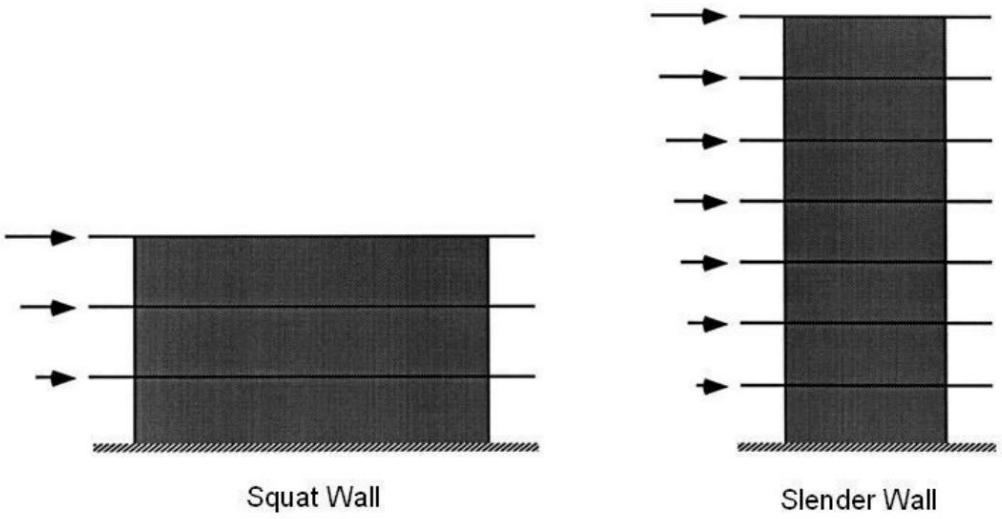


Figure 2.1 Types of cantilever structural walls (Aejaz and Wight, 1990)

Structural walls are commonly connected to adjacent walls or frames through coupling beams or floor slabs. When these walls also function as partitions, they often require openings for windows, doors, or other architectural features. As illustrated in Figure 2.2, there are three primary wall system configurations: coupled walls, wall-frame systems, and pierced walls. Although both coupled and pierced wall systems include openings aligned vertically, their structural behavior differs significantly. In coupled wall systems, the openings are large enough to separate the wall segments, and energy dissipation primarily occurs through the nonlinear behavior of coupling beams. In contrast, a pierced wall system acts more like a monolithic wall, where the impact of openings may be negligible depending on the opening to wall area ratio. The classification of a wall system as either coupled or pierced is largely governed by the shear span to depth ratio of the coupling beams (Aejaz and Wight, 1990).

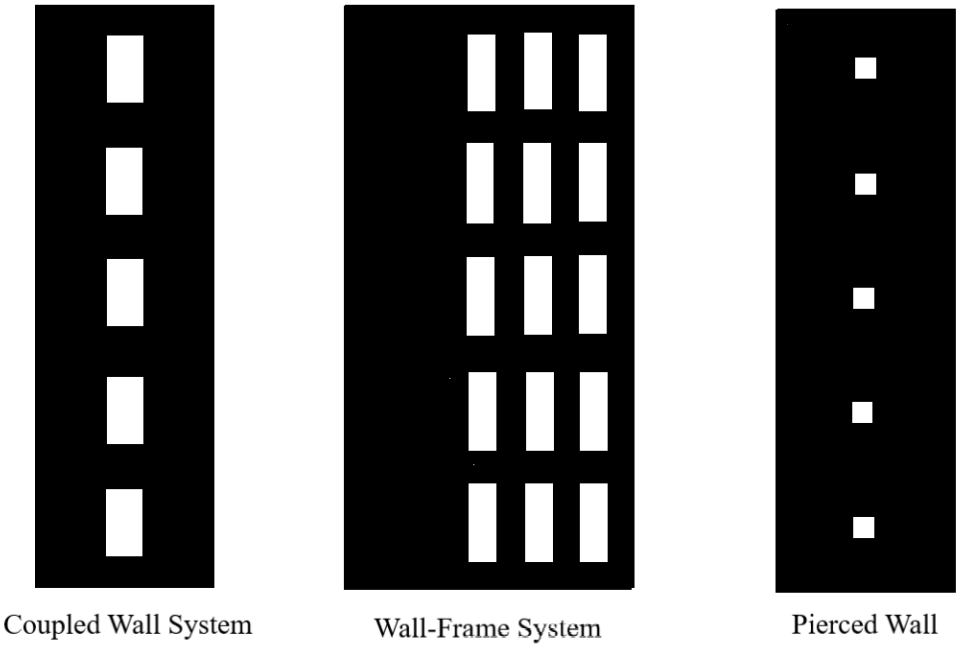


Figure 2.2 Structural wall systems (Aejaz and Wight, 1990)

2.2 Nonlinear Modeling of Structural Walls

The nonlinear modeling of structural walls plays a significant role in the representation of the actual behavior of structures under various loading conditions, as these elements have a great impact on the overall structural response. During the 1970s and 1980s, extensive experimental and analytical studies were conducted to examine and model the nonlinear behavior of reinforced concrete (RC) structural systems incorporating structural walls, such as wall-frame systems. These investigations revealed that many analytical models struggled to accurately capture the nonlinear characteristics of such systems. Some analytical studies (Aktan & Bertero, 1984; Aktan & Nelson, 1988) verified that the inadequacy of the analytical models used for structural walls was a key factor contributing to the discrepancy between analytical and observed responses.

Modeling methods for structural walls are generally divided into two categories: macroscopic modeling and microscopic modeling. Macroscopic modeling refers to simplified modeling approaches in which structural walls are represented using

idealized structural components that capture the overall behavior of the wall. This method is widely used in practice due to its lower computational demand and efficiency in analyzing entire structure. However, macroscopic models are generally limited in representing detailed local phenomena such as cracking, crushing, bond slip or reinforcement buckling. Microscopic modeling involves a more refined representation of the wall by modeling its material properties and internal components in greater detail. This allows for more accurate simulation of local behavior including shear failure mechanisms, crack propagation and nonlinear stress distribution. Although more precise, microscopic modeling requires significantly more computational effort and detailed input data. The selection between macroscopic and microscopic modeling depends on the objectives of the analysis, the scale of the structure, computational resources and the desired level of detail in analytical results.

2.2.1 Macroscopic Modeling of Structural Walls

The macroscopic modeling of structural walls includes several idealized approaches that are widely accepted in literature for their effectiveness in representing global structural behavior. These models, some of which are discussed next, are commonly utilized in the structural analysis and the seismic performance evaluation of reinforced concrete structural walls.

2.2.1.1 Vertical-Line-Element Model (VLEM)

The Vertical-Line-Element Model is further divided into three subcategories: the One-Vertical-Line-Element Model, the Three-Vertical-Line-Element Model, and the Multiple-Vertical-Line-Element Model, depending on the level of discretization of the wall section.

2.2.1.1.1 One-Vertical-Line-Element Model (OVLEM)

Vulcano et al. (1988) introduced the equivalent beam model as one of the earliest macro modeling techniques for structural walls within frame-wall systems. Similar approaches had been proposed earlier by Kabeyasawa et al. (1983), who termed it the equivalent column model, and by Fischinger et al. (1990), who referred to it as the beam-column element model. This modeling strategy simplifies the entire wall into a single element aligned along its centroidal axis, which is then rigidly connected to the frame beams or coupling beams. A typical representation of an OVLEM is presented in Figure 2.3.

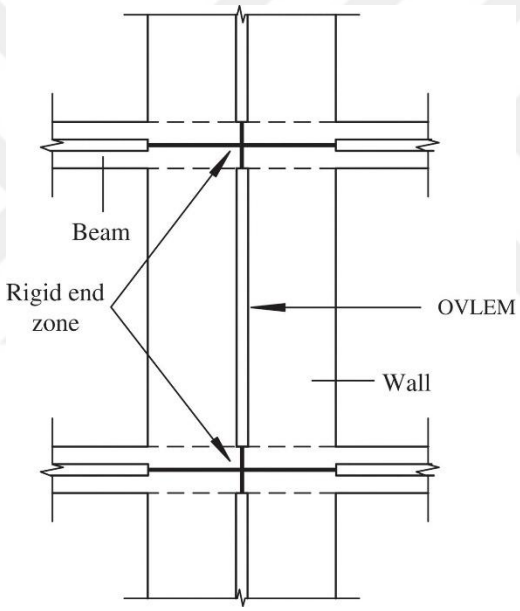


Figure 2.3 Typical representation of One-Vertical-Line-Element Model

OVLEMs can be categorized into several types, including the one-component model (Giberson, 1969), the two-component model (Clough et al., 1965), and the multiple spring model (Takayanagi, 1977). Different types of OVLEMs are presented in Figure 2.4. Among these, the one-component model is the most widely adopted one. This model comprises a perfectly elastic component with two inelastic rotational springs located at its ends, implying that the inelastic behavior of the member is

concentrated in these springs, or plastic hinges which have zero length, while the remaining portion is considered to remain elastic.

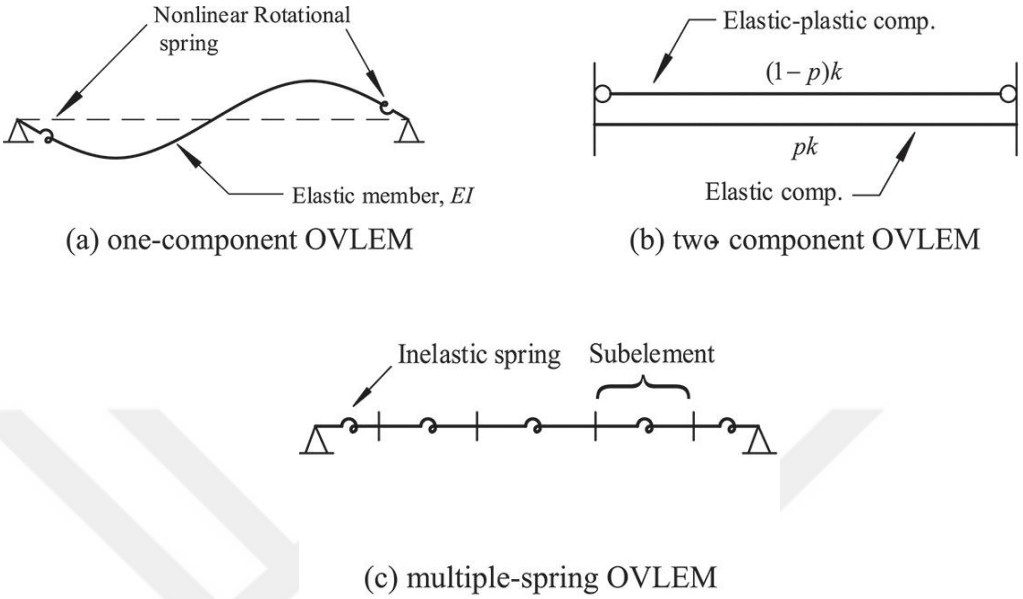


Figure 2.4 Types of OVLEMs

The simplicity of OVLEMs can offer computational convenience at the cost of accuracy. Within these models, it is assumed that the section of the wall rotates about its centroidal axis, which corresponds to a fixed neutral axis during the entire analysis. Nonetheless, experimental investigations conducted on three distinct structural wall specimens (Schuler, 2024) have demonstrated that the neutral axis undergoes a shift caused by notable elongation in the tension side boundary element, accompanied by comparatively minor shortening on the compression side. Vulcano (1988) states that while the equivalent beam model effectively represents flexural behavior, under high shear forces, it needs to be improved to accurately capture the hysteretic shear response as well as the flexural and shear displacements.

2.2.1.1.2 Three-Vertical-Line-Element Model (TVLEM)

Kabeyasawa et al. (1983) carried out a full scale test on a seven story reinforced concrete frame-wall system and to address the limitations of traditional OVLEMs,

introduced TVLEM. This model represents the wall using three vertical line elements connected by infinitely rigid beams at the top and bottom floor levels, as depicted in Figure 2.5. The two outer elements model the axial stiffness of the boundary zones, while the central element corresponds to the wall web. This central element incorporates vertical, horizontal, and rotational springs to simulate the axial, shear, and flexural behavior of the web, respectively.

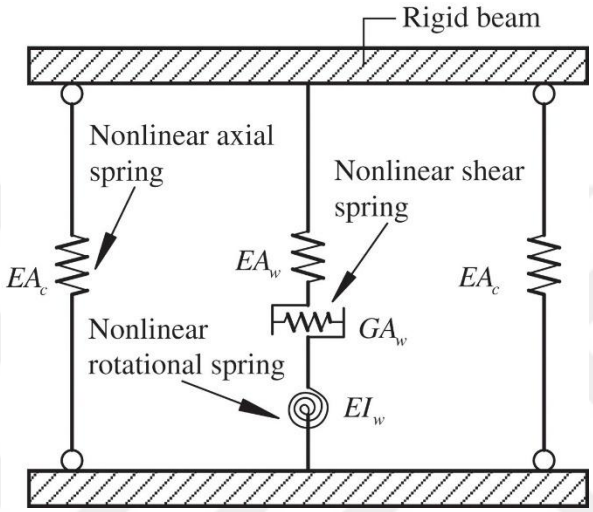


Figure 2.5 Three-Vertical-Line-Element Model (Kabeyasawa et al., 1983)

To represent the axial hysteretic behavior of all vertical springs in the TVLEM, Kabeyasawa et al. (1983) proposed the Axial-Stiffness Hysteresis Model (ASHM). The hysteretic responses of the horizontal and rotational springs were modeled using the Origin-Oriented Hysteresis Model (OOHM). Shear stiffness degradation was incorporated into the model; however, the effects of concrete cracking were not considered.

The two exterior axial springs enable the model to capture the shifting of the neutral axis of the wall cross section, rocking response, and the outrigger like interaction with adjoining frame components. However, due to the use of only three vertical elements, the model is unable to accurately represent the depth of the compression zone within the wall section, resulting in only an approximation of the neutral axis variation. Furthermore, the deformations represented by the elongation and

shortening of the exterior springs, associated with the boundary elements, are often incompatible with those captured by the vertical and rotational springs of the interior element. Vulcano and Bertero (1987) replaced the ASHM with the Two-Axial-Element-in-Series Model (AESM), which divides the axial component into two distinct elements rather than using a single spring. As illustrated in Figure 2.6, the first element consists of a single spring representing the contribution of steel and uncracked concrete, while the second element, composed of two springs, accounts for the remaining steel and the cracked concrete with bond degradation. A bond deterioration parameter, λ, was introduced to define the relative lengths of these elements. Despite the continued use of the Origin-Oriented Hysteresis Model (OOHM) to represent shear hysteresis, discrepancies were noted between the analytical predictions and experimental results for squat walls subjected to high stress levels. Regarding the previously mentioned compatibility issue, although a softening stiffness was assigned to the rotational spring to improve consistency, this approach proved insufficient in terms of reliability and efficiency.

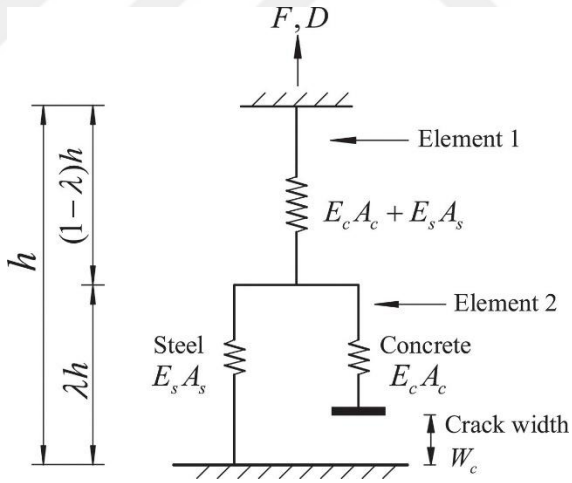


Figure 2.6 Two-Axial-Element-in-Series Model (Vulcano and Bertero, 1986)

Linde and Bachmann (1994) also attempted to resolve this issue by modifying the TVLEM. Their approach excluded the rotational spring from the interior element, instead using three vertical springs to capture both axial and flexural behavior (Figure 2.7), along with a horizontal spring to simulate the shear stiffness of the wall.

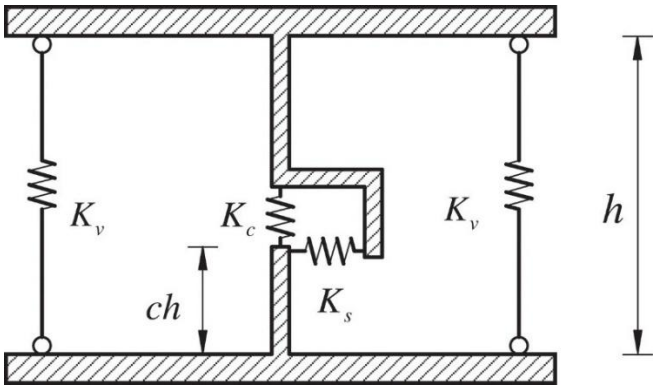


Figure 2.7 Modified TVLEM (Linde and Bachmann, 1994)

2.2.1.1.3 Multiple-Vertical-Line-Element Model (MVLEM)

The MVLEM, also called the multi component in parallel model, proposed by Vulcano et al. (1988), was developed through a geometric refinement of the TVLEM and the implementation of more advanced hysteretic models. The axial stiffness of the boundary elements (K_1 and K_2) continues to be represented by the two exterior springs. Meanwhile, the additional interior elements, at least two with axial stiffnesses K_3 to K_n, are introduced to model the axial and flexural responses of the wall web region (Figure 2.8). As in the four spring model proposed by Linde and Bachmann (1994), the rotational spring is excluded in the present model due to challenges in ensuring deformation compatibility. However, the horizontal spring with stiffness K_h is retained.

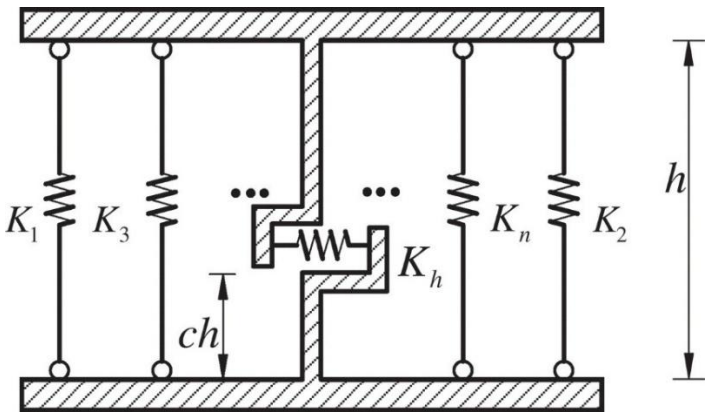


Figure 2.8 Multiple-Vertical-Line-Element Model (Vulcano et al., 1988)

Following the approach of Vulcano and Bertero (1988), the relative rotation of the wall between the top and bottom levels is assumed to occur at a height ch from the base, where the parameter c (ranging from 0 to 1) is selected based on the anticipated curvature distribution along the wall height. In terms of hysteretic behavior, Element 1 of the original AESM (Figure 2.6) is modified to consist of two parallel components, representing the uncracked concrete and the steel contribution separately, while the remainder of the model remains unchanged (Figure 2.9).

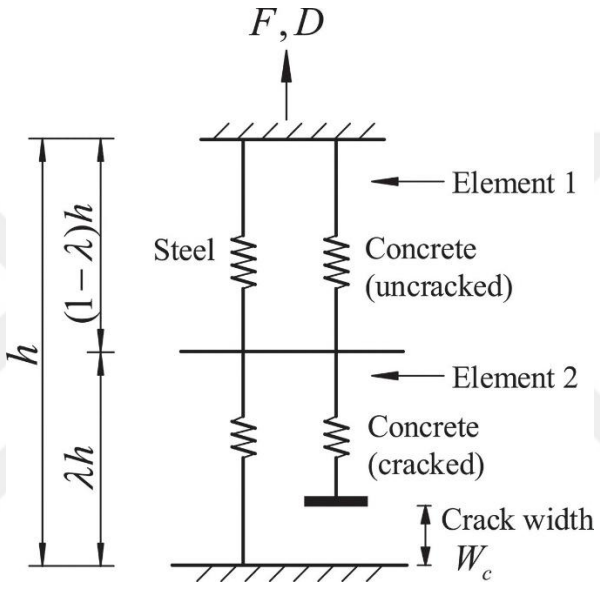


Figure 2.9 Modified AESM

By replacing the single axial and rotational springs at the web centroid with multiple interior elements, the MVLEM resolves the compatibility issues present in the TVLEM. Due to the increased number of vertical elements, the MVLEM is also able to more accurately capture the variation of the neutral axis of the wall cross section. Numerical studies by Vulcano et al. (1988) demonstrated that the MVLEM provides better agreement with experimental results than the TVLEM, particularly in simulating the 1/3 scale RC wall test by Vallenas et al. (1979). However, it is reported that the model does not adequately represent nonlinear shear deformations, particularly under high shear stress conditions (Colotti, 1993). It is important to note that while axial-flexural interaction is included, the interaction between flexure and

shear remains neglected in the MVLEM. The uncoupling mode between flexural and shear deformation is illustrated in Figure 2.10.

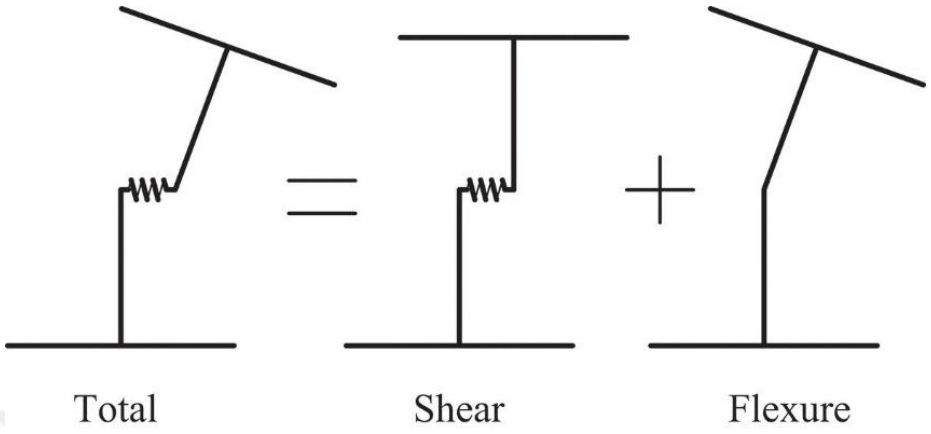


Figure 2.10 Uncoupling mode of deflection in MVLEM

2.2.1.2 2D Shear Panel Element Model (2D SPEM)

Colotti (1993) enhanced the original MVLEM by introducing a shear panel element to capture shear behavior and shear-flexure interaction more accurately, particularly under high shear stress conditions. The shear panel is based on the Modified Compression Field Theory (MCFT) developed by Vecchio and Collins (1986). In this model, the horizontal spring of the MVLEM is replaced by the shear panel, while vertical uniaxial elements are incorporated to represent boundary regions. The panel assumes an orthogonal grid of reinforcement that resists only axial forces, neglecting dowel action, and is subjected to uniform axial and shear stresses. The stress state of the shear panel is illustrated in Figure 2.11.

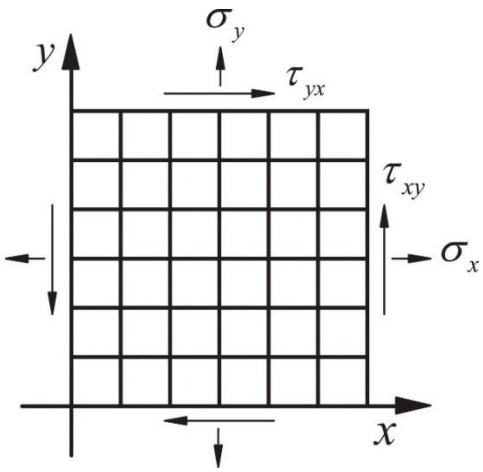


Figure 2.11 Stress state of shear panel element

Chen and Kabeyasawa (2000) used a 2D nonlinear panel element to simulate the nonlinear behavior of the structural wall (Figure 2.12). Two types of elements were utilized to model the wall web: an iso-parametric element and an incompatible element. The iso-parametric element (Figure 2.13a), which was a 4 node panel under biaxial loading, was unable to accurately capture the flexural deformation. To address this predicament, the incompatible element (Figure 2.13b) included an additional shape function to account for the internal deformation, allowing flexural behavior to be represented more accurately.

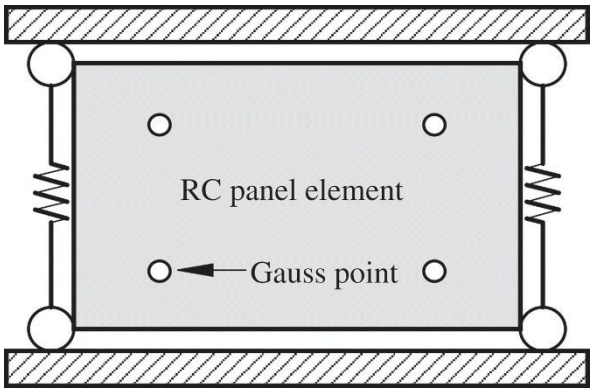


Figure 2.12 2D nonlinear panel element model (Chen et al., 2000)

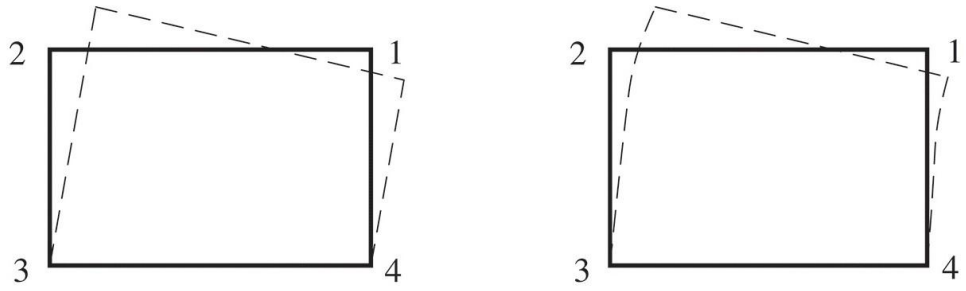


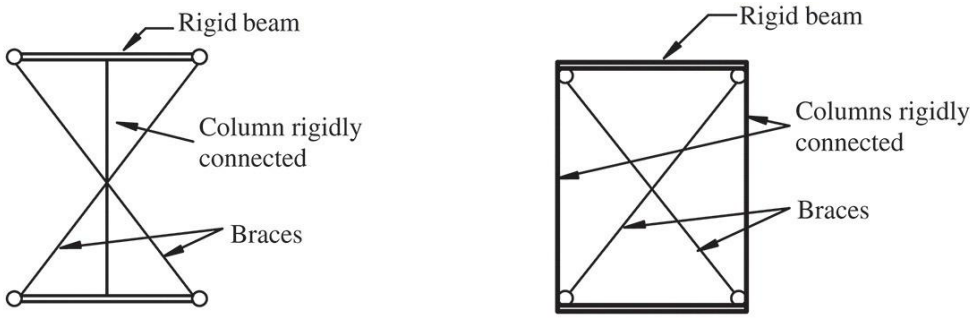
Figure 2.13 Two types of wall web elements (Chen et al., 2000)

A comparison between analytical and experimental results for T-shaped structural walls tested by Kabeyasawa et al. (1995) indicated that, in flexural yielding cases, the iso-parametric panel element tended to overestimate shear deformation, while the incompatible element produced results more consistent with the experimental data. For walls that experienced shear failure, both panel elements gave similar outcomes. This modeling approach was also applied to a full scale six story RC frame-wall structure, yielding satisfactory results (Chen et al., 2007).

2.2.1.3 Equivalent Truss Model (ETM)

Earliest forms of Equivalent Truss Model (ETM) were derived from the wide column model concept. It includes a central column element, rigid horizontal beams at the top and bottom, and two hinge ended diagonal braces connected at the ends of the rigid beams (Figure 2.14a). Smith and Girgis (1984) referred to this as the braced wide column analogy and used it to analyze a 15 story elevator core wall. In this model, the bending stiffness of the wall is provided by the column element, while shear stiffness comes from both the column and the horizontal components of the brace stiffness. The vertical components of brace stiffness and the axial stiffness of the column contribute to the axial stiffness of the wall. In a variation of this model

(Figure 2.14b), also proposed by Smith and Girgis (1984), the central column was replaced with two edge columns. This braced frame analogy allows for symmetric and asymmetric forms, enabling independent rotation of adjacent columns in full width models.



(a) braced wide-column analogy model (b) braced frame analogy model

Figure 2.14 Equivalent Truss Models

2.2.1.4 Fiber Model

The fiber model represents a cross section by dividing it into multiple discrete fibers. Each fiber is assigned a uniaxial hysteretic material model, and the overall section behavior is derived by enforcing kinematic compatibility and equilibrium. While the fiber model is well regarded for accurately capturing the interaction between axial force and bending moment, it typically neglects shear and bond slip effects due to the assumption that presumes plane sections remain plane during bending. The fiber model has been applied in different ways by researchers. Some, such as Kaba and Mahin (1983), considered it as a simplified form of the finite element method, suggesting a microscopic classification. Others, like Lai et al., 1984), viewed it as a complex variant of a multiaxial spring macroscopic model. With the advancement of microscopic modeling techniques, the fiber model is gradually transitioning toward being classified as a macroscopic model in structural analysis.

In general, two distinct finite element formulations are commonly used: displacement based and force based elements. A key limitation of the displacement

based approach is its reliance on a linear curvature distribution assumption along the element, which becomes inaccurate in regions of significant inelastic deformation. As a result, a fine mesh is often required to achieve acceptable accuracy. In contrast, force based elements do not require such mesh refinement, as their force interpolation functions inherently satisfy equilibrium conditions, allowing for more accurate modeling of inelastic behavior. Pugh et al. (2015) validated the force based fiber model using experimental data from 21 slender wall tests and introduced a generalized constitutive model to enhance prediction accuracy.

Several fiber models developed for simulating the nonlinear behavior of structural walls are conceptually derived from the MVLEM. Orakcal et al. (2004) proposed a macroscopic fiber based model incorporating modern cyclic constitutive laws for concrete and reinforcement, replacing the traditional hysteretic models such as AESM and OOHH. The model was validated using experimental results from rectangular and T-shaped wall specimens (Thomsen & Wallace, 2004), demonstrating good agreement in terms of lateral load capacity, displacement profiles, and average rotations. However, the model tended to underestimate peak compressive strains. Wallace (2007) attributed this to a common limitation of fiber models, the lack of coupling between shear and flexural responses.

To address the shear-flexure interaction (SFI) in structural walls, several fiber based models have been developed. Petrangeli et al. (1999) introduced a fiber model incorporating shear mechanisms at the fiber level. Building on this, Massone et al. (2016) modified the model by Orakcal (2004) by assigning shear springs to each vertical element, effectively coupling shear and flexural responses using panel models like the rotating-angle softened-truss model. Although this model captured SFI under monotonic loading, it had limitations in post peak prediction. To improve cyclic response simulation, Kolozvari et al. (2015) proposed the SFI-MVLEM, replacing uniaxial elements with RC panel elements governed by the extended fixed-strut-angle-model (Figure 2.15). This model effectively captured SFI under cyclic loading but showed reduced accuracy for squat walls with aspect ratios less than 1.0 due to the zero resultant horizontal stress assumption.

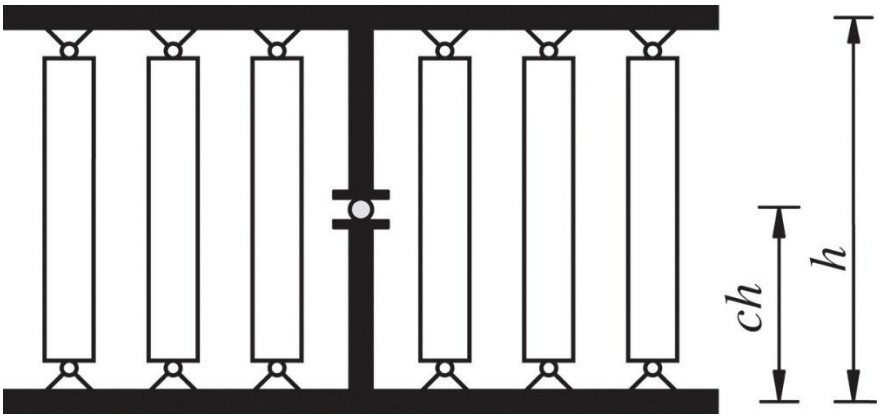


Figure 2.15 SFI-MVLEM (Kolozvari et al., 2015)

2.2.2 Microscopic Modeling of Structural Walls

The microscopic modeling of reinforced concrete structural walls generally involves the use of the finite element method to accurately capture both the global structural response and the local material behavior within the elements. The concrete matrix and reinforcing steel are modeled as distinct components to accurately capture localized nonlinear behavior, including cracking, crushing, and reinforcement yielding. Concrete is typically represented using either 2D plane stress-strain or 3D solid elements, along with advanced constitutive models that can simulate tension softening, compression hardening, and stiffness degradation. Reinforcement is commonly modeled using truss or beam elements, while the bond behavior between concrete and steel can be idealized as perfect or explicitly represented through interface elements.

Commonly adopted concrete models include the Concrete Damaged Plasticity model (Lubliner et al., 1989), smeared crack (Dahlblom et al., 1990) or discrete crack models (Cervenka et al., 2022), and fracture energy based approaches. The overall behavior of reinforced concrete is also simulated using material formulations such as the Modified Compression Field Theory (Vecchio & Collins, 1986), the Distributed Stress Field Model (Vecchio, 2000) and the Fixed Strut Angle Model

(Gullu et al., 2019), which differ primarily in their treatment of crack orientation, stress transfer mechanisms and the interaction between shear and normal stresses.

2.3 Structural Wall Ratio

Buildings are exposed to lateral forces during earthquakes, resulting in horizontal deformations. The extent of these deformations, which is directly related to the structural stiffness, serves as a primary indicator of potential damage. In reinforced concrete buildings, incorporating structural walls is among the most effective means of enhancing lateral stiffness. Therefore, the structural wall area to floor area ratio, referred to as the structural wall ratio, can be utilized to estimate the anticipated level of seismic damage.

Under earthquake loading, the roof and interstory drifts observed in reinforced concrete buildings serve as the key indicators for predicting the potential extent of structural damage. Structural walls in reinforced concrete systems significantly enhance stiffness and help mitigate lateral deformations. Contemporary approaches for evaluating the seismic performance of such buildings primarily focus on assessing the degree of local plasticity in individual structural members, as plastic deformations are closely associated with lateral displacements. Consequently, information on the structural wall ratio is crucial for determining, limiting, or predicting the expected level of seismic damage in these buildings.

An analytical approach was proposed by Wallace (1994) to determine the need to provide transverse reinforcement at the boundaries of reinforced concrete structural walls. The magnitude and distribution of normal strain within the wall were determined by establishing a relationship between the expected displacement demands on the building and the local deformations that occurred in the wall cross section. The calculation of transverse reinforcement required for concrete confinement and the determination of the confined length of the wall section were carried out using the computed wall strain distribution.

The roof drift ratios for several wall aspect ratios were estimated and plotted against structural wall ratio, presented in Figure 2.16. It was observed that the roof drift decreased nonlinearly with increasing structural wall ratio, exhibiting an asymptotic trend that gradually stabilized at higher wall ratios.

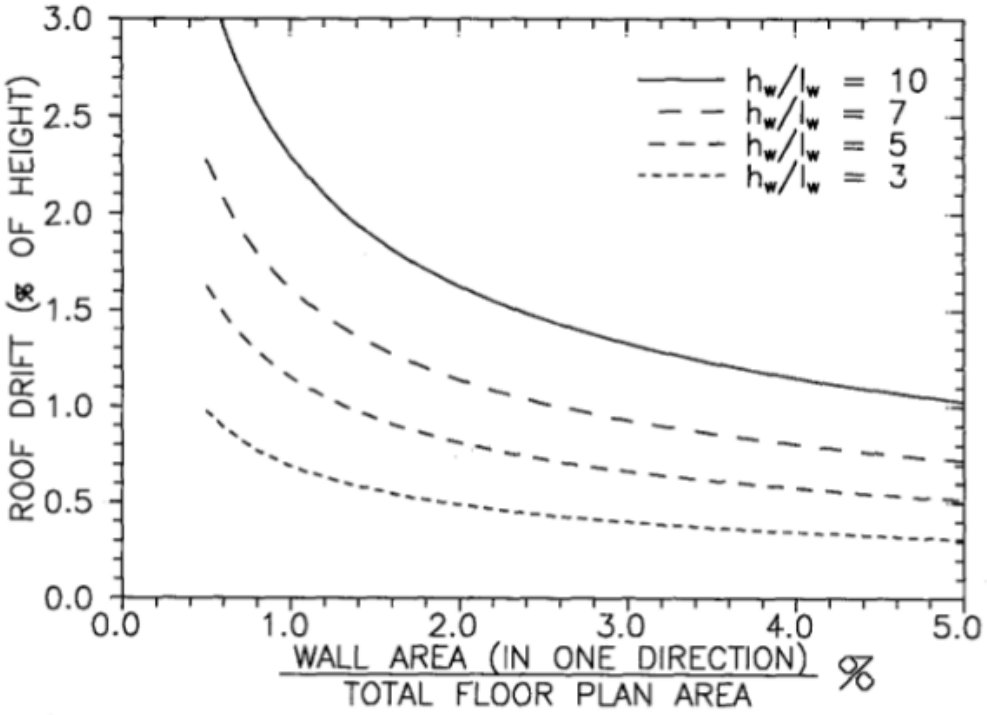


Figure 2.16 Roof drift vs. structural wall ratio (Wallace, 1994)

The extreme wall fiber strain was computed and plotted against increasing structural wall ratio, as presented in Figure 2.17. The results indicated that the wall extreme fiber strains and roof drifts showed similar trends with varying wall ratio.

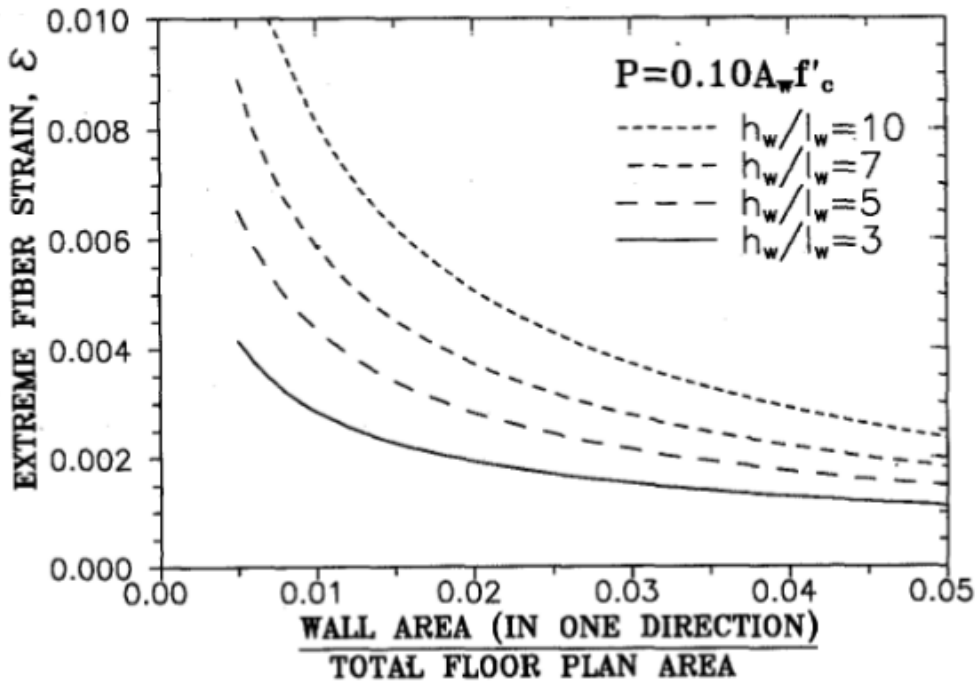


Figure 2.17 Extreme fiber strain vs. structural wall ratio (Wallace, 1994)

A simplified approach for assessing the seismic vulnerability of low rise (up to five story) monolithic reinforced concrete buildings was proposed by Hassan and Sozen (1997). The method ranks buildings according to their expected damage potential by employing two parameters: the wall index (WI) and the column index (CI). These indices are plotted on a two dimensional graph, presented in Figure 2.18, with CI on the x-axis and WI on the y-axis, where the position of buildings indicate their relative vulnerability levels. The method was applied to 46 institutional buildings that experienced varying damage levels during the 1992 Erzincan Earthquake, leading to the establishment of empirical boundary lines separating different vulnerability regions.

In this study, the wall index, WI, was defined as:

$$WI = \frac{A_{wt}}{A_{ft}} x100$$

where,

$A_{wt} = A_{cw} + (A_{mw}/10) =$ effective cross sectional area of the walls in a given horizontal direction

$A_{cw} =$ total cross sectional area of the reinforced concrete walls in one horizontal direction at the base of the structure

$A_{mw} =$ cross sectional area of nonreinforced masonry filler walls in one horizontal direction at the base

$A_{ft} =$ total floor area above the base

while, the column index, CI, was defined as:

$$CI = \frac{A_{ce}}{A_{ft}} x100$$

where,

$A_{ce} = A_{col}/2 =$ effective cross sectional area of columns at the base of the structure

$A_{col} =$ total cross sectional area of columns above the base, computed by summing up the column areas at each floor above the base.

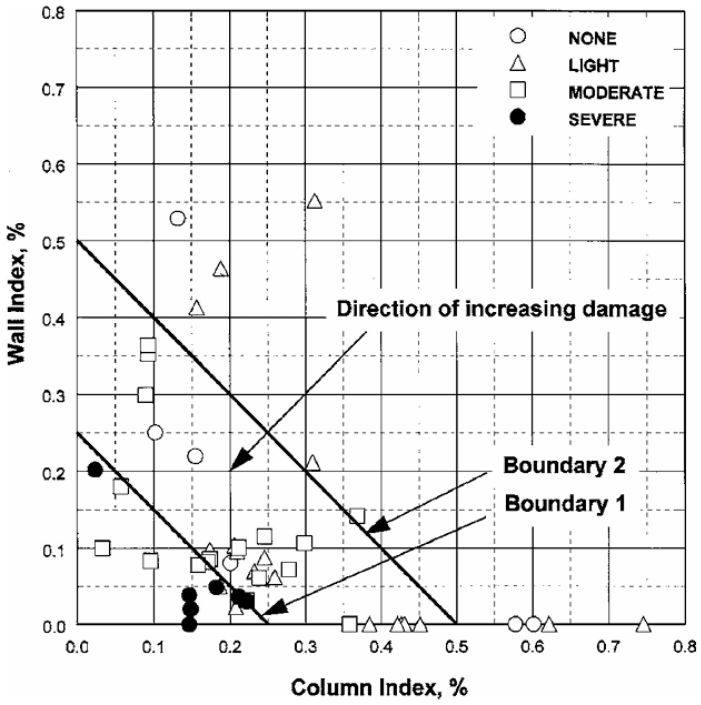


Figure 2.18 Proposed evaluation method (Hassan and Sozen, 1997)

The triangular area enclosed by the first boundary line and the index axes denotes the most critical region, corresponding to a higher probability of severe damage. Although the method does not incorporate material strength, number of stories, or detailed frame characteristics, its simplicity and reliance on basic geometric parameters make it an efficient tool for rapid seismic vulnerability screening of existing structures and preliminary design evaluations.

Another model for the preliminary assessment of the seismic vulnerability of existing reinforced concrete buildings is proposed by Ozcebe et al. (2003). In this method, number of stories (n), minimum normalized lateral stiffness index (mnlstfi), minimum normalized lateral strength index (mnlsi), normalized redundancy score (nurse), soft story index (ssi) and overhang ratio (or) were selected as the parameters influencing structural response.

Minimum normalized lateral stiffness indices (mnlstfi) were defined as:

MNLSTFI = min (I_{nx}, I_{ny})

$$I_{nx} = \frac{\sum(I_{col})_x + \sum(I_{sw})_x}{A_{tf}} \times 1000$$

$$I_{ny} = \frac{\sum(I_{col})_y + \sum(I_{sw})_y}{A_{tf}} \times 1000$$

where,

$\sum(I_{col})_x$ and $\sum(I_{col})_y$: Summation of moment of inertias of all columns about their centroidal X- and Y-axes, respectively,

$\sum(I_{sw})_x$ and $\sum(I_{sw})_y$: Summation of moment of inertias of all structural walls about their centroidal X- and Y-axes, respectively,

I_{nx} and I_{ny} : Normalized indices about X- and Y-axes, respectively,

A_{tf} : Total floor area at the base of a building.

Minimum normalized lateral strength indices (mnlsi) were defined as:

MNLSI = max (A_{nx}, A_{ny})

$$A_{nx} = \frac{\sum(A_{col})_x + \sum(A_{sw})_x + (0.1 \times \sum(A_{mw})_x)}{A_{tf}} \times 1000$$

$$A_{ny} = \frac{\sum(A_{col})_y + \sum(A_{sw})_y + (0.1 \times \sum(A_{mw})_y)}{A_{tf}} \times 1000$$

where,

$\sum(A_{col})_x$ and $\sum(A_{col})_y$: Summation of effective cross sectional areas of all columns in X- and Y directions, respectively,

$\sum(A_{sw})_x$ and $\sum(A_{sw})_y$: Summation of effective cross sectional areas of all structural walls in X- and Y-directions, respectively,

$\sum(A_{mw})_x$ and $\sum(A_{mw})_y$: Summation of effective cross sectional areas of all masonry walls in X- and Y-directions, respectively,

A_{nx} and A_{ny} : Normalized lateral strength indices in X- and Y-directions, respectively.

The parameters mnlstfi and mnlsi were directly related to the cross sectional properties of the columns and structural walls, as well as the ratio of the summation of their effective area to total floor area. This study had a building damage database of 484 mid to low rise reinforced concrete buildings, which were evaluated by the survey teams after the 1999 Duzce Earthquake. The proposed method was then validated on the damage data assessed from the 1992 Erzincan and 2002 Afyon earthquakes. It was stated that the model was found to be quite satisfactory and the classification rates of the damaged buildings support the predictive ability of the proposed statistical model.

Gulkan and Utkutug (2003) utilized the elastic displacement response spectrum defined in the Turkish Earthquake Code (1998) to determine the required design criteria for ensuring the safety of school buildings. In this study, the relationship between the structural wall ratio and roof drift for reinforced concrete buildings with varying aspect ratios was investigated. A parabolic relationship between roof drift and the structural wall ratio was obtained for specified wall aspect ratios (Figure 2.19).

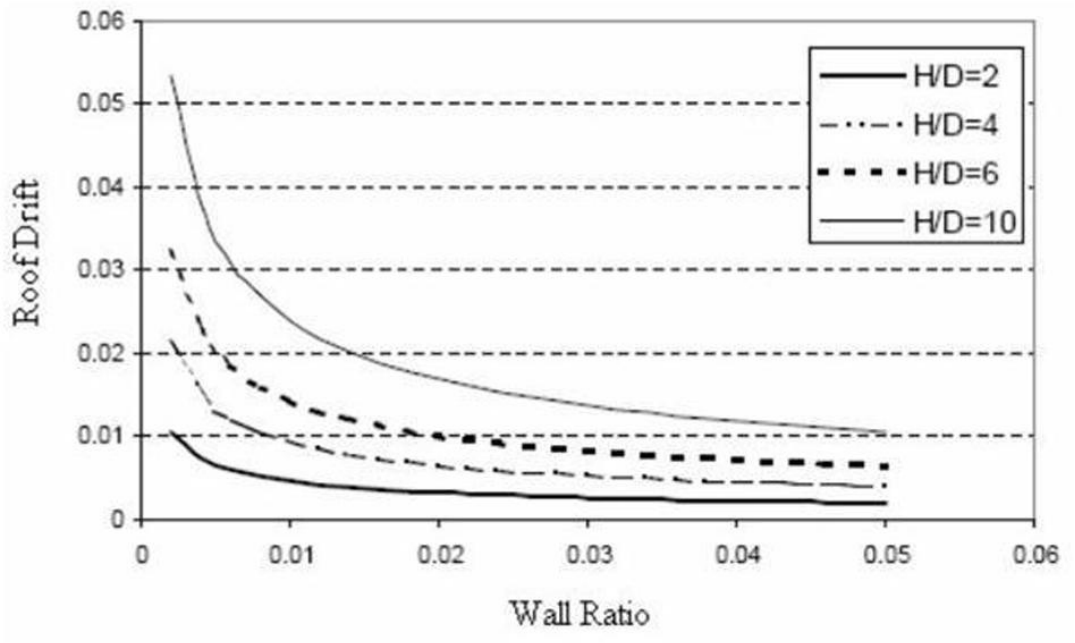


Figure 2.19 Roof Drift vs. Wall Ratio (Gulkan and Utkutug, 2003)

Furthermore, the influence of wall ratio on the maximum compressive concrete strains was investigated. It was stated that satisfying the strain limit of 0.003 requires higher structural wall ratios, especially for slender walls or those subjected to high axial loads. Ultimately, it was concluded that a structural wall ratio of approximately 1.50% was required to provide sufficient strain capacity and ensure structural safety.

Yakut and Soydas (2009) conducted an analytical study to assess the influence of wall index on the seismic performance of low to midrise reinforced concrete buildings, with the objective of guiding the preliminary assessment and design stages prior to the structural analyses. In this study, 45 buildings with 2, 5, and 8 stories, featuring structural wall ratios between 0.53% and 3.60%, were designed in accordance with the Turkish Earthquake Code (2007). Structural wall ratio was computed as the ratio of structural wall area to floor area ratio. Linear elastic and nonlinear static pushover analyses were carried out on the models to examine the variation of roof and interstory drifts with increasing structural wall ratio. In Figure 2.20, the variation of maximum interstory drifts in the x-direction of buildings is plotted against increasing structural wall ratio.

The results of the elastic analyses indicated that 2, 5 and 8 story buildings were observed to exhibit similar trends. The maximum interstory drift decreased with increasing structural wall ratio, although the rate of decrease reduced at higher wall ratios and the maximum calculated interstory drift did not exceed 1.00%. It was concluded that the interstory drift limit prescribed by Turkish Seismic Code (2007) was not the governing parameter in the evaluation of the performance of low to midrise reinforced concrete buildings with wall-frame systems. Instead, the influence of structural wall ratio on the performance was observed to depend on the number of stories, the ductility of the structural system and the location of the walls.

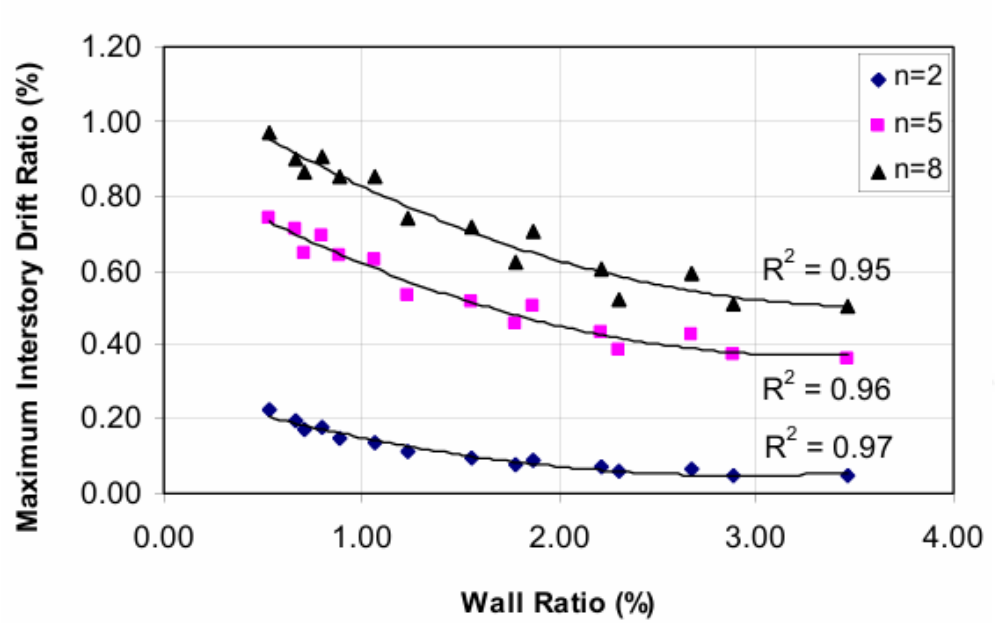


Figure 2.20 Maximum interstory drift vs. structural wall ratio (Soydas, 2009)

Burak and Comlekoglu (2009) conducted an analytical study to investigate the influence of structural walls on the seismic performance of midrise reinforced concrete buildings. In this study, nonlinear time history analyses were performed on 24 buildings, which were symmetric, regular in plan and free of torsional irregularities, that had 5 and 8 stories with structural wall ratios ranging between 0.51% and 2.17% in both directions. The modeling method for the structural walls was selected as the wide column analogy, which was validated by comparing the analytical results with the experimental results of a full scale seven story reinforced

concrete shear wall building tested under the U.S.-Japan Cooperative Research Program in 1981 (Wight et al., 1983). It was indicated by the analytical results that a minimum shear wall ratio of 1.0% was required in the design of midrise buildings to minimize the observed drift. In addition, it was observed that no significant improvement in seismic performance was achieved when the shear wall ratio was increased beyond 1.5%.

Following the same modeling approach validated by Burak and Comlekoglu (2009), an analytical study was performed by Burak and Gunel (2013) to evaluate the influence of structural wall ratio on the behavior of existing midrise reinforced concrete buildings with torsional irregularities under earthquake loading. The seismic performance of five existing school buildings and their strengthened counterparts which had structural wall ratios between 0.00% and 2.50% in both longitudinal and transverse directions were evaluated. Nonlinear time history analyses were performed on total of 24 buildings, each subjected to 7 ground motion records. It was stated that increasing the structural wall ratio reduced roof drifts and plastic deformations, though the rate of reduction diminished at higher wall ratios. Buildings with approximately 1.0% wall ratio exhibited significantly lower deformations, while ratios around 1.5% further minimized them, beyond which additional walls had only a minor influence on seismic performance. These findings verified the observations reported by Burak and Comlekoglu (2009).

Yurdakul et al. (2014) investigated the influence of structural wall ratio on the seismic performance of reinforced concrete buildings exhibiting significant structural deficiencies, including low concrete strength, poor detailing, and irregular configurations, conditions commonly observed in most structures affected by earthquakes. Two buildings that experienced heavy damage during the 1999 Kocaeli Earthquake were analytically modeled, incorporating estimated material strengths representative of the Turkish building stock. Nonlinear response history analyses were conducted using the ground motion recorded at the Duzce station, and models with structural wall ratios varying between 0.0% and 2.0% were evaluated. The results demonstrated that buildings without structural walls exhibited substantially

worse seismic performance, consistent with the observed earthquake response, whereas increasing the structural wall ratio significantly reduced both roof and interstory drifts. The analyses identified a structural wall ratio of approximately 1.0% as critical for achieving acceptable drift limits, aligning with the 2.0% interstory drift threshold defined in TEC 2007. Moreover, buildings with at least 1.0% wall ratio were shown to reach life safety performance level, behaving more like a cantilever wall. It was concluded that an optimal structural wall ratio of around 1.0% is appropriate for low rise reinforced concrete buildings with regular structural plans.

Dahesh, Tuken and Siddiqui (2015) conducted a parametric study to determine the optimum arrangement of shear walls for a 10 story reinforced concrete building with a square plan, assumed to be located in a seismically active region in Saudi Arabia. The investigation evaluated the influence of various parameters, including wall thickness, height, configuration and opening locations, on the lateral response of the structure under seismic loading. The study highlighted the substantial impact of the structural wall area to floor area ratio on the lateral stiffness of the building. It was reported that increasing the structural wall ratio from 0.56% to 1.29% resulted in a reduction of roof displacement by 38% to 72% compared to the bare frame model without structural walls.

Tunc and Al-Ageedi (2020) performed an analytical investigation on 40 reinforced concrete building models, varying both in height and structural wall ratios. The models incorporated structural wall ratios ranging from 0.0% to 2.0% and included buildings of 20, 30, and 40 stories. Each model was analyzed using a response spectrum approach. The analytical results demonstrated that the optimal structural wall to floor area ratios were 1.5% for 20 story buildings and 2.0% for 30 story buildings. It was noted that, for the 40 story building, a slightly higher wall ratio was required; however, upon revising the wall layout for the model with the 2.0% wall ratio, the demand was efficiently satisfied, signifying that a 2.0% wall area ratio could also be considered suitable for the 40 story building.

Khelaifia, Chebili, and Zine (2023) carried out an analytical study to evaluate the effect of different structural wall arrangements and ratios on the seismic performance of an eight story reinforced concrete building. The study employed nonlinear pushover analysis in accordance with FEMA 356 (Federal Emergency Management Agency, 2000) guidelines. The reduction in interstory drifts was observed to be substantial when structural walls were concentrated in the middle of the structure and formed compound shapes (e.g., Box, U, and L) compared to the peripheral arrangements. It was recommended that a shear wall ratio of 1.0% was required to satisfy validation criteria for interstory drift and structural damage, whereas exceeding this ratio resulted in more than required performance, proving uneconomical as the structural members remained primarily in the elastic range.

Alam et al. (2024) investigated the influence of varying structural wall area to floor area ratios on the seismic performance of a 15 story reinforced concrete building with an irregular U-shaped plan. The study employed response spectrum analysis using ETABS software. Nine different models with structural wall ratios ranging between 0.6% and 2.2% were analyzed to assess parameters such as story displacement, interstory drift and base shear. The analytical results indicated that increasing the structural wall ratio reduced the lateral displacements but increased the base shear. It was concluded that a structural wall ratio of 1.8% provided the optimal balance between structural efficiency and performance. The study further indicated that increasing the wall ratio beyond 1.8% did not yield proportional improvements in structural resistance, providing diminishing returns.

Khelaifia, Zine, Guettala and Chebili (2024) conducted a comprehensive study to investigate the optimal positioning of structural walls and the ideal structural wall area to floor area ratio in relation to building height. Utilizing both nonlinear static and nonlinear dynamic analyses, the seismic performance of reinforced concrete buildings with varying heights was evaluated. The findings of the study indicated that increasing the structural wall ratio not only enhanced structural rigidity, but also improved reliability in terms of controlling the interstory drift. Specifically, the analyses revealed that a structural wall ratio of 1.0% was imperative for 7 story

structures, whereas a higher ratio of 1.5% was required for 14 story structures to effectively meet the performance based design conditions. Furthermore, the study highlighted that shear walls arranged in compound forms (such as Box, U, and L shapes) offered enhanced reliability compared to dispersed frame arrangements.

Shah, Parmar and Shah (2025) conducted an analytical study to determine the optimum structural wall area to floor area ratio for midrise reinforced concrete buildings with varying concrete grades. The investigation focused on a set of 10 story residential building models located in a high seismic zone, incorporating concrete grades of C25, C30, and C35. The study employed the response spectrum method to analyze fifteen different models, where the structural wall ratio was incrementally varied from 0% (bare frame) to 4%. The key seismic response parameters, including base shear, maximum story displacement and interstory drift are evaluated. The analytical results demonstrated that increasing the structural wall ratio significantly reduces lateral displacements and drift demands; however, this improvement is accompanied by a notable increase in the base shear due to the added stiffness and seismic weight. The study highlighted that while higher concrete grades contribute to rigidity, the shear wall quantity plays a more dominant role in controlling the global seismic response of the structure.

Shah et al. (2025) conducted a comprehensive review of recent studies investigating the effects of structural wall location and wall ratio on the seismic behavior of reinforced concrete buildings. The review highlighted a strong consensus in the literature that symmetrically placed shear walls, particularly those forming a core or located at the corners, provide superior seismic performance compared to asymmetrical or peripheral arrangements. Furthermore, the study emphasized that the structural wall area to floor area ratio is a critical parameter influencing structural response, with numerous studies recommending an optimal range between 1.0% and 2.0% depending on the building height and plan configuration. It was concluded that while lateral drifts were generally reduced by increasing the shear wall ratio, a balance between rigidity requirements and cost efficiency was required for optimal design.

CHAPTER 3

VALIDATION OF NONLINEAR MODELING

Accurate nonlinear modeling of reinforced concrete structural members is essential for precise seismic performance assessment, especially in systems where structural walls provide primary lateral resistance. To verify the accuracy of the proposed method, two nonlinear models are constructed in ETABS (Computers and Structures, Inc. [CSI], 2024) and validated by comparing analytical results with experimental data. First, a reinforced concrete wall specimen, RW2, that was tested under pseudo dynamic loading (Thomsen, 1995) is analyzed to obtain the base shear vs. displacement response. Then, a seven story reinforced concrete building (Wight, 1983) is analyzed for the verification of the interaction between structural walls, beams, columns, and slabs. In both models, fiber hinges and layered shell elements are utilized and the validation is carried out by comparing the base shear vs. time and roof displacement vs. time histories, as well as base shear vs. roof displacement response.

3.1 RW2 Structural Wall Specimen

The structural wall specimen designated as RW2 was experimentally investigated by Thomsen et al. (1995) to assess the seismic response. In this study, the wall is modeled in ETABS (Computers and Structures, Inc. [CSI], 2024) using both fiber hinge and layered shell modeling approaches. The geometry of the RW2 specimen is illustrated in Figure 3.1. The wall has a rectangular cross section with a width of 1.22 m and a thickness of 0.102 m, and an overall height of 3.66 m, resulting in an aspect ratio of 3.0.

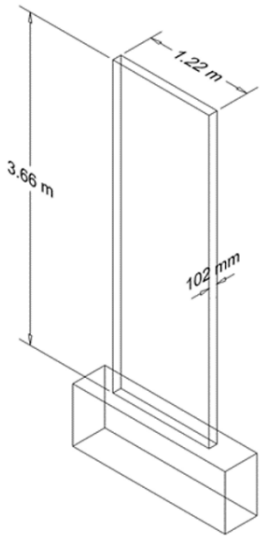


Figure 3.1 Geometry of RW2 specimen (Thomsen, 1995)

The experimental setup for the RW2 specimen is shown in Figure 3.2. Cyclic lateral loading was imposed at the top of the wall by hydraulic actuators.

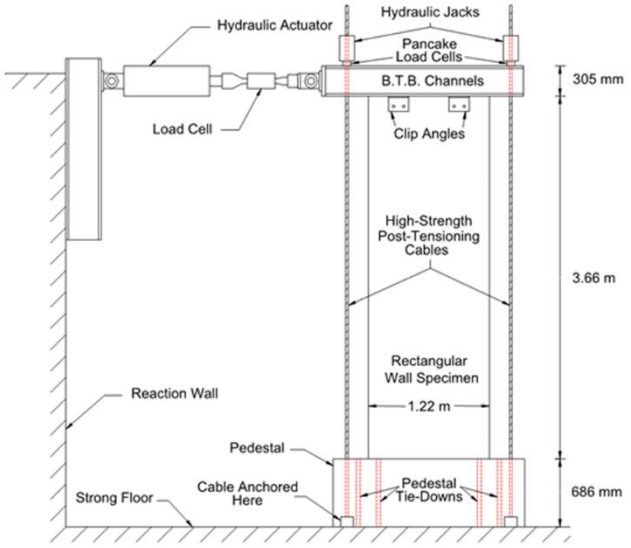


Figure 3.2 Test setup of RW2 specimen (Thomsen, 1995)

The reinforcement layout for the cross section and elevation views are shown in Figures 3.3 and 3.4, respectively. Boundary elements were placed to provide confinement at both ends of the wall. 8 #3 bars (9.53 mm diameter) were used in the

confinement zones, while the hoop reinforcement in the boundary region consists of #1.5 bars (4.76 mm diameter) spaced at 76 mm intervals. Two rows of #2 bars (6.35 mm diameter) were provided for both longitudinal and transverse web reinforcement, spaced at 191 mm.

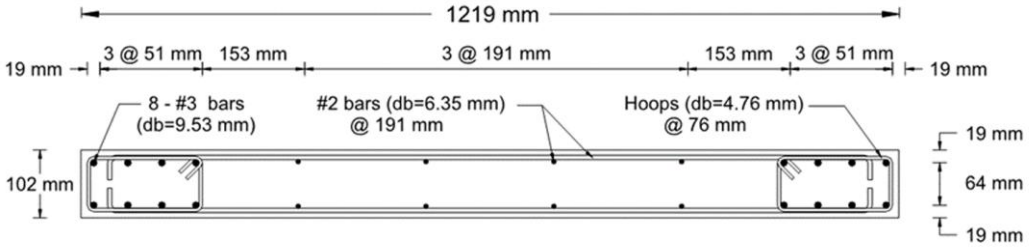


Figure 3.3 Cross section view of RW2 specimen (Thomsen, 1995)

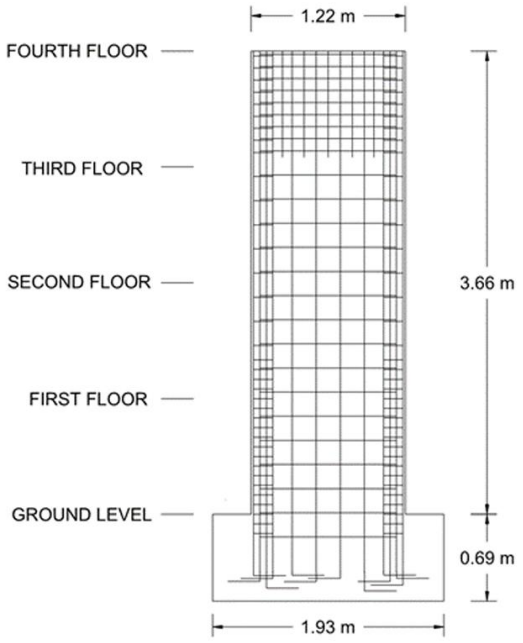


Figure 3.4 Elevation view of RW2 specimen (Thomsen, 1995)

Concrete compressive strength of 27.6 MPa and steel yield strength of 413 MPa, given as the design material properties, are utilized in the analytical model. Hognestad model (Hognestad, 1955) is selected to generate the complete stress-strain curve including the nonlinear behavior for concrete. The modeling parameters

used for both concrete and steel materials are shown in Figure 3.5 and Figure 3.6, respectively. Parameters shown in Figure 3.6 are numerically presented in Table 3.1.

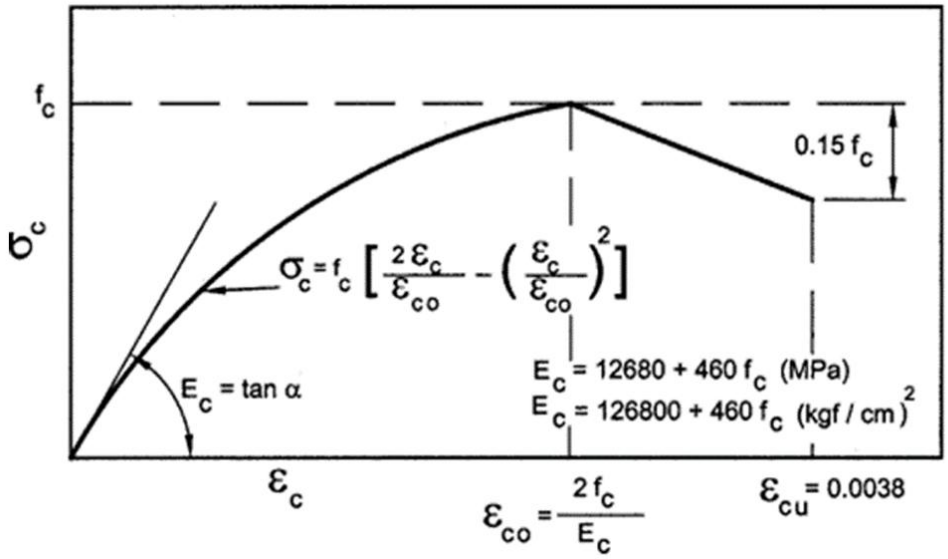


Figure 3.5 Hognestad model for concrete (Hognestad, 1955)

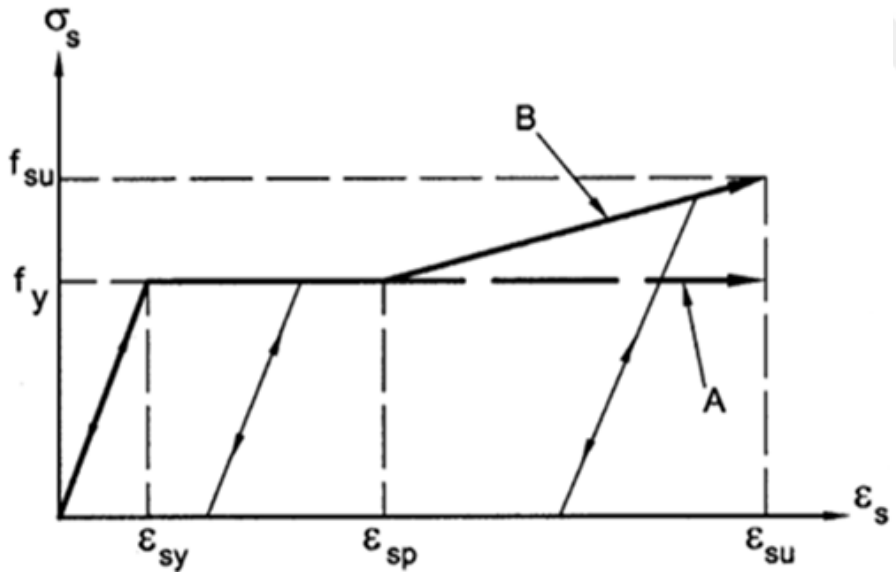


Figure 3.6 Steel stress-strain curve used for modeling RW2 specimen

Table 3.1 Steel stress-strain curve parameters used for modeling RW2 specimen

Parameter	*Value*
E_s	200 GPa
f_y	413 MPa
f_{su}	1.3 f_y
ε_{sy}	f_y / E_s
ε_{sp}	0.01
ε_{su}	0.11

3.1.1 Fiber Hinge Model of RW2 Structural Wall Specimen

The fiber hinge model of the RW2 specimen is constructed using the commercially available structural analysis software, ETABS (Computers and Structures, Inc. [CSI], 2024). The structural wall is modeled as a four story cantilever member, and fixed end boundary conditions are assigned at the base. Elevation view of the structural wall is shown in Figure 3.7.

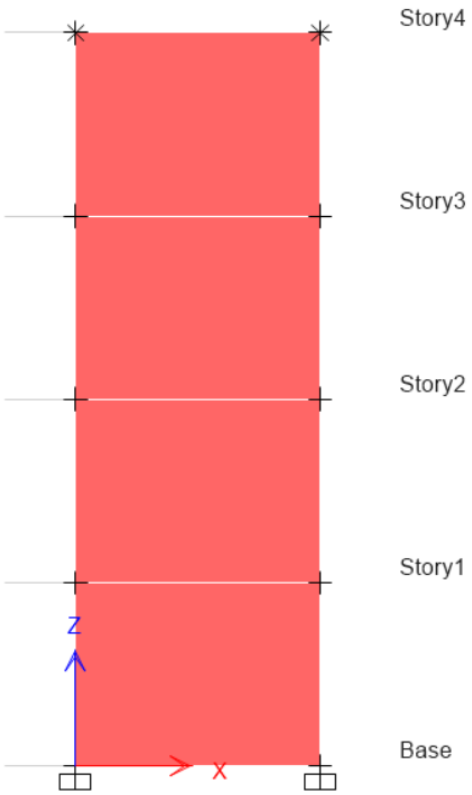


Figure 3.7 Elevation view of RW2 specimen with fiber hinge model

Gravity load of 189 kN is applied to each of the two joints located at the fourth story level, resulting in a total applied gravity load of 378 kN. Their effect on stiffness and displacements is considered as initial conditions for the nonlinear time history analysis. To impose displacement controlled loading, a lateral unit displacement pattern of 1 mm is assigned to the same two joints and scaled by a displacement vs. time record presented in Figure 3.8. The loads applied to the wall are provided in Figure 3.9. To represent the pseudo static analysis as realistically as possible, the lateral displacement is applied at a constant rate of 1 mm/s.

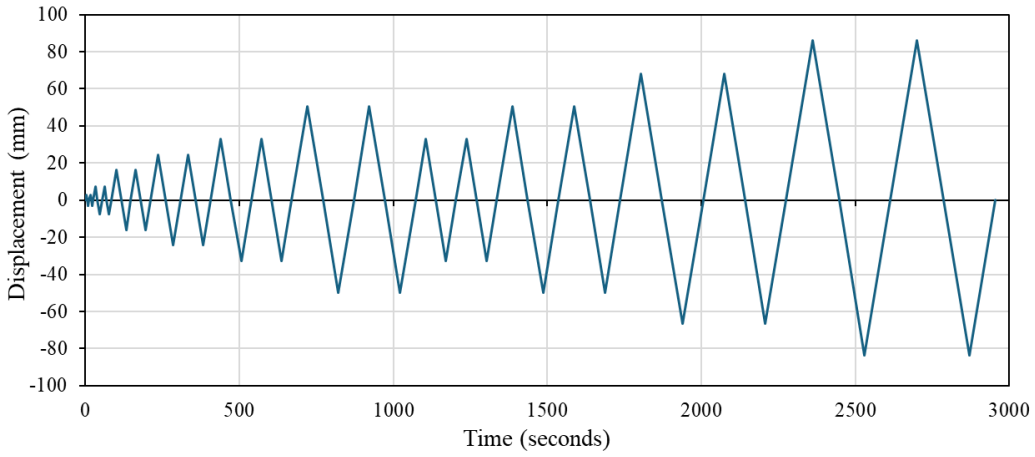


Figure 3.8 Displacement vs. time history of RW2

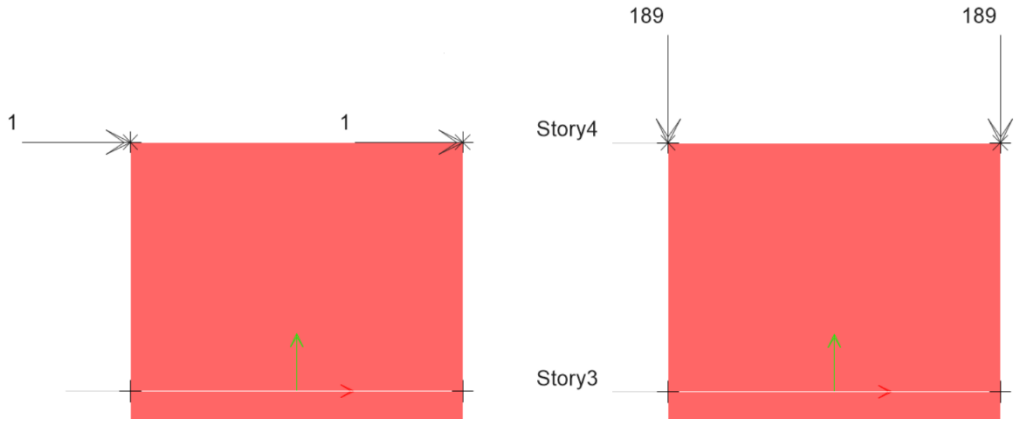


Figure 3.9 Load pattern of RW2 specimen

To account for the stiffness degradation in cracked sections, first the effective stiffness modifiers (ESM) specified in ASCE 41-23 are adopted in the analyses. Although different ESM are defined in ASCE 41-23 for linear and nonlinear analyses, these values are the same for reinforced concrete structural walls. Hysteresis behavior of concrete and steel materials are provided in Appendix A in Figures A.1 and A.2.

In the fiber model approach, the cross section of a structural element is divided into discrete fibers, each having distinct material properties and dimensions, to capture

the nonlinear behavior of the member. The cross section of the structural wall idealized with the fiber model is presented in Figure 3.10.

In this figure, the table labeled “Fiber Definition Data” lists the identification number, area required to compute stress from applied forces, location in the local 2-direction, and material properties used to define the stress-strain relationship for each fiber. The number of fibers representing reinforcing bars does not correspond to the actual number of bars, instead, groups of two or four bars are idealized using a single representative steel fiber placed at the centroid of each group. The concrete, being a continuous material, must also be idealized using finite elements, in this case, fibers. An important aspect of defining the concrete and steel materials with fibers is ensuring that the total area and stiffness represented by the fibers are consistent with the actual area and stiffness of the member. Confined concrete material properties are assigned to fibers located within the boundary regions, while unconfined concrete properties are assigned to fibers in the web region. The geometric locations of the defined concrete and steel fibers within the section are displayed in the top right corner. It is important to note that the axial-flexural interaction is effectively captured by fiber hinges, while the shear-flexural interaction and local damage mechanisms such as bar buckling, bond slip, crack propogation or concrete spalling are neglected.

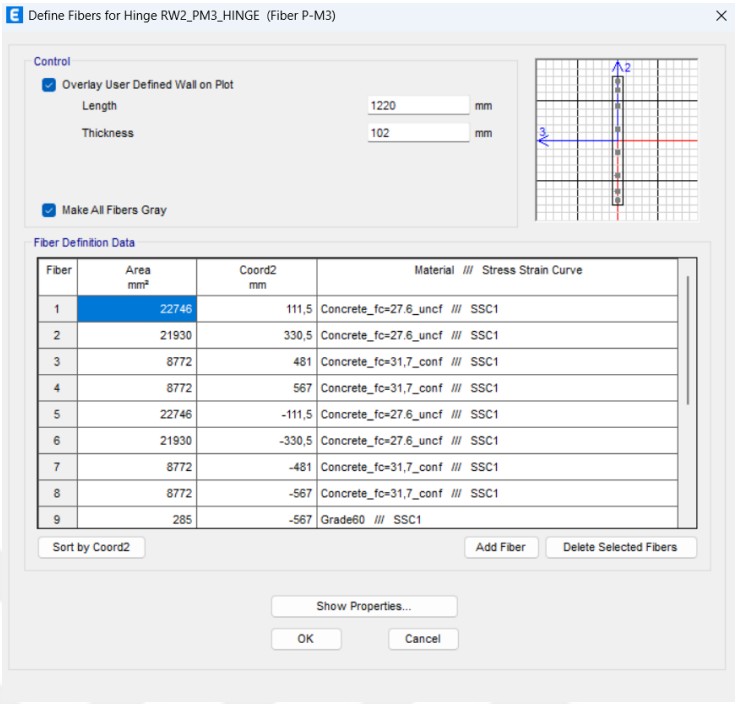


Figure 3.10 RW2 specimen model fiber hinge definition

The comparison of analytical and experimental results for the RW2 structural wall modeled using the fiber hinge approach are illustrated in Figure 3.11. The analytical results indicate that the initial stiffness is well represented by the fiber model; however, the capacity is reached during the early loading cycles, which deviates from the experimental response. The ultimate load carrying capacity shows a close correlation with the test data, while the pinching behavior appears slightly more pronounced than the experimental outcome.

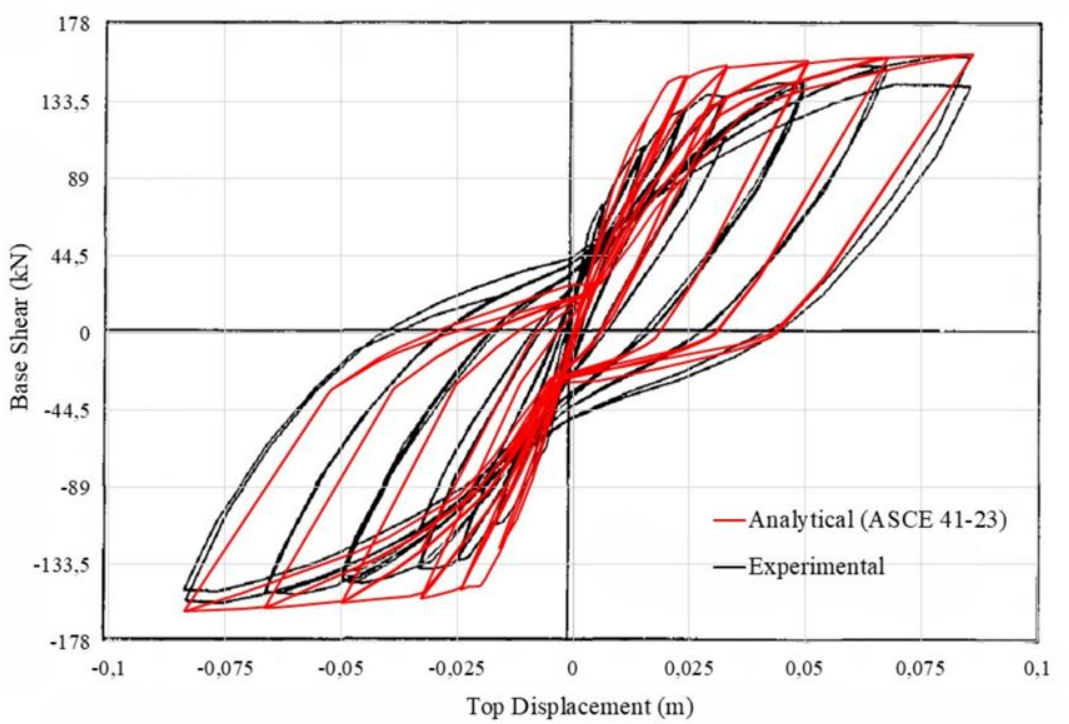


Figure 3.11 Base Shear vs. Top Displacement of RW2 with fiber hinge model (ASCE 41-23)

To evaluate the reliability of the stiffness modifiers specified in ASCE 41-23, the analysis is repeated using the ESM prescribed in TBEC-2018 and ACI 318-19. The corresponding modifiers are summarized in Table 3.2.

Table 3.2 Effective stiffness modifiers

Structural Member	ASCE 41-23 Linear			ASCE 41-23 Nonlinear			ACI 318-19			TBEC-2018		
	Flexural	Shear	Axial	Flexural	Shear	Axial	Flexural	Shear	Axial	Flexural	Shear	Axial
Beams	0.30	0.40	1.00	0.20	0.40	1.00	0.35	1.00	1.00	0.35	1.00	1.00
Columns with compression caused by design gravity loads > 0.5 $A_g f_c$	0.70	0.40	1.00	0.70	0.40	1.00	0.70	1.00	1.00	0.70	1.00	1.00
Columns with compression caused by design gravity loads < 0.1 $A_g f_c$	0.30	0.40	1.00	0.20	0.40	1.00	0.70	1.00	1.00	0.70	1.00	1.00
Walls	0.25	0.15	1.00	0.25	0.15	1.00	0.35	1.00	1.00	0.35	0.25	1.00

The analytical results of the RW2 specimen, obtained utilizing the ESM specified in TBEC-2018 and ACI 318-19, are presented in Figures 3.12 and 3.13, respectively. The comparison of analytical results with different ESM is presented in Figure 3.14.

For all models incorporating different ESM, the ultimate load carrying capacity exhibits a strong correlation with the experimental data. However, when the ESM from TBEC-2018 are applied, the accuracy in capturing the pinching behavior decreases. The initial stiffness of models using ESM from both ACI 318-19 and TBEC-2018 are similar, with both cases overestimating the experimental stiffness. Among these models, the ESM from ASCE 41-23 exhibits the highest correlation.

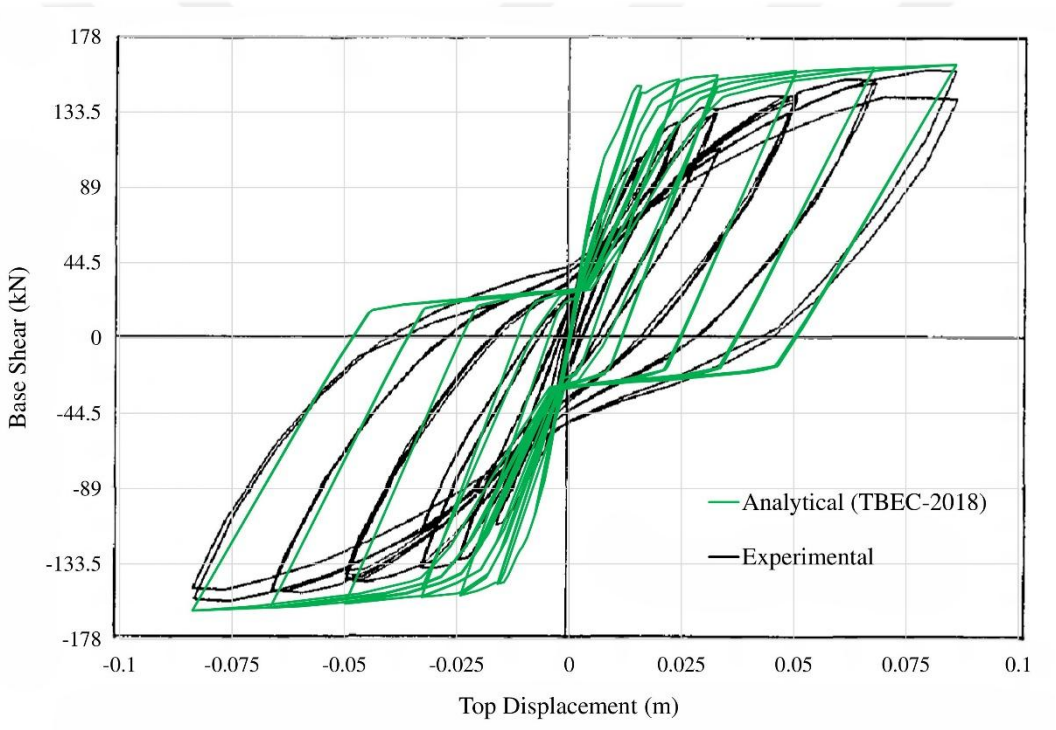


Figure 3.12 Base Shear vs. Top Displacement of RW2 with fiber hinge model (TBEC-2018)

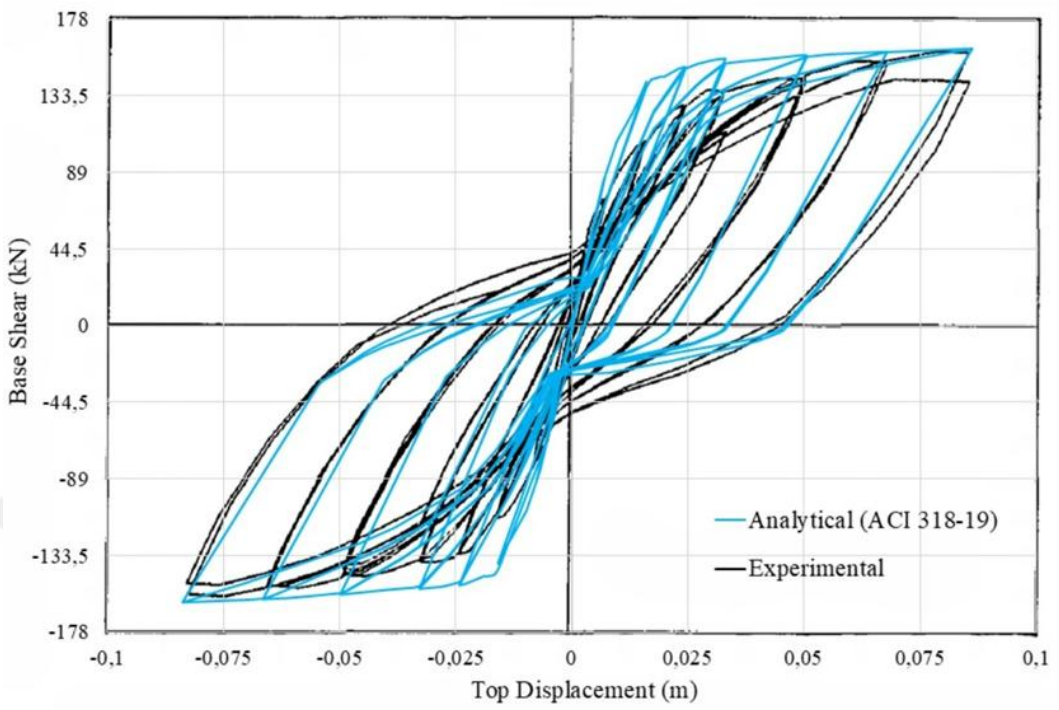


Figure 3.13 Base Shear vs. Top Displacement of RW2 with fiber hinge model (ACI 318-19)

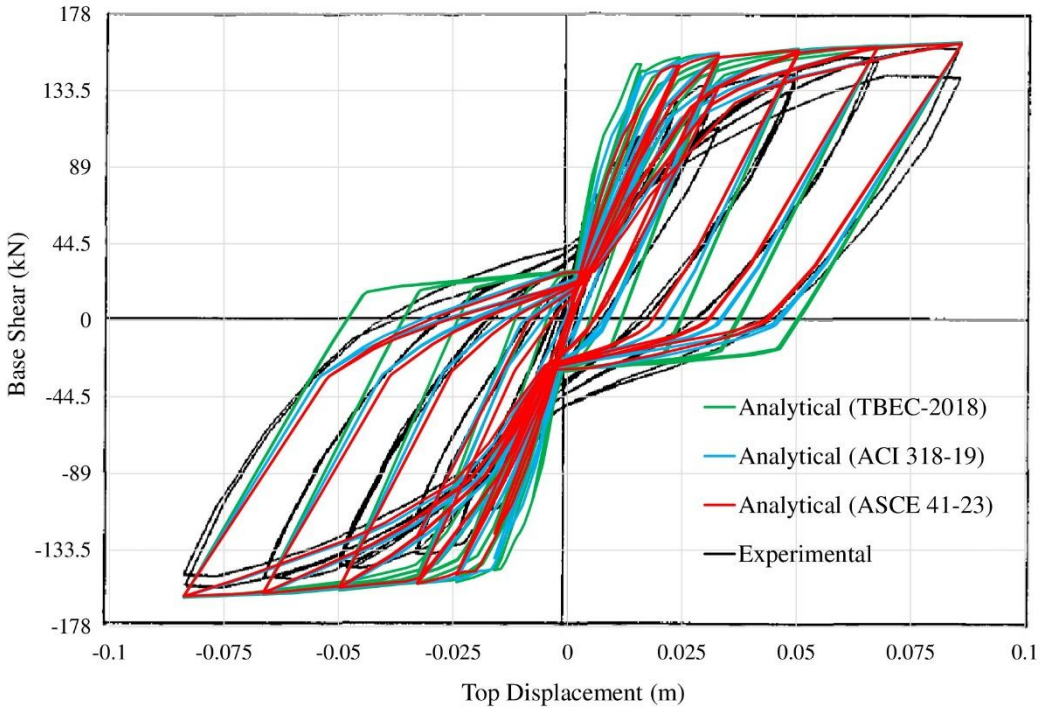


Figure 3.14 Comparison of Base Shear vs. Top Displacement of RW2 with different ESM

3.1.2 Layered Shell Model of RW2 Structural Wall Specimen

As an alternative modeling technique, the behavior of the RW2 specimen is investigated utilizing the layered shell model available in ETABS (Computers and Structures, Inc. [CSI], 2024). Unlike the fiber model, which discretizes the section in one dimension and is limited to capturing the nonlinear in plane axial and flexural behavior, the layered shell model employs two dimensional shell elements that can simulate both in plane and out of plane responses. In this approach, concrete and reinforcing bars are defined as separate shell layers assigned with discrete thickness and material properties allowing for a more comprehensive representation of the nonlinear structural response.

During the construction of the layered shell model of RW2 specimen, same support and initial conditions, material properties, load pattern, and load-displacement

history as in the fiber hinge model are utilized to ensure a coherent comparison of the two models. The ASCE 41-23 effective stiffness modifier (ESM) values, which correlate best with the experimental results, are utilized in the analysis. The web and confinement zones of the structural wall are modeled using separate shell elements to accurately capture their distinct behavioral characteristics, accounting for differences in reinforcement ratio through adjustments in the corresponding layer thickness. The elevation view, the definition of the layered shell element for the confinement zone and the web are provided in Figures 3.15-3.17, respectively.

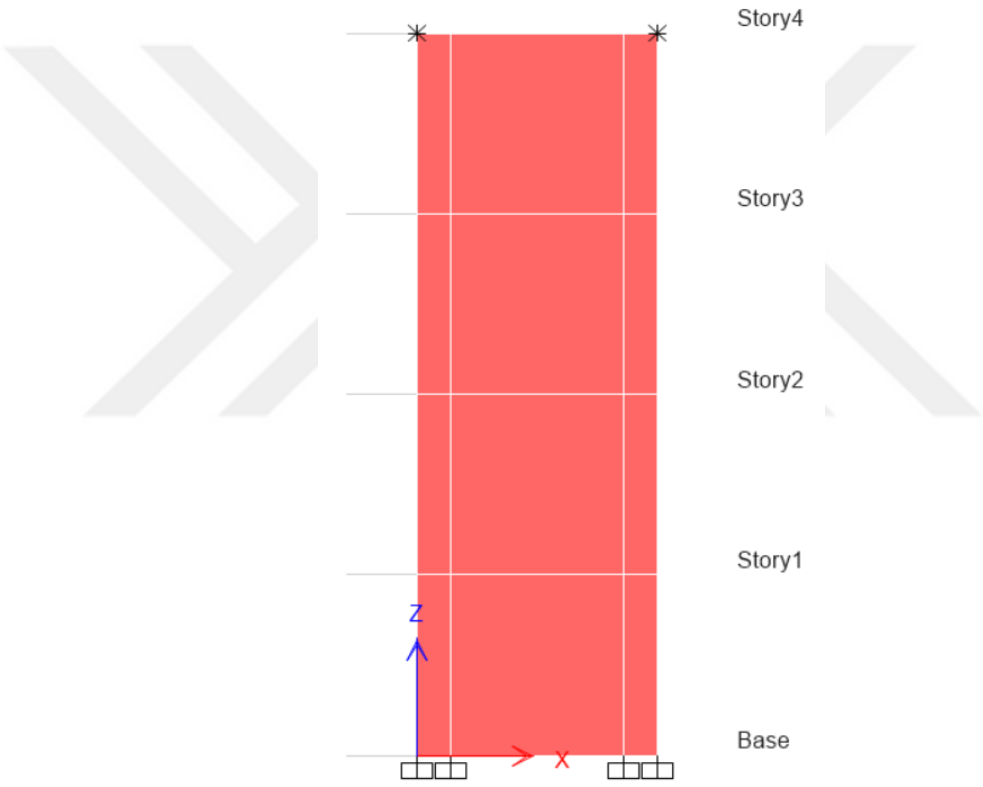


Figure 3.15 Elevation view of RW2 specimen with layered shell model

In Figures 3.16 and 3.17, the first layer labeled “ConcS” represents the concrete material, while the remaining layers (“Pos3Bar1”, “Pos3Bar2”, “Neg3Bar1” and “Neg3Bar2”) correspond to the groups of longitudinal and transverse reinforcement. Each layer is assigned an equivalent thickness that reflects the area of the material it represents. The layer modeling type can be defined as “Membrane”, “Shell” or

“Plate”, where Membrane captures only in plane behavior, Shell represents full in plane and out of plane behavior, and Plate models only out of plane response.

As per the default settings of the analytical program, the concrete layer is integrated using three points through the thickness to better capture nonlinear stress distribution and stiffness degradation. Reinforcement layers, being uniaxial, require only a single integration point. The material angle is measured counterclockwise from the local 1 axis of the shell element to the assigned material direction, i.e. the length of the wall for concrete material; in this configuration, an angle of 90° corresponds to longitudinal reinforcement, while 0° is assigned to transverse bars and concrete.

The material behavior option can be set to either “Directional” or “Coupled”. The Directional formulation allows independent control of the S11, S22, and S12 components, whereas the Coupled option enforces nonlinear behavior in all three directions using the Modified Darwin-Pecknold 2D concrete model (Darwin and Pecknold, 1977). Validation studies indicated that the selected behavior type has negligible influence on the overall analytical response.

S11 denotes the normal stress-strain response along the local 1 axis of the shell element, aligned with the longitudinal reinforcement. This component is modeled as nonlinear, as it governs the primary nonlinear behavior of the structural wall. S22 represents the normal response along the local 2 axis, perpendicular to S11. Since the transverse dimension of the longitudinal reinforcement is significantly small relative to the bar length, its nonlinear contribution is insignificant; therefore, S22 is set to inactive for reinforcement layers. S12 corresponds to the in plane shear response. Although slender walls are not expected to exhibit pronounced nonlinear shear behavior, S12 is defined as nonlinear to be conservative, however, setting this parameter to linear or inactive has not led to any difference in the analytical results.

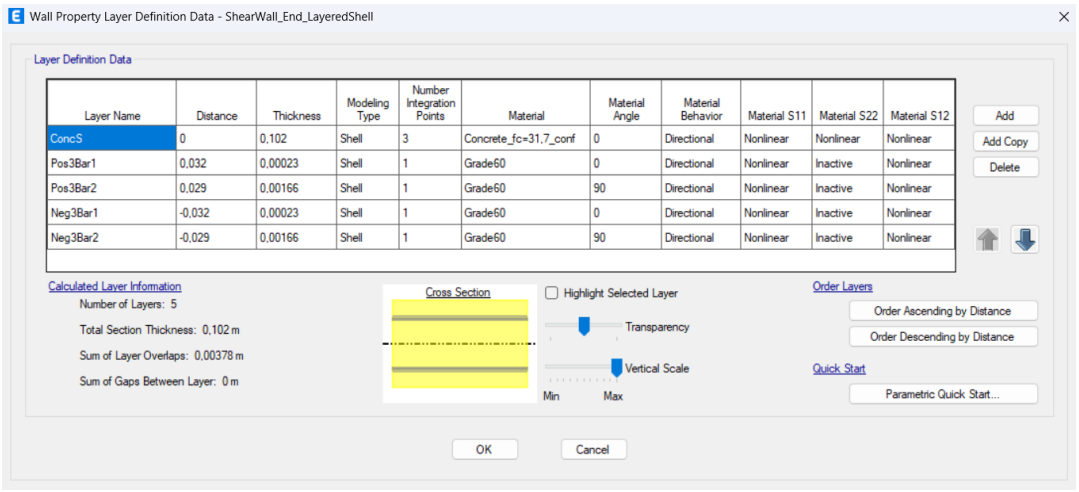


Figure 3.16 Definition of the layered shell element for the confinement zone of RW2 specimen

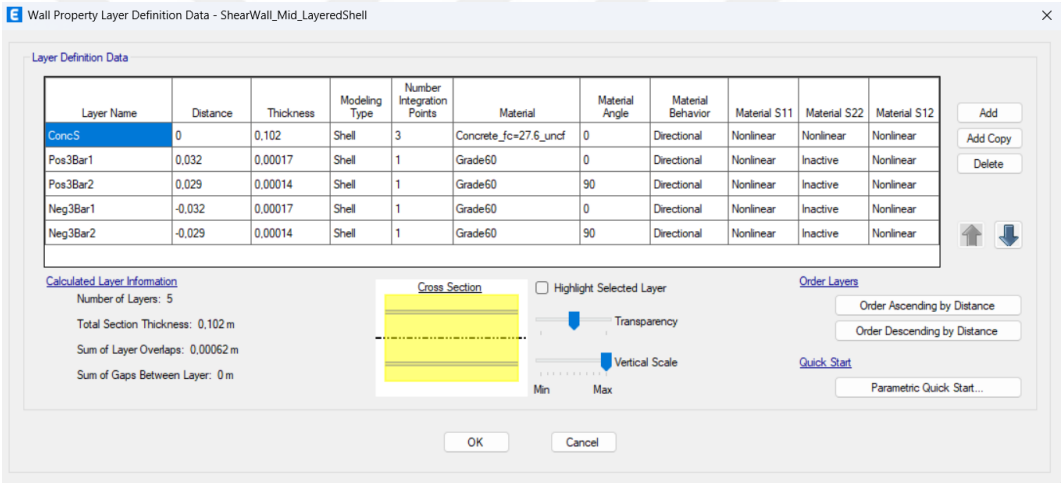


Figure 3.17 Definition of the layered shell element for the web of RW2 specimen

The comparison of the analytical and experimental results for the RW2 structural wall with the layered shell model are presented in Figure 3.18. Furthermore, the comparison between the layered shell and fiber hinge models of RW2 specimen is illustrated in Figure 3.19. The most notable difference is observed in the initial stiffness, which is overestimated by the layered shell model. Similar to the fiber hinge model, the predicted ultimate lateral load capacity closely matches with the experimental results, and the pinching behavior appears more pronounced. Compared to the fiber model, a slight difference is observed in the unloading

stiffness; however, this minor deviation is considered to be negligible. Overall, the fiber hinge model is observed to provide a more accurate representation of the base shear vs. roof displacement response when compared to the layered shell model for this experimental study.

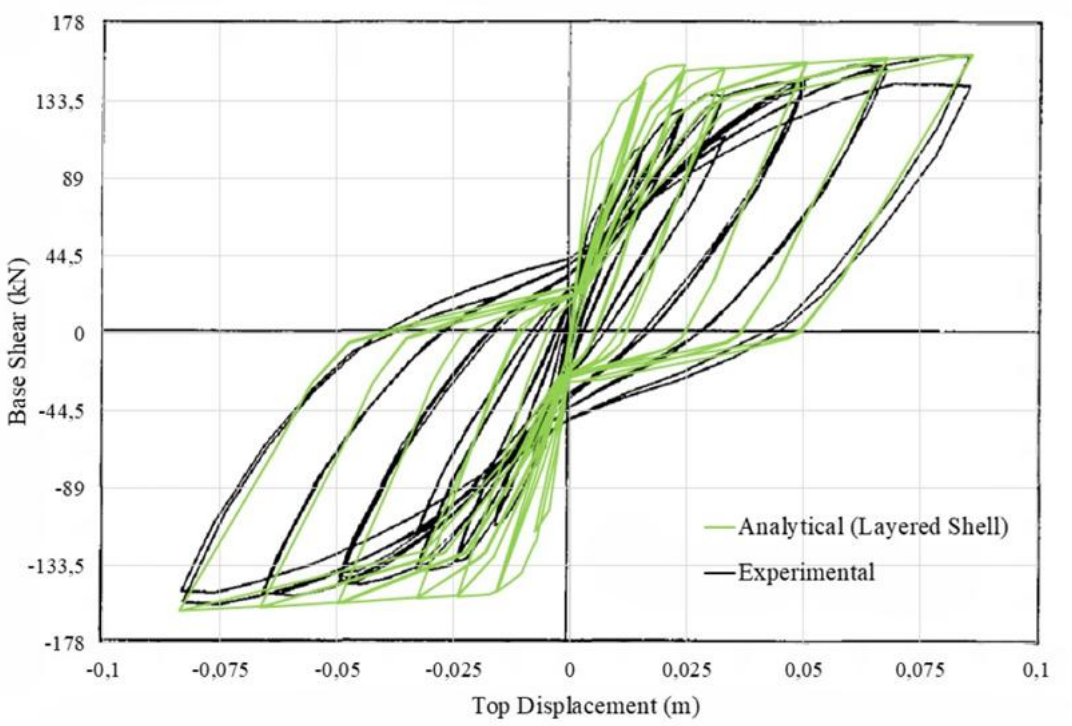


Figure 3.18 Comparison of Base Shear vs. Top Displacement Response of RW2 specimen with layered shell model

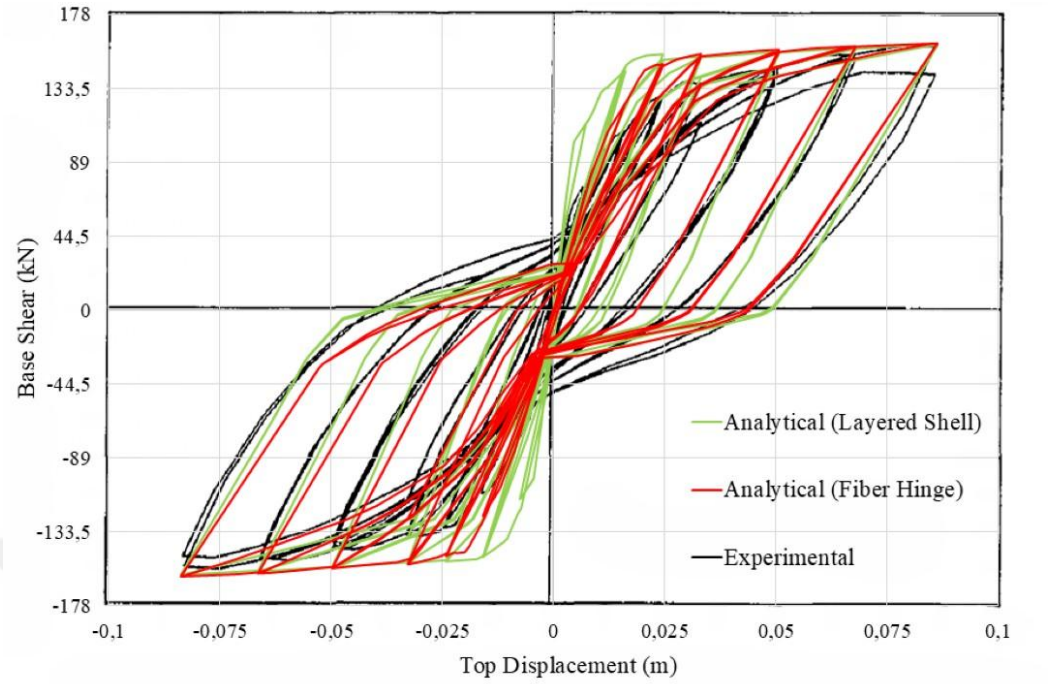


Figure 3.19 Comparison of Base Shear vs. Top Displacement Response of RW2 specimen with both layered shell and fiber hinge models

3.2 Seven Story Full Scale Building

Within the framework of the U.S.-Japan Cooperative Research Program on Large Scale Testing Facilities, a full scale, seven story reinforced concrete building was designed, constructed, and tested at the Building Research Institute under the Ministry of Construction in Japan (Wight, 1983).

The structure consisted of three three bay frames in the loading direction and four two bay frames in the transverse direction, with spans of 6.0 m-5.0 m-6.0 m and 6.0 m, respectively. Story heights were 3.75 m at the first level and 3.0 m for the upper stories. A continuous structural wall, without girders, was placed in the central bay of the central frame from the first to the seventh story. The structure was rigidly anchored to the test floor, and soil-structure interaction was not considered. Columns are 50 cm × 50 cm across all stories. From the second floor up to the roof, the cross sectional dimensions of girders parallel to the loading direction are 30 cm by 50 cm.

The thickness of the structural walls is 20 cm, while the floor slabs have a uniform thickness of 12 cm. Plan and elevation views of the structure are shown in Figures 3.20 and 3.21, respectively.

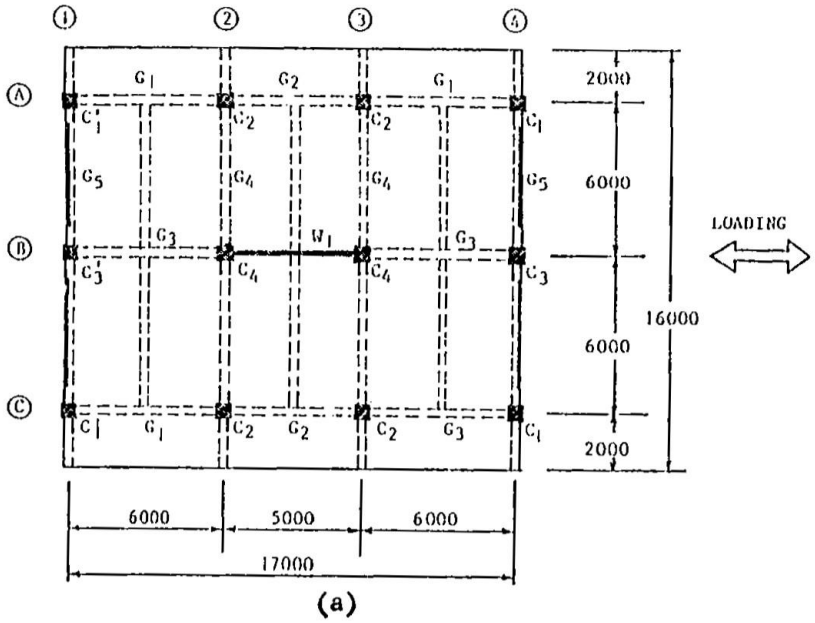


Figure 3.20 Plan view of the seven story validation building

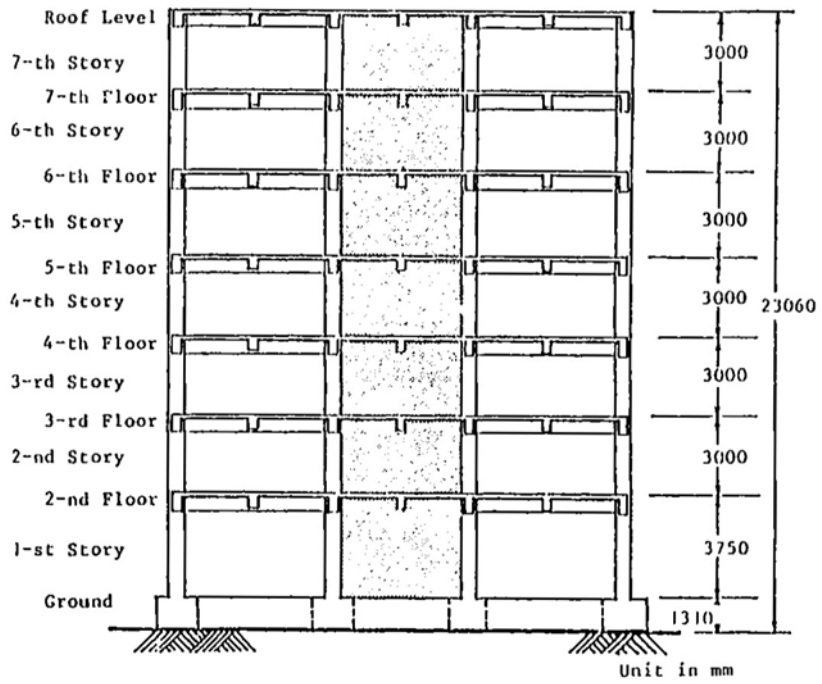


Figure 3.21 Elevation view of the seven story validation building

The floor plan is rectangular, with dimensions of 17 m along the X-axis and 16 m along the Y-axis, resulting in a total floor area of 272 m². The structure comprises three frames in the X-direction and four frames in the Y-direction. The overall height of the seven story building is 21.75 m. The model maintains plan symmetry about both the centroidal X and Y axes.

Initially, the building, excluding nonstructural elements, was tested under loading conditions ranging from elastic response to high intensity seismic loading inducing significant damage. After the first test series, the damaged structure was repaired and strengthened, and nonstructural elements were added. Subsequently, the structure underwent retesting using the same protocol as in the original test series. A brief overview of the test program for the full scale seven story reinforced concrete building and the reinforcement detailing are provided in Table 3.3 and Appendix B in Figure B.1, respectively.

Table 3.3 Brief description of the seven story building test series

Test No.	Brief Description
VT - 1	Free and Forced Vibration Tests
FLL - 1	Each Floor Level Loading Test
SL - 1	Static Test under Inverted Triangular Load Distribution Dmax* = 342 mm, Smax** = 400 kN
SPD - 1	Pseudo - Dynamic Earthquake Test Modified Miyagi-ken Oki Earthquake (1978) Dmax = 2.52 mm, Smax = 315 kN, Amax***= 23.5 cm/s²
SPD - 2	Pseudo - Dynamic Earthquake Test Modified Miyagi-ken Oki Earthquake (1978) Dmax = 32.5 mm, Smax = 2260 kN, Amax***= 105 cm/s²
SPD - 3	Pseudo - Dynamic Earthquake Test Modified Tehachapi Shock (1952) Dmax = 238 mm, Smax = 4110 kN, Amax***= 320 cm/s²
SPD - 4	Pseudo - Dynamic Earthquake Test Tokachi Oki Earthquake (1968) Dmax = 342 mm, Smax = 4390 kN, Amax***= 350 cm/s²
FLL - 2	Each Floor Level Loading Test
VT - 2	Free and Forced Vibration Tests
	Repair of Test Structure by Epoxy Injection
VT - 3	Free and Forced Vibration Tests
FLL - 3	Each Floor Level Loading Test
	Placement of Nonstructural Elements in Test Structure
VT - 4	Free and Forced Vibration Tests
FLL - 4	Each Floor Level Loading Test
SL - 2	Static Test under Inverted Triangular Load Distribution Dmax* = 4 mm, Smax** = 220 kN
SPD - 5	Pseudo - Dynamic Earthquake Test Modified Miyagi-ken Oki Earthquake (1978) Dmax = 3.03 mm, Smax = 267 kN, Amax***= 23.5 cm/s²
SPD - 6	Pseudo - Dynamic Earthquake Test Modified Miyagi-ken Oki Earthquake (1978) Dmax = 65.3 mm, Smax = 2340 kN, Amax***= 105 cm/s²
SPD - 7	Pseudo - Dynamic Earthquake Test Modified Tehachapi Shock (1952) Dmax = 244 mm, Smax = 5970 kN, Amax***= 320 cm/s²
SL - 3	Static Test under Uniform Load Distribution Dmax* = 4 mm, Smax** = 220 kN
VT - 5	Free and Forced Vibration Tests

* Dmax : Maximum roof level displacement (mm)

** Smax : Maximum base shear (kN)

*** Amax: Maximum acceleration of input ground motion (cm/s²)

3.2.1 Fiber Hinge Model of the Seven Story Full Scale Building

The plan view of the first story of the generated model and the elevation view of the central frame, which contains the structural wall and aligned with the loading direction, are presented in Figure 3.22 and Figure 3.23, respectively. Since the foundation was rigidly anchored to the test floor, fixed base support condition is considered.

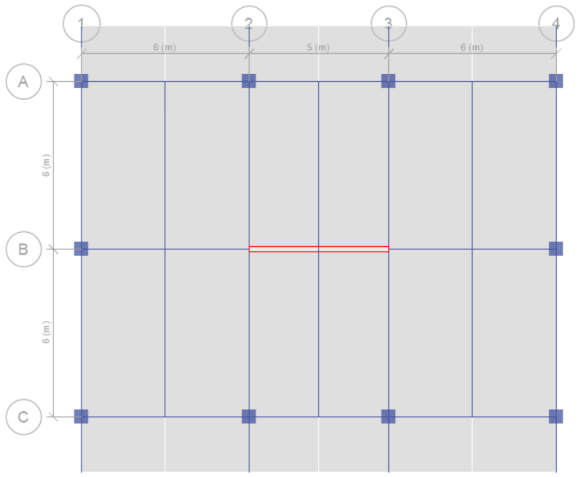


Figure 3.22 Plan view of the fiber hinge model of the seven story building

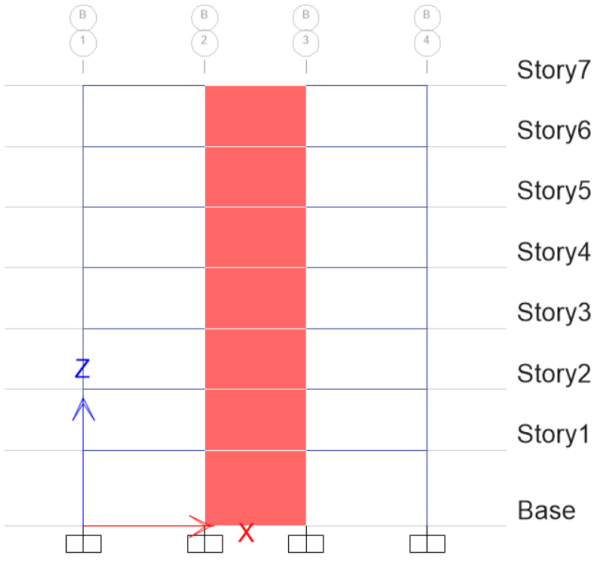


Figure 3.23 Elevation view of the fiber hinge model of the seven story building

In the analysis, based on the experimental data, the compressive strength and elastic modulus of concrete are taken as 28.4 MPa (corresponding to a strain of 0.0021) and 23.2 GPa, respectively. The mechanical properties of the reinforcing bars with varying diameters are presented in Table 3.4.

Table 3.4 Mechanical properties of the reinforcing bars in the seven story building

Bar Size	*Nominal Area (mm^2)*	*Yield Strength (MPa)*	*Strain Hardening Strain*	*Tensile Strength (MPa)*	*Fracture Strain*
D10	71	380	0.018	556	0.17
D16	199	378	0.019	560	0.18
D19	287	353	0.017	561	0.20
D22	387	346	0.012	563	0.21

In the experimental program, a series of tests are conducted on the structure, including retrofitting and testing the damaged specimen, the details of which are provided in Table 3.3. Analyzing the retrofitted structure inherently requires the damaged state of the structure as the initial condition. Although the initial conditions representing the damaged state can be defined in the analytical software, incorporating retrofit measures simultaneously alters the model, therefore, the retrofitted specimens are not considered. Examination of the experimental data indicates that the majority of the experimental results are provided for the SPD-3 test, and as such, the SPD-2 and SPD-3 tests are selected for analysis. The SPD-2 test is employed to define the initial conditions for the SPD-3 test. Since no cracking was reported in the SPD-1 test and elastic response was observed, SPD-1 test step is not included in the analysis.

The applied time histories for the SPD-2 and SPD-3 tests are presented in Figures 3.24 and 3.25, respectively.

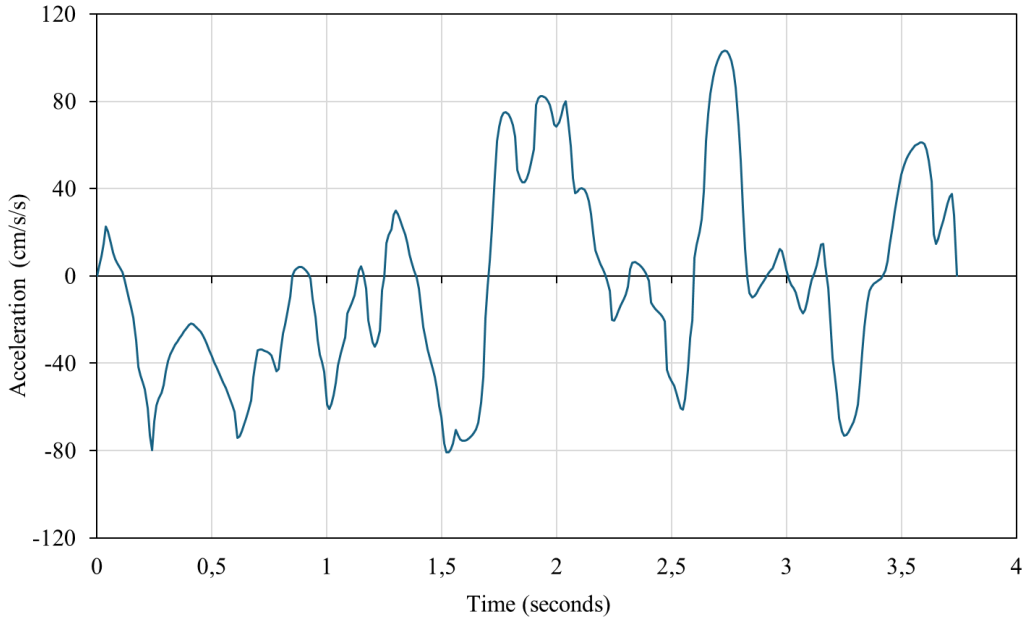


Figure 3.24 Acceleration vs. time history of SPD-2 test

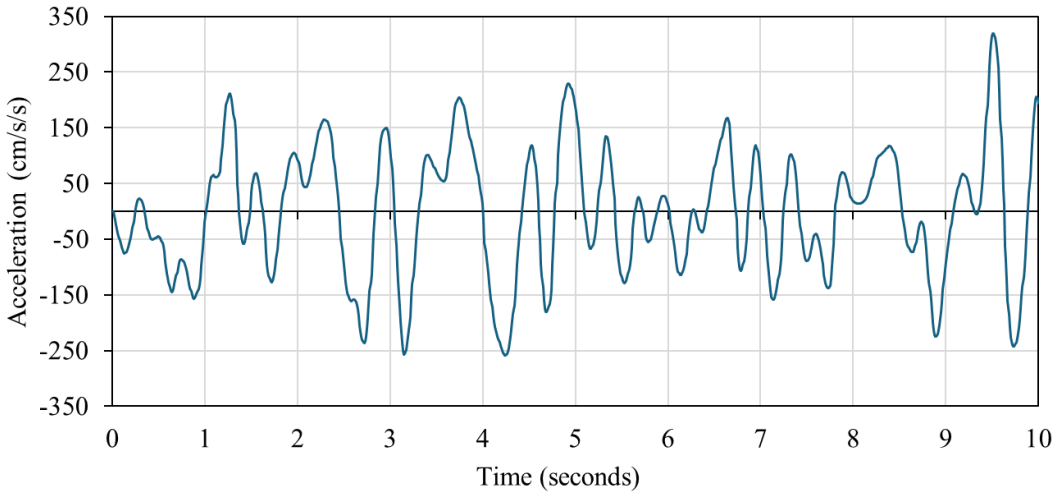


Figure 3.25 Acceleration vs. time history of SPD-3 test

In the development of the fiber model for the full scale seven story building, M3 moment-rotation hinges are assigned to the beams, P-M2-M3 fiber hinges to the columns, and P-M3 fiber hinges to the structural walls. The M3 and P-M2-M3 hinges are modeled as zero length elements and placed at both ends of each corresponding frame element. The P-M3 hinges are placed at the midheight of the structural wall

element on each story. Representative illustrations for the definition of each hinge type are provided in Figures 3.26, 3.27, and 3.28.

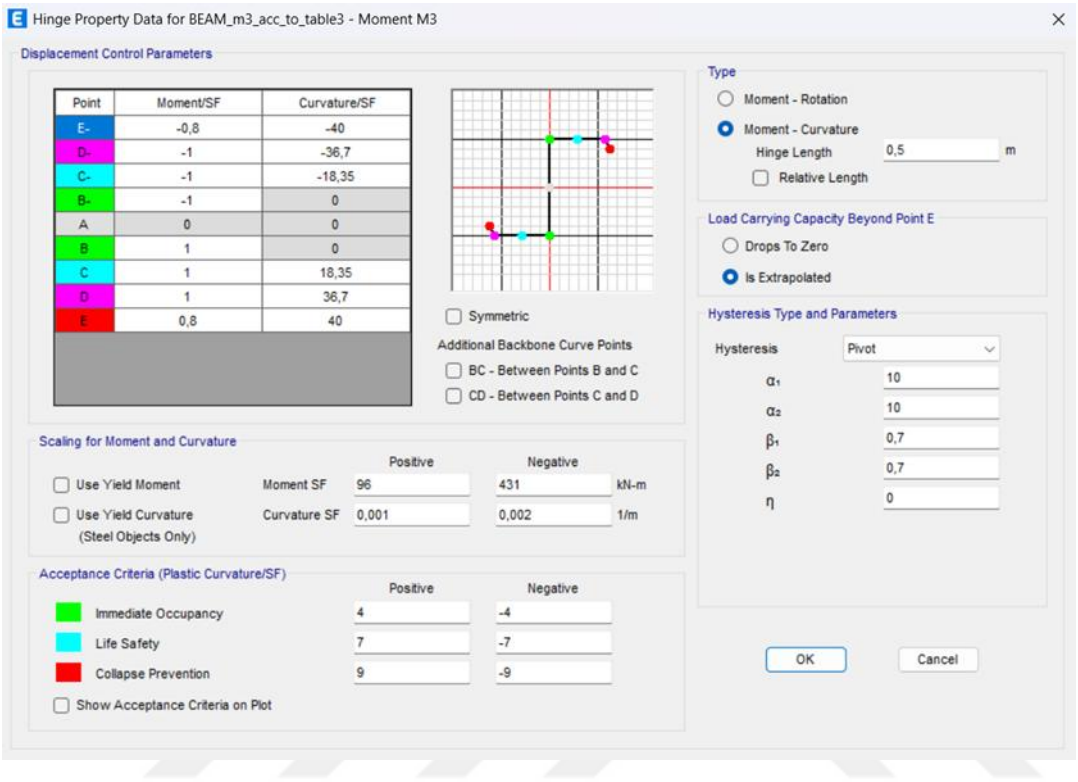


Figure 3.26 Representative M3 moment-rotation hinge



Fiber	Area m²	Coord2 m	Material	Color
5	0,0997	-0,5	C28.4MPa	
6	0,0997	0	C28.4MPa	
7	0,0997	0,5	C28.4MPa	
8	0,0997	1	C28.4MPa	
9	0,0997	1,5	C28.4MPa	
10	0,0997	2	C28.4MPa	
11	0,0498	2,375	C28.4MPa	
12	0,0003	-2,25	Mat_D10_Rebar	
13	0,0003	-1,75	Mat_D10_Rebar	

Figure 3.27 Representative P-M3 fiber hinge

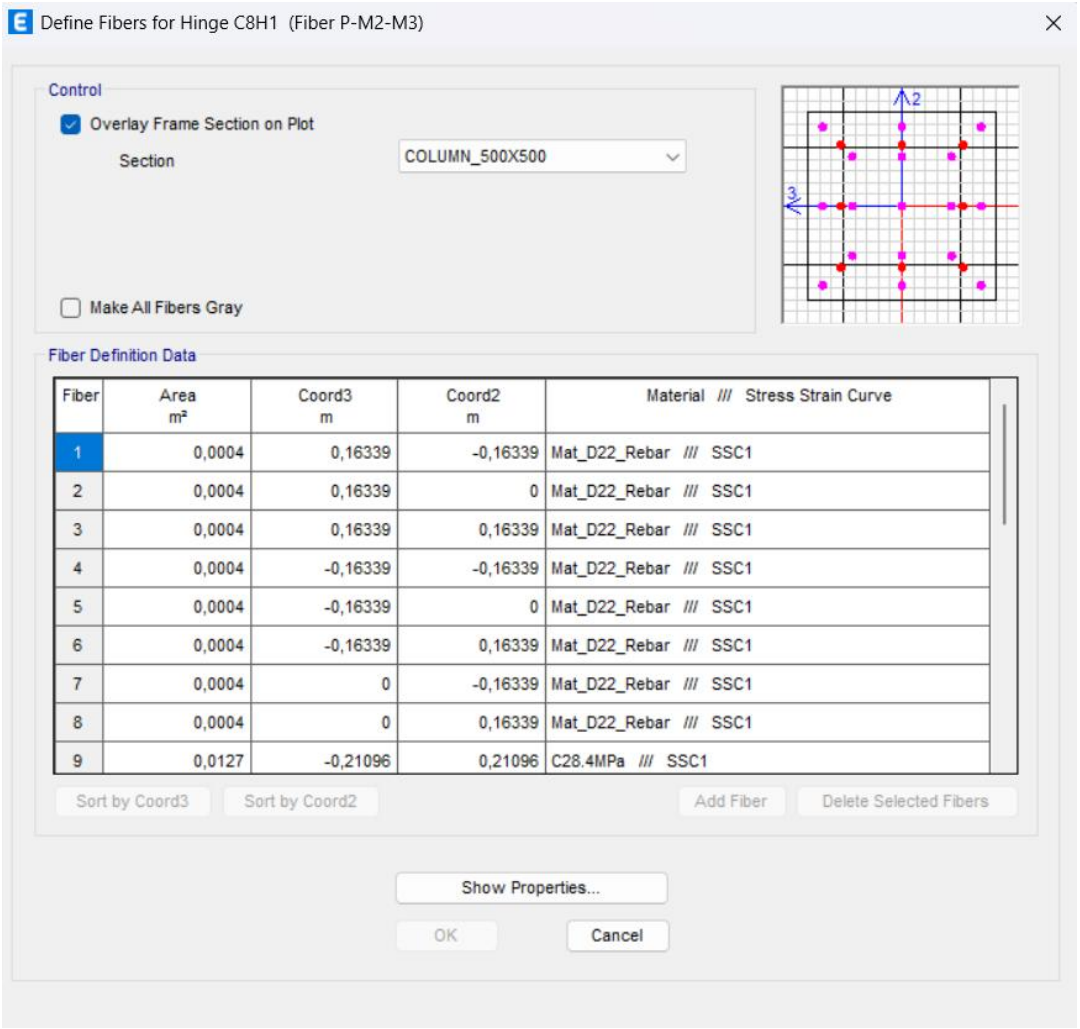


Figure 3.28 Representative P-M2-M3 fiber hinge

In Figure 3.26, the moment-curvature relationship for the beam section is idealized in ETABS. In this definition, point ‘A’ corresponds to the yield point on the moment-curvature relationship, while the coordinates of all other points are entered as multiples of the coordinates of point ‘A’. The moment and curvature values corresponding to point ‘A’ are assigned in the fields labeled “Moment SF” and “Curvature SF”, respectively.

In ETABS, the M3 hinge formulation is fundamentally based on curvature rather than rotation. The hinge output can be set to rotation or curvature using the options in the upper right corner. When curvature is selected, the hinge length must be

specified and rotation is obtained by multiplying the curvature by the hinge length. The hinge length is taken as the section depth, as recommended by ACI 318-19.

If the option “Load Carrying Capacity Beyond Point E” is set to “Drops to Zero”, the plastic hinge does not carry moment beyond point E, which may lead to convergence issues in the analysis. When “Extrapolated” is selected, the behavior beyond point E is extrapolated using the slope defined by point E and the preceding point. Based on the validation studies, the hysteresis type is selected as “Pivot”, with default parameters. The details of these parameters are provided in Appendix A in Figure A.6.

A detailed explanation regarding the P-M3 fiber hinges assigned to the structural walls, as shown in Figure 3.27, is provided in Section 3.1.1. The same principles apply to the P-M2-M3 hinges shown in Figure 3.28, with the key difference that these hinges capture nonlinear response in both the 2- and 3-directions. Therefore, when defining the fibers for P-M2-M3 hinges, the coordinates must be specified for both directions. The total area and the stiffness of the fibers in both directions must match the actual member.

In ETABS (Computers and Structures, Inc. [CSI], 2024), unlike frame elements which are line objects with distinct end points where hinges can be explicitly assigned, wall elements are defined as area objects. Therefore, hinges in shell walls are automatically located at the midheight of the object, where the software obtains internal forces (P, M3, etc.) at a single control station. This definition corresponds to a one point Gauss integration scheme, meaning that the hinge acts as a lumped nonlinearity at the object level rather than at the finite element level. If the expected plastic hinge length is shorter, the wall object should be subdivided so that the midpoint of each sub-object coincides with the intended hinge region. Since plastic hinges are assigned to shell walls at every story, and nonlinear response in slender walls is typically concentrated in the first few stories (i.e., 1-3), this modeling approach is generally sufficient to capture the nonlinear behavior. The hinge

locations for the frame elements and shell elements are illustrated in Figures 3.29 and 3.30, respectively.

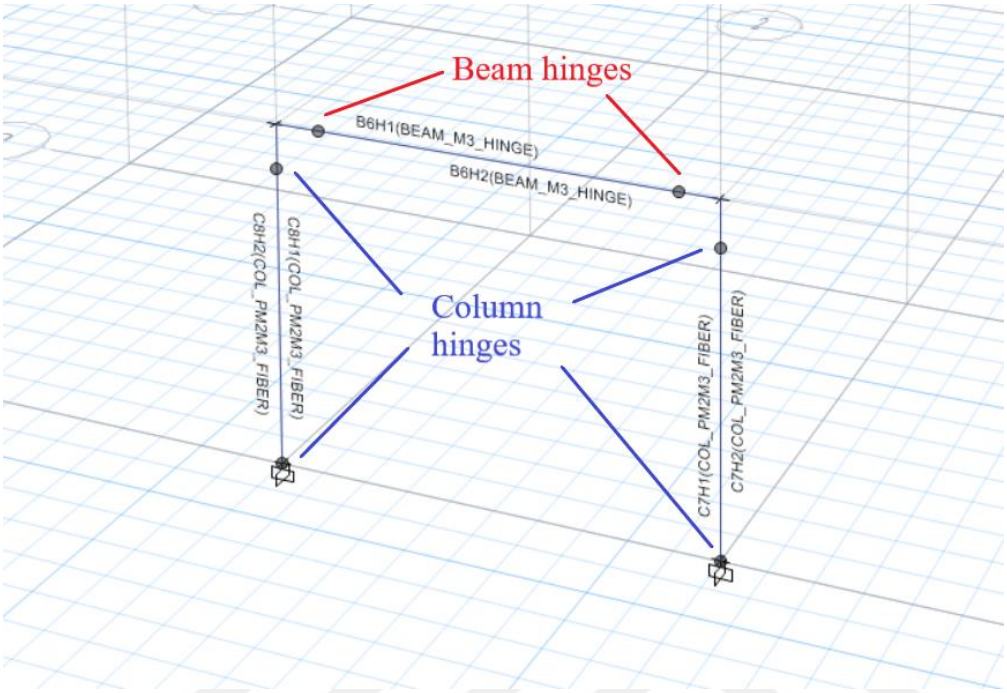


Figure 3.29 Location of frame hinges

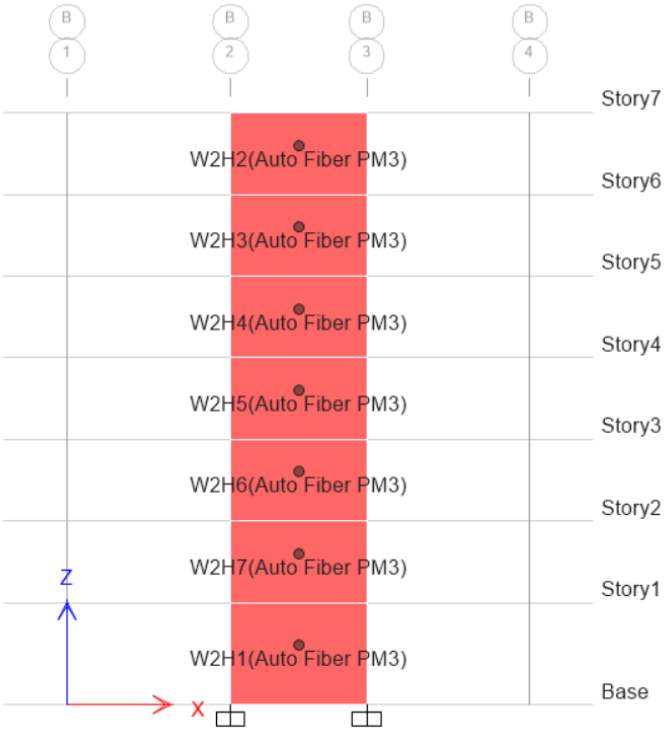


Figure 3.30 Location of shell hinges

During the analysis, to account for the stiffness reduction due to cracking of the sections, the effective stiffness modifiers (ESM) provided in ASCE 41-23, ACI 318-19 and TBEC-2018 are utilized. ASCE 41-23 specifies different ESM for linear and nonlinear analyses. In the validation study of the seven story full scale building, all modifiers provided in the above mentioned design codes are utilized to compare the effect on the structural response. Figures 3.31-3.38 illustrate the analytical results obtained with effective stiffness modifiers recommended by ASCE 41-23 Nonlinear Analysis (ESM-ANA), ASCE 41-23 Linear Analysis (ESM-ALA), ACI 318-19 (ESM-ACI 318-19) and TBEC-2018 (ESM-TBEC-2018).

The best fit with the experimental results is obtained when the effective stiffness modifiers (ESM) recommended by ASCE 41-23 for linear analysis are adopted, both in terms of roof displacement vs. time and base shear vs. time responses. The analytical results obtained by utilizing ESM definitions of ACI 318-19 and TBEC-2018 are nearly identical due to their similar stiffness modifiers, both leading to an

underestimation of roof displacements. In contrast, the ESM-ANA case produced an overestimation of roof displacements, which can be attributed to the relatively low flexural stiffness modifiers specified for structural walls, beams, and columns compared to the other investigated design codes. For all models, the experimental response up to the 4-second mark is not adequately captured. The initial mismatch is believed to be caused by the difference in the periods of the model and the experiment. As nonlinear behavior dominated the response, the period of the model is observed to merge towards that of the experiment. The parameters that significantly affect the period are observed to be the effective stiffness modifiers. To validate this observation, the model is reanalyzed without applying the effective stiffness modifiers, the results of which are presented in Figures 3.39 and 3.40.

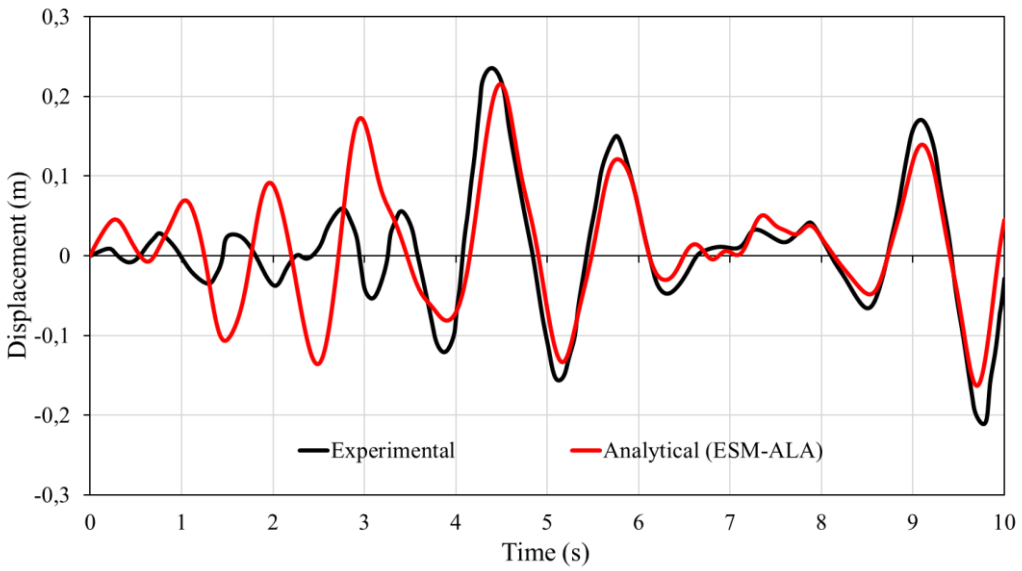


Figure 3.31 Roof displacement vs. time (ESM-ALA)

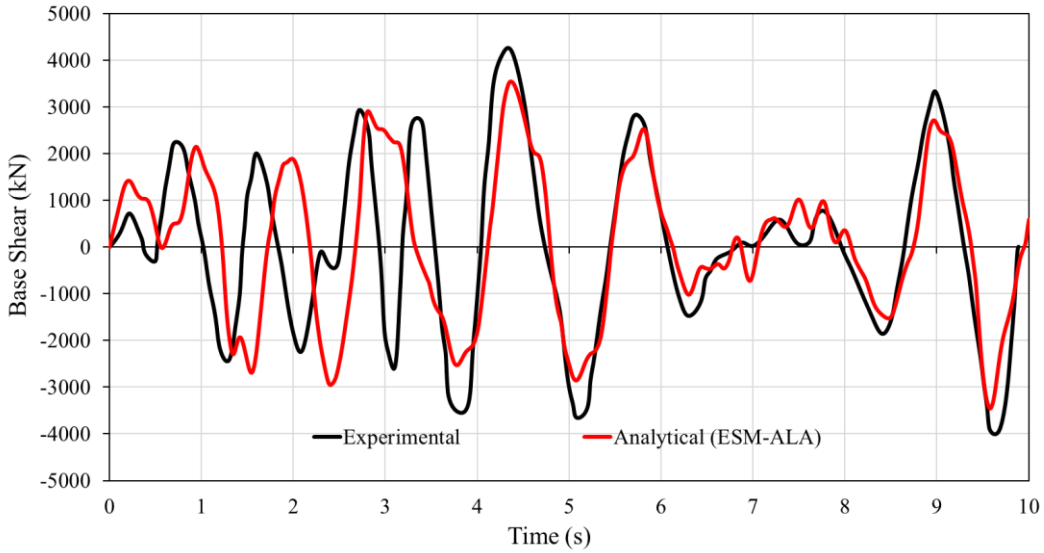


Figure 3.32 Base shear vs. time (ESM-ALA)

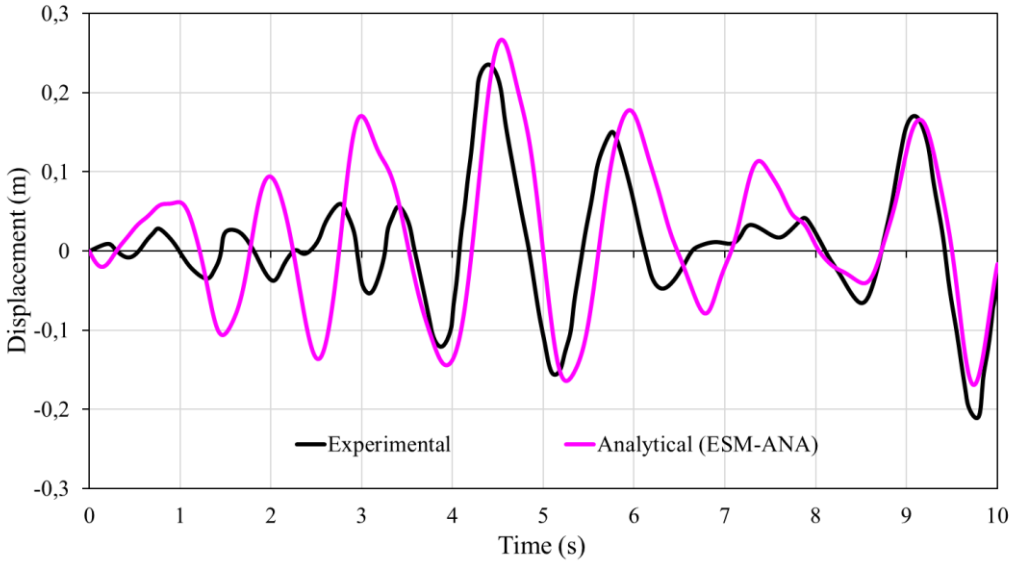


Figure 3.33 Roof displacement vs. time (ESM-ANA)

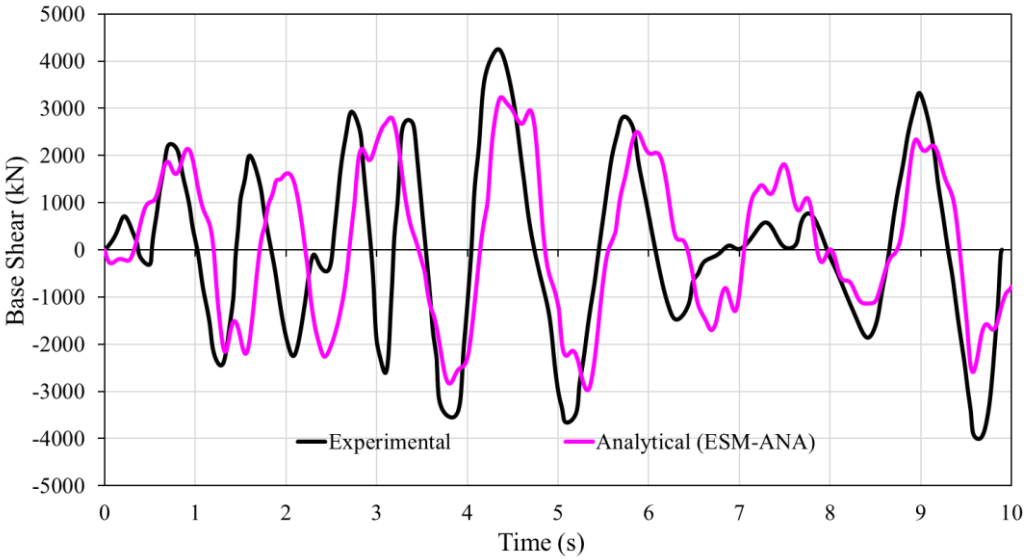


Figure 3.34 Base shear vs. time (ESM-ANA)

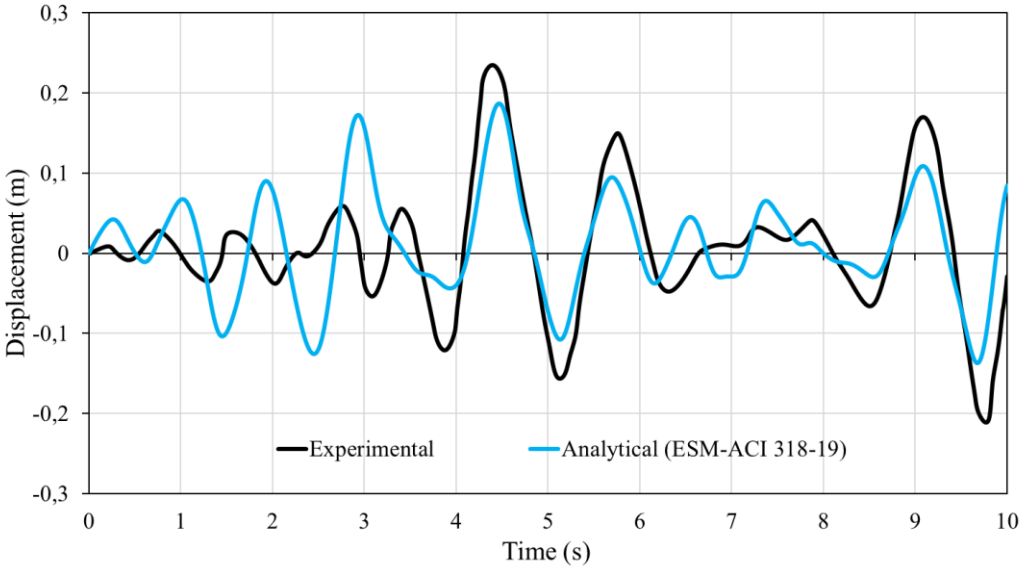


Figure 3.35 Roof displacement vs. time (ESM-ACI 318-19)

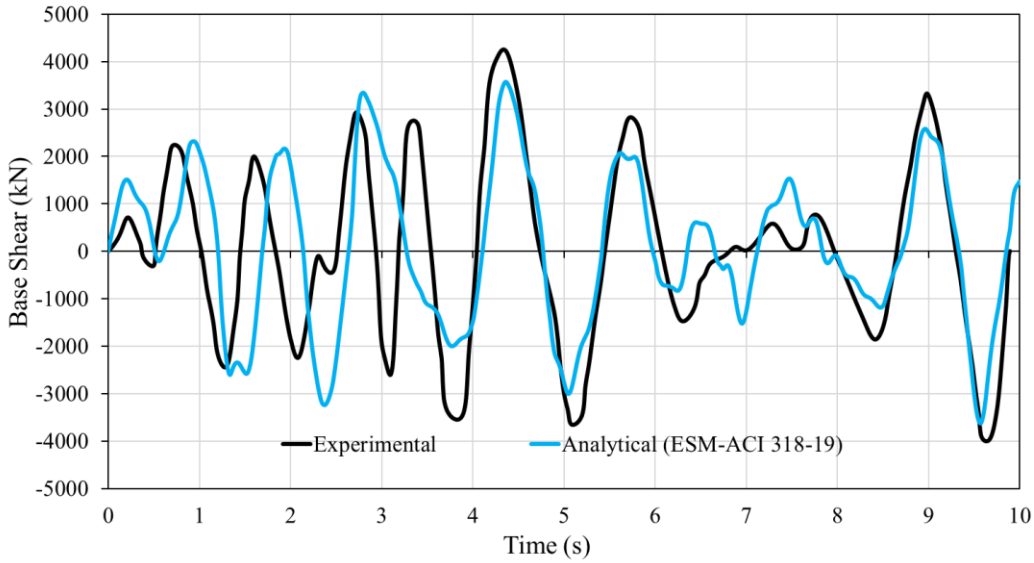


Figure 3.36 Base shear vs. time (ESM-ACI 318-19)

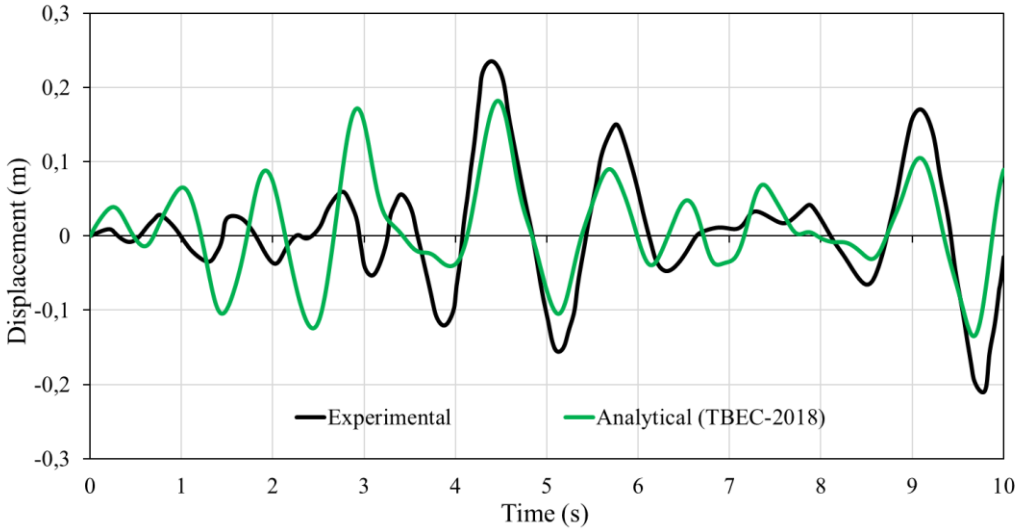


Figure 3.37 Roof displacement vs. time (ESM-TBEC-2018)

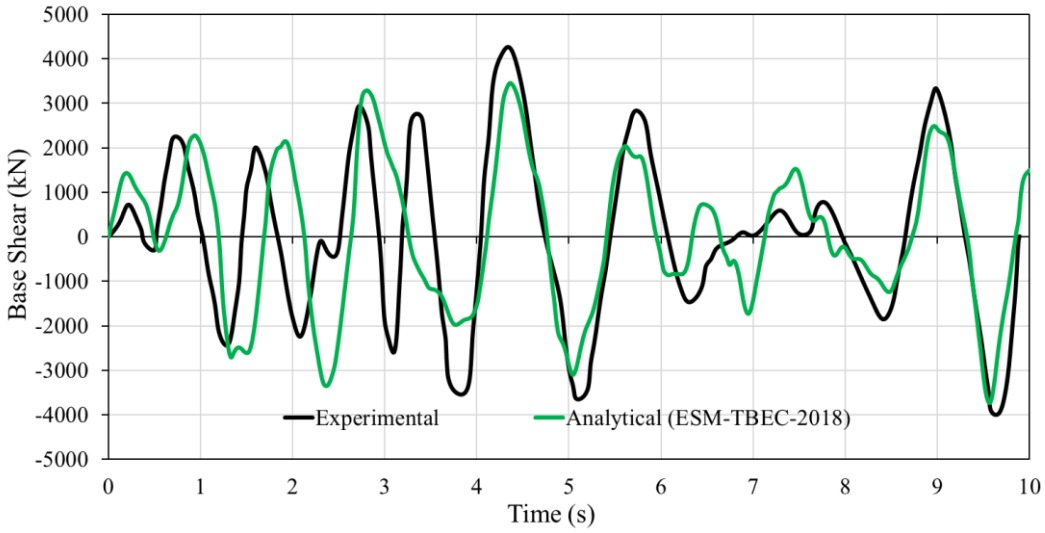


Figure 3.38 Base shear vs. time (ESM-TBEC-2018)

When the effective stiffness modifiers are not utilized, a good agreement with the experimental results in both the roof displacement vs. time and base shear vs. time responses is achieved up to the 4-second mark.

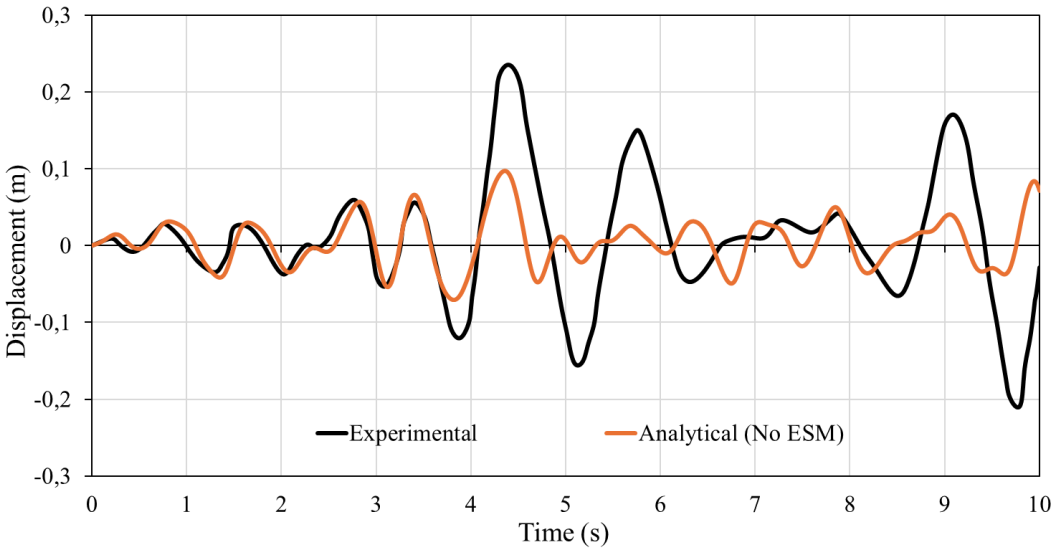


Figure 3.39 Roof displacement vs. time (no ESM)

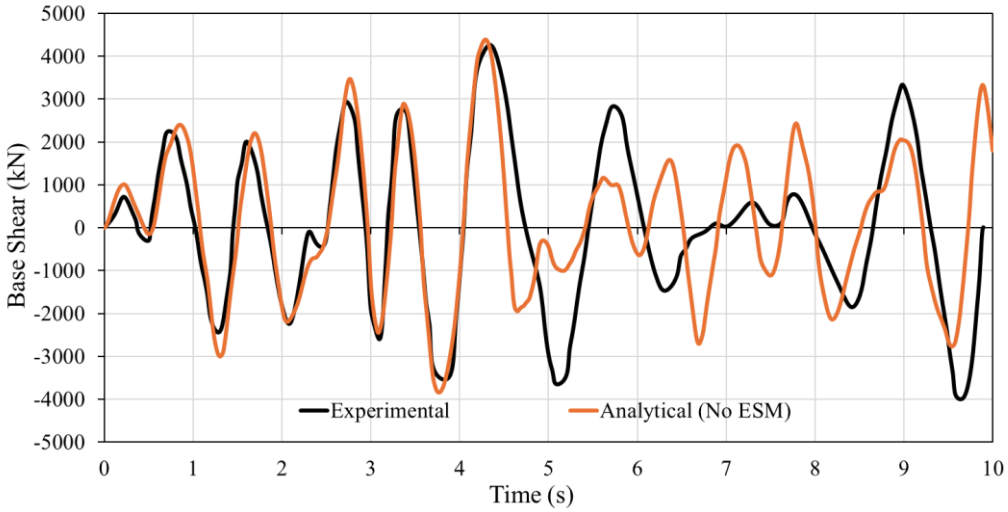


Figure 3.40 Base shear vs. time (no ESM)

To strengthen the argument presented for the differences before and after the 4-second mark, the models with different ESM are subjected to free vibration analysis before and after SPD-2, and also before and after SPD-3. Then, the periods are calculated.

Before SPD-3, the experimental period is captured by the model without ESM, while after SPD-3, the period is better represented by the model with ESM-ALA. Due to the limitations of the analytical software, cracked stiffness values can only be specified prior to the analysis and cannot be modified at an intermediate time step. As a result, when nonlinear behavior becomes dominant during the experiment, the response prior to that stage can only be captured without effective stiffness modifiers, while the latter response is more adequately represented when the modifiers are utilized. However, both stages cannot be captured simultaneously within a single analysis. Additionally, the curves obtained from the pushover analyses of models with different ESM are superimposed on the experimental roof displacement vs. base shear hysteresis graph. In the pushover analyses, the stiffness of the structure after SPD-2 is considered to be the initial condition. The corresponding results are provided in Table 3.5 and Figure 3.41.

Table 3.5 Variation of periods before and after SPD tests with different ESM

Period (s) / ESM	Experiment	ESM-ALA	ESM-ANA	ACI 318-19	TBEC-2018	No ESM
Before SPD-2	0,43	0,82	0,86	0,76	0,75	0,59
Between SPD-2 &SPD-3	0,55	0,89	0,94	0,85	0,83	0,59
After SPD-3	1,15	1,10	1,20	1,01	0,97	0,70

The results of the pushover analyses indicate that the initial stiffness is better captured by the model without ESM, whereas the ultimate capacity is attained by the model with ESM-ALA. The models with ESM-ANA, ESM-ACI 318-19 and ESM-TBEC-2018 could not accurately estimate neither the initial stiffness nor the ultimate capacity.

Overall, these findings support the argument that a significant stiffness reduction occurred as the nonlinear behavior dominated around the 4- second mark of the SPD-3 test. Since the primary scope of this study focuses on the nonlinear behavior, the effective stiffness modifiers provided in ASCE 41-23 for linear analysis are adopted in the subsequent analyses.

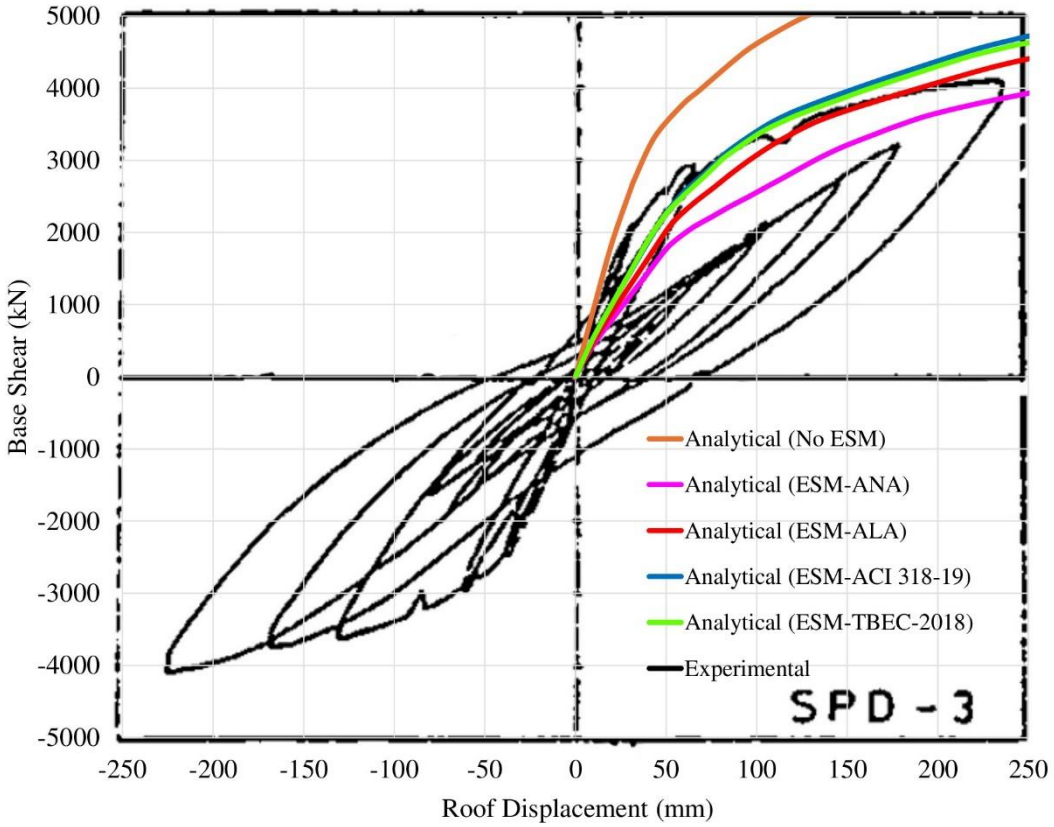


Figure 3.41 Pushover curves of models with different ESM superimposed on experimental the base shear vs. roof displacement hysteresis

3.2.2 Layered Shell Model of the Seven Story Full Scale Building

Following the same procedure as for the RW2 specimen, the seven story full scale building is reanalyzed utilizing the layered shell approach to model the central structural wall. Material properties, initial conditions, and acceleration vs. time history records are kept the same. To account for the stiffness degradation due to cracking, ESM-ALA values are selected.

Different shell elements are used to represent the web and confinement zones of the structural wall. The elevation view of the central frame containing the structural wall, the definition of the layered shell element for the confinement zone and the web are provided in Figures 3.42-3.44.

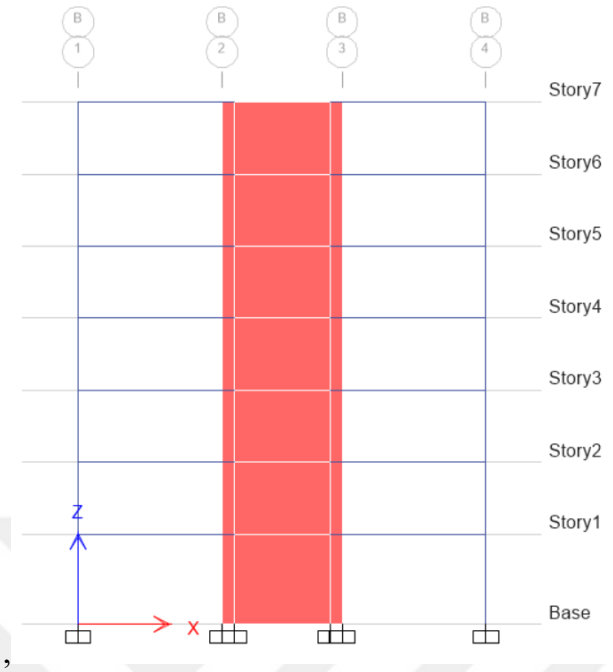


Figure 3.42 Elevation view of the layered shell model of the seven story full scale building

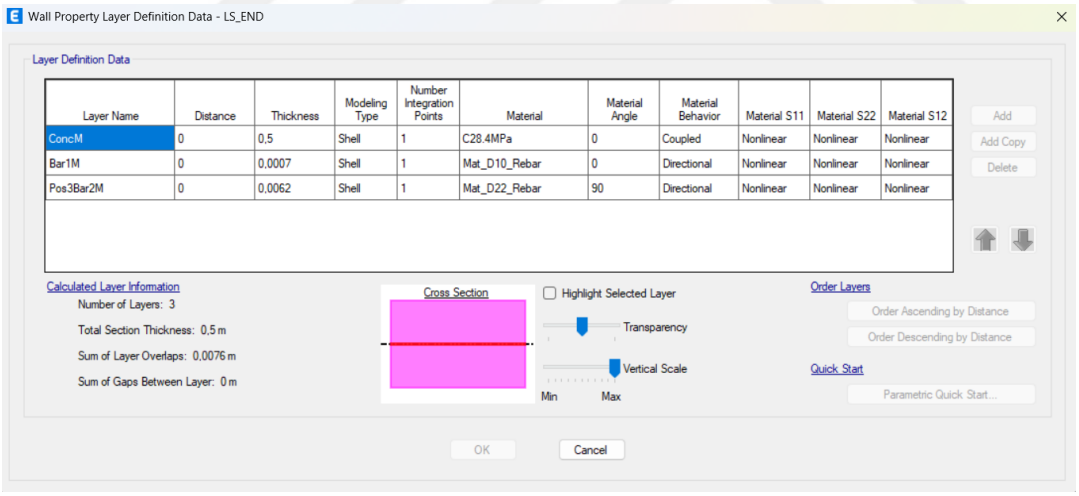


Figure 3.43 Definition of the layered shell element for the confinement zone

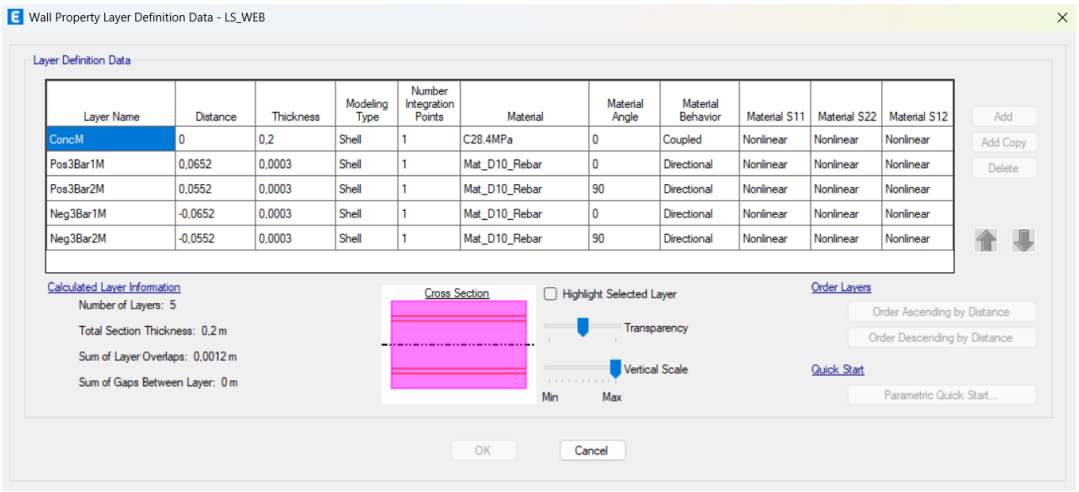


Figure 3.44 Definition of the layered shell element for the web

The base shear vs. time and top displacement vs. time responses obtained from the analysis of the seven story full scale building modeled with layered shell elements, in comparison with the fiber model, are presented in Figures 3.45 and 3.46.

An almost exact match is observed between the fiber hinge model and the layered shell model in terms of the base shear vs. time and top displacement vs. time responses of the seven story full scale building.

Based on the superior estimation of the initial stiffness for the RW2 specimen, along with the modeling convenience and reduced time required for analysis, the fiber hinge model is adopted for the subsequent analyses presented in the following sections.

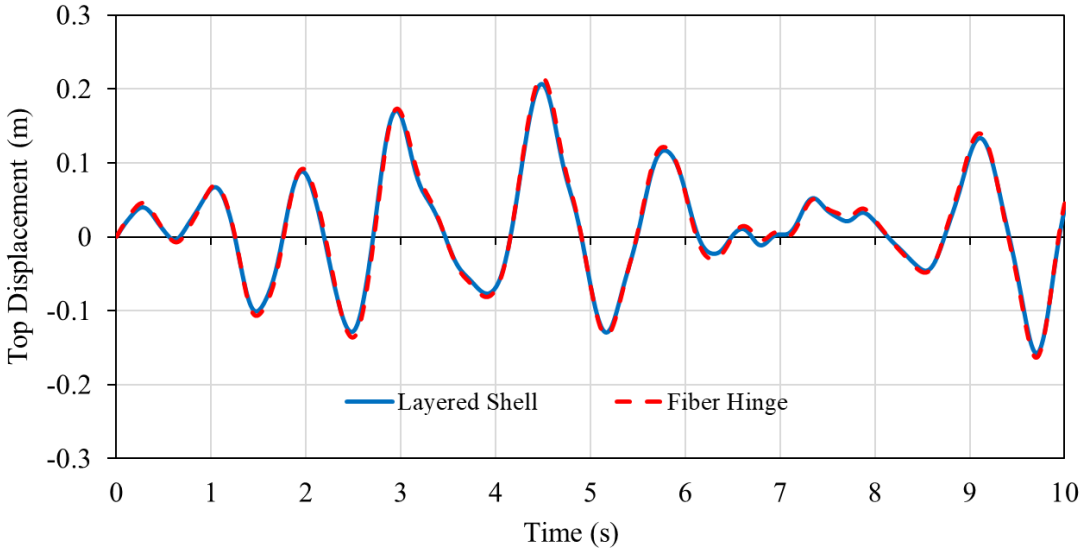


Figure 3.45 Comparison of the top displacement vs. time responses of seven story full scale building for the layered shell model and fiber hinge model

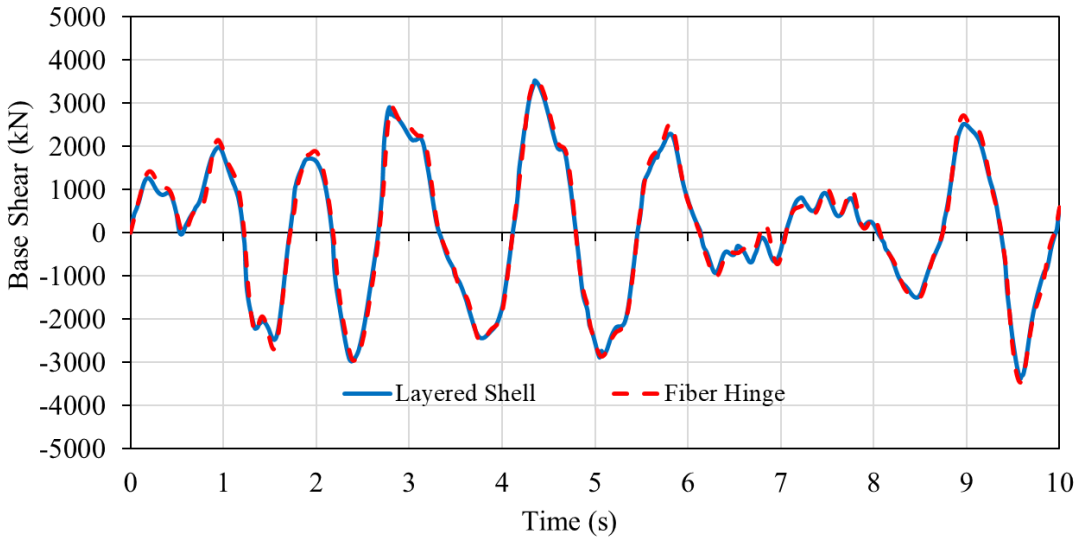


Figure 3.46 Comparison of the base shear vs. time responses of the seven story full scale building for the layered shell model and fiber hinge model

3.3 Results of the Validation of Nonlinear Modeling

The nonlinear time history analyses presented in the subsequent chapters are conducted based on the conclusions drawn from this validation study. The main findings are summarized below:

- Based on the analytical results of both the RW2 specimen and the seven story building modeled using the fiber hinge approach, it is observed that among ASCE 41-23, ACI 318-19, and TBEC-2018, the effective stiffness modifiers provided in ASCE 41-23 for linear analyses yielded the closest agreement with the experimental results, despite conducting a nonlinear analysis.
- When the effective stiffness modifiers specified in ASCE 41-23 for linear analysis are utilized, the comparison between the fiber hinge and layered shell modeling approaches indicated that for the RW2 specimen, experimental initial stiffness is more accurately captured by the fiber hinge model, while for the seven story building, the roof displacement vs. time and the base shear vs. time responses are captured by both approaches with only minor and negligible differences.
- Due to the limitations of the analytical software, effective stiffness modifiers can only be assigned at the beginning of the analysis. Consequently, as the nonlinear behavior, represented by these modifiers, dominates the response at a certain stage of the experiment, only the response before or after that stage can be accurately captured in the analysis. This study focuses on the nonlinear behavior; therefore, the effective stiffness modifiers are applied in all subsequent analyses.

CHAPTER 4

ANALYTICAL MODELING AND BUILDING GENERATION

4.1 Introduction

The purpose of this study is to examine the effect of structural wall area to floor area ratio on the overall seismic performance of mid to high rise buildings with no torsional irregularities. First, a five story frame building without structural walls is modeled in ETABS (Computers and Structures, Inc. [CSI], 2024). The slab thickness, column and beam dimensions, and corresponding reinforcement detailing are determined by designing the initial building under site specific seismic forces. The building is assumed to be in a seismically active region, located in California, United States, representing a high seismic hazard level that can impose significant demands on the structures without leading to total collapse. The seismic design is carried out in accordance with TS500 (Turkish Standards Institution, 2000), TBEC-2018 (Ministry of Environment and Urbanization, 2018), ACI 318-19 (American Concrete Institute, 2019), ASCE 7-22 (American Society of Civil Engineers, 2022) and ASCE 41-23 (American Society of Civil Engineers, 2023) requirements. Subsequent buildings are generated by replicating stories vertically and modifying the structural wall ratio through the addition of structural walls, the capacities of which are verified to avoid failure. In addition, the column transverse reinforcement in the generated buildings, as well as the designed 5 story frame building, is governed by the detailing required for the 30 story frame building without structural walls, ensuring that the minimum confinement demands are fulfilled to prevent collapse. In total, 35 building models are constructed by combining five different number of stories (5, 7, 10, 20, and 30) with seven structural wall ratios (0.0%, 0.5%, 1.0%, 1.5%, 2.0%, 2.5%, and 3.0%). Eleven time history records, scaled by spectral matching, the details of which are provided in the following sections, are applied to

all building models. The seismic response of each building is then evaluated based on the results obtained from these nonlinear analyses.

To denote the building models efficiently, a notation system is adopted in the format Sxx_Ryy, where Sxx represents the number of stories and Ryy indicates the structural wall ratio in percentage (multiplied by 100 and written without a decimal). For instance, the 5 story building with a 1.5% structural wall ratio is denoted as S05_R15, while the 30 story frame building with no structural walls is denoted as S30_R00.

4.2 Seismic Design of Model S05_R00

In the preliminary design, the structural system is selected first and then the story heights and span lengths are determined. The story height is set to 3 meters, and the plan dimensions are defined as 25 meters in both X and Y directions, divided into 5 bays per direction. This results in 6 columns along each axis, totaling 36 columns. The four innermost central columns and the four outermost corner columns have square cross sections, while the remaining columns are rectangular. There are concentric beams in all axes connecting the columns. The effective stiffness modifiers specified for linear analysis in ASCE 41-23 (American Society of Civil Engineers, 2023) are assigned to the beams and columns, as these modifiers provided better agreement with the results of the validation study compared to the modifiers recommended by other structural codes. The seismic design is performed following the ACI 318-19 requirements. To reduce the number of required analyses by half, torsional irregularity is intentionally avoided, and orthogonal symmetry is targeted in the plan configuration. As a result, for the time history analyses of the generated buildings, there is no need to reapply the ground motions by switching directions along the X and Y axes, as required in both TBEC-2018 and ASCE 7-22 provisions. The plan view of the preliminary floor layout is presented in Figure 4.1.

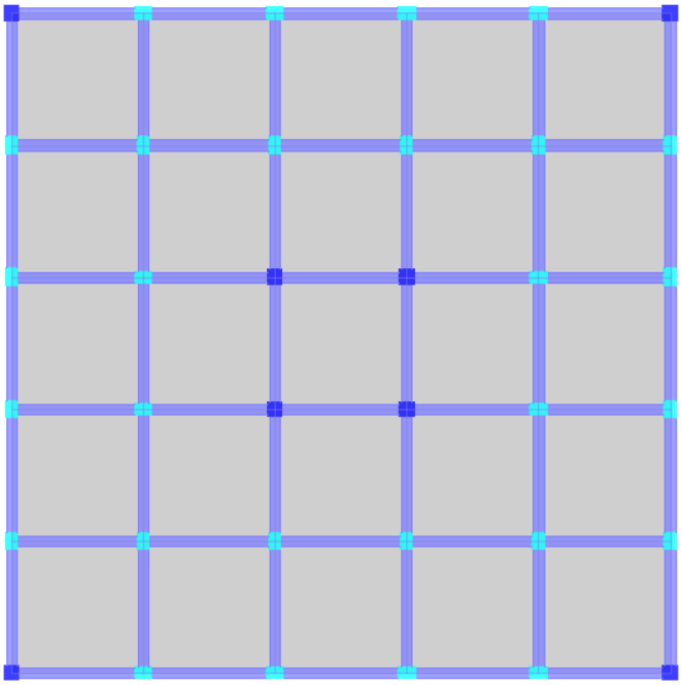


Figure 4.1 Preliminary floor layout

Linear dynamic analysis is employed for the seismic design of model S05_R00, using the modal response spectrum method. The design spectrum parameters are obtained using the ASCE Hazard Tool, as recommended by the ASCE 7-22 provisions.

Three input parameters are required to obtain the spectral parameters using the ASCE Hazard Tool: risk category, site soil class, and geographic location. In this study, the building is assumed to be located in the United States, near Los Angeles, California, at coordinates latitude 34.187394 and longitude -118.858845. Model S05_R00, along with all other buildings derived from it, is classified as Risk Category II according to ASCE 7-22 Table 1.5-1, based on the assumption that the structures serve residential purposes. According to ASCE 7-22 Article 11.4.2.1, in the absence of site specific soil properties, spectral response acceleration values should be determined using the most conservative values among Site Classes C, CD, and D. Accordingly, Site Class CD is selected in this study, as it resulted in the most critical spectral acceleration values.

ASCE 7-22 defines two types of design spectrum: the Multi-Period Design Spectrum and the Two-Period Design Spectrum, as presented in Figure 4.2. These spectra are generated using the ASCE Hazard Tool based on the user defined input parameters (site class, risk category and location). Since the Multi-Period Design Spectrum is not defined in TBEC-2018, the Two-Period Design Spectrum is adopted in this study to ensure consistency with both design codes.

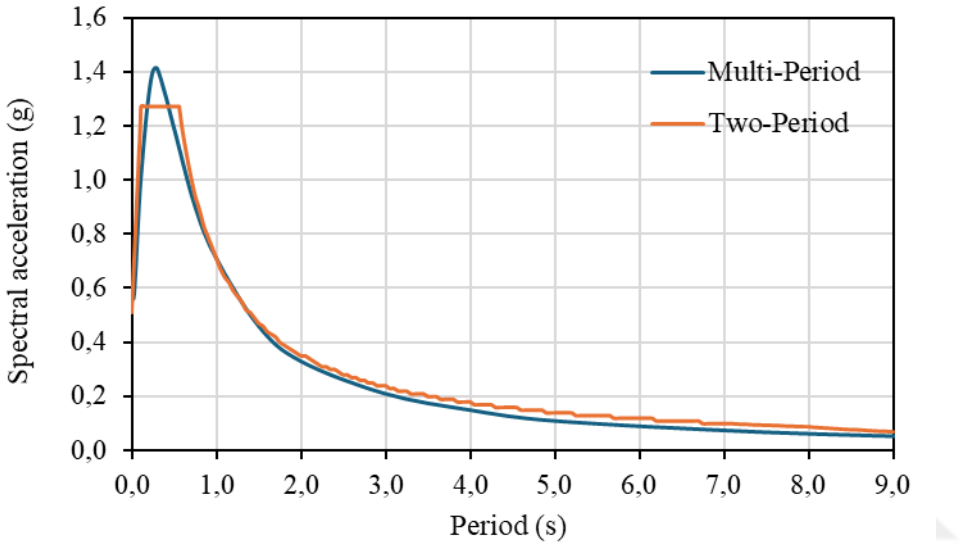


Figure 4.2 Two types of design spectra

For Model S05_R00, the seismic force resisting system is classified as Special Reinforced Concrete Moment Resisting Frame. The response modification factor, R, is taken as 8, based on ASCE 7-22 Table 12.2-1 and TBEC-2018 Table 4.1, which are consistent for this classification.

4.2.1 Material Properties of Model S05_R00

Prior to the structural design, the concrete class is designated as C40/50 to prevent compression failure in the columns, considering the increase in gravity loads resulting from the upward replication of stories in the generated buildings. The stress-strain curve parameters for concrete and reinforcing steel are determined in accordance with the provisions of ACI 318-19. For the rebar material properties,

steel reinforcement with a yield strength of 420 MPa is employed, and its stress-strain behavior is idealized as bilinear. The stress-strain relationships of the unconfined concrete, reinforcing steel and confined concrete assigned to columns and wall boundaries are illustrated in Figures 4.3-4.6, respectively. To model the behavior of confined concrete, the equations proposed by Mander et al. (1988) are utilized. The parameters that define these curves are presented in Table 4.1.

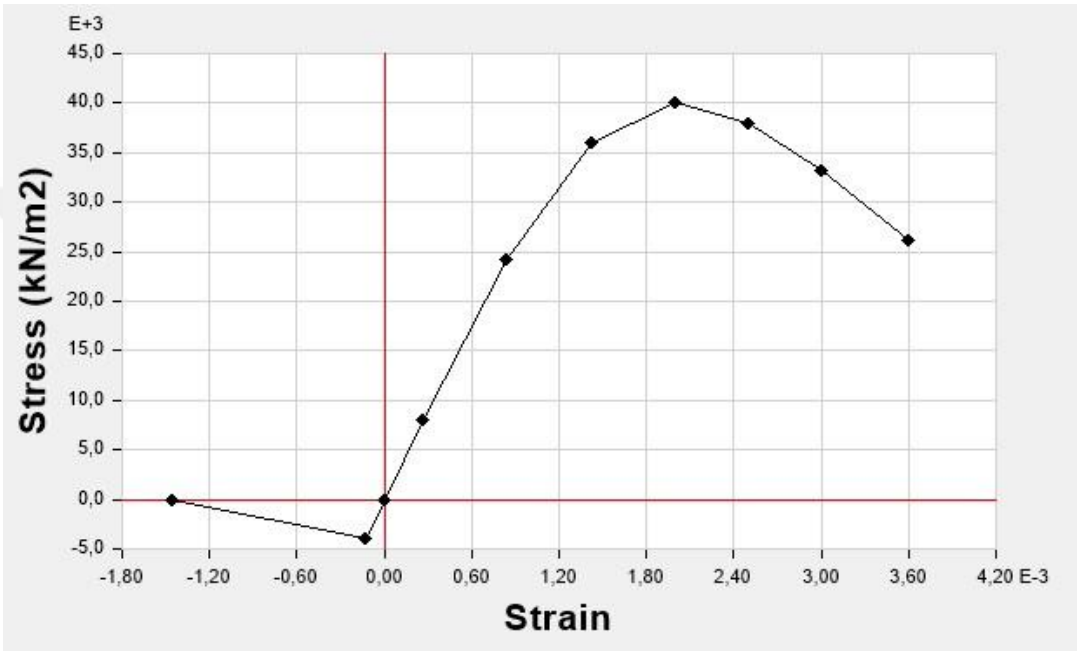


Figure 4.3 Unconfined concrete stress-strain relationship

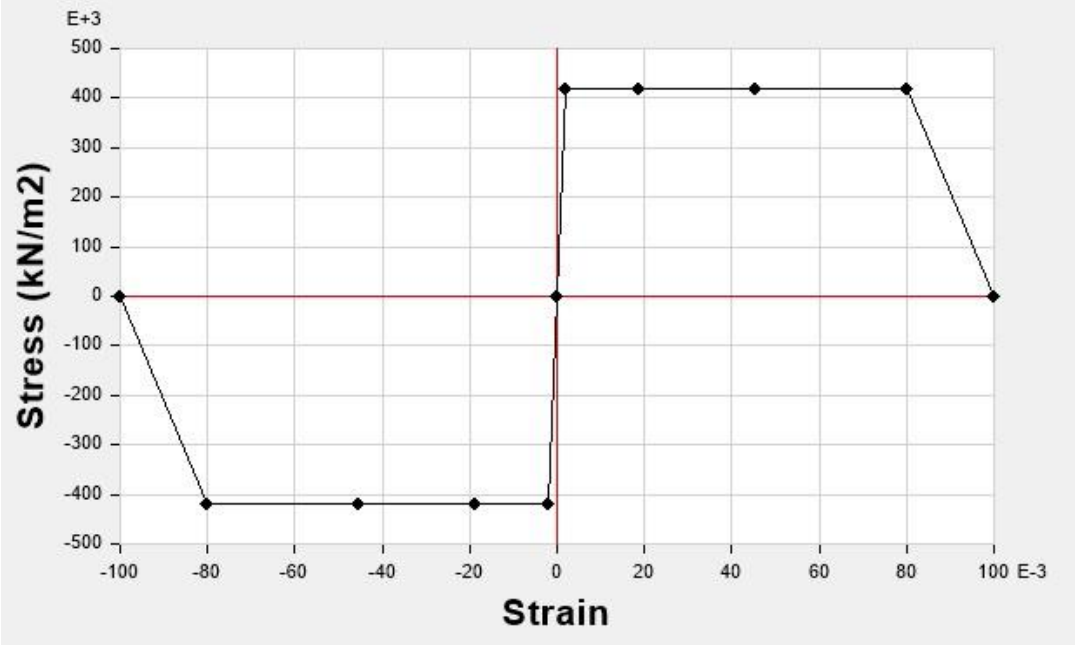


Figure 4.4 Reinforcing steel stress-strain relationship

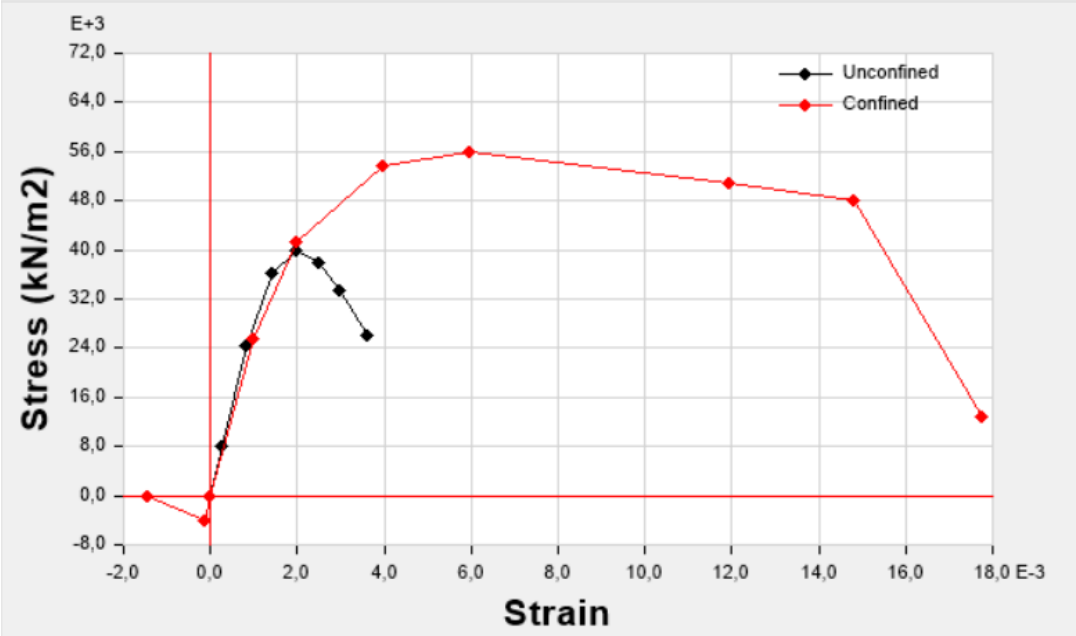


Figure 4.5 Confined concrete stress-strain relationship (columns)

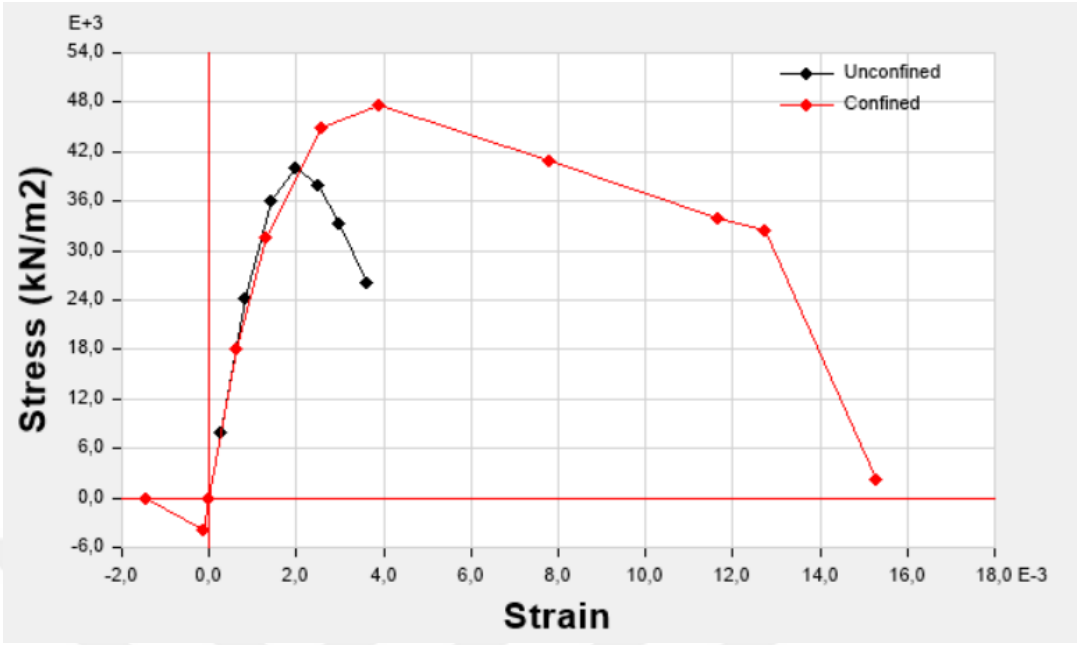


Figure 4.6 Confined concrete stress-strain relationship (wall boundaries)

Table 4.1 Stress-strain parameters for unconfined concrete and reinforcing steel materials

Material	*Elastic Modulus (MPa)*	*Peak Strength (MPa)*	*Strain at Peak*	*Ultimate Strain*	*Ultimate Strength (MPa)*
Reinforcing steel	200000	420	0.0021	0.08	420
Unconfined concrete	29725	40	0.002	0.003	34
Confined concrete (columns)	29630	56	0.006	0.015	46
Confined concrete (wall boundaries)	29084	48	0.004	0.013	32

4.2.2 Member Dimensions and Reinforcement Detailing of Model S05_R00

The column and beam dimensions for Model S05_R00 are determined through seismic design using the modal response spectrum method. For all other building models derived from this reference model, these member dimensions and reinforcement detailing are kept constant. Model S05_R00 contains no structural walls. For building models with a structural wall ratio greater than 0.0%, the structural walls are not seismically designed; instead, their dimensions and detailing are determined according to the minimum requirements specified in TS500, TBEC-2018, ACI 318-19, and ASCE 41-23. In cases where provisions from these codes conflict, the most conservative requirement is adopted to ensure consistency with all regulations. Transverse reinforcement detailing for frame members, namely columns and beams, are specified for the confinement zones of the sections, where plastic hinges are assigned in the nonlinear analyses.

4.2.2.1 Column Dimensions and Reinforcement Detailing

Two different column cross sections and reinforcement detailing are selected in the seismic design. The first column type has a 600 mm × 600 mm square cross section, while the second type has a 500 mm × 700 mm rectangular cross section.

For 600 mm × 600 mm square columns, the ratio of reinforcement area to the gross cross sectional area, referred to as the reinforcement ratio, is 1.75%. These columns contain six longitudinal bars along each principal axis, resulting in a total of 20 longitudinal bars with a diameter of 20 mm. Confined concrete material properties are assigned to the core concrete, and the stress-strain behavior of the core is computed considering six legs of confinement reinforcement in each direction, with a diameter of 10 mm and a spacing of 100 mm. The cross section of the 600 x 600 mm column is illustrated in Figure 4.7.

For 500 mm × 700 mm rectangular columns, the reinforcement ratio is determined as 1.8%. These columns contain seven longitudinal bars along the major axis and five longitudinal bars along the minor axis, resulting in a total of 20 longitudinal bars with a diameter of 20 mm. Confinement reinforcement has seven legs along the major axis and five legs along the minor axis, with a diameter of 10 mm and a spacing of 100 mm. The cross section of the 500 mm × 700 mm column is illustrated in Figure 4.8.

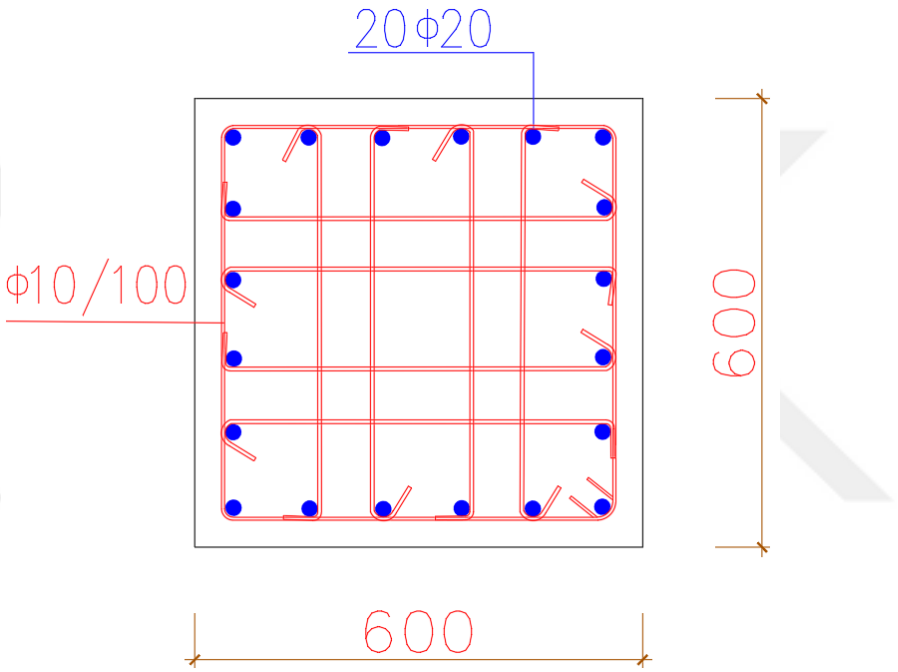


Figure 4.7 Reinforcement detailing of 600 × 600 mm columns

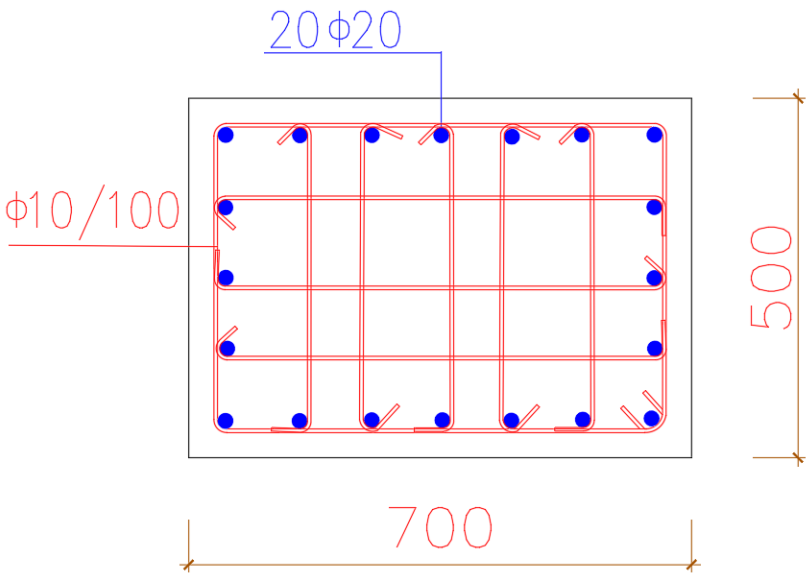


Figure 4.8 Reinforcement detailing of 500 × 700 mm columns

4.2.2.2 Beam Dimensions and Reinforcement Detailing

All beams have a depth of 600 mm and a width of 300 mm. Each beam contains four 20 mm diameter longitudinal bars at the top and four 20 mm diameter longitudinal bars at the bottom of the section, resulting in a total of eight longitudinal bars. No web reinforcement is provided. Transverse reinforcement consists of 10 mm diameter stirrups spaced at 100 mm. The cross section of the 300 mm x 600 mm beams is illustrated in Figure 4.9.

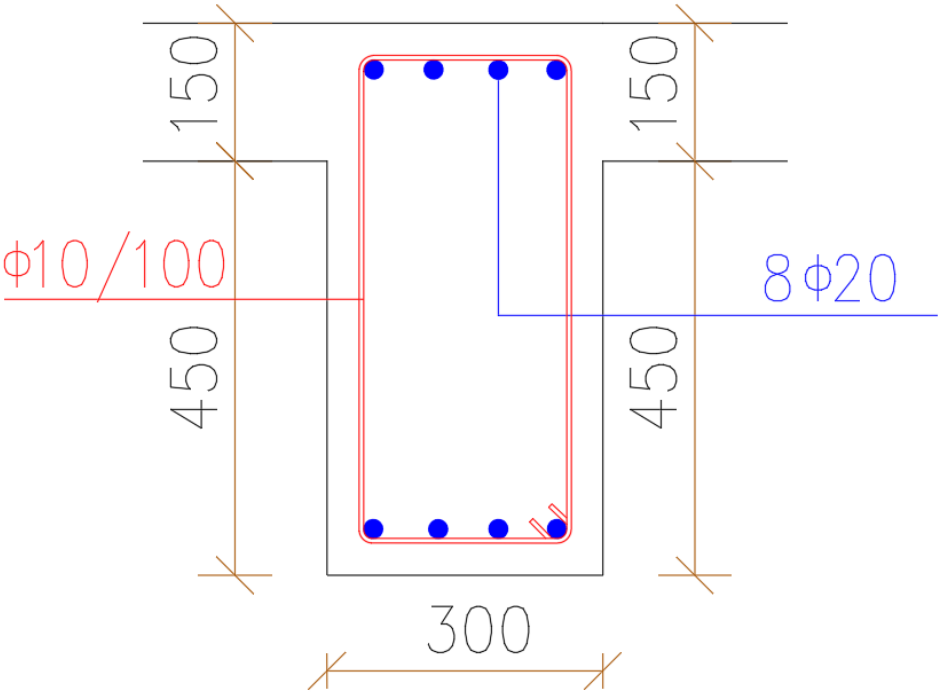


Figure 4.9 Reinforcement detailing of 300 × 600 mm beams

4.2.2.3 Slab Dimensions

The slab thickness throughout the building is set to 150 mm. No seismic design or reinforcement detailing is provided, as the slabs are assumed to remain in the elastic range in nonlinear time history analyses. Rigid diaphragm constraints are assigned to all joints at each story level. The self weight of the structural members is automatically calculated by the analytical software. In addition to the self weight, slabs are subjected to 2 kN/m^2 superimposed dead load and 2 kN/m^2 live load.

4.2.2.4 Structural Wall Dimensions and Reinforcement Detailing

Structural walls are not designed under seismic loads, instead their dimensions and reinforcement detailing are determined according to most conservative provisions of TS500, TBDY2018, ASCE 41-23 and ACI 318-19. The thickness of the structural

walls is set to 300 mm. As the walls are placed on the overall span, each wall has a length of 5000 mm, resulting in a single section. The effective stiffness modifiers specified for linear analysis in ASCE 41-23 are assigned to all structural wall sections, as well. Confined concrete material properties are assigned only for the wall boundary regions, whereas the web region is modeled as unconfined, since the web transverse reinforcement is not detailed with closed hoops, which is considered a conservative approach. The cross section of the 300 mm x 5000 mm structural walls is illustrated in Figure 4.10.

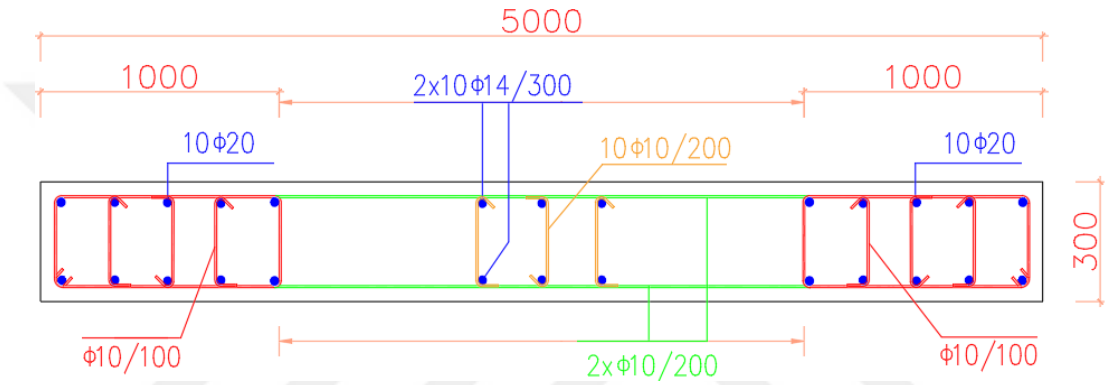


Figure 4.10 Reinforcement detailing of 300 × 5000 mm structural walls

4.3 Building Generation

A total of 35 buildings are generated by combining five different number of stories (5, 7, 10, 20, and 30) with seven structural wall area to floor area ratios. Although the exact ratios do not exactly match the predefined ratios due to structural dimensions (i.e., 0.00%, 0.48%, 0.96%, 1.44%, 1.92%, 2.40%, and 2.88%), they are rounded to the nearest half percent for simplicity in classification and presentation (i.e., 0.0%, 0.5%, 1.0%, 1.5%, 2.0%, 2.5%, and 3.0%). Figures 4.11 through 4.17 illustrate the plan configurations of the generated buildings with progressively increasing structural wall area to floor area ratios.

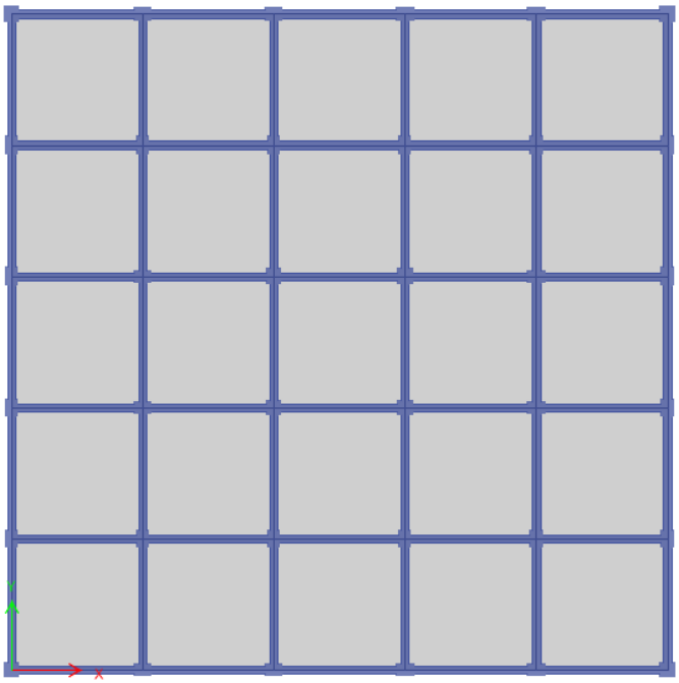


Figure 4.11 Plan configuration of the generated buildings with 0.0% structural wall ratio

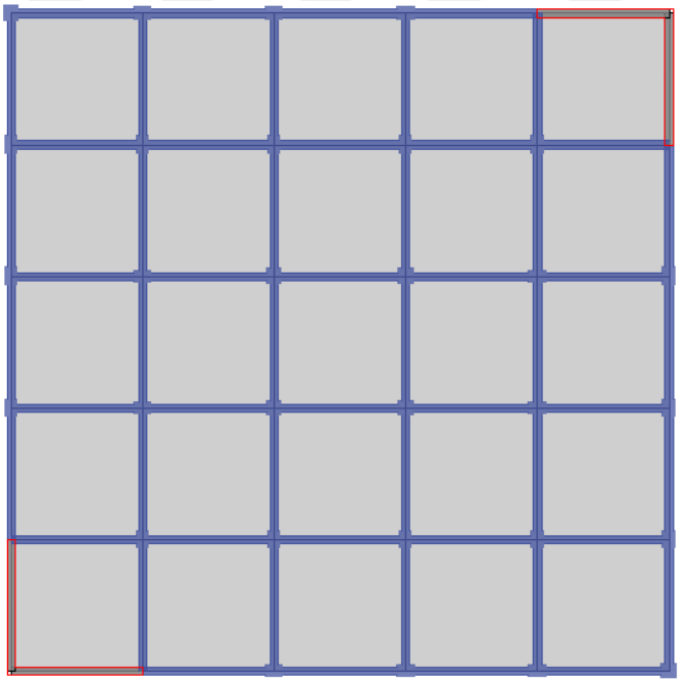


Figure 4.12 Plan configuration of the generated buildings with 0.5% structural wall ratio

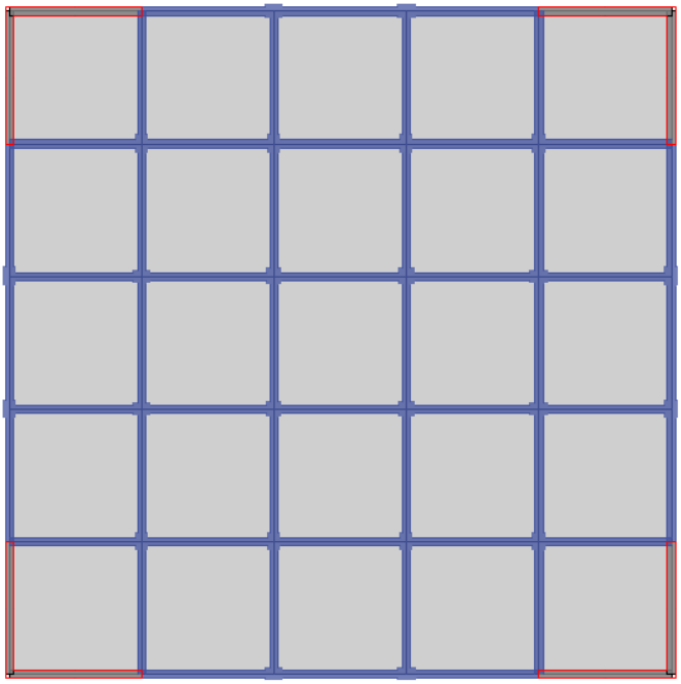


Figure 4.13 Plan configuration of the generated buildings with 1.0% structural wall ratio

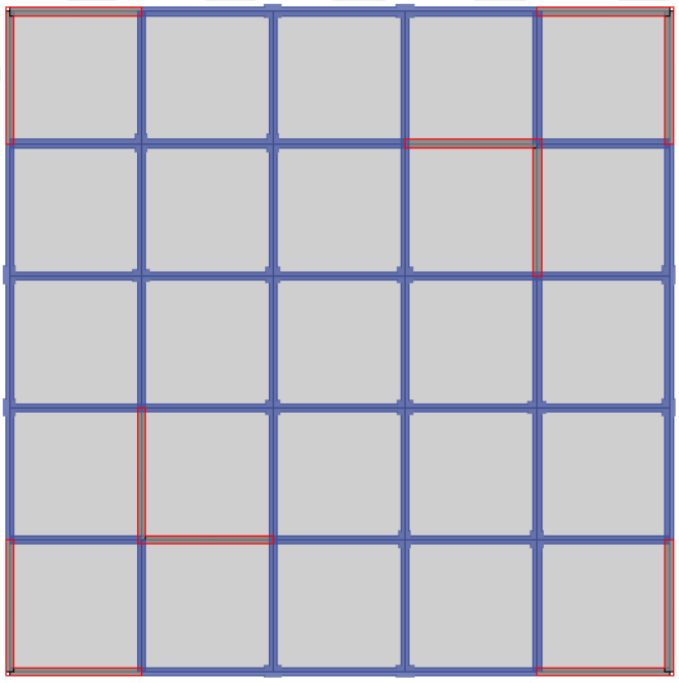


Figure 4.14 Plan configuration of the generated buildings with 1.5% structural wall ratio

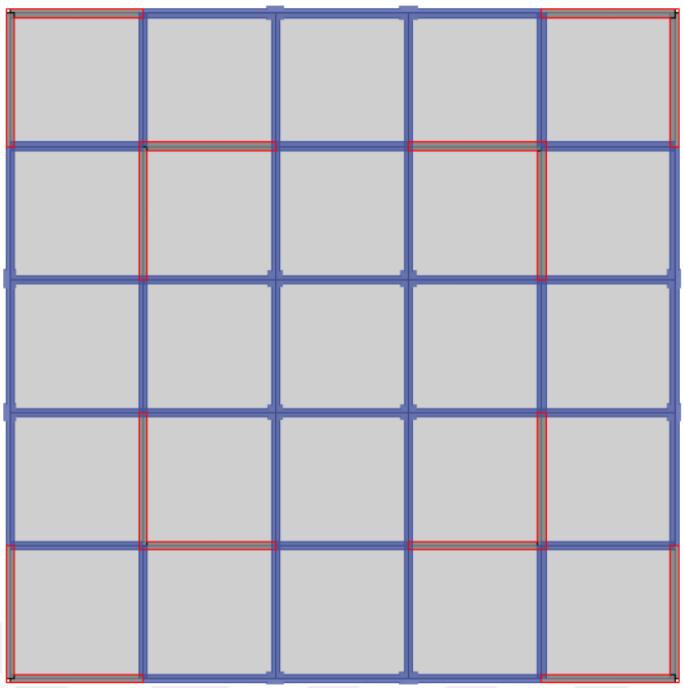


Figure 4.15 Plan configuration of the generated buildings with 2.0% structural wall ratio

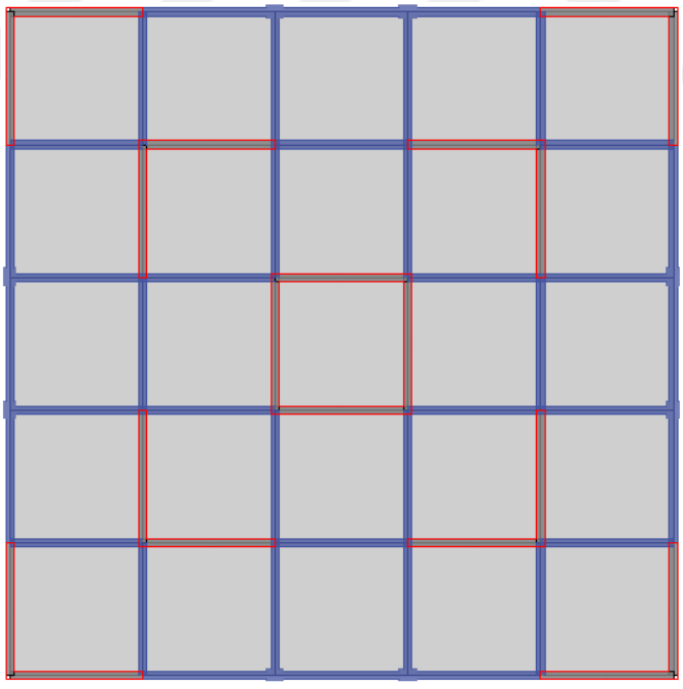


Figure 4.16 Plan configuration of the generated buildings with 2.5% structural wall ratio

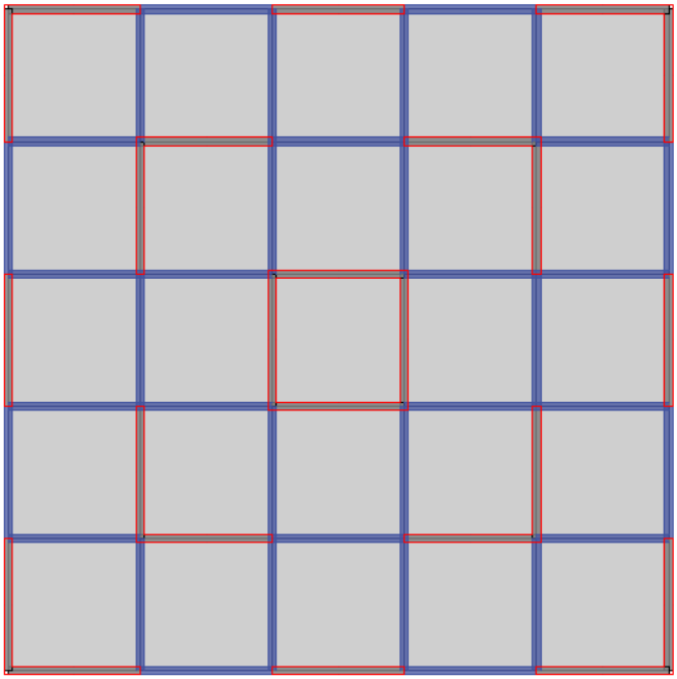


Figure 4.17 Plan configuration of the generated buildings with 3.0% structural wall ratio

4.4 Selection of Ground Motion Records

A set of eleven ground motion records is obtained from the Pacific Earthquake Engineering Research Center (PEER) database to fulfill the requirement for the use of at least 11 records specified by ASCE 7-22 and TBEC-2018 for nonlinear time history analyses. Each ground motion includes a pair of horizontal components oriented in orthogonal directions. Vertical ground motion components are excluded from the analyses since ASCE 7-22 specifies that they may be neglected when no vertical discontinuities are present in the structure. General information about the selected ground motion records is given in Table 4.2. In this table, Record Sequence Number (RSN) is a unique identifier assigned to each ground motion record in the PEER database for organized data management and referencing. Rupture Distance (Rrup) refers to the shortest distance from the site to the fault rupture surface.

The ground motion records with rupture distances less than 10 km are classified as near fault records, which typically exhibit pulse like characteristics, whereas those

with higher distances are classified as far field records (Yamada, 2014). Accordingly, the Imperial Valley, Erzincan, Northridge, and Duzce earthquake records are categorized as near fault (NF), while the remaining records are classified as far field (FF).

Table 4.2 Selected ground motion records

Name	*RSN*	*Country*	*Station*	*Year*	*Magnitude*	*Mechanism*	*Rrup (km)*
Imperial Valley	6	USA	El Centro Array#9	1940	6.95	Strike slip	6.09 (NF)
Loma Prieta	735	USA	APEEL 7-Pulgas	1989	6.93	Reverse oblique	41.86 (FF)
Erzincan	821	Turkey	Erzincan	1992	6.69	Strike slip	4.38 (NF)
Landers	850	USA	Desert Hot Springs	1992	7.28	Strike slip	21.78 (FF)
Northridge	1086	USA	Sylmar-Olive View Med FF	1994	6.69	Reverse	5.3 (NF)
Kobe	1104	Japan	Fukushima	1995	6.90	Strike slip	17.85 (FF)
Kocaeli	1160	Turkey	Fatih	1999	7.51	Strike slip	55.48 (FF)
Chi-chi	1186	Taiwan	CHY014	1999	7.62	Reverse oblique	34.18 (FF)
Duzce	1615	Turkey	Lamont 1062	1999	7.14	Strike slip	9.14 (NF)
El Mayor-Cucapah	5823	USA	Chihuahua	2010	7.20	Strike slip	19.47 (FF)
Christchurch	8062	New Zealand	Canterbury Aero Club	2011	6.20	Reverse oblique	14.41 (FF)

4.5 Scaling of Time History Records

Both ASCE 7-22 and TBEC-2018 specify two scaling methods for ground motions: amplitude scaling and spectral matching. Amplitude scaling involves applying the same scale factor to both horizontal components of each ground motion so that the average response spectrum matches the target spectrum over a defined period range. In contrast, spectral matching modifies the frequency content of each ground motion so that the average spectrum matches over the same range. In both standards, the lower and upper bounds of the period range for scaling are defined as 0.2 times and 1.5 times the fundamental period of the structure, respectively.

Amplitude scaling is the simpler method, and the PEER website can automatically determine appropriate scale factors for different ground motion records when a target spectrum is provided. An exact match can be achieved either at a single period or over a specified period range by minimizing the mean square error (MSE). However, in both cases, a perfect match across the entire spectrum is not feasible. In single period scaling, significant mismatch occurs at untargeted periods, while in the MSE based approach, increasing the period range often leads to inadequate results. Since the same ground motions are applied to all thirty five generated buildings, the period range covers most of the target spectrum. Therefore, the spectral matching method is adopted for scaling the selected time history records.

The target spectrum to which the eleven time history records are scaled is selected as the 5% damped Maximum Considered Earthquake (MCE_R), as defined and recommended in ASCE 7-22. The site conditions, geographic location and risk category are kept consistent with the designed reference model S05_R00. MCE_R response spectrum, obtained from ASCE Hazard Tool, is presented in Figure 4.18.

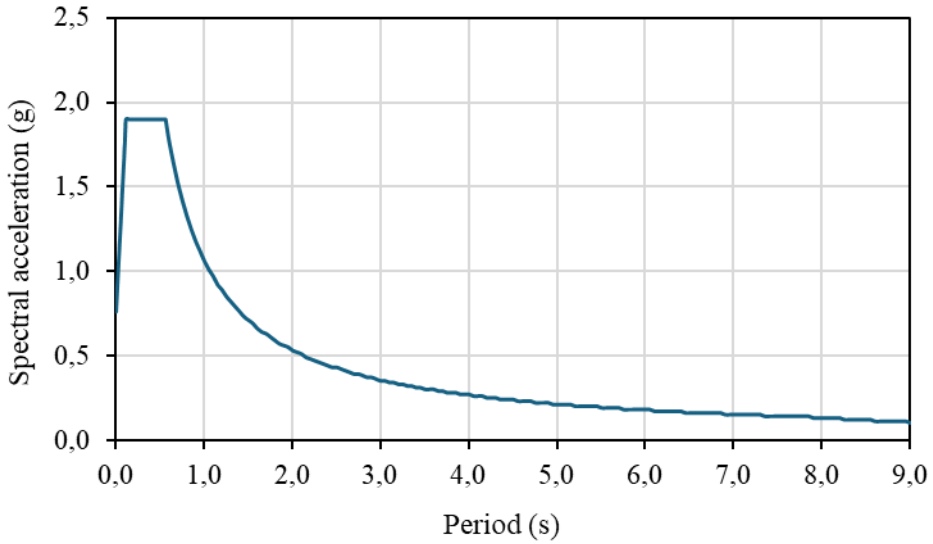


Figure 4.18 MCE_R response spectrum

Spectral matching is performed using the built in tool in ETABS. All records are modified so that their average response spectrum matches the MCE_R response spectrum. The matching is carried out in the frequency domain, and the pulse characteristics of the near fault ground motions are preserved, as required by ASCE 7-22 when spectral matching is performed. The procedure involves generating the response spectrum of the reference record corresponding to the specified damping ratio and computing its Fourier amplitude spectrum through a Fast Fourier Transform (FFT). A scale factor is then determined for each frequency within the defined range as the ratio of the target spectrum acceleration to the reference spectrum acceleration. The Fourier amplitudes are multiplied by these scale factors, and an inverse FFT is applied to obtain the modified time history compatible with the target response spectrum (Computers and Structures Inc., 2025). The average of 22 response spectra obtained from the scaled time history records are compared with the MCE_R response spectrum, presented in Figure 4.19. The comparison between the original and scaled acceleration vs. time histories, along with their corresponding response spectra for all ground motions, is presented in Appendix C in Tables C.1-C.11.

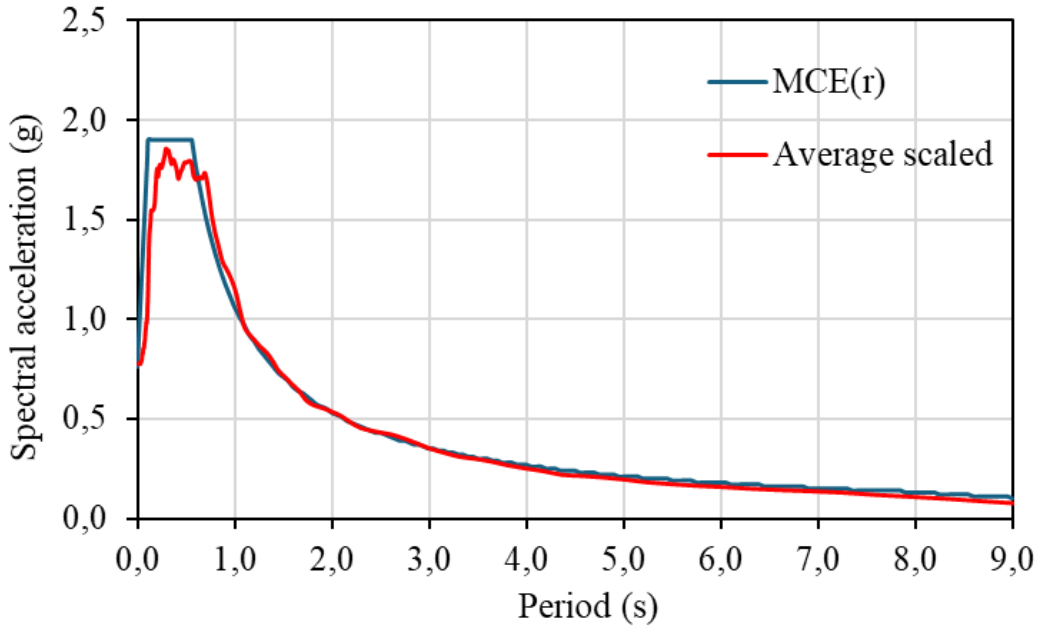


Figure 4.19 Average of scaled spectrum compared with MCE_R design spectrum

4.6 Modeling of Nonlinear Behavior

Throughout the nonlinear time history analyses, the nonlinear behavior of structural members is represented by assigning plastic hinges at locations where inelastic deformations are expected to occur. For frame members, namely columns and beams, zero length plastic hinges are assigned at both ends of each member. For shell members, namely structural walls, a single plastic hinge is assigned at the midheight of each shell element as explained in Chapter 3.

4.6.1 Plastic Hinge Definition of Beams

Zero length, M3 moment-curvature hinges are assigned at the end zones of beams, where nonlinear behavior is expected. To obtain the moment-curvature relationship of the beam end sections, the Section Designer tool available in the analytical software SAP2000 v25.1.0 (Computers and Structures, Inc., 2023) is utilized. The beam section created in the Section Designer tool of SAP2000, the corresponding

moment-curvature relationship, and the definition of the plastic hinges assigned to the beams in ETABS are illustrated in Figures 4.20, 4.21, and 4.22, respectively. The details of the definition of M3 hinges in ETABS are provided in Chapter 3.

In Figure 4.20, the beam sectional dimensions and the location, diameter, and material properties of the longitudinal reinforcing bars are defined in a 2D plane. Although the stirrup layout is not visually represented, the cover concrete is assigned the stress-strain relationship shown in Figure 4.3, while the stress-strain relationship of the confined core concrete is computed by SAP2000 using the confinement reinforcement illustrated in Figure 4.5, based on the equations proposed by Mander et al. (1988).

In Figure 4.21, the moment-curvature response obtained from the Section Designer tool for the beam section defined in Figure 4.20 is presented. In this menu, it is important to assign a value of zero to the cell labeled ‘P’, which represents the axial load on the beam, since the M3 hinges assigned to the beams do not incorporate flexure-axial load interaction. The cell titled ‘No. of Points’ controls the number of points used to generate the moment-curvature relationship, while the cell labeled ‘Angle (Deg)’ is used to rotate the neutral axis. The default value of 0° corresponds to the neutral axis being oriented parallel to the local 3-direction.

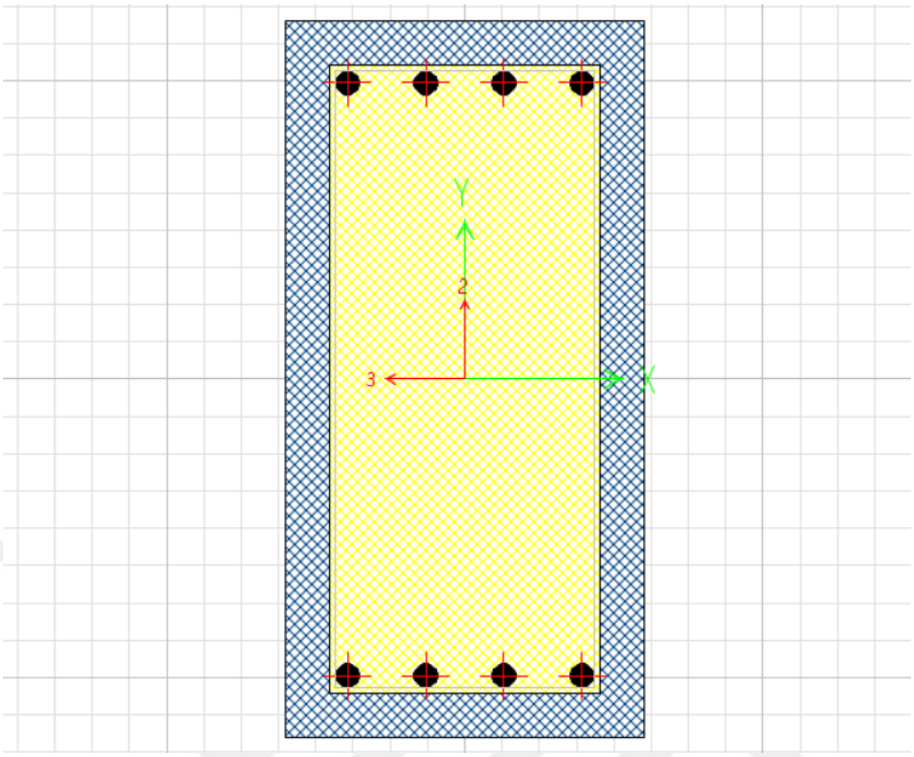


Figure 4.20 Beam section in SAP2000 Section Designer tool

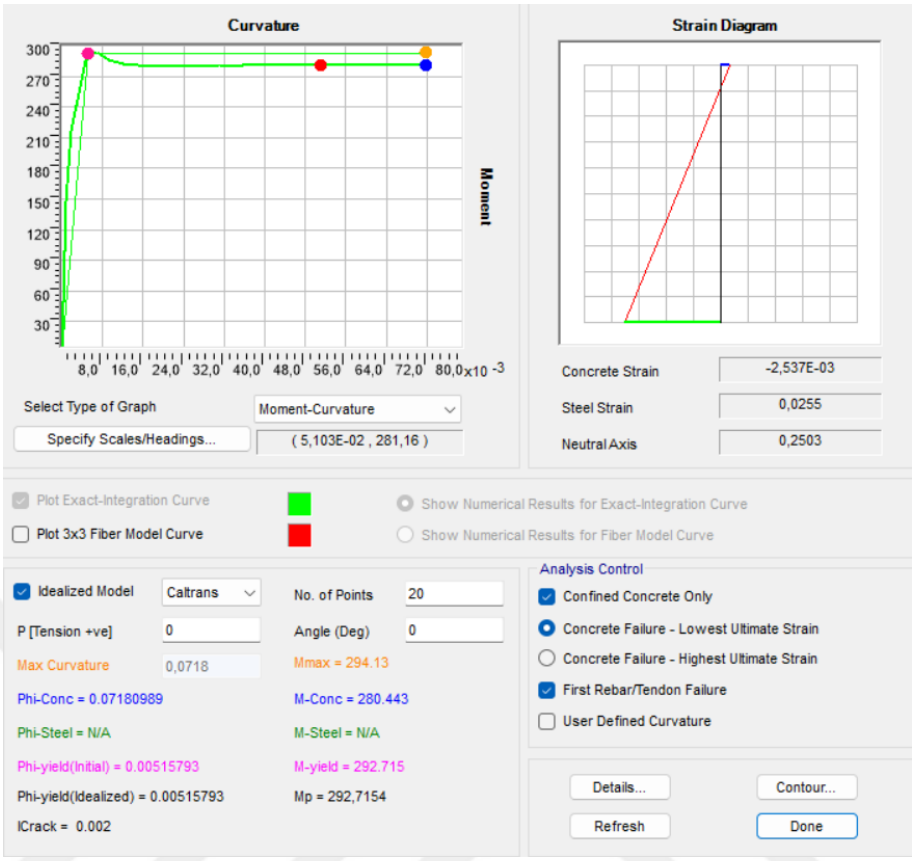


Figure 4.21 Moment vs. curvature relationship of beams

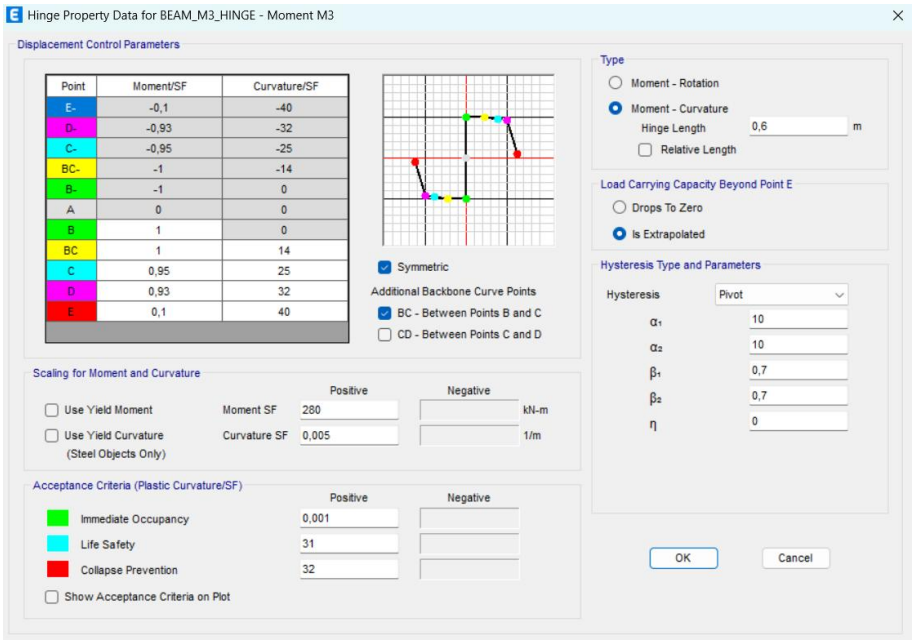


Figure 4.22 Definition of M3 moment-curvature beam hinges

4.6.2 Plastic Hinge Definition of Columns

Zero length, P-M2-M3 fiber hinges are assigned to both ends of columns. In fiber hinges, the column sections are represented by fibers, each having different locations, material properties, and dimensions within the section. Although the fibers have no physical dimensions in a geometric sense, their defined dimensions are utilized during the analysis to compute stresses based on the applied forces acting on them. In the P-M2-M3 hinges, the axial load is coupled with the moments about the 2 and 3 axes in the analytical software, where the moment components about the 2 and 3 directions are computed independently from each other. Two distinct fiber hinge definitions are assigned to the column sections used in the buildings, namely 500 × 700 mm and 600 × 600 mm, as illustrated in Figures 4.23 and 4.24, respectively. The detailed definition of P-M2-M3 hinges is provided in Chapter 3.

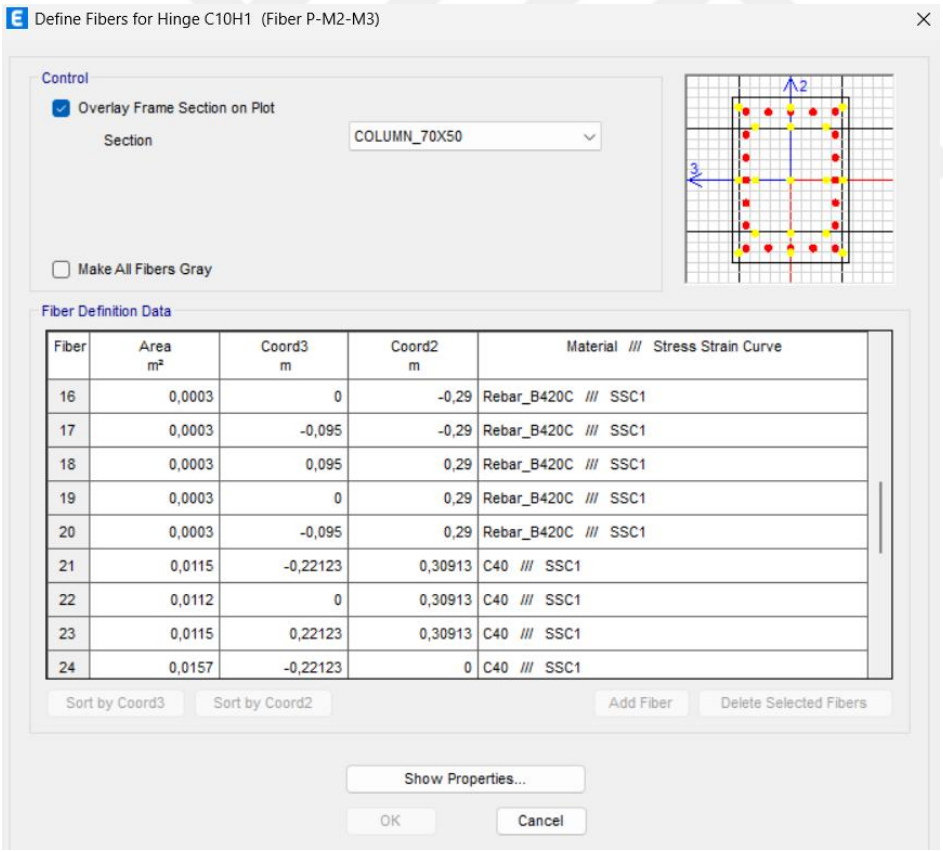


Figure 4.23 Fiber hinge definition of 500 x 700 mm columns

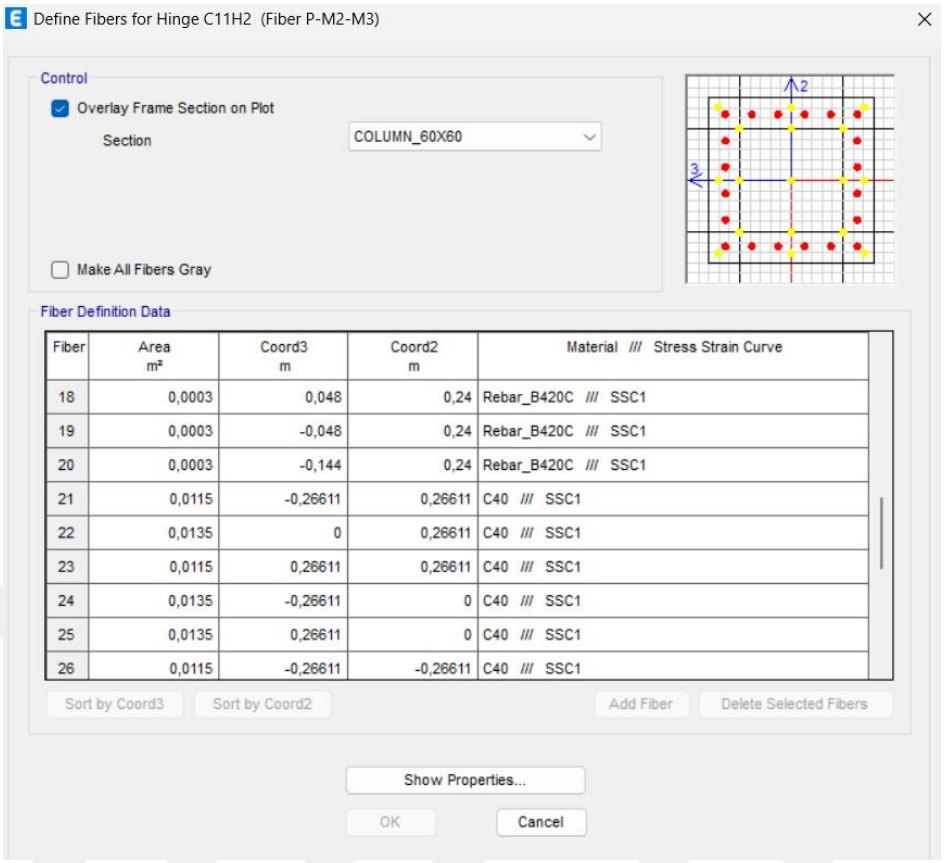


Figure 4.24 Fiber hinge definition of 600 x 600 mm columns

4.6.3 Plastic Hinge Definition of Structural Walls

The P-M3 hinges are placed at the midheight of the structural wall elements in each story, as wall elements in ETABS are defined as area objects, with hinges automatically positioned at the midpoint where internal forces are obtained, effectively capturing the nonlinear response of the wall. Detailed explanation of these hinges is provided in Chapter 3. In the P-M3 hinges, the axial load is coupled with the moment about the 3-axis, which represents the in plane direction, while no interaction is considered with the moment about the 2-axis, corresponding to the out of plane direction. The fiber hinge definition of P-M3 hinges is illustrated in Figure 4.25.



Figure 4.25 Fiber hinge definition of structural walls

CHAPTER 5

ANALYTICAL RESULTS

The analytical results obtained from 385 time history analyses, conducted on 35 buildings, each subjected to 11 ground motion records, are processed and presented in this chapter. The records are grouped as near fault and far field based on the rupture distance between the fault rupture and the recording station, where near fault motions correspond to distances less than 10 km (4 records) and far field motions correspond to greater distances (7 records). The results include modal period, average maximum roof and interstory drifts, distribution of interstory drift and story shear, total base shear, base shear resisted by structural walls and the percentage of members with reinforcement yielding. Additionally, the interactions among these parameters and their variation with increasing structural wall ratio and number of stories are discussed. To denote the building models efficiently, a notation system is adopted in the format Sxx_Ryy, where Sxx and Ryy represent the number of stories and structural wall ratio (%), respectively, i.e., S07_R25 for a 7 story building with 2.5% wall to floor area ratio.

5.1 Modal Period

The first modal period, evaluated with respect to the varying structural wall ratio, is observed to decrease as the wall ratio increases. In all buildings, the rate of reduction becomes considerably less pronounced beyond a structural wall ratio of 1.0%. This trend is more evident in the 5 and 7 story buildings, where the periods become almost identical after 1.5% wall ratio. The first modal periods of all buildings are presented in Figure 5.1.

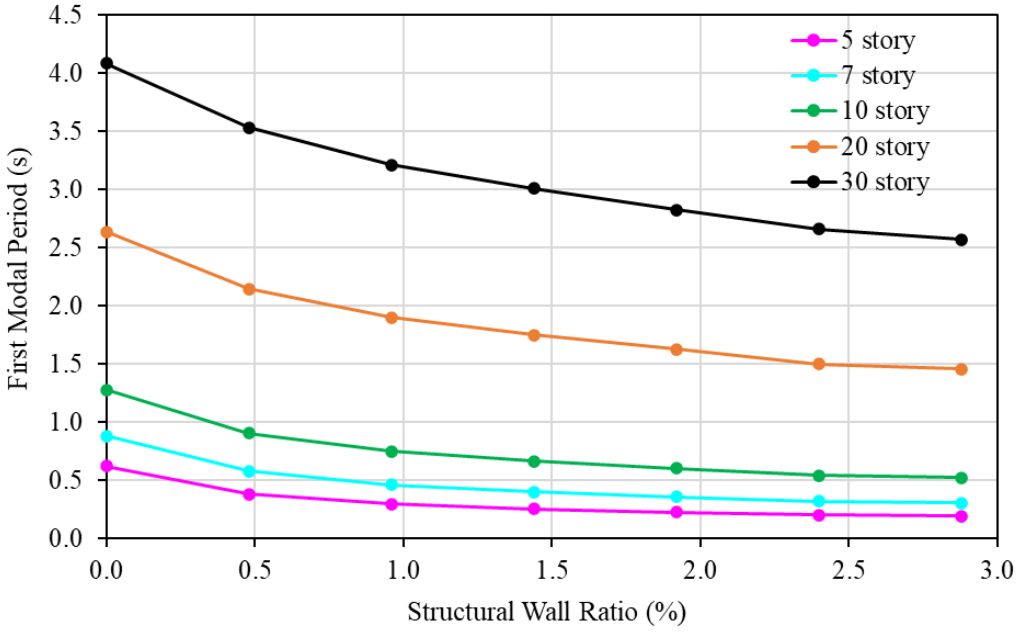


Figure 5.1 First modal period vs. structural wall ratio

5.2 Percentage of Base Shear Carried by Structural Walls

In order to evaluate the relationship between the structural wall ratio and the contribution of reinforced concrete structural walls to lateral load resistance, a series of nonlinear time history analyses are conducted for buildings with 5, 7, 10, 20, and 30 stories. Each building is subjected to 11 ground motion records, and the base shear carried by the structural walls is obtained separately in the X and Y directions. The results from both directions are then averaged, as the structural configuration featured orthogonal symmetry and is free of torsional irregularity, leading to nearly identical responses in both directions. The average percentage of base shear resisted by structural walls is then plotted against the corresponding structural wall ratio, presented in Figure 5.2 to investigate the variation of shear force carried by structural walls with increasing wall ratio and building height.

The resulting curves for different number of stories indicate a strong overlap, confirming that the contribution of structural walls to lateral load carrying capacity primarily depends on the wall area to floor area ratio, with minimal influence from

building height within the examined range. Even a structural wall ratio of 0.5% is adequate for the walls to carry more than half of the base shear, approximately 65.0%, significantly reducing the lateral load applied on columns. As the wall ratio increases, the fraction of shear force carried by the walls continues to increase, but the rate of change decreases. This reduction in slope becomes more evident after 1.5% wall ratio, indicating that beyond this point, adding more structural walls results in diminishing returns in terms of base shear contribution.

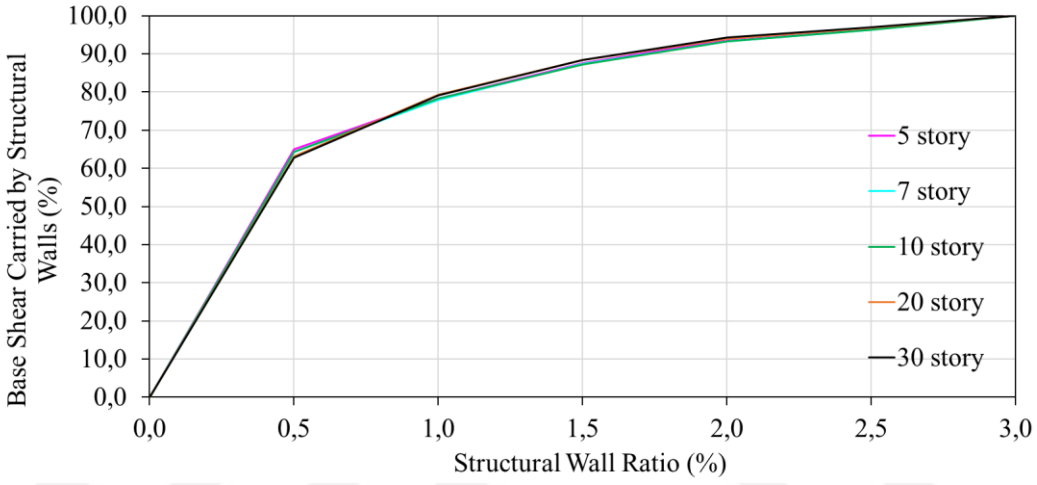


Figure 5.2 Base shear contribution of structural walls vs. structural wall ratio

5.3 Distribution of Story Shear

The distribution of story shear is presented through two graphs for each time history analysis in the principal x and y directions. For practical representation, two ground motion records that impose the highest displacement demands are selected, namely the Christchurch Earthquake from the far field set and the Erzincan Earthquake from the near fault set. The results are presented for the 5, 10 and 30 story buildings, as these heights are considered sufficient to demonstrate the general trend of how the distribution of story shear is influenced by varying structural wall ratios across different building heights. The results for the distribution of story shear for the 5, 10 and 30 story buildings under the Christchurch and Erzincan Earthquakes are illustrated in Figures 5.3 and 5.4, respectively.

In Figure 5.3, a gradual increase in story shear is observed in all buildings as the structural wall ratio increases, attributed to the corresponding increase in the rigidity of the buildings. In the 5 and 10 story buildings, the overall trend of story shear distribution is maintained despite the increase in the wall ratio. However, in the 30 story building, higher story shears are observed above the 20th story compared to the ones between the 10th and 20th stories as the structural wall ratio increases. This type of story shear distribution indicates the presence of the whiplash effect, which refers to the amplified motion and inertial forces occurring in the upper stories of tall, flexible buildings during dynamic excitation, similar to the rapid snapping motion observed at the tip of a whip (Wan-Xie & Jia-Hao, 1987).

In Figure 5.4, similar results to those obtained under the Christchurch Earthquake are observed for the 5 and 10 story buildings subjected to the Erzincan Earthquake. In the 30 story building, however, the increase in story shear at the upper stories is more pronounced. For the 30 story buildings, variations in story shear distribution with increasing structural wall ratio are observed to be more irregular compared to behavior under the Christchurch Earthquake. This indicates that due to their pulse like characteristics, near fault earthquakes such as the Erzincan Earthquake, may lead to a more irregular structural response.

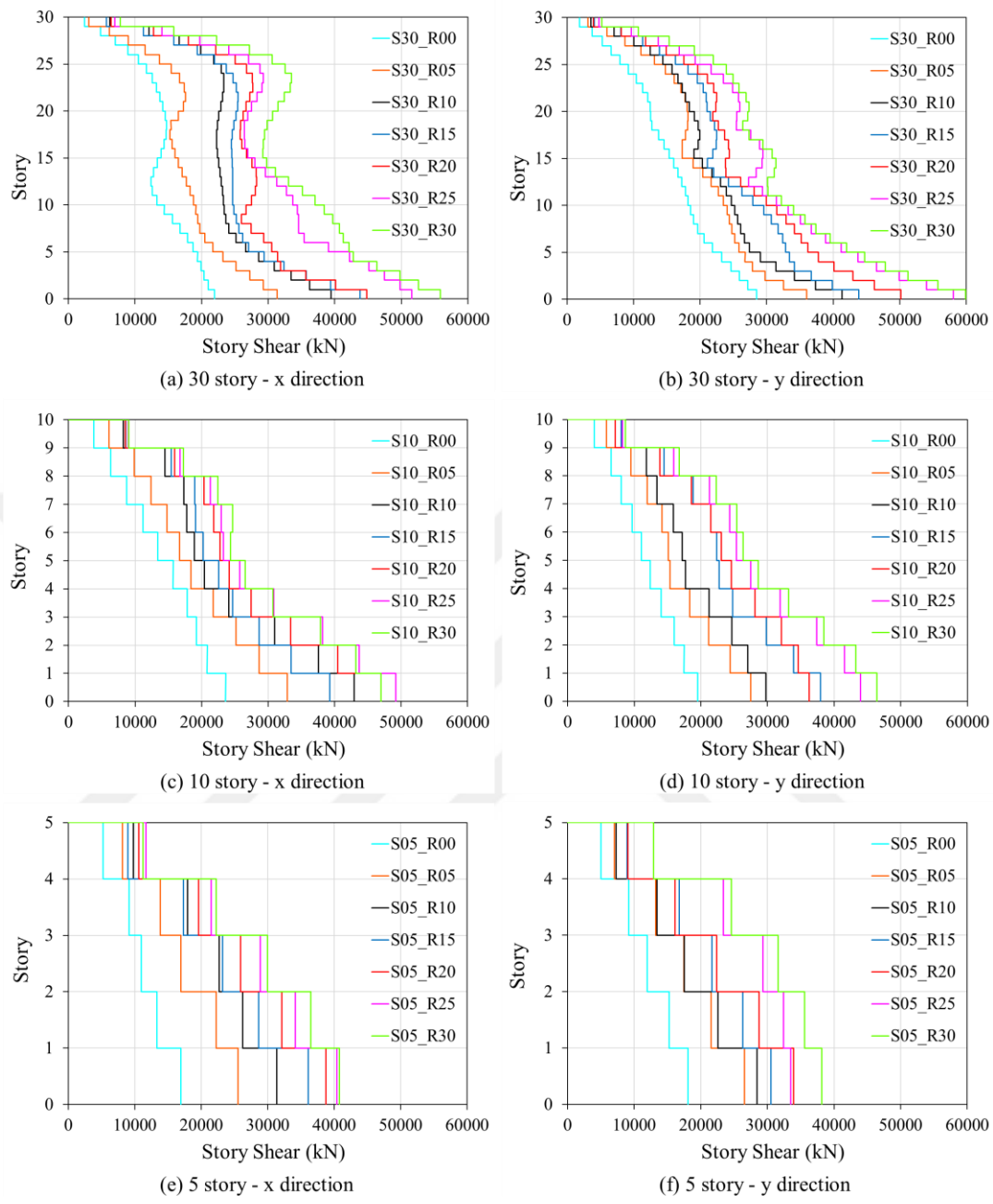


Figure 5.3 Distribution of story shear under the Christchurch Earthquake

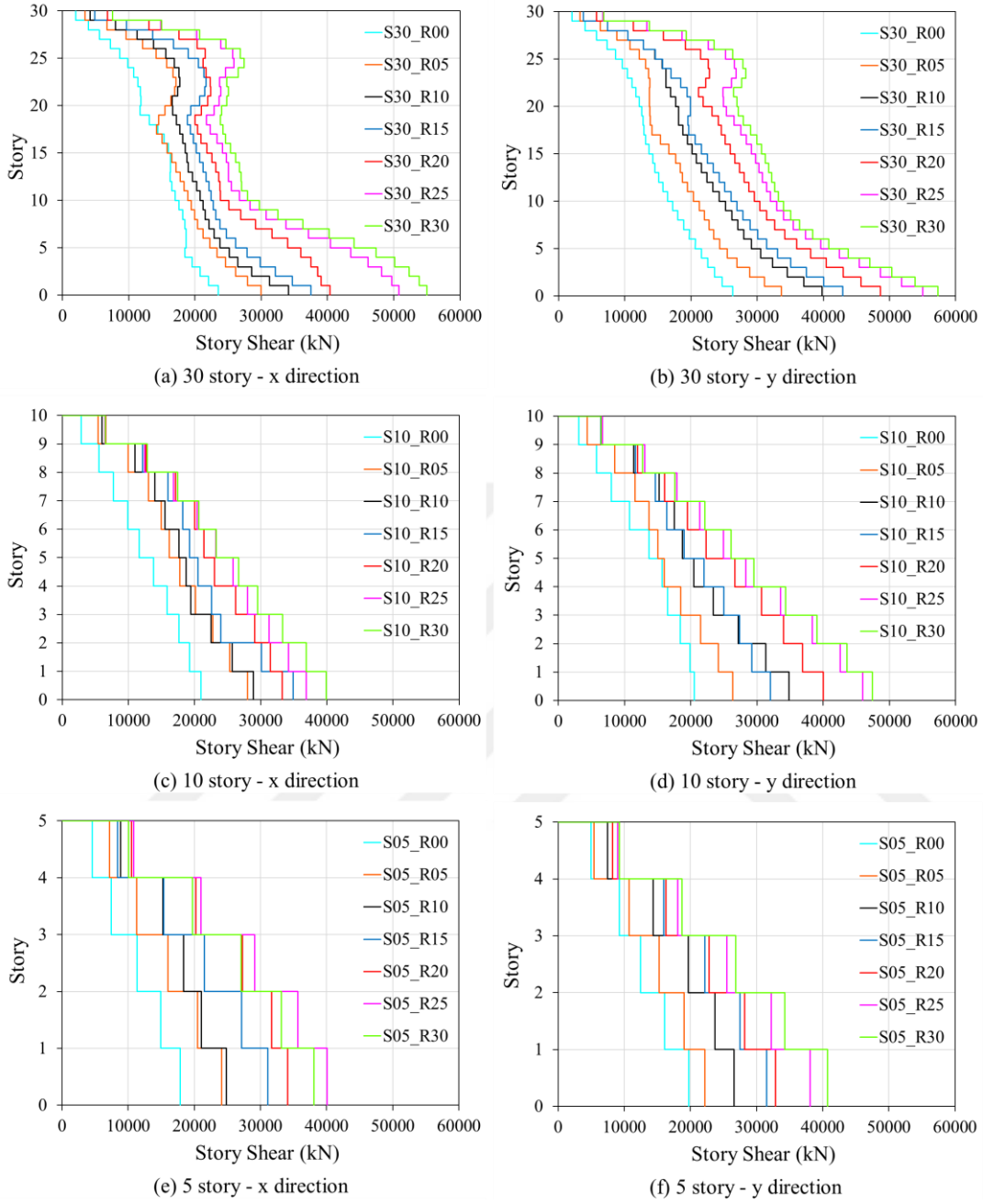


Figure 5.4 Distribution of story shear under the Erzincan Earthquake

5.4 Maximum Roof Drift Ratio

For each building, nonlinear time history analyses are performed using 11 ground motion records. From each analysis, four maximum roof drift values are obtained,

corresponding to the +X, -X, +Y, and -Y directions. The absolute maximum among these four values is selected as the representative roof drift for that ground motion. As a result, one maximum drift value is assigned per record, and the average of these 11 values is computed to determine the overall roof drift for each building.

Furthermore, the roof drift values in each graph are normalized with respect to both 1.0% and 1.5% structural wall area to floor area ratios for comparative evaluation of the effectiveness of these wall ratios. These reference ratios are selected to demonstrate the diminishing reduction in drift beyond these wall ratios.

The variation of roof drift with respect to the structural wall area to floor area ratio for buildings with different story levels are presented in Figure 5.5. In Figures 5.5(a), (d), and (g), the average roof drift ratios obtained from far field, near fault, and all ground motion records are illustrated respectively. The corresponding normalized results with respect to 1.0% and 1.5% wall ratios are presented in Figures 5.5(b), (e), (h) and Figures 5.5(c), (f), (i), respectively.

When the average results of all records are examined (Figure 5.5(g)), a consistent decrease in the roof drift is observed with increasing structural wall ratio for 5, 7 and 10 story buildings. For 20 and 30 story buildings, an increase in roof drift is observed for 0.5% structural wall ratio. When the structural wall ratio is increased to 1.0%, the roof drift is decreased compared to the 0.5% wall ratio case but remains higher than the average value obtained for buildings without structural walls. Beyond 1.0% wall ratio, the reduction in roof drift is not as significant as those observed for the 5, 7, and 10 story buildings.

The average roof drifts for near fault ground motions (Figure 5.5(a)) are obtained to be higher than those for far field ground motions (Figure 5.5(d)), which are lower than that of the average of all ground motions, as expected. Although the roof drift values vary, the overall trends of the roof drift vs. structural wall ratio curves for varying building heights remain consistent across the different averaging approaches, namely the average of all 11 ground motions, the average of far field records, and the average of near fault records.

When the normalized graphs are examined, it is observed that for all averaging approaches the reduction in maximum roof drift becomes less pronounced with increasing number of stories and structural wall ratio. The reduction in drift is observed to be more significant for the far field records, indicating that the effectiveness of additional structural walls decreases as the source to site distance reduces.

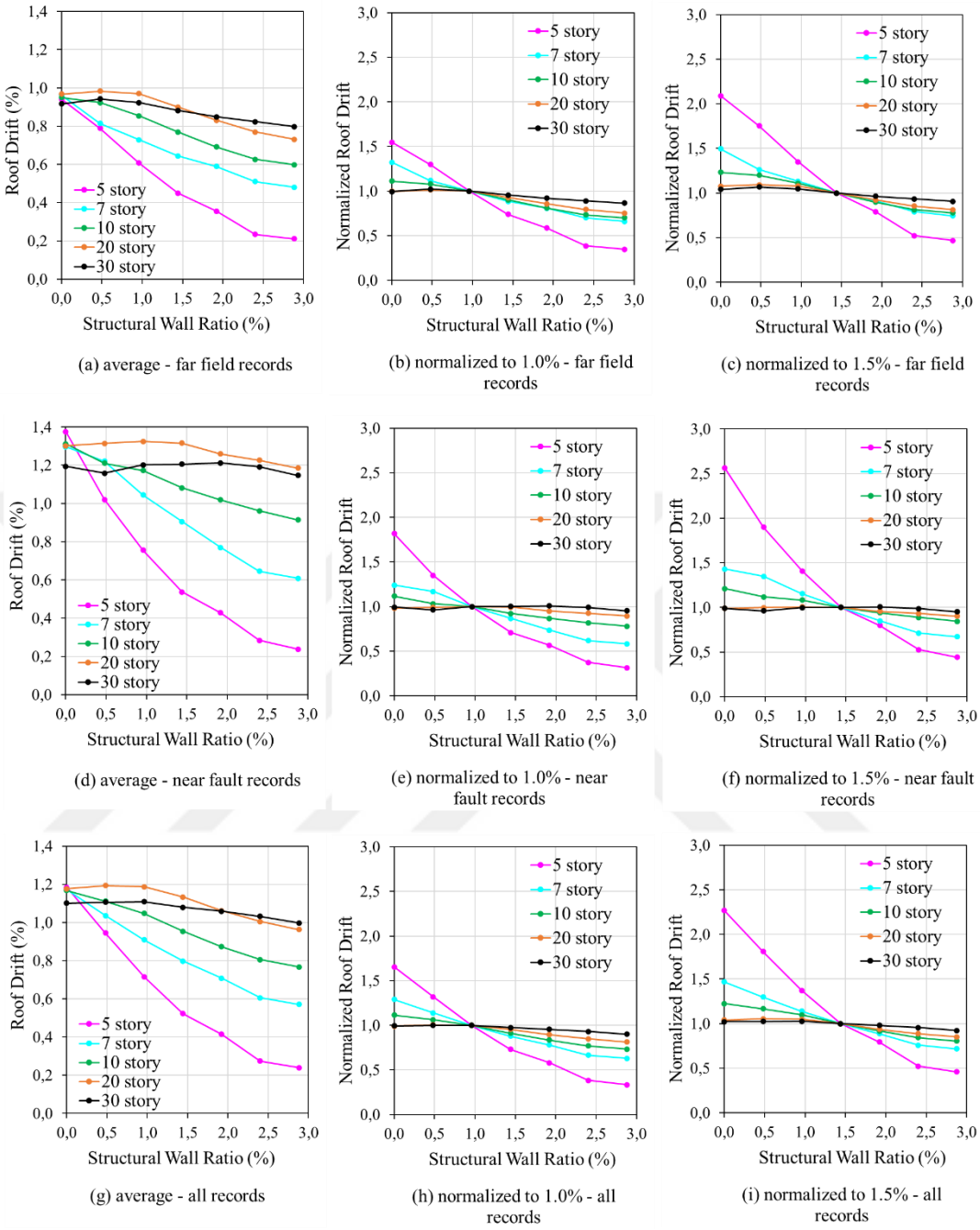


Figure 5.5 Maximum roof drift vs. structural wall ratio

5.5 Roof Drift vs. Time Response

In total, 770 roof drift vs. time response graphs are obtained from the analyses, corresponding to two principal directions for each ground motion, eleven records per

building, and thirty five buildings. Near fault earthquake records, which have a rupture distance of less than 10 km, generally exhibit pulse like characteristics resulting in larger lateral displacements and impose the most critical demands on structures. Accordingly, the focus is placed on the Y-axis component of Northridge Earthquake, as this record produces one of the highest roof displacements among the eleven records and displays distinct pulse characteristics.

Figure 5.6 presents the roof drift vs. time responses under the Northridge Earthquake for frame buildings that have 0.0% structural wall ratio. To improve clarity, 5, 7 and 10 story buildings are grouped together since they exhibit similar trends in the variation of maximum roof drift with different structural wall ratios, while 20 and 30 story buildings are presented as a separate group due to their comparable behavior (Figure 5.5). The grouped results are presented in Figures 5.7 through 5.20.

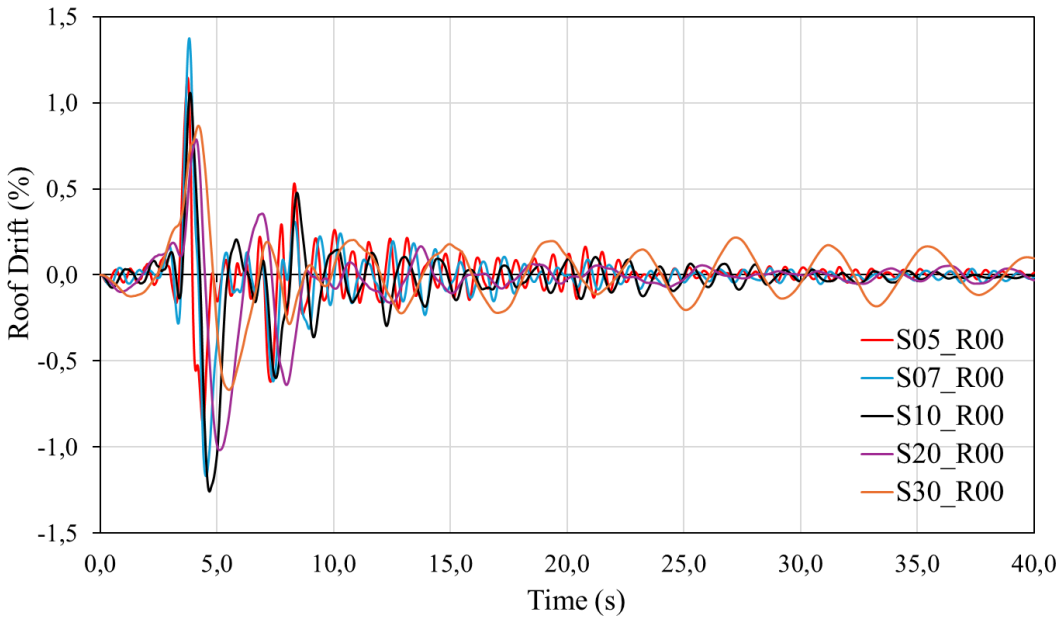


Figure 5.6 Roof drift vs. time response of Northridge Earthquake for buildings with 0.0% structural wall ratio

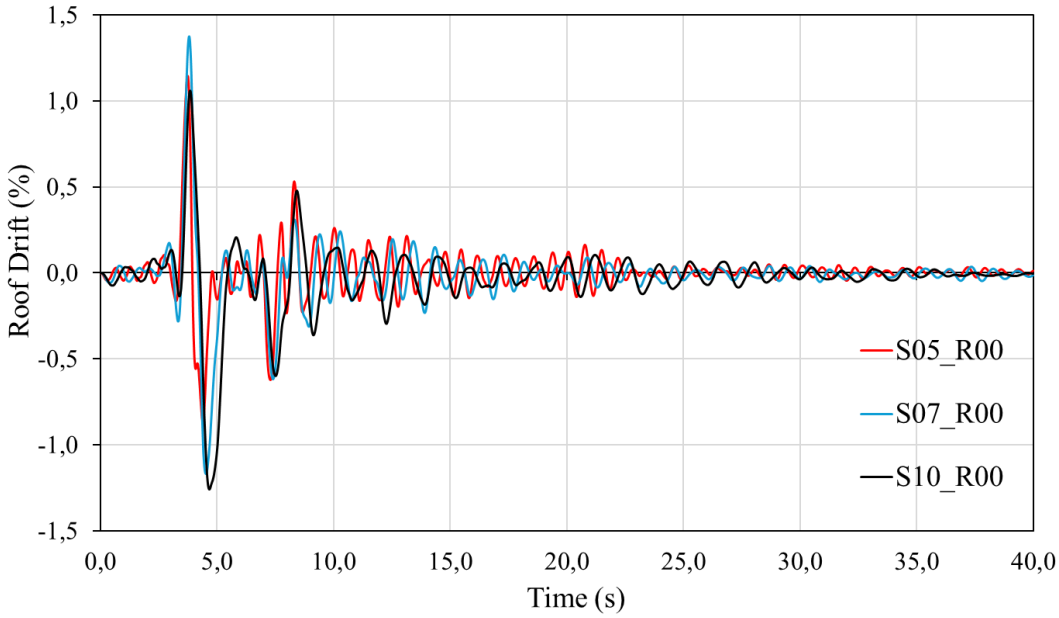


Figure 5.7 Roof drift vs. time response for Northridge Earthquake for S05_R00, S07_R00 and S10_R00

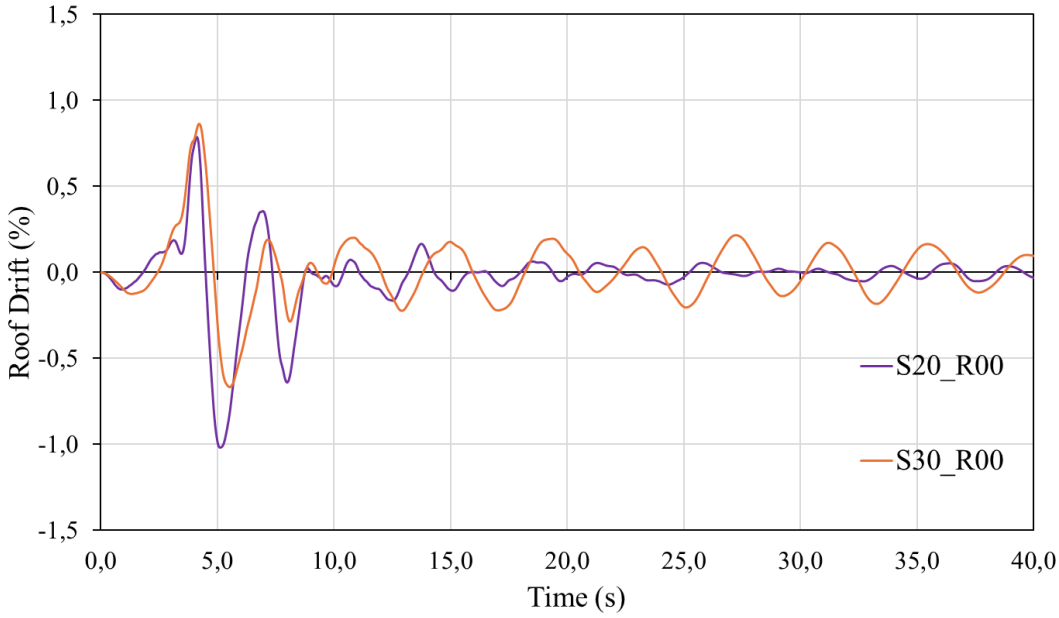


Figure 5.8 Roof drift vs. time response for Northridge Earthquake for S20_R00 and S30_R00

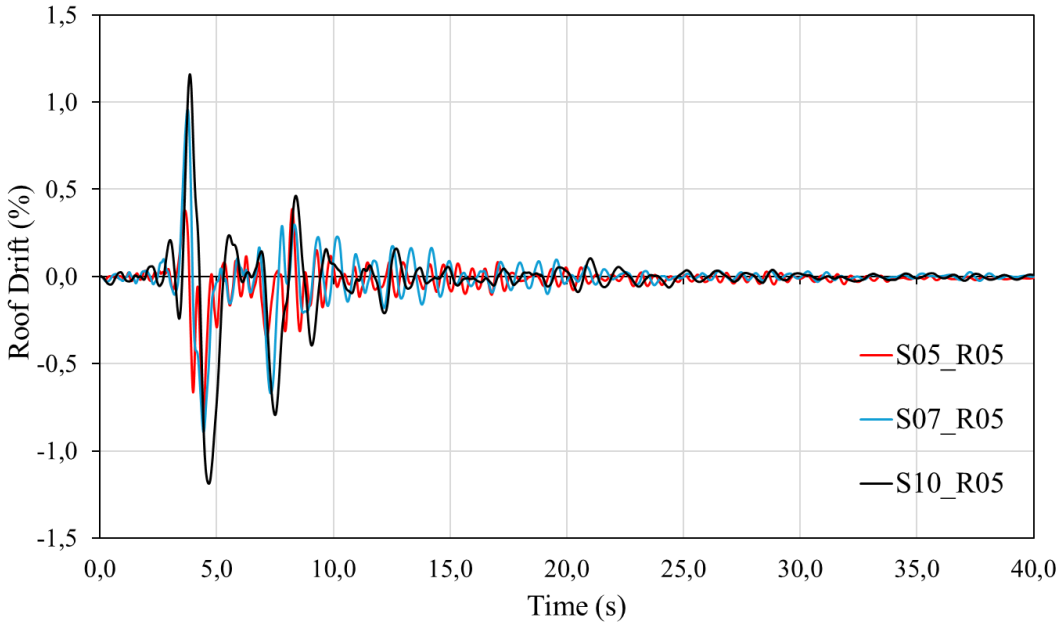


Figure 5.9 Roof drift vs. time response for Northridge Earthquake for S05_R05, S07_R05 and S10_R05

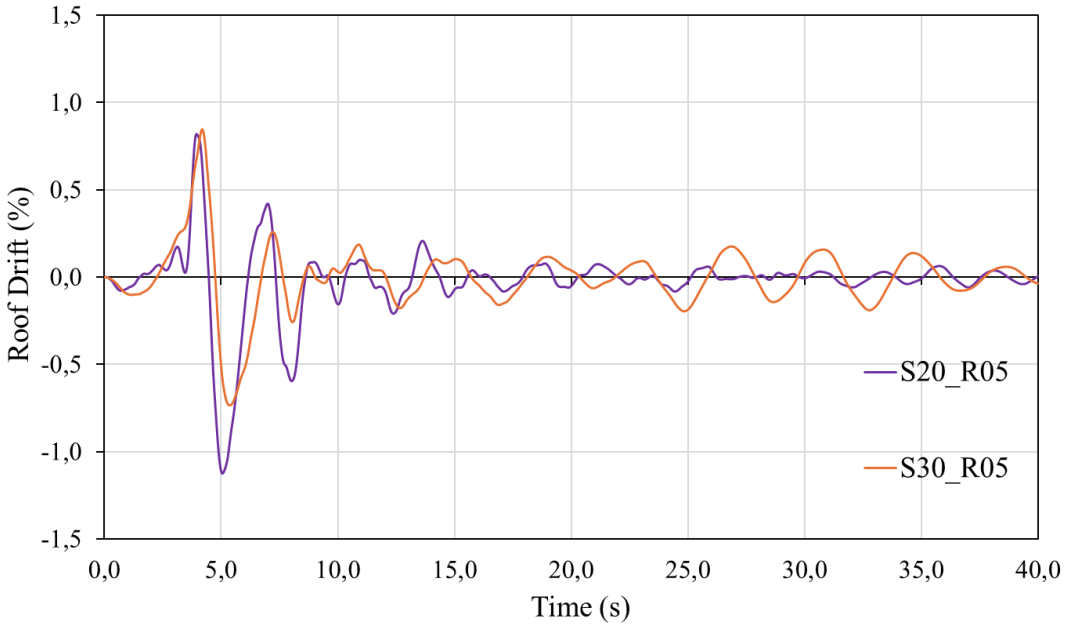


Figure 5.10 Roof drift vs. time response for Northridge Earthquake for S20_R05 and S30_R05

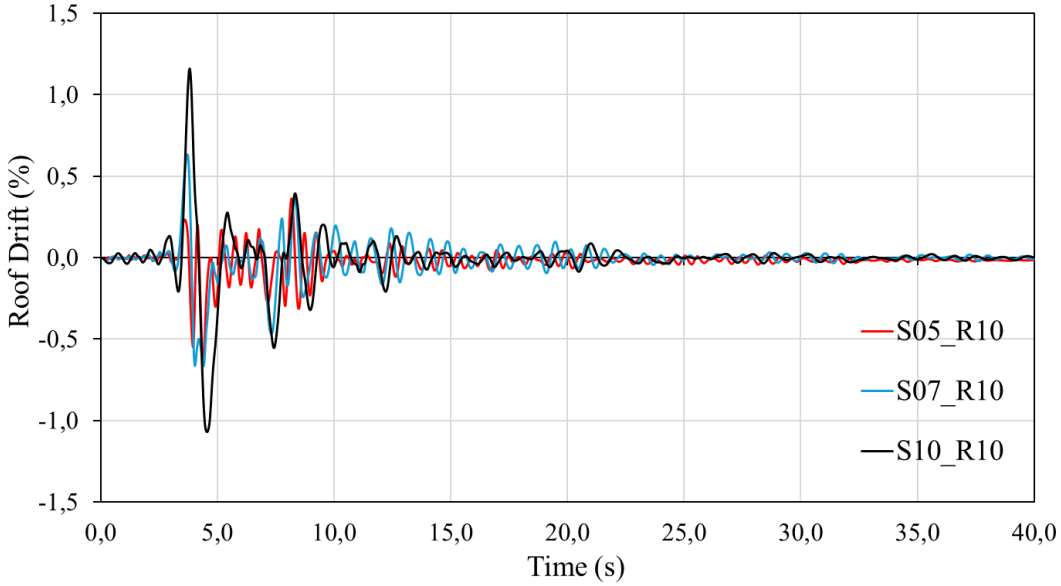


Figure 5.11 Roof drift vs. time response for Northridge Earthquake for S05_R10, S07_R10 and S10_R10

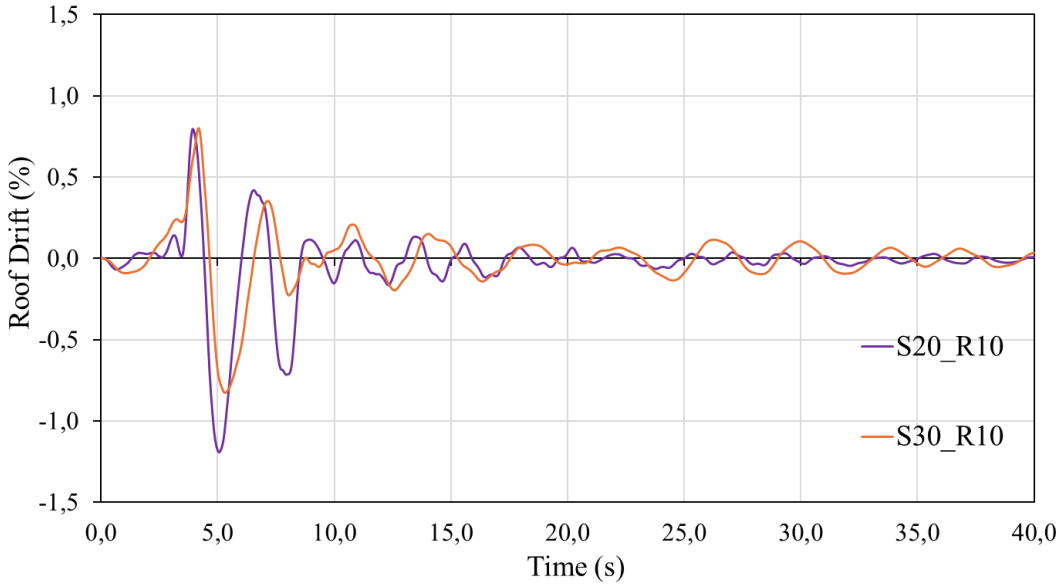


Figure 5.12 Roof drift vs. time response for Northridge Earthquake for S20_R10 and S30_R10

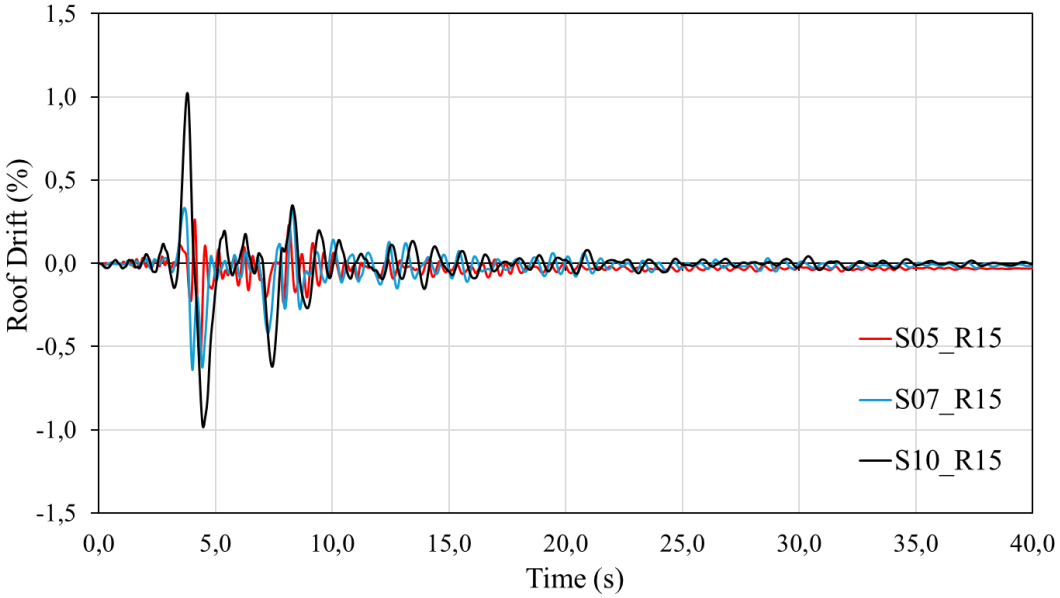


Figure 5.13 Roof drift vs. time response for Northridge Earthquake for S05_R15, S07_R15 and S10_R15

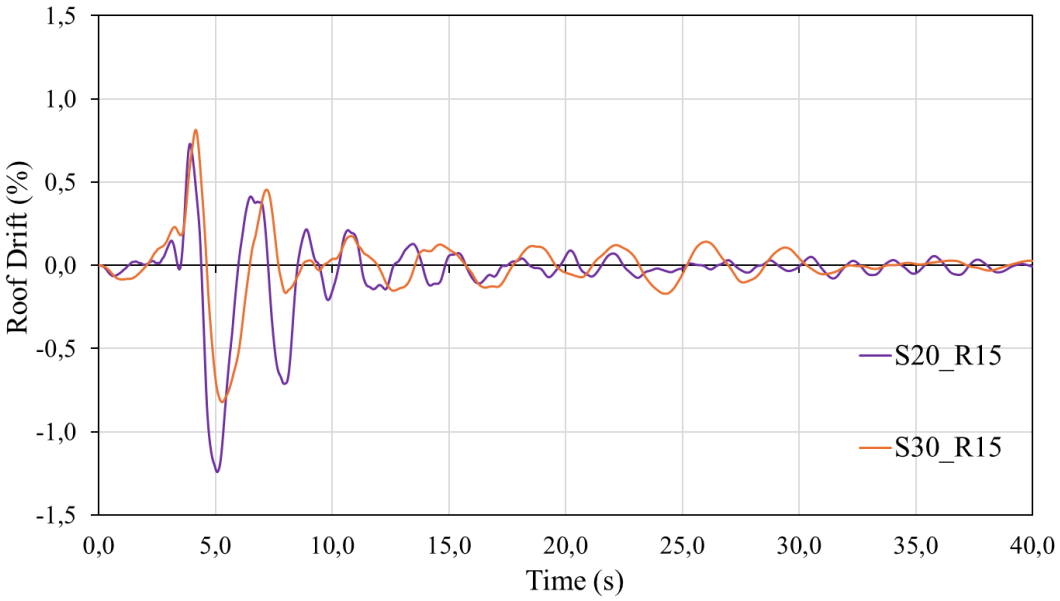


Figure 5.14 Roof drift vs. time response for Northridge Earthquake for S20_R15 and S30_R15

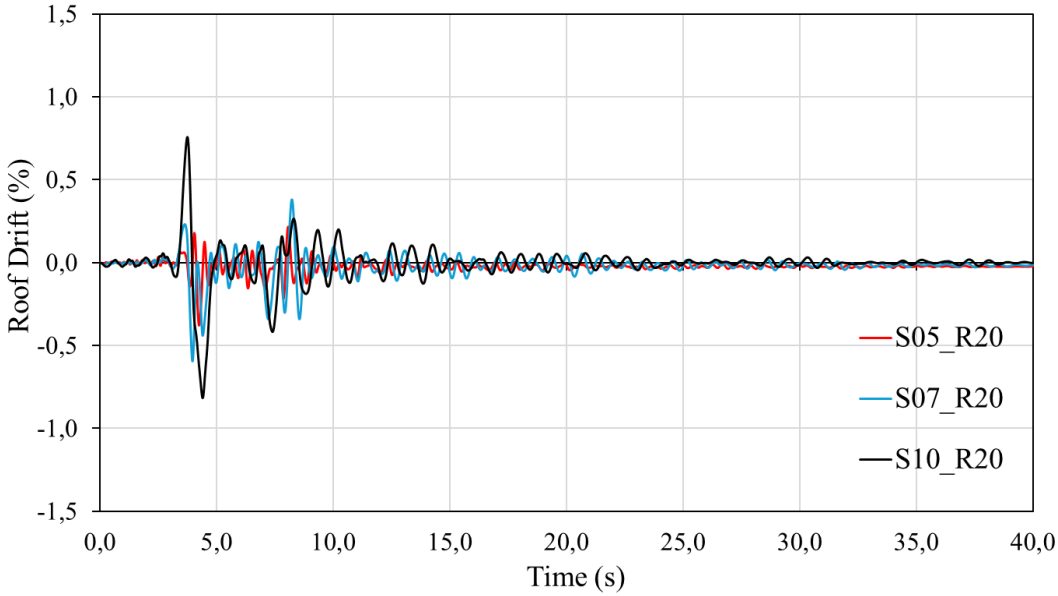


Figure 5.15 Roof drift vs. time response for Northridge Earthquake for S05_R20, S07_R20 and S10_R20

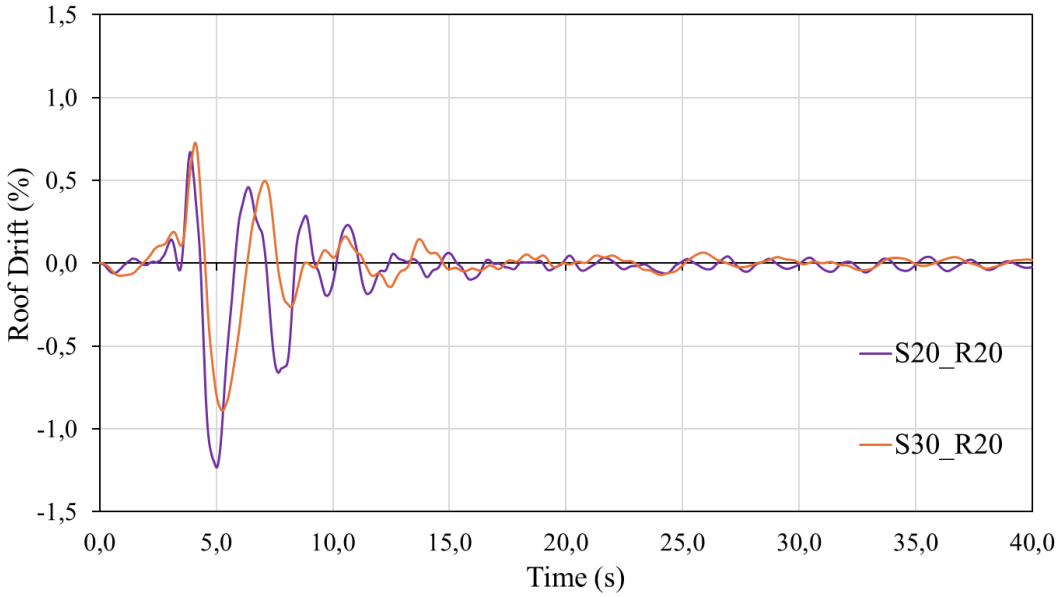


Figure 5.16 Roof drift vs. time response for Northridge Earthquake for S20_R20 and S30_R20

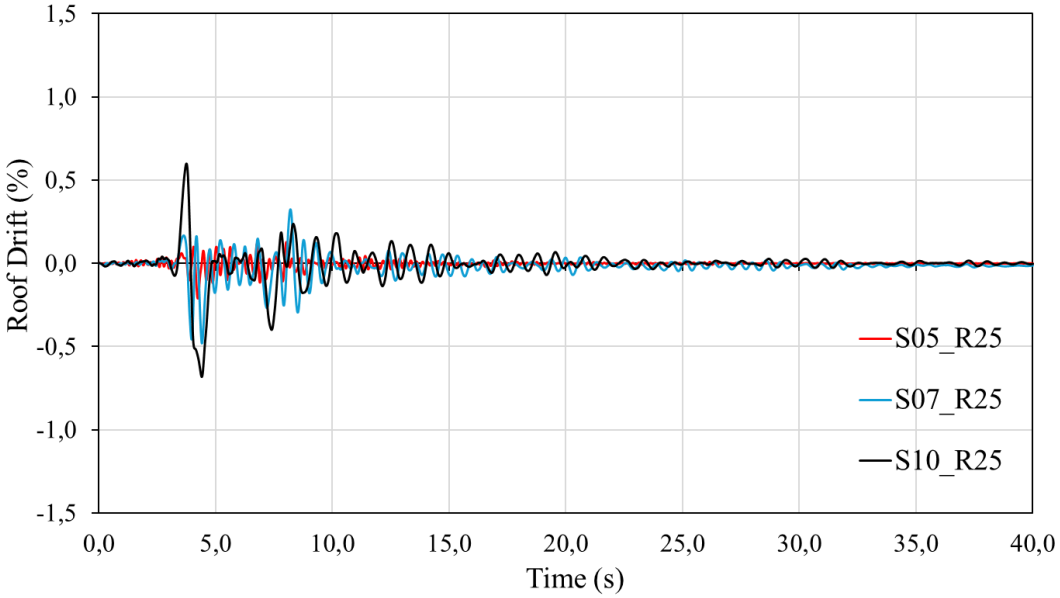


Figure 5.17 Roof drift vs. time response for Northridge Earthquake for S05_R25, S07_R25 and S10_R25

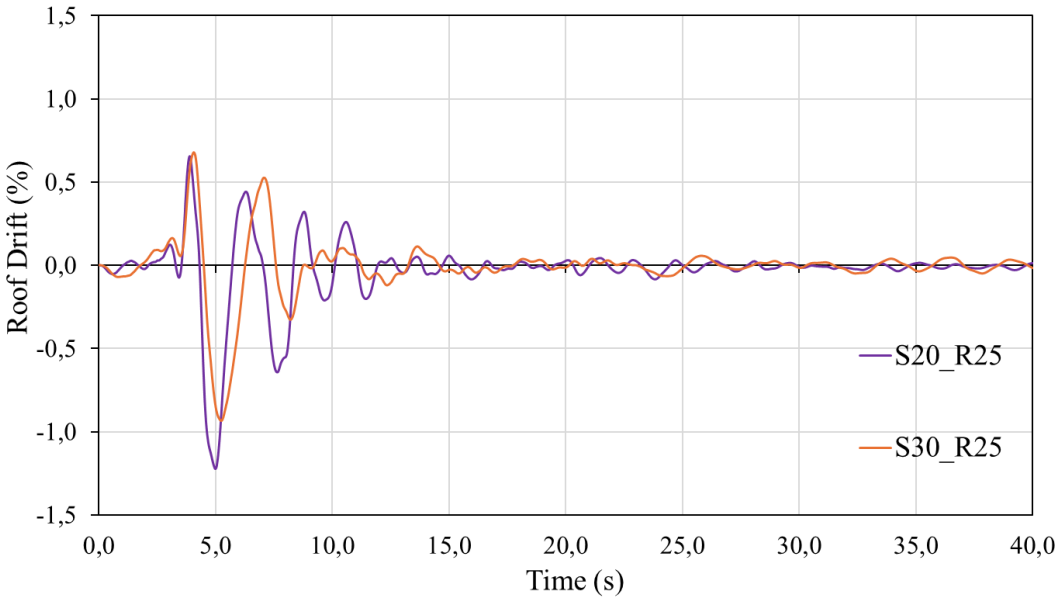


Figure 5.18 Roof drift vs. time response for Northridge Earthquake for S20_R25 and S30_R25

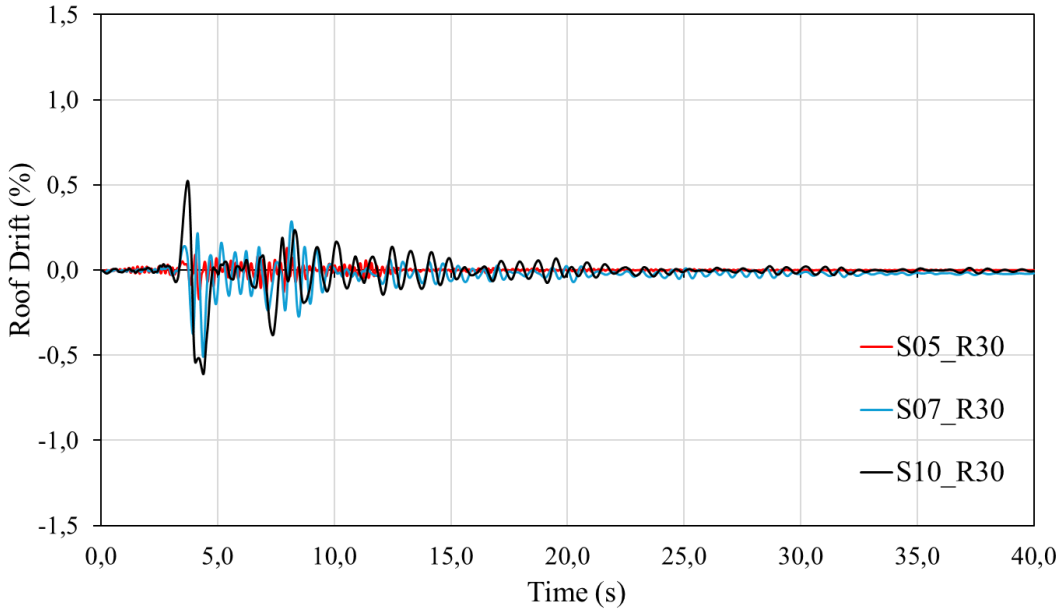


Figure 5.19 Roof drift vs. time response for Northridge Earthquake for S05_R30, S07_R30 and S10_R30

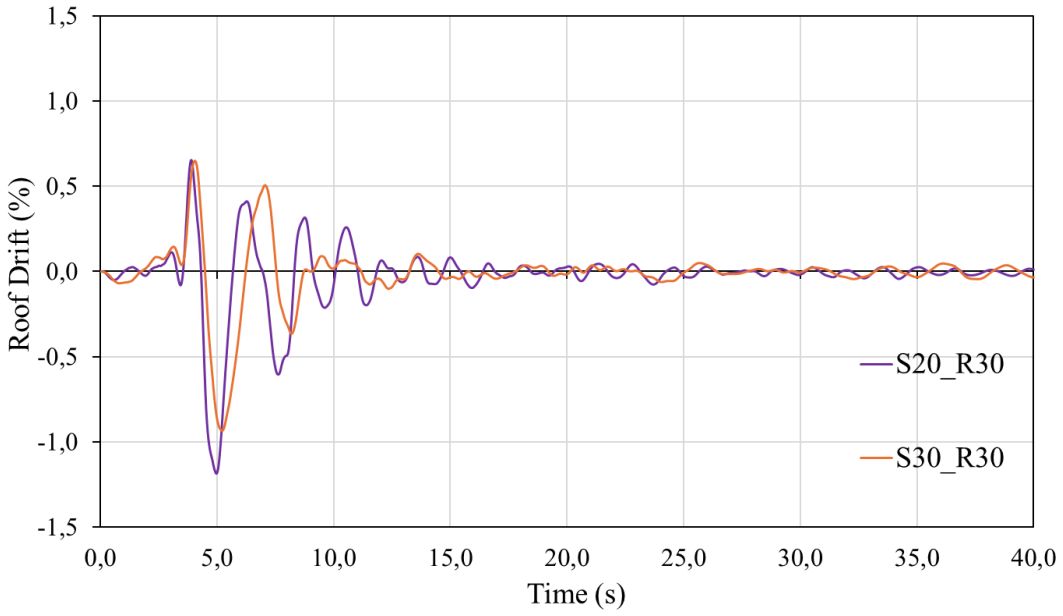


Figure 5.20 Roof drift vs. time response for Northridge Earthquake for S20_R30 and S30_R30

An examination of the roof drift vs. time responses under the Y-axis component of the Northridge Earthquake reveals that reduction in roof drift is obtained for the 5,

7, and 10 story buildings as the structural wall ratio increases. When the structural wall ratio is 0.0%, the observed roof drifts are around 1.0% in these buildings (Figure 5.7); however, as the structural wall ratio increases up to 3.0%, the roof drifts are reduced to half, reaching approximately 0.5% (Figure 5.19). This reduction is attained at relatively low wall ratios, around 0.5% to 1.0% in the 5 and 7 story buildings (Figures 5.9, 5.11), whereas a noticeable decrease in the roof drift is obtained in the 10 story building only at a higher wall ratio of 2.0% (Figure 5.15).

For the 20 and 30 story buildings, the characteristics of the roof drift vs. time response is quite different. At a structural wall ratio of 0.0%, roof drift values of approximately 1.0% are recorded (Figure 5.8). As the wall ratio increases up to 2.0%, a gradual increase in the roof drift up to 1.2% is observed (Figure 5.16). Between wall ratios of 2.0% and 3.0%, the roof drift values remain nearly constant (Figures 5.16, 5.18 and 5.20). This behavior is observed to be contradictory to the average results of all records, which are predominantly governed by far field records rather than by earthquakes with distinct pulse characteristics, highlighting that the relative number of near fault ground motions within the selected set can significantly influence the average response.

5.6 Maximum Interstory Drift

A similar procedure, previously applied to obtain a single representative value from the maximum roof drift results, is applied for the interstory drift, where the absolute maximum interstory drift among the four loading directions is considered for each story. The absolute maximum interstory drift observed over the height of the building is selected to represent the maximum response in the +X, -X, +Y, and -Y directions for each ground motion record. Then, these interstory drifts are normalized with respect to 1.0% and 1.5% structural wall ratios and grouped for different averaging approaches. The variation of maximum interstory drift with increasing wall ratio for buildings with varying number of stories is presented in Figure 5.21.

As can be observed from Figure 5.21(g), which includes all ground motion records, the maximum interstory drift consistently decreases with increasing structural wall ratio for all building heights. The reduction is more pronounced in 5, 7 and 10 story buildings, while in 20 and 30 story buildings, the rate of decrease is lower, particularly beyond 1.0-1.5% wall ratio. For 20 and 30 story buildings, the normalization graphs indicate that the reduction in interstory drifts after 1.5% structural wall ratio becomes less compared to the reduction before this threshold. The normalized results of the 5 story buildings are found to be significantly different from the rest of the curves, suggesting that the reduction in maximum interstory drifts before and after 1.0%-1.5% is greater than that observed in buildings with higher number of stories. This behavior can be attributed to the average response spectrum obtained after spectral matching. The periods of the 5 story buildings correspond to the plateau region of the response spectrum. Although the addition of structural walls increases the stiffness and the natural frequency of the buildings, the seismic forces acting on them remain constant and may even decrease due to fluctuations in the plateau region (Figure 4.19).

In Figure 5.21(d), for near fault records, 5, 7 and 10 story buildings have a similar trend, although the absolute maximum interstory drift values are obtained to be larger compared to the average results of all records. The most notable difference between the average results of all records and those of near fault records is observed for 20 and 30 story buildings, where the reduction in interstory drifts reaches a plateau between 1.0% and 1.5% structural wall ratio for near fault records, and subsequently begins to decrease again after 2.0% wall ratio. This indicates that the effectiveness of structural walls in reducing interstory drifts is less significant for 20 and 30 story buildings subjected to near fault records that exhibit pulse characteristics.

In Figure 5.21(a), for far field records, a more consistent decrease in interstory drifts is observed for all buildings. The normalization graphs indicate that the rate of reduction after 1.0% and 1.5% wall ratios are significantly lower when compared to other methods of averaging, namely average of all 11 records and average of near fault records.

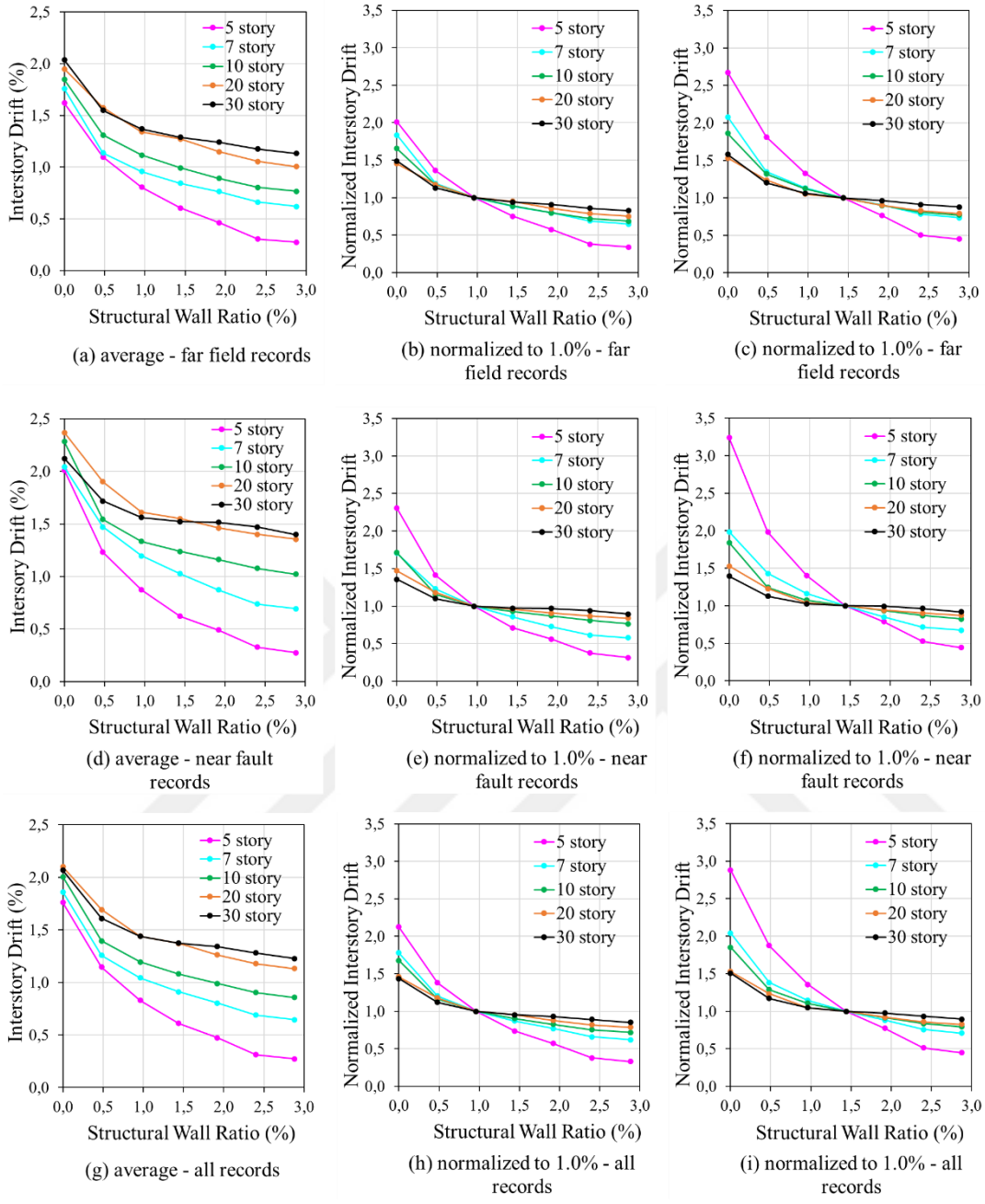


Figure 5.21 Maximum interstory drift vs. structural wall ratio

The standard deviation (SD) and the coefficient of variation (COV) of the maximum interstory drifts are computed for each model considering the eleven ground motions. The results for different averaging approaches, namely the average of all records, the average of far field (FF) records and the average of near fault (NF) records, are presented in Table 5.1. The relationship between the coefficient of variation and the

structural wall ratio for buildings with different number of stories is illustrated in Figure 5.22.

It is observed that no clear correlation or trend emerges between the coefficient of variation (COV) of the maximum interstory drift and the structural wall ratio (Figure 5.22). This behavior is attributed to the different frequency content of the ground motions and the wide period range of the building models, leading to varying sensitivity to individual records. Overall, the COV values remain around 20% for most configurations, indicating an acceptable level of variability considering the diversity of both the input motions and the dynamic characteristics of the buildings.

Table 5.1 Statistical parameters for maximum interstory drift

Model	Standard Deviation			Coefficient of Variation (%)		
	ALL	FF	NF	ALL	FF	NF
S05_R00	0,31	0,21	0,33	17,65	12,77	16,19
S05_R05	0,22	0,25	0,13	19,23	23,16	10,77
S05_R10	0,12	0,10	0,16	14,61	12,71	17,84
S05_R15	0,13	0,15	0,09	20,53	24,70	13,98
S05_R20	0,08	0,10	0,07	17,87	20,71	14,11
S05_R25	0,07	0,08	0,06	23,81	27,68	18,95
S05_R30	0,08	0,09	0,07	29,64	33,19	26,98
S07_R00	0,40	0,39	0,41	21,69	22,12	20,31
S07_R05	0,27	0,18	0,31	21,80	15,61	20,76
S07_R10	0,19	0,11	0,20	17,79	11,83	16,92
S07_R15	0,17	0,15	0,13	18,40	18,25	12,91
S07_R20	0,14	0,13	0,13	16,95	17,04	15,29
S07_R25	0,11	0,09	0,13	15,53	13,22	18,24
S07_R30	0,10	0,08	0,13	15,26	12,32	18,28
S10_R00	0,43	0,45	0,22	21,34	24,29	9,55
S10_R05	0,25	0,20	0,29	18,03	15,59	18,50
S10_R10	0,25	0,24	0,23	20,68	21,21	17,06
S10_R15	0,22	0,19	0,17	19,98	19,55	13,79
S10_R20	0,20	0,15	0,16	20,18	16,97	13,71
S10_R25	0,18	0,10	0,15	20,03	12,72	14,28
S10_R30	0,17	0,09	0,15	19,66	11,90	14,94
S20_R00	0,42	0,25	0,57	20,16	13,03	23,86
S20_R05	0,38	0,21	0,55	22,28	13,08	28,78
S20_R10	0,30	0,22	0,38	21,14	16,76	23,65
S20_R15	0,29	0,21	0,36	21,21	16,41	23,30
S20_R20	0,26	0,20	0,26	20,78	17,51	17,51
S20_R25	0,27	0,23	0,21	23,30	22,01	14,73
S20_R30	0,28	0,24	0,19	24,53	24,19	13,91
S30_R00	0,21	0,24	0,16	10,06	11,63	7,56
S30_R05	0,24	0,19	0,31	14,95	12,48	17,88
S30_R10	0,25	0,18	0,34	17,49	12,79	22,02
S30_R15	0,25	0,17	0,33	18,32	13,16	21,47
S30_R20	0,24	0,16	0,26	17,60	13,23	17,27
S30_R25	0,23	0,16	0,25	18,32	13,28	16,80
S30_R30	0,23	0,15	0,26	18,60	13,19	18,86

FF = Far field, NF = near fault

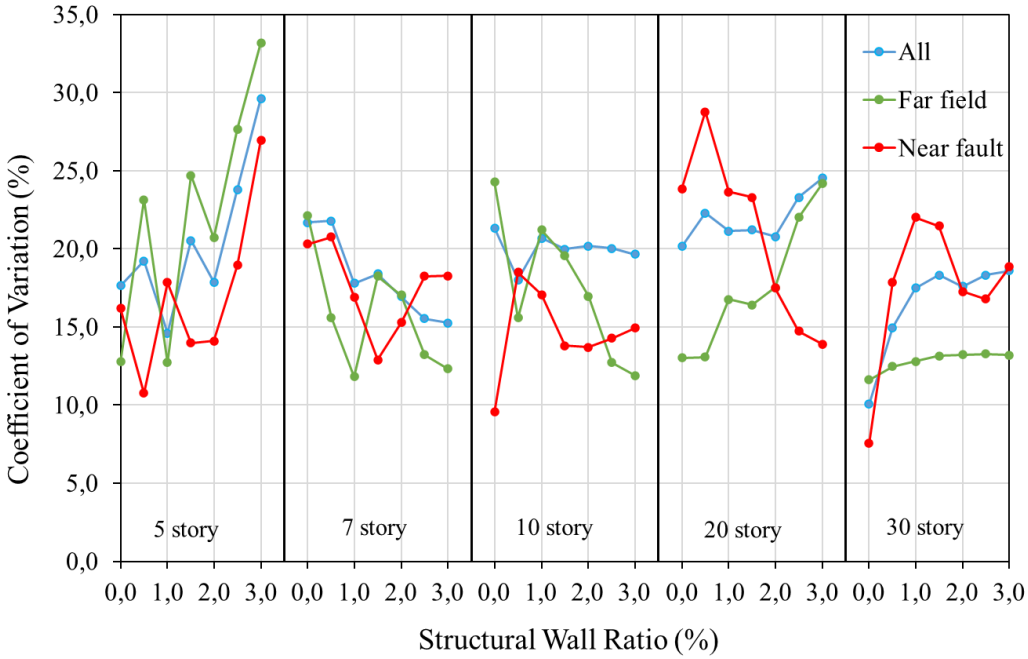


Figure 5.22 Coefficient of variation vs. structural wall ratio

5.7 Distribution of Maximum Interstory Drifts

For the distribution of maximum interstory drifts, due to the large data set, the results of two critical ground motion records, one from the far field group and one from the near fault group, are presented. Upon examination of all results, the Christchurch earthquake is identified as the most critical ground motion within the far field set, producing the highest interstory drifts, while the Erzincan earthquake is identified as the most critical within the near fault set. The distribution of maximum interstory drift results for all earthquakes corresponding to S30_R00 and S30_R20 are presented in Figures 5.23 and 5.24, respectively.

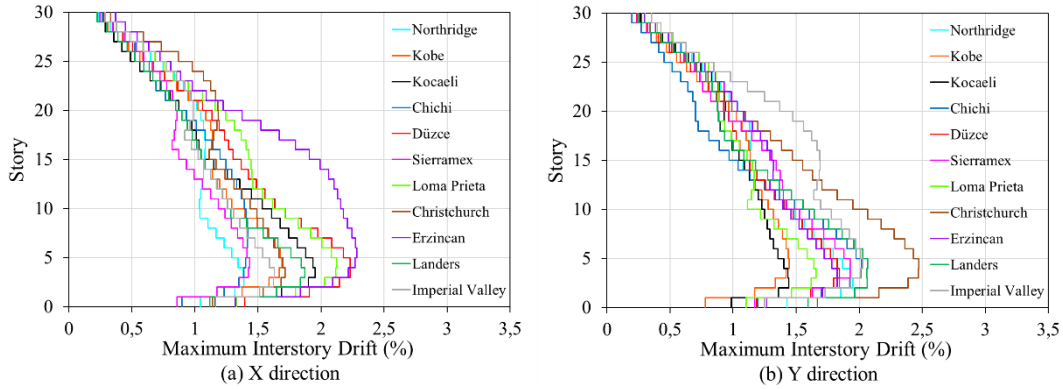


Figure 5.23 Distribution of maximum interstory drift for S30_R00

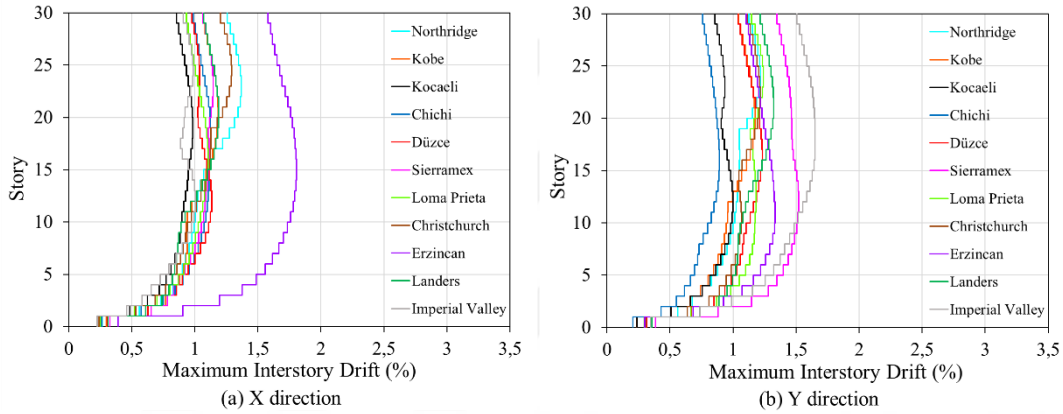


Figure 5.24 Distribution of maximum interstory drift for S30_R20

In Figures 5.25 and 5.26, the distribution of maximum interstory drifts with increasing structural wall ratio is illustrated for 30, 10, and 5 story buildings subjected to the Christchurch and Erzincan earthquakes, respectively.

As can be observed from Figures 5.25(a) and (b), for the 30 story buildings subjected to the Christchurch earthquake, the increase in structural wall ratio causes the interstory drift demand to shift from the lower stories (0-10) toward the higher stories (15-30), while the interstory drift distribution becomes more uniform. As the wall ratio is increased, the overall structural behavior of the buildings is observed to transition from frame-dominated behavior to cantilever structural wall-dominated behavior. This behavioral shift is found to become pronounced at structural wall ratios of 1.5% and more.

A similar trend is observed in Figures 5.25(c) and (d), where, as the structural wall ratio is increased, the interstory drift demand shifts from the lower stories (0-5) to higher (2-10) stories. Unlike the gradual increase observed in the 30 story buildings, once the behavioral shift occurs, the interstory drifts are nearly identical from the 2nd story to the roof. In this case, a structural wall ratio of 1.0% is sufficient to induce the transition from frame-dominated to cantilever wall-dominated behavior.

In Figures 5.25(e) and (f), it is observed that the behavior of 5 story buildings under the Christchurch Earthquake is similar to that of the 10 story buildings. In both cases, the behavioral transition is observed at a 1.0% wall ratio, and when the structural wall ratio is higher than 1.0%, the interstory drifts above the 2nd story are almost the same.

As can be observed in Figures 5.26(a) and (b), the behavioral shift for 30 story buildings subjected to the Erzincan earthquake occurs at structural wall ratios of approximately 2.0%, indicating that buildings of such height require higher structural wall ratios to undergo behavioral transition when exposed to ground motions with pulse characteristics.

In Figures 5.26(c) through (f), it is observed that the 5 and 10 story buildings subjected to the Erzincan earthquake exhibit trends similar to those under the Christchurch earthquake. However, the interstory drift values are found to be significantly higher for 5 story buildings, particularly at a structural wall ratio of 0.0%, which emphasizes the role of structural walls in the lateral load resisting system.

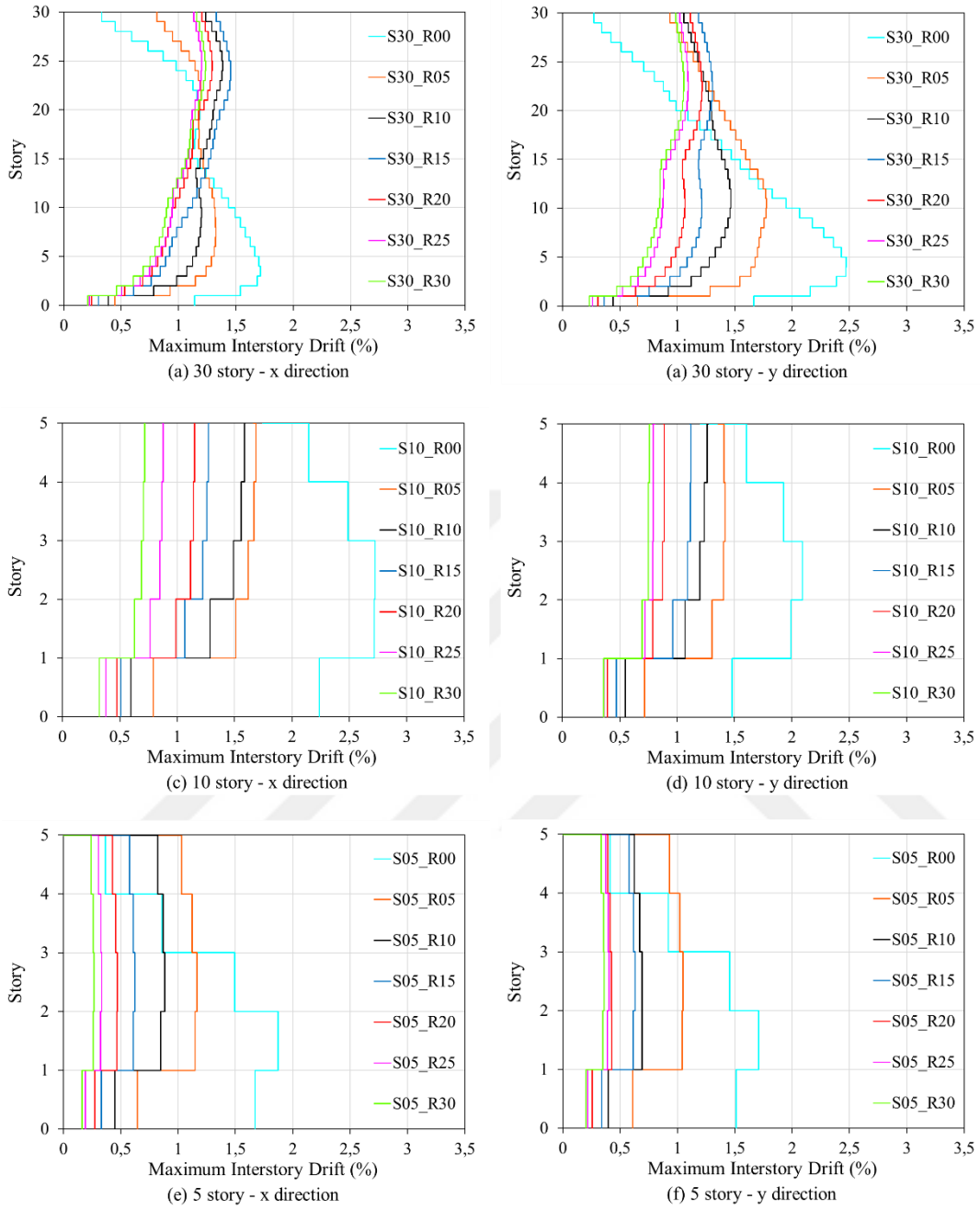


Figure 5.25 Distribution of maximum interstory drift of buildings under the Christchurch Earthquake

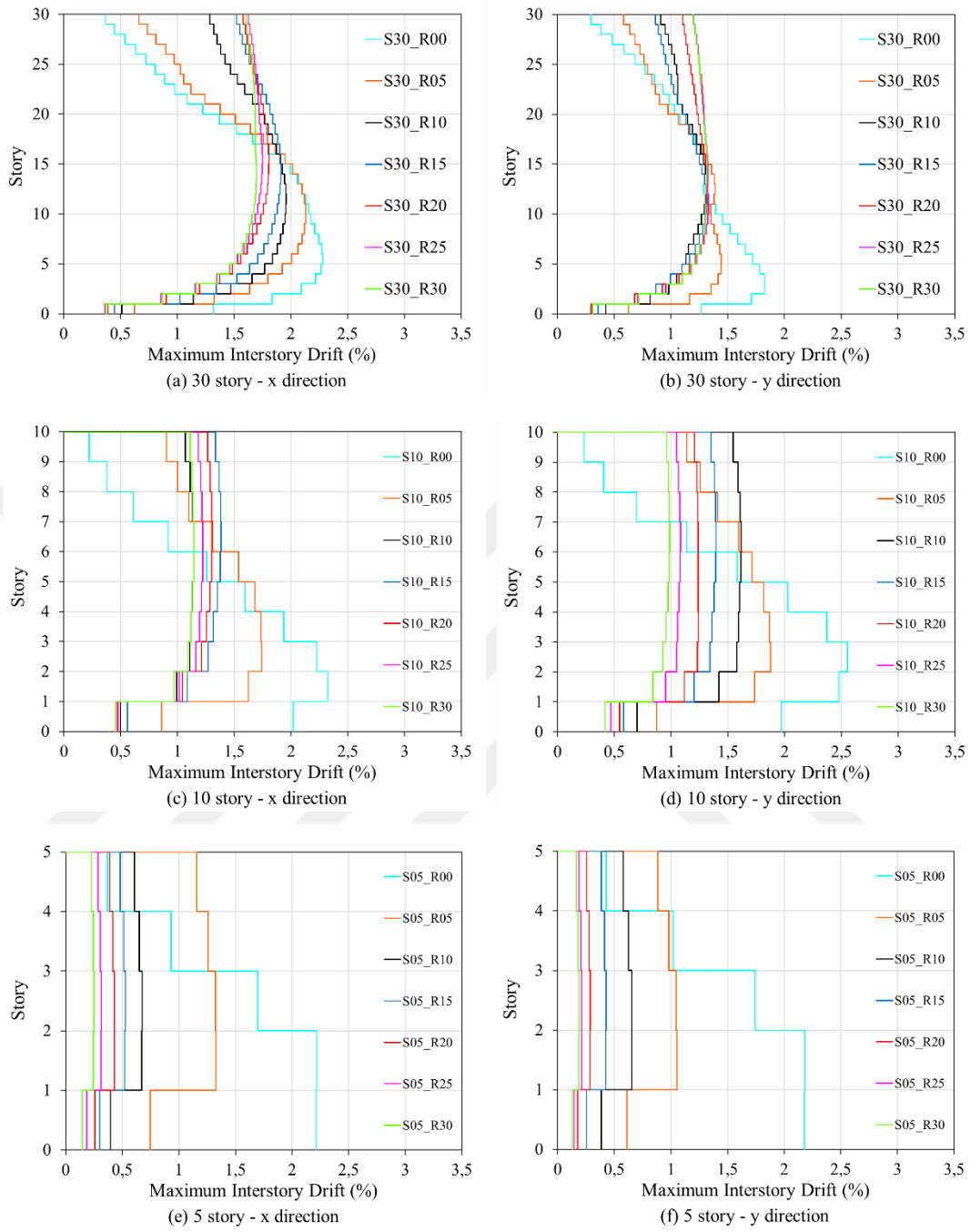


Figure 5.26 Distribution of maximum interstory drift of buildings under the Erzincan Earthquake

5.8 Roof Drift vs. Base Shear Response

The results of the roof drift vs. base shear response for the 30, 10, and 5 story buildings are presented in Figures 5.27-5.29 for the Erzincan Earthquake, and in Figures 5.30-5.32 for the Christchurch Earthquake, respectively. Each figure is composed of nine graphs, (a) through (g), corresponding to structural wall ratios of 0.0%, 0.5%, 1.0%, 1.5%, 2.0%, 2.5%, and 3.0%, respectively.

As can be observed from Figures 5.27 and 5.28, the nonlinear behavior is dominant for all 30 and 10 story buildings with different structural wall ratios under the Erzincan Earthquake and the change in maximum roof drifts with increasing structural wall ratio is negligible. However, a significant increase in stiffness and energy dissipation capacity is observed as the structural wall ratio increases, particularly beyond 2.0% wall ratio.

In Figure 5.29, the response of the 5 story buildings under the Erzincan Earthquake is observed to approach elastic behavior as the structural wall ratio increases beyond 1.0%, indicating a significant reduction in nonlinear response. When 5.29 (c) is compared with 5.29 (a) and (b), a significant reduction in maximum roof drift and a notable increase in rigidity are observed. As the structural wall ratio reaches 1.5%, the behavior of the structure is observed to become almost fully elastic, indicating that a ratio between 1.0% and 1.5% can be considered as efficient for 5 story buildings. Buildings with wall ratios exceeding 1.5% are also observed to behave almost elastically.

In Figure 5.30, for 30 story buildings subjected to the Christchurch Earthquake, the maximum roof displacement remains nearly constant with increasing structural wall ratio up to 1.5%, after which a slight reduction in drift is observed. The rigidity of the buildings is observed to be increasing with higher structural wall ratios, resulting in higher energy dissipation capacity; however, the increase in rigidity becomes negligible beyond a structural wall ratio of 1.5% when compared to lower wall ratios. The nonlinear behavior is dominant throughout all buildings.

In Figure 5.31(a), for the 10 story building with no structural walls, most of the loading cycles overlap, except for a single cycle that comprises the majority of the plastic deformation of the building. As the structural wall ratio increases, the plastic deformations gradually reduce and the structure becomes more rigid.

In Figure 5.32, similar to the results of 5 story buildings under the Erzincan Earthquake, the rigidity of the structures subjected to the Christchurch Earthquake increases significantly at a wall ratio of 1.0% when compared to 0.0%. Beyond 1.5% wall ratio, the nonlinear response of the 5 story buildings becomes noticeably less pronounced compared to that of taller buildings with the same wall ratios.

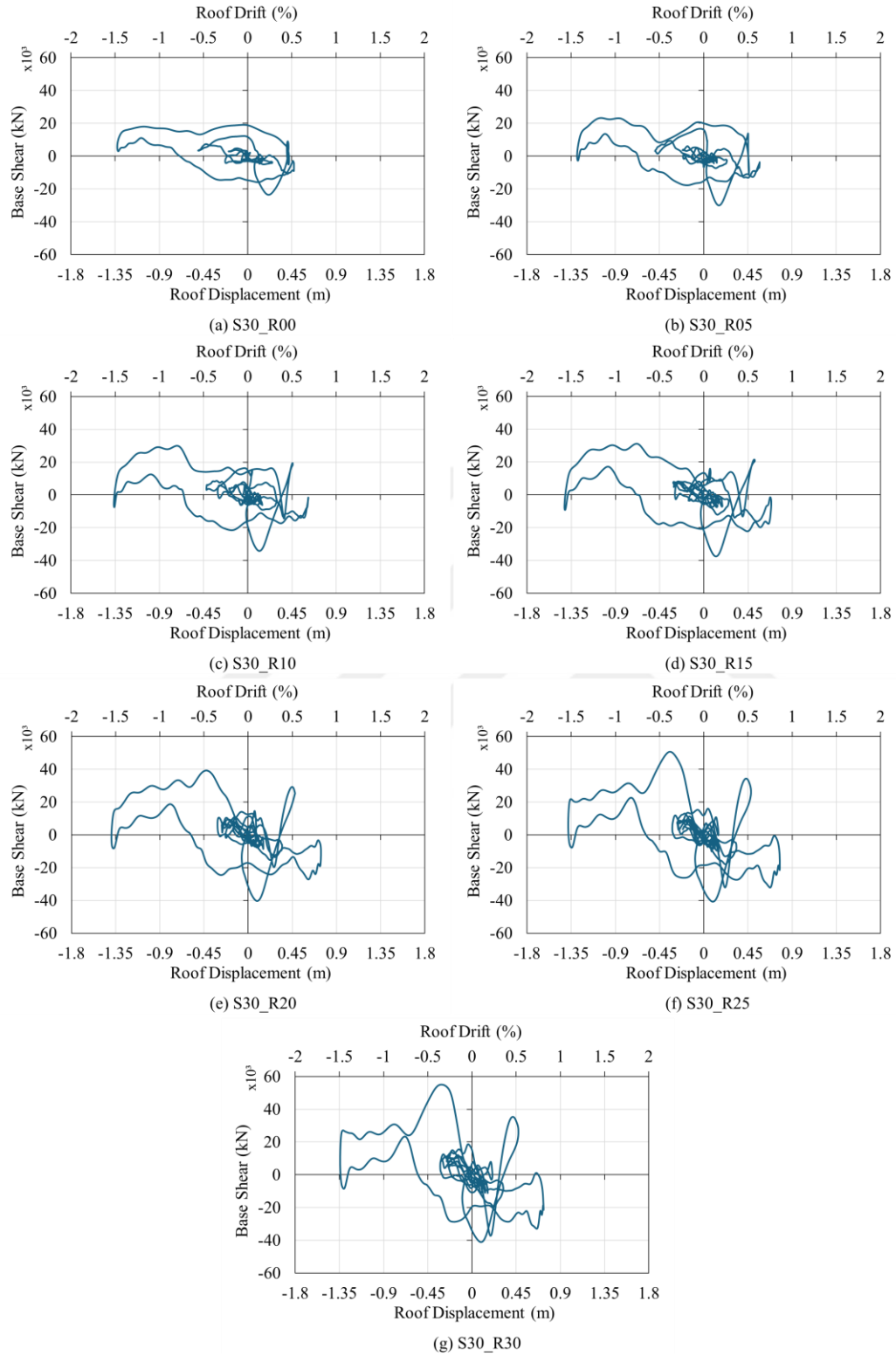


Figure 5.27 Roof drift vs. base shear under the Erzincan Earthquake for 30 story buildings

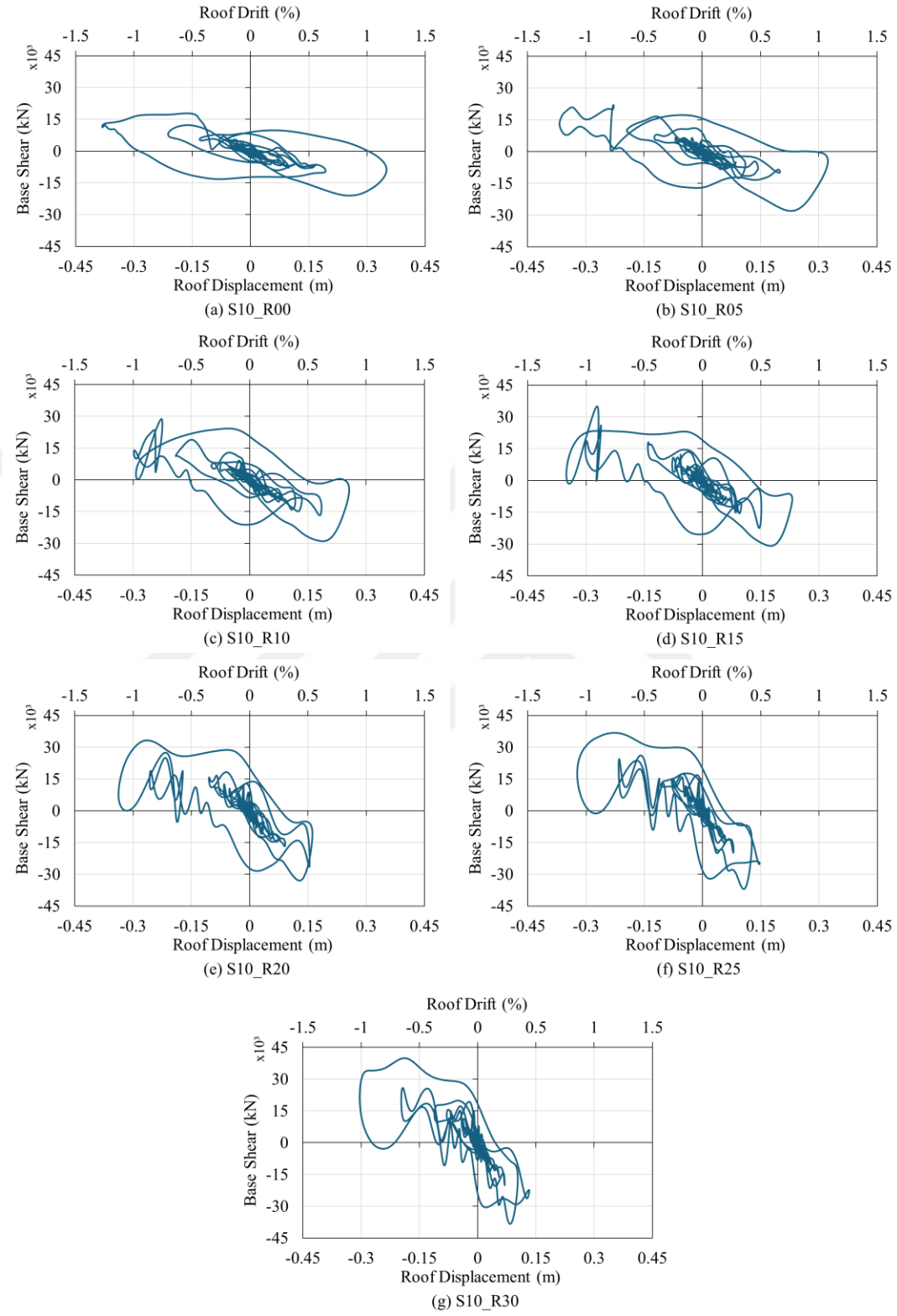


Figure 5.28 Roof drift vs. base shear under the Erzincan Earthquake for 10 story buildings

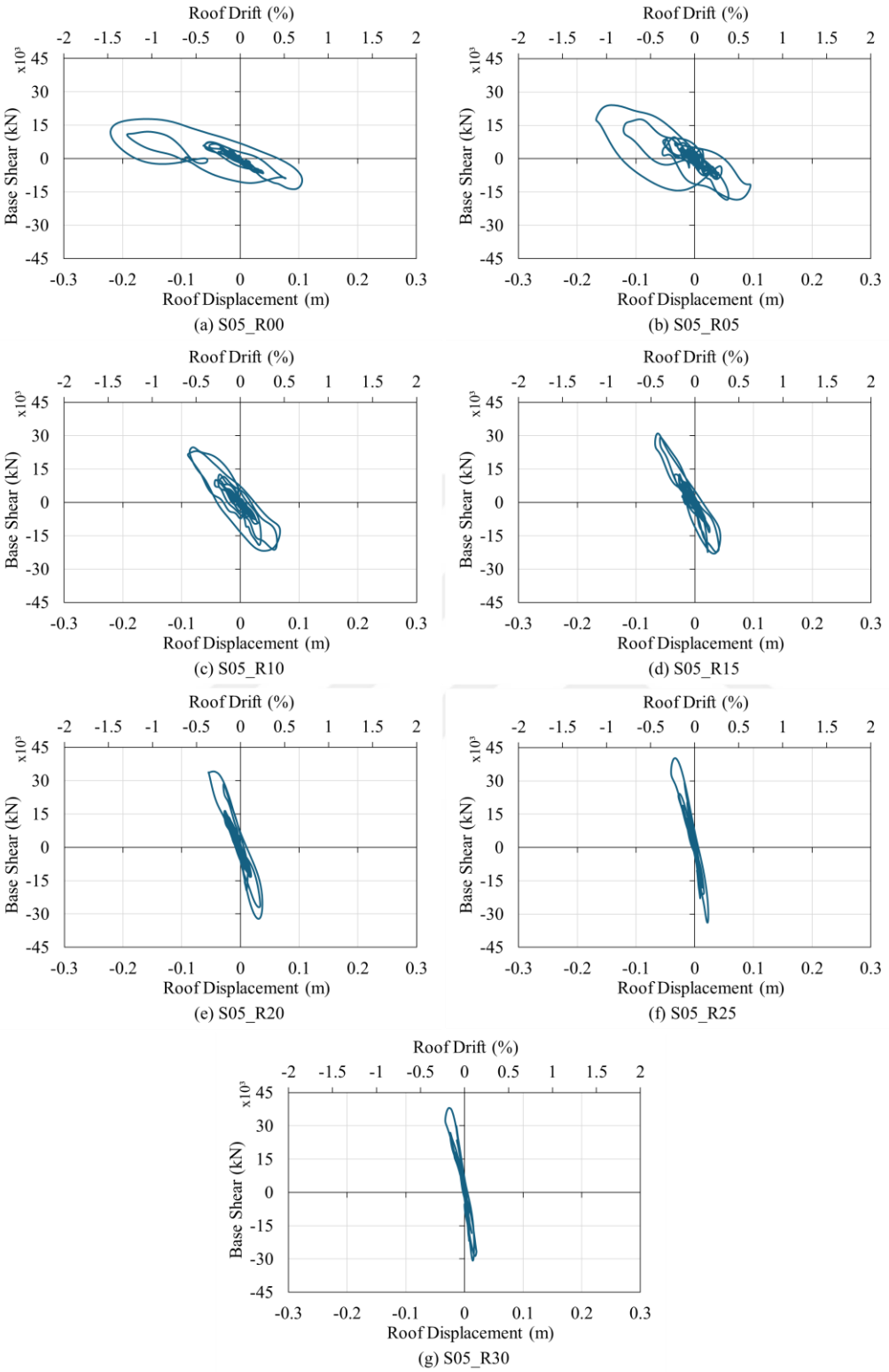


Figure 5.29 Roof drift vs. base shear under the Erzincan Earthquake for 5 story buildings

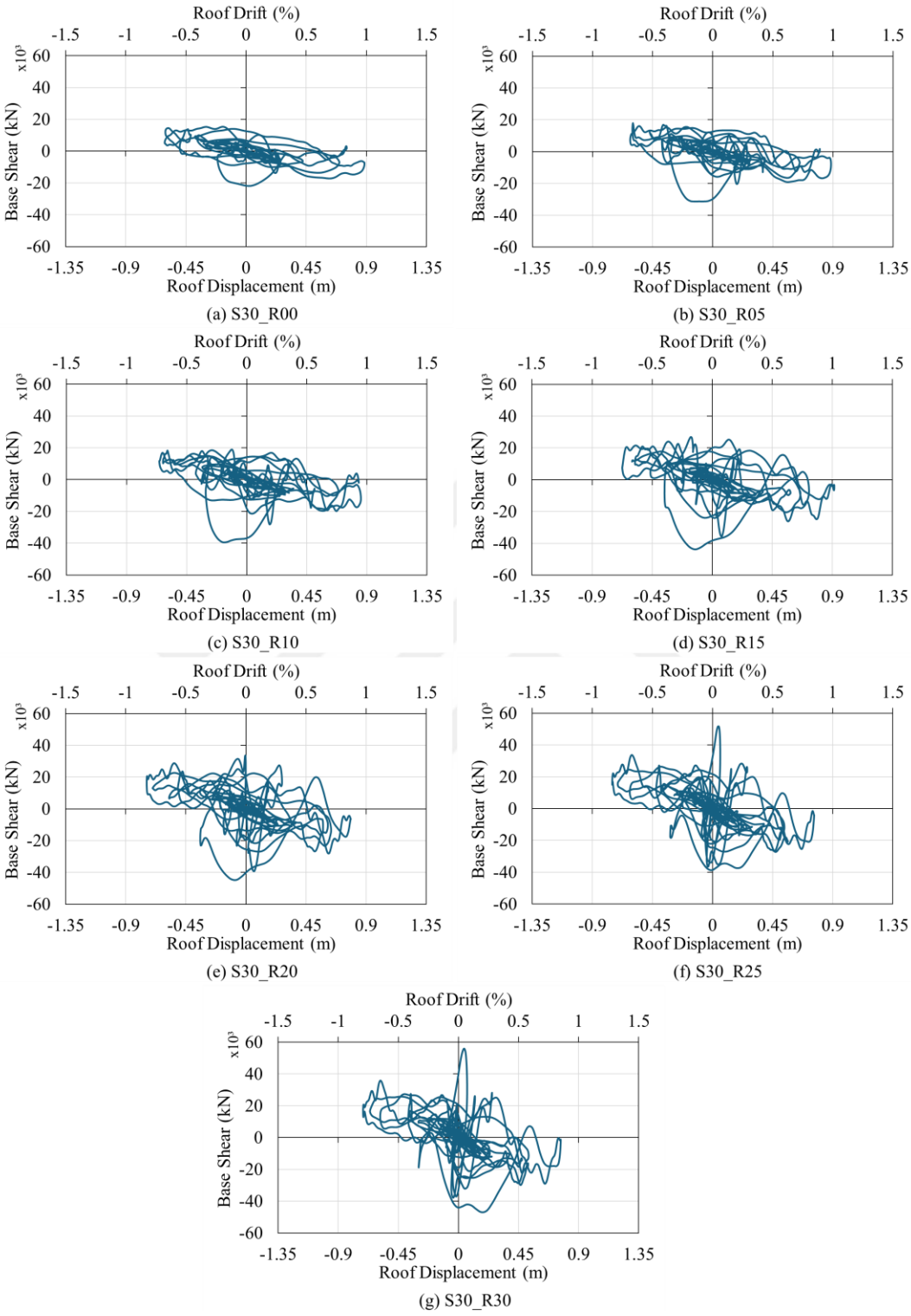


Figure 5.30 Roof drift vs. base shear under the Christchurch Earthquake for 30 story buildings

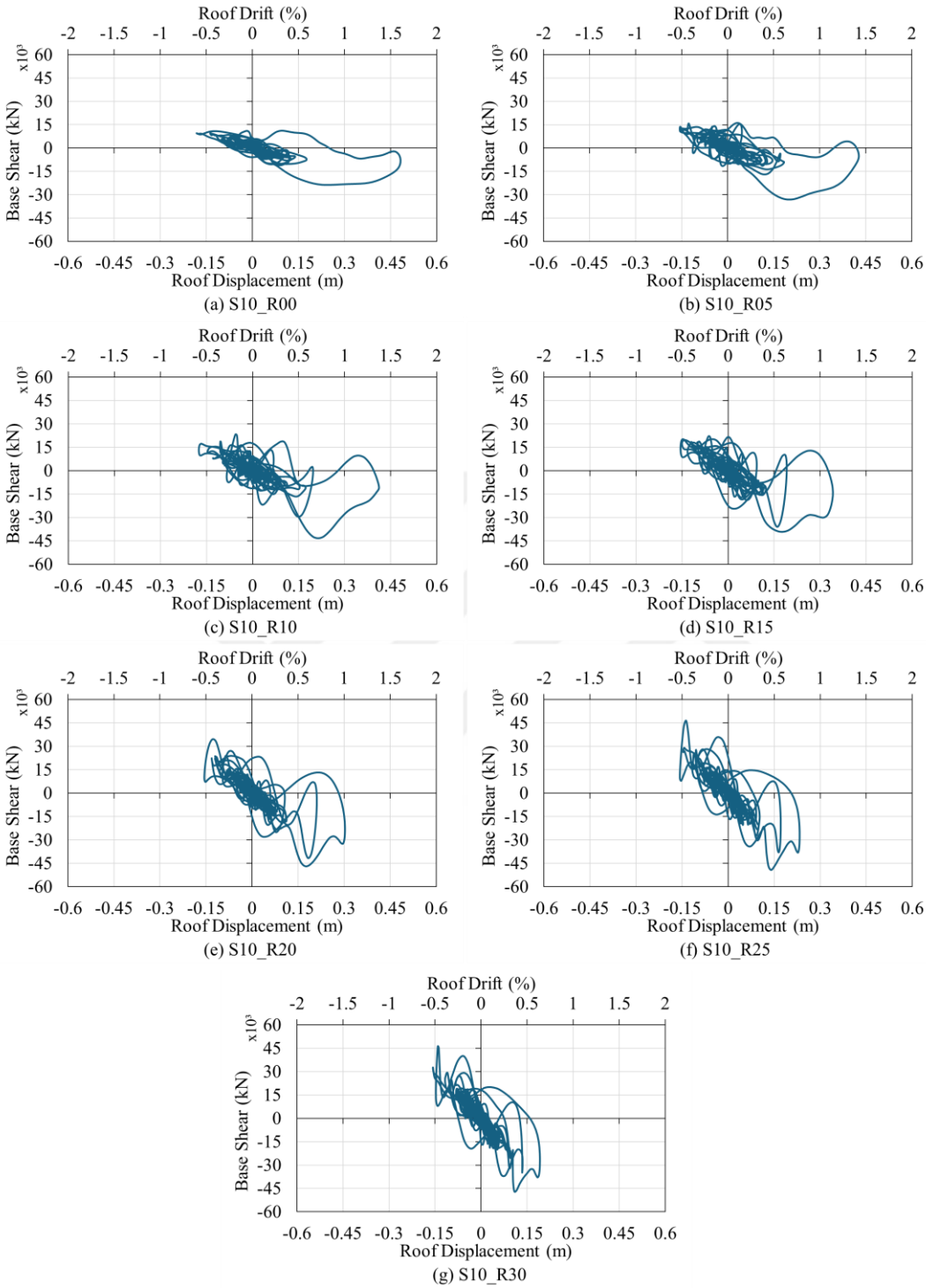


Figure 5.31 Roof drift vs. base shear under the Christchurch Earthquake for 10 story buildings

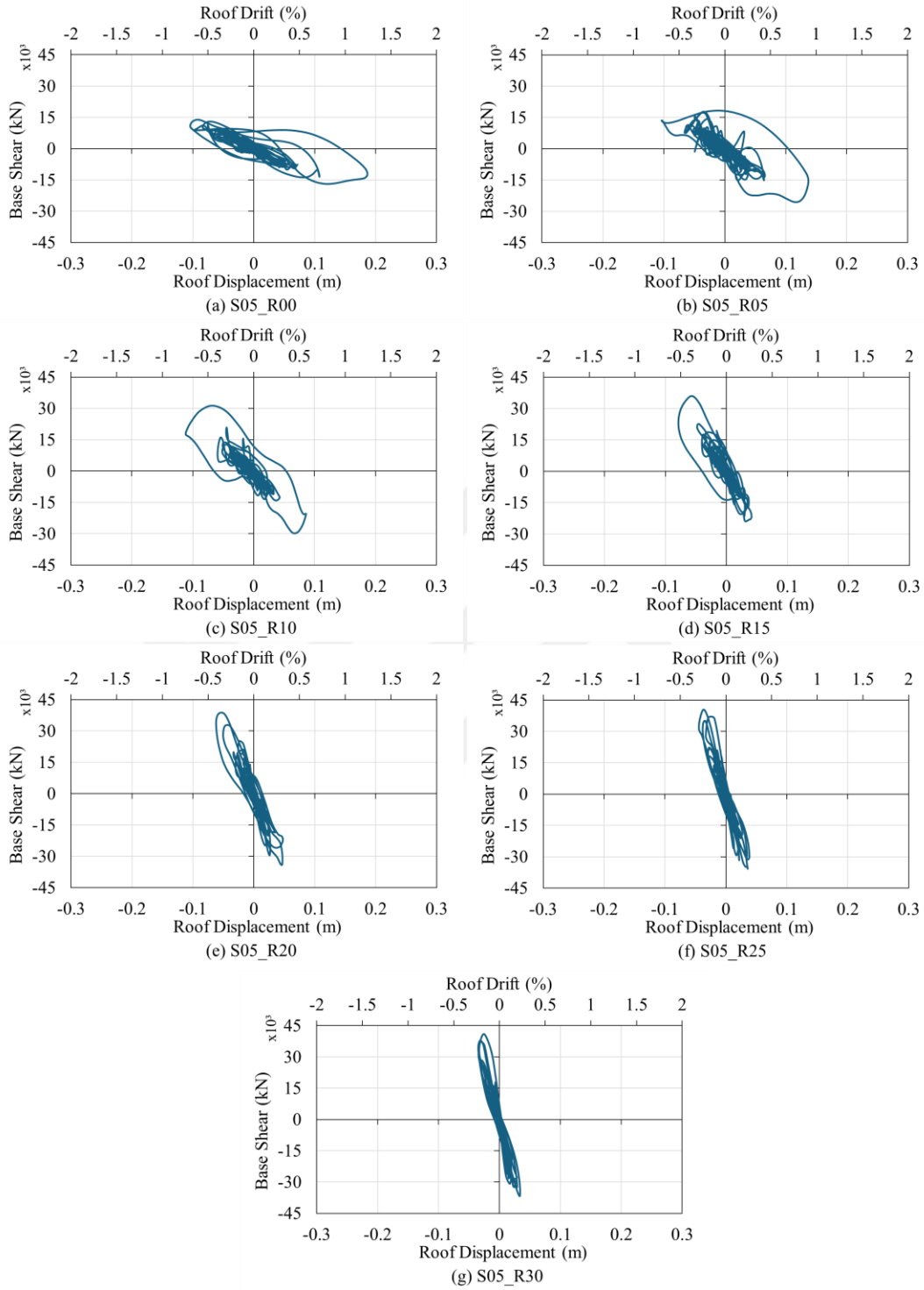


Figure 5.32 Roof drift vs. base shear under the Christchurch Earthquake for 5 story buildings

5.9 Percentage of Members with Reinforcement Yielding

In the time history analyses, M3 moment-curvature hinges are assigned to the beams, while fiber hinges are utilized for the structural walls and columns. For the moment-curvature hinges, the yield point on the moment-curvature response of the beam is defined as the point at which at least one of the steel longitudinal reinforcing bars reaches its yield strain. In the case of structural walls and columns, where fiber hinges are employed, a structural member is considered to be yielded when any of its steel fibers reaches the yield strain.

The percentage of yielded structural walls, beams, and columns at each story for 5 story buildings is presented in Table 5.2, while the percentage of yielded structural members for 7, 10, 20 and 30 story buildings is provided in Appendix D in Tables D.1-D.4. The yielded member percentage is calculated by dividing the total area of yielded members at a given story by the total member area at that story.

When the results of the time history analyses for all buildings are examined, it is observed that, for the case with a structural wall ratio of 0.0%, all beams at each story, except the top story, exhibit yielding in at least one longitudinal reinforcement. For structural wall ratios more than 0.0%, almost all beams at all stories exhibit reinforcement yielding. Therefore, the structural wall ratio or the building height has a minimal influence on the percentage of beams with reinforcement yielding, as this behavior is primarily governed by the strong column-weak beam design principle Only when the overall structural response approaches a fully elastic state, the percentage of beams with reinforcement yielding decreases.

As can be observed from the tables, in the absence of structural walls (0.0% wall ratio), yielding in column bars extends up to the 5th story in the 5, 7, and 10 story buildings (Tables 5.2, D.1 and D.2) and up to the 8th and 12th stories in the 20 and 30 story buildings, respectively (Tables D.3 and D.4), indicating a frame-dominated behavior. As the structural wall ratio increases, yielding in the columns progressively diminishes, while the longitudinal wall reinforcements in the first few stories begin

to yield and eventually structural walls dominate the lateral load resistance mechanism.

In 5, 7 and 10 story buildings, even a low wall ratio (i.e., 0.5%) significantly reduces the yielding of column bars and limit it to the first two stories, while promoting yielding in the walls at the base. For wall ratios above 1.0%, the column bars remain mostly elastic throughout the height, and yielding becomes concentrated in the reinforcing bars of the first story walls, demonstrating an almost fully wall-dominated mechanism (Tables 5.2, D.1 and D.2).

In 20 and 30 story buildings, yielding of column bars is observed at all wall ratios, indicating that the frame action continues to contribute to the overall lateral resistance. However, the yielding of column bars is distributed along the height, while the yielding of wall bars is extended to higher stories, reflecting the significant influence of flexural deformation in taller structures. As the structural wall ratio increases, yielding of the column bars gradually decreases and the lateral load resistance shifts towards the structural walls. Beyond a wall ratio around 2.0%, the contribution of columns to the overall lateral resistance becomes notably limited and the structural response is predominantly governed by the yielding of wall reinforcing bars near the base (Tables D.3 and D.4).

Furthermore, for cases with structural walls, yielding is often concentrated at the top story columns, which can be attributed to the reduced rigidity contribution from walls at higher elevations and the relatively larger story shear demands in those regions, especially for 20 and 30 story buildings. Overall, the results confirm that the introduction of structural walls shifts the resisting mechanism from frame-dominated to wall-dominated behavior, with a corresponding reduction in column yielding and concentration of plasticity in the walls near the base.

Table 5.2 Percentage of members with reinforcement yielding - 5 story buildings

Model	Story	NOR			KOB			KOC			CHI			DUZ			SM			LOM			CC			ERZ			LAN			IMP		
		W	C	B	W	C	B	W	C	B	W	C	B	W	C	B	W	C	B	W	C	B	W	C	B	W	C	B	W	C	B	W	C	B
S05_R00	1	-	100	100	-	100	100	-	100	100	-	100	100	-	100	100	-	100	100	-	100	100	-	100	100	-	100	100	-	100	100	-	100	100
	2	-	81	100	-	0	100	-	0	100	-	0	100	-	36	100	-	94	100	-	25	100	-	22	100	-	94	100	-	89	100	-	94	100
	3	-	94	100	-	33	100	-	67	100	-	39	100	-	92	100	-	94	100	-	92	100	-	94	100	-	100	100	-	94	100	-	100	100
	4	-	56	100	-	0	100	-	0	100	-	0	100	-	78	100	-	81	100	-	75	100	-	83	100	-	100	100	-	81	100	-	94	100
	5	-	0	3	-	0	0	-	0	0	-	0	0	-	0	30	-	0	5	-	0	0	-	0	0	-	0	0	-	0	0	-	0	0
S05_R05	1	100	100	100	100	60	100	100	23	100	100	37	100	100	50	100	100	57	100	100	100	100	100	83	100	100	100	100	100	100	100	100	100	100
	2	25	3	100	0	0	100	0	0	100	0	0	100	0	0	100	25	10	100	25	37	100	0	0	100	0	80	100	0	97	100	0	7	100
	3	0	0	100	0	0	100	0	0	100	0	0	100	0	0	100	0	0	100	0	0	100	0	0	100	0	0	100	0	0	100	0	0	100
	4	0	0	100	0	0	100	0	0	100	0	0	100	0	0	100	0	0	100	0	0	100	0	0	100	0	0	100	0	0	100	0	0	100
	5	0	77	100	0	67	100	0	63	96	0	13	100	0	67	100	0	77	100	0	93	100	0	53	100	0	93	100	0	93	100	0	87	100
S05_R10	1	100	0	96	100	0	100	100	0	100	100	0	100	100	0	98	100	17	100	100	4	100	100	0	100	100	0	100	100	38	100	100	29	100
	2	13	0	98	0	0	100	0	0	100	0	0	100	0	0	100	0	0	100	0	0	100	0	0	100	0	0	100	0	0	100	0	0	100
	3	0	0	96	0	0	100	0	0	100	0	0	100	0	0	100	0	0	100	0	0	100	0	0	100	0	0	100	0	0	100	0	0	100
	4	0	0	96	0	0	100	0	0	100	0	0	100	0	0	100	0	0	100	0	0	100	0	0	100	0	0	100	0	0	100	0	0	100
	5	0	8	96	0	17	87	0	4	83	0	4	92	0	8	90	0	75	94	0	29	92	0	17	94	0	0	90	0	79	94	0	63	100

Table 5.2 Percentage of members with reinforcement yielding - 5 story buildings (cont'd)

Model	Story	NOR			KOB			KOC			CHI			DUZ			SM			LOM			CC			ERZ			LAN			IMP		
		W	C	B	W	C	B	W	C	B	W	C	B	W	C	B	W	C	B	W	C	B	W	C	B	W	C	B	W	C	B	W	C	B
S05_R15	1	100	0	92	100	0	90	100	0	92	100	0	85	100	0	98	100	0	100	100	0	96	100	0	96	100	0	90	100	6	98	100	0	100
	2	0	0	100	0	0	94	0	0	98	0	0	96	0	0	100	0	0	100	0	0	98	0	0	100	0	0	92	0	0	98	0	0	100
	3	0	0	100	0	0	94	0	0	98	0	0	96	0	0	100	0	0	100	0	0	96	0	0	100	0	0	92	0	0	96	0	0	100
	4	0	0	96	0	0	92	0	0	98	0	0	96	0	0	100	0	0	100	0	0	96	0	0	100	0	0	92	0	0	96	0	0	100
	5	0	0	85	0	0	44	0	0	71	0	0	69	0	0	88	0	0	88	0	0	92	0	6	88	0	0	77	0	56	94	0	0	88
S05_R20	1	100	0	82	100	0	43	100	0	77	100	0	43	100	0	95	100	0	89	100	0	86	100	0	95	100	0	57	100	0	91	100	0	98
	2	0	0	93	0	0	57	0	0	95	0	0	61	0	0	100	0	0	95	0	0	93	0	0	98	0	0	68	0	0	95	0	0	100
	3	0	0	93	0	0	57	0	0	93	0	0	64	0	0	100	0	0	95	0	0	93	0	0	98	0	0	68	0	0	95	0	0	100
	4	0	0	93	0	0	57	0	0	93	0	0	64	0	0	100	0	0	95	0	0	93	0	0	98	0	0	64	0	0	95	0	0	100
	5	0	0	66	0	0	39	0	0	64	0	0	32	0	0	89	0	0	80	0	0	73	0	0	91	0	0	48	0	0	80	0	0	93
S05_R25	1	90	0	30	0	0	0	100	0	48	90	0	15	100	0	80	100	0	80	100	0	58	100	0	75	90	0	28	100	0	50	100	0	58
	2	0	0	33	0	0	0	0	0	55	0	0	25	0	0	95	0	0	90	0	0	70	0	0	95	0	0	45	0	0	65	0	0	78
	3	0	0	30	0	0	0	0	0	55	0	0	25	0	0	90	0	0	88	0	0	65	0	0	95	0	0	43	0	0	68	0	0	78
	4	0	0	30	0	0	0	0	0	55	0	0	25	0	0	90	0	0	88	0	0	65	0	0	95	0	0	43	0	0	70	0	0	78
	5	0	0	20	0	0	0	0	0	35	0	0	15	0	0	58	0	0	63	0	0	43	0	0	65	0	0	23	0	0	43	0	0	48
S05_R30	1	46	-	0	0	-	0	100	-	53	0	-	0	96	-	58	100	-	72	100	-	50	100	-	67	79	-	28	92	-	42	100	-	44
	2	0	-	17	0	-	0	0	-	61	0	-	0	0	-	72	0	-	81	0	-	56	0	-	72	0	-	39	0	-	47	0	-	50
	3	0	-	17	0	-	0	0	-	61	0	-	3	0	-	75	0	-	81	0	-	56	0	-	72	0	-	44	0	-	50	0	-	53
	4	0	-	19	0	-	0	0	-	64	0	-	6	0	-	75	0	-	78	0	-	56	0	-	72	0	-	44	0	-	53	0	-	53
	5	0	-	6	0	-	0	0	-	53	0	-	0	0	-	53	0	-	61	0	-	47	0	-	56	0	-	31	0	-	39	0	-	39

Note: NOR = Northridge; KOB = Kobe; KOC = Kocaeli; CHI = Chi Chi; DUZ = Duzce; SM = Sierramex; LOM = Loma prieta; CC = Christchurch; ERZ = Erzincan; LAN = Landers; IMP = Imperial Valley; W = Structural wall; C = Column; B = Beam

CHAPTER 6

SUMMARY AND CONCLUSIONS

6.1 Summary

In this study, the effect of the structural wall area to floor area ratio on the seismic performance of mid to high rise reinforced concrete buildings is investigated. First, a five story frame building without structural walls is modeled and designed in accordance with TS500 (2000), TBEC-2018, ACI 318-19, ASCE 41-23 and ASCE 7-22 requirements. In order to prevent failure even for 30 story buildings, the transverse reinforcement ratio in the columns is intenionally increased to enhance the confinement effect, ensuring that the columns can sustain the increased gravity load demands. Then, without altering the material properties, member dimensions, or reinforcement detailing, structural walls are added and the number of stories is increased to generate 35 buildings, representing the combination of seven structural wall ratios (0.0%, 0.5%, 1.0%, 1.5%, 2.0%, 2.5%, 3.0%) and five building heights (5, 7, 10, 20, and 30 stories).

The reliability of the selected software and the user defined nonlinear modeling approach is validated through comparison with two experimental studies: one investigating a cantilever structural wall and the other a full scale building. Following this validation, eleven nonlinear time history analyses are conducted on each of the 35 generated buildings using the widely adopted commercial software ETABS v22.4.0 (Computers and Structures Inc. [CSI], 2024).

The variation of roof drift, maximum interstory drift, distribution of maximum interstory drifts, base and story shear forces, base shear vs. roof drift response, percentage of shear force carried by structural walls and percentage of members with reinforcement yielding as the structural wall ratio increases is discussed for all buildings with different number of stories.

6.2 Conclusions

Based on the results of the nonlinear analyses, the following conclusions are drawn:

- Even a structural wall ratio as low as 0.5% reduces the percentage of base shear force carried by columns by more than half. As the structural wall ratio increases, the base shear force resisted by structural walls also increases, although the rate of increase gradually diminishes and becomes significantly less pronounced beyond a structural wall ratio of approximately 1.5%. When the floor plan remains the same, the influence of the number of stories, or overall building height, on the percentage of base shear carried by structural walls is negligible.
- Story shear forces increase with building height due to higher building weight and further rise with increased structural wall ratios as a result of enhanced lateral rigidity. In 5, 7 and 10 story buildings, story shear forces gradually reduce toward the upper stories for all structural wall ratios. However, in 20 and 30 story buildings, as the structural wall ratio increases, shear forces observed in upper stories (stories 10-15 for 20 story buildings and 20-25 for 30 story buildings) are higher compared to lower stories. This behavior is attributed to the substantial rigidity provided by structural walls at the base and their reduced effectiveness at higher elevations, which limits the reduction of lateral forces, combined with increased modal participation in the upper stories, resulting in a whiplash effect.
- As the structural wall ratio increases, the average maximum roof drifts decrease for 5, 7 and 10 story buildings. For frame buildings of these heights without structural walls (0.0% structural wall ratio), the observed average maximum roof drifts are quite similar. However, with increasing structural wall ratio, the reduction in roof drift becomes less pronounced as building height increases. The roof drift results of 5 story buildings exhibit an asymptotic trend, with the effect of increasing structural wall ratio on roof

drift gradually diminishing. In contrast, the trend of reduction in roof drift for 7 and 10 story buildings is closer to linear. For 20 and 30 story buildings, the influence of increasing structural wall ratios on roof drift differs from that of 5, 7 and 10 story buildings. Considering the average results of all earthquake records, a minimal increase in roof drift is observed up to a 1.0% structural wall ratio, while beyond this ratio, roof drifts decrease, but the reduction is considerably lower compared to the 5, 7 and 10 story buildings. When the average results of only near fault earthquakes are considered, the ineffectiveness of increasing structural wall ratio in reducing roof drifts of 20 and 30 story buildings becomes even more pronounced. This indicates that the number of near fault records in a selected set of ground motions can significantly affect the average seismic response results.

- The maximum interstory drift asymptotically decreases with increasing structural wall ratio for all building heights. The reduction in maximum interstory drift for 5, 7 and 10 story buildings is more pronounced compared to 20 and 30 story buildings. For all building heights, the rate of reduction beyond a structural wall ratio of approximately 1.0-1.5% is significantly smaller compared to lower wall ratios. As expected, interstory drifts observed for near fault records are higher than those observed for far field records, highlighting the importance of the proportion of near fault records within a selected ground motion set in shaping the average structural response.
- The roof drift and interstory drift results for 20 and 30 story buildings contradict each other. Although increasing the structural wall ratio leads to very limited or no reduction in roof drift, a clear reduction is observed in interstory drift. Since local damage in structural members is more closely associated with the relative displacement between two consecutive stories rather than overall roof displacement, roof drift is considered to be a misleading parameter for predicting structural damage for buildings of these heights. This behavior is also attributed to the significant contribution of higher modes in tall buildings.

- The increase in structural wall ratio causes the interstory drift demand to shift from the lower stories toward the higher stories, while the interstory drift distribution becomes more uniform. As the wall ratio is increased, the overall structural behavior of the buildings is observed to transition from frame-dominated behavior to cantilever structural wall-dominated behavior. For 5, 7 and 10 story buildings, a structural wall ratio of approximately 1.0% is adequate to induce the behavioral transition, whereas 20 and 30 story buildings require approximately 1.5-2.0% structural wall ratio to exhibit similar behavior.
- In roof drift vs. base shear response, a significant increase in stiffness and energy dissipation capacity is observed as the structural wall ratio increases, for 10, 20 and 30 story buildings, particularly beyond 2.0% wall ratio. In these buildings, nonlinear behavior is dominant across all structural wall ratios. For 5 and 7 story buildings, however, the nonlinear response significantly reduces beyond 1.0% structural wall ratio, while the building behavior is remarkably closer to linear elastic after 2.0% wall ratio. The roof drift vs. base shear response of 5 and 7 story buildings resembles that of a single degree of freedom system (SDOF), whereas the response of the 10, 20 and 30 story buildings is more dispersed and deviates significantly from SDOF like behavior, validating the significant contribution of higher modes.
- In all buildings, almost all beams at each story exhibit reinforcing bar yielding, consistent with the strong column-weak beam design principle. In 5, 7 and 10 story buildings, even a small wall ratio of 0.5% significantly reduces the yielding of column bars to the first few stories, while promoting bar yielding in the walls at the base. For wall ratios beyond 1.0%, the column bars remain mostly elastic throughout the height and yielding becomes concentrated in the reinforcing bars of the first story walls, demonstrating a wall-dominated mechanism. In 20 and 30 story buildings, the yielding of column bars is more scattered across the height for all structural wall ratios, reflecting the greater influence of flexural deformation at higher elevations

in tall structures. Beyond the wall ratio of 2.0%, the contribution of columns to the overall lateral resistance becomes notably limited and structural wall response is governed by the yielding of wall reinforcing bars near the base.

- The structural wall ratio of 1.0% is highly effective in reducing the maximum interstory drifts across all buildings. Considering the interstory drift distributions, roof drift vs. base shear responses, and the percentage of members exhibiting reinforcement yielding, 1.0% wall ratio is sufficient to shift the behavior of the 5, 7 and 10 story buildings from frame-dominated to cantilever wall-dominated behavior. In contrast, achieving a similar behavioral transition in 20 and 30 story buildings requires a structural wall ratio of at least 1.5% for far field earthquakes, with the required ratio of 2.0% for near fault earthquakes.

6.3 Future Research Recommendations

- The beam-column connections are assumed to be rigid. Panel zone models can be implemented to improve the accuracy of the connection behavior in the analytical models.
- Shear-flexure interaction in structural walls is not considered in the fiber hinge models. Incorporating this interaction can yield more realistic results, particularly under shear failure conditions.
- The aspect ratio of the structural walls is kept constant throughout all analyses. The effect of the structural wall area to floor area ratio on seismic performance could be further examined using walls with varying aspect ratios.
- The influence of different structural wall configurations on the seismic performance is not evaluated in this study. Future research may examine buildings of buildings with various wall layouts while maintaining a constant structural wall ratio.

- The seismic performance of the analyzed buildings is highly sensitive to the selected ground motion records. Additional analyses can be performed using ground motion records with different frequency content and intensity characteristics.
- Rectangular, L-shaped, and box shaped structural walls are used in this study. The influence of other wall configurations, such as C-shaped or H-shaped walls, can also be investigated.
- The maximum number of stories analyzed is limited to 30 in this study. Given the trend of increasing building heights in real world applications, the behavior of taller buildings can be studied in future research.
- Vertical components of ground motion are not considered in this study. Including vertical excitations may improve the accuracy of the results.
- Soil-structure interaction is not considered and the supports are idealized as infinitely rigid. This assumption can be refined by modeling the interaction using spring elements, allowing for a more detailed representation of different soil conditions beyond their influence on the target response spectrum.
- Torsional and vertical irregularities, soft or weak story mechanisms, and openings in structural walls are intentionally avoided in all building models. Future studies may investigate the seismic performance of buildings incorporating such irregularities.

REFERENCES

Abdullah, S. A. (2019). Reinforced concrete structural walls: Test database and modeling parameters. University of California, Los Angeles.

Aejaz, B. A., & Wight, J. K. (1991). RC Structural Walls with Staggered Door Openings. Journal of Structural Engineering, 117(5), 1514–1531. https://doi.org/10.1061/(ASCE)0733-9445(1991)117:5(1514)

Aktan, A. E., & Bertero, V. v. (1984). Seismic Response of R/C Frame-Wall Structures. Journal of Structural Engineering, 110(8). https://doi.org/10.1061/(asce)0733-9445(1984)110:8(1803)

Alam, T., Banerjee, R., Mahadeven, V., Gupta, N., & Parashar, A. K. (2024). Assessment of shear wall quantity on seismic performance of high-rise building. Asian Journal of Civil Engineering, 25, 3815–3822. https://doi.org/10.1007/s42107-024-01013-z

American Concrete Institute. (2019). Building code requirements for structural concrete (ACI 318-19) and commentary (ACI 318R-19). American Concrete Institute.

American Concrete Institute. (2019). Building code requirements for structural concrete (ACI 318-19) and commentary (ACI 318R-19).

American Society of Civil Engineers. (2022). Minimum design loads and associated criteria for buildings and other structures (ASCE/SEI 7-22).

American Society of Civil Engineers. (2023). Seismic evaluation and retrofit of existing buildings (ASCE/SEI 41-23).

American Society of Civil Engineers. (2023). Seismic evaluation and retrofit of existing buildings (ASCE/SEI 41-23).

Aniket, W., Nijagunappa, K., … L. P.-… R. J. of, & 2018, undefined. (2018). Analysis of RC Structure With and Without Shear Wall and Optimum Location of Shear Wall. Academia.EduW Aniket, K Nijagunappa, L Pranav, S Kanhaiyya, P Krishnakant, BM MalagimaniInternational Research Journal of Engineering and Technology (IRJET), 2018•academia.Edu. https://www.academia.edu/download/57068052/IRJET-V5I627.pdf

Binici, B., Yakut, A., Kadas, K., Demirel, O., Akpinar, U., Canbolat, A., Yurtseven, F., Oztaskin, O., Aktas, S., & Canbay, E. (2023). Performance of RC buildings after Kahramanmaraş Earthquakes: lessons toward performance based design. Earthquake Engineering and Engineering Vibration, 22(4). https://doi.org/10.1007/s11803-023-2206-8

Burak, B., & Comlekoglu, H. G. (2013). Effect of shear wall area to floor area ratio on the seismic behavior of reinforced concrete buildings. Journal of Structural Engineering, 139(11), 1928-1937.

Cervenka, V., Rimkus, A., Gribniak, V., & Cervenka, J. (2022). Simulation of the crack width in reinforced concrete beams based on concrete fracture. Theoretical and Applied Fracture Mechanics, 121, 103428. https://doi.org/10.1016/J.TAFMEC.2022.103428

Chen, S., & Kabeyasawa, T. (2000). Modeling of Reinforced Concrete Shear Wall for Nonlinear Analysis. 12WCEE, Twelfth World Conference on Earthquake Engineering, New Zealand, 1596.

Chen, S., Matsumori, T., & Kabeyasawa, T. (2007). Simulation of the six-story full-scale wall-frame test. Ascelibrary.OrgS Chen, T Matsumori, T KabeyasawaStructural Engineering Research Frontiers, 2007•ascelibrary.Org. https://doi.org/10.1061/40944(249)9

Clough, R. W., Benuska, K. L., & Wilson, E. L. (1965). Inelastic earthquake response of tall buildings. In Proceedings of the third world conference on earthquake engineering (Vol. 2, pp. 68–84). New Zealand National Committee on Earthquake Engineering.

Colotti, V. (1993). Shear Behavior of RC Structural Walls. Journal of Structural Engineering, 119(3). https://doi.org/10.1061/(asce)0733-9445(1993)119:3(728)

Computers and Structures, Inc. (2024). ETABS (Version 22.4.0) [Computer software]. https://www.csiamerica.com/products/etabs

CRED. (2023). EM-DAT: The International Disaster Database. Université catholique de Louvain. https://emdat.be

Dahesh, M. A., Tuken, A., & Siddiqui, N. A. (2015). Controlling the earthquake-induced lateral displacement of RC buildings using shear walls: Parametric study. Arabian Journal of Geosciences, 8(8), 5929–5939. https://doi.org/10.1007/s12517-014-1635-0

Dahlblom, O., mechanics, N. O.-J. of engineering, & 1990, undefined. (1990). Smeared crack analysis using generalized fictitious crack model. Ascelibrary.OrgO Dahlblom, NS OttosenJournal of Engineering Mechanics, 1990•ascelibrary.Org, 116(1), 55–76. https://doi.org/10.1061/(ASCE)0733-9399(1990)116:1(55)

Dere, Y. (2017). Assessing a Retrofitting Method for Existing RC Buildings with Low Seismic Capacity in Turkey. Journal of Performance of Constructed Facilities, 31(2), 04016098.

Disaster and Emergency Management Authority [AFAD]. (2023). 06 Şubat 2023 Pazarcık-Elbistan (Kahramanmaraş) Mw: 7.7 – Mw: 7.6 depremleri raporu [Report on the February 6, 2023 Pazarcık-Elbistan (Kahramanmaraş) Mw: 7.7 – Mw: 7.6 earthquakes]. https://deprem.afad.gov.tr/assets/pdf/Kahramanmaraş%20Depremi%20%20Ra poru_02.06.2023.pdf

Disaster and Emergency Management Presidency. (2018). Türkiye bina deprem yönetmeliği [Turkish building earthquake code].

Fintel, M. (1995). Performance of buildings with shear walls in earthquakes of the last thirty years. PCI Journal, 40(3), 62–80. https://doi.org/10.15554/PCIJ.05011995.62.80

Fischinger, M. A. T. E. J., Vidic, T. O. M. A. Z., & Fajfar, P. (1992). Nonlinear Seismic Analysis of Structural Walls Using the Multiple-Vertical-Line-Element Model' (pp. 191-202). Elsevier Science Publishers Ltd, London and New York.

Giberson, M. F. (1969). Two Nonlinear Beams With Definitions of Ductility. Journal of the Structural Division, 95(2). https://doi.org/10.1061/jsdeag.0002184

Gulkan, P., & Utkutug, D. (2003). Okul binalarının deprem güvenliği için minimum dizayn kriterleri [Minimum design criteria for earthquake safety of school buildings]. Türkiye Mühendislik Haberleri, 425, 13–22.

Gullu, M. F., Orakcal, K., & Kolozvari, K. (2019). The fixed-strut-angle finite element (FSAFE) model for reinforced concrete structural walls. Bulletin of Earthquake Engineering, 17(12), 6463–6489.

Günel, A. O. (2013). Influence of the Shear Wall Area to Floor Area Ratio on the Seismic Performance of Existing Reinforced Concrete Buildings (Order No. 31670149). Available from ProQuest Dissertations & Theses Global. (3122726547). https://www.proquest.com/dissertations-theses/influence-shear-wall-area-floor-ratio-on-seismic/docview/3122726547/se-2

Hassan, A. F., & Sozen, M. A. (1997). Seismic vulnerability assessment of low-rise buildings in regions with infrequent earthquakes. ACI structural journal, 94(1), 31-39.

Hognestad, E., Hanson, N. W., & McHenry, D. (1955). Concrete stress distribution in ultimate strength design. ACI Journal Proceedings, 52(4), 455–479.

Institution of Structural Engineers. (2019). 1985 Mexico City earthquake: EEFIT reconnaissance report (Report No. EEFIT/2019/0809). Institution of Structural Engineers.

Johnson, K., Villani, M., Bayliss, K., Brooks, C., Chandrasekhar, S., Chartier, T., Chen, Y., Garcia-Pelaez, J., Gee, R., Styron, R., Rood, A., Simionato, M., & Pagani, M. (2023). Global Earthquake Model (GEM) seismic hazard map (version 2023.1 - June 2023). GEM Foundation. https://doi.org/10.5281/zenodo.8409647

Kaba, S. A., & Mahin, S. A. (1983). Interactive computer analysis methods for predicting the inelastic cyclic behavior of structural sections. https://nehrpsearch.nist.gov/static/files/NSF/PB84192012.pdf

Kabeyasawa, T., & Matsumoto, K. (1995). Tests and analyses of T-shaped shear walls. Proceedings of the Japan Concrete Institute, 17(2), 1195–1200.

Khelaifia, A., Zine, A., Guettala, S., & Chebili, R. (2024). Assessment of the position and quantity of shear walls their correlation with building height on the seismic nonlinear performance. Asian Journal of Civil Engineering, 25(8), 5925–5937.

Khelaifia, A., Zine, A., Guettala, S., & Chebili, R. (2024). Optimizing building designs: A comprehensive study on shear wall positioning, ratios, and height correlation. Asian Journal of Civil Engineering, 25, 2685–2703. https://doi.org/10.1007/s42107-023-00947-0

Khelaifia, L., Chebili, R., & Zine, A. (2023). Effect of shear wall arrangement and ratio on the seismic performance of RC buildings. Asian Journal of Civil Engineering, 24(5), 1485–1499.

Kolozvari, K., Orakcal, K., Structural, J. W.-J. of, & 2015, undefined. (2015). Modeling of cyclic shear-flexure interaction in reinforced concrete structural walls. I: Theory. Ascelibrary.OrgK Kolozvari, K Orakcal, JW WallaceJournal of Structural Engineering, 2015•ascelibrary.Org, 141(5). https://doi.org/10.1061/(ASCE)ST.1943-541X.0001059

Lai, S., Will, G. T., & Otani, S. (1984). Model for Inelastic Biaxial Bending of Concrete Members. Journal of Structural Engineering, 110(11). https://doi.org/10.1061/(asce)0733-9445(1984)110:11(2563)

Linde, P., & Bachmann, H. (1994). Dynamic modelling and design of earthquake-resistant walls. Earthquake Engineering & Structural Dynamics, 23(12). https://doi.org/10.1002/eqe.4290231205

Lindenberg, M., & Schuler, H. (2020). Flexural and shear deformation of basement-clamped reinforced concrete shear walls. Proceedings of the 17th World Conference on Earthquake Engineering (17WCEE), Sendai, Japan.

Lubliner, J., Oliver, J., Oller, S., & Oñate, E. (1989). A plastic-damage model for concrete. International Journal of Solids and Structures, 25(3), 299–326. https://doi.org/10.1016/0020-7683(89)90050-4

Mander, J. B., Priestley, M. J., & Park, R. (1988). Theoretical stress-strain model for confined concrete. Journal of structural engineering, 114(8), 1804-1826.

Massone, L., Orakcal, K., Publication, J. W.-S., & 2006, undefined. (2016). Shear-flexure interaction for structural walls. Researchgate.NetLM Massone, K Orakcal, JW WallaceSpecial Publication, 2006•researchgate.Net. https://www.researchgate.net/profile/Leonardo-Massone/publication/284079633_Shear-flexure_interaction_for_structural_walls/links/578cd64808ae59aa66814914/Shear-flexure-interaction-for-structural-walls.pdf

Orakcal, K., Wallace, J. W., & Conte, J. P. (2004). Flexural modeling of reinforced concrete walls: Model attributes. ACI Structural Journal, 101(5), 688–698.

Otani, S., Kabeyasawa, T., Shiohara, H., & Aoyama, H. (1985). ANALYSIS OF THE FULL SCALE SEVEN STORY REINFORCED CONCRETE TEST STRUCTURE. In Publication SP - American Concrete Institute.

Ozcebe, G., Yücemen, M. S., Aydoğan, V., & Yakut, A. (2003). Statistical assessment of seismic vulnerability of existing reinforced concrete buildings in Turkey (Final Report No. 98-03-03-03). Middle East Technical University.

Pacific Earthquake Engineering Research Center. (n.d.). PEER ground motion database [Data set]. University of California, Berkeley. https://ngawest2.berkeley.edu/

Petrangeli, M., Pinto, P. E., & Ciampi, V. (1999). Fiber Element for Cyclic Bending and Shear of RC Structures. I: Theory. Journal of Engineering Mechanics, 125(9). https://doi.org/10.1061/(asce)0733-9399(1999)125:9(994)

Pugh, J. S., Lowes, L. N., & Lehman, D. E. (2015). Nonlinear line-element modeling of flexural reinforced concrete walls. Engineering Structures, 104, 174–192. https://doi.org/10.1016/J.ENGSTRUCT.2015.08.037

Republic of Turkey Ministry of Environment and Urbanization. (2018). Turkish Building Earthquake Code (TBDY 2018). Ankara, Turkey.

Shah, D., Parmar, A., & Shah, S. (2025). Effect of different location and shear wall area ratio on the seismic behavior of the building: A review paper. Eksplorium, 46(1), 712–720.

Shah, D., Parmar, A., & Shah, S. (2025). Effect of shear wall percentage and grade of concrete on seismic performance of G+10 reinforced residential building: An analytical study. International Journal of Environmental Sciences, 11(10s), 213–221.

Smith, B. S., & Girgis, A. (1984). Simple Analogous Frames for Shear Wall Analysis. Journal of Structural Engineering, 110(11). https://doi.org/10.1061/(asce)0733-9445(1984)110:11(2655)

Sonmez, E., Eryilmaz Yildirim, M., Aydin, M. F., & Koroglu, F. B. (2025). Seismic performance assessment of structural systems in the aftermath of the 2023 Kahramanmaraş earthquakes: Observations and fragility analyses. Earthquake Spectra, 41(1), 198–218.

Soydaş, O. (2009). Evaluation of shear wall indexes for reinforced concrete buildings (Master's thesis, Middle East Technical University (Turkey)).

Takayanagi, T. (1977). Computed behavior of reinforced concrete coupled shear walls [Doctoral dissertation, University of Illinois at Urbana-Champaign].

Thomsen, J. H., & Wallace, J. W. (1995). Displacement-based design of RC structural walls: An experimental investigation of walls with rectangular and T-shaped cross-sections (Report No. CU/CEE-95/06). Clarkson University.

Thomsen, J. H., & Wallace, J. W. (2004). Displacement-Based Design of Slender Reinforced Concrete Structural Walls—Experimental Verification. Journal of Structural Engineering, 130(4), 618–630. https://doi.org/10.1061/(ASCE)0733-9445(2004)130:4(618)

Thomsen, J. H., & Wallace, J. W. (2004). Displacement-Based Design of Slender Reinforced Concrete Structural Walls—Experimental Verification. Journal of Structural Engineering, 130(4), 618–630. https://doi.org/10.1061/(ASCE)0733-9445(2004)130:4(618)

TMMOB Chamber of Civil Engineers. (2010). Assessment of Earthquake Reality of Turkey.

Tunc, G., & Al-Ageedi, A. H. (2020). Determination of optimum shear wall ratio in high-rise reinforced concrete buildings. Challenge Journal of Structural Mechanics, 6(2), 73–81. https://doi.org/10.20528/cjsmec.2020.02.003

Turkish Standards Institution. (2000). Betonarme yapıların tasarım ve yapım kuralları [Requirements for design and construction of reinforced concrete structures] (TS 500).

Vallenas, J. M., Bertero, V. v, & Popov, E. P. (1979). Hysteric behavior of reinforced concrete structural walls. NASA STI/Recon Technical Report N, 80(August 1979).

Vecchio, F. J. (2000). Disturbed Stress Field Model for Reinforced Concrete: Formulation. Journal of Structural Engineering, 126(9), 1070–1077. https://doi.org/10.1061/(ASCE)0733-9445(2000)126:9(1070)

Vecchio, F. J., & Collins, M. P. (1986). The modified compression-field theory for reinforced concrete elements subjected to shear. ACI Journal Proceedings, 83(2), 219–231.

Vulcano, A., & Bertero, V. (1987). Analytical models for predicting the lateral response of RC shear walls: Evaluation of their reliability. https://nehrpsearch.nist.gov/article/PB88-178983/XAB

Vulcano, A., Bertero, V. v., & Colotti, V. (1988). Analytical modeling of R/C structural walls. 9th World Conference on Earthquake Engineering.

Wallace, J. W. (1994). New methodology for seismic design of RC shear walls. Journal of Structural Engineering, 120(3), 863–884.

Wan-Xie, Z., & Jia-Hao, L. (1987). The whiplash effect on tall buildings. In Progress in Applied Mechanics: The Chien Wei-zang Anniversary Volume (pp. 371-378). Dordrecht: Springer Netherlands.

Wight, J. K. (1985). U.S.-Japan cooperative research program: Construction and testing of a full-scale reinforced concrete seven-story structure. In J. K. Wight (Ed.), Earthquake effects on reinforced concrete structures: U.S.-Japan research (Publication No. SP-84, pp. 59–82). American Concrete Institute.

Yamada, M. (2014). Estimation of fault rupture extent using near-source records for earthquake early warning. In Early Warning for Geological Disasters: Scientific Methods and Current Practice (pp. 29-47). Berlin, Heidelberg: Springer Berlin Heidelberg.

Yurdakul, Ö., Avşar, Ö., & Tunaboyu, O. (2014, July). *Effects of shear wall ratio on the seismic behavior of buildings having inadequate seismic resistance*. In Proceedings of the 10th U.S. National Conference on Earthquake Engineering (NCEE 2014).

APPENDICES

A. Material Hysteresis Models

Hysteresis refers to the process of energy dissipation through deformation. In ETABS, various hysteretic models are available to characterize the material behavior, each differing in the amount of energy dissipated during a given deformation cycle.

For fiber elements representing concrete material in P-M2-M3 hinges assigned to columns and P-M3 hinges assigned to structural walls, Concrete Hysteresis Model is utilized. This model, designed for unreinforced concrete and similar materials, serves as the default option for concrete and masonry in ETABS. In this model, tensile and compressive responses are defined independently, and the formulation is primarily intended for axial behavior. The fibers assigned in this model deform only under axial tension and compression, and the flexural response arises from the differences in these axial forces and deformations along the section. The Concrete Hysteresis Model is illustrated in Figure A.1.

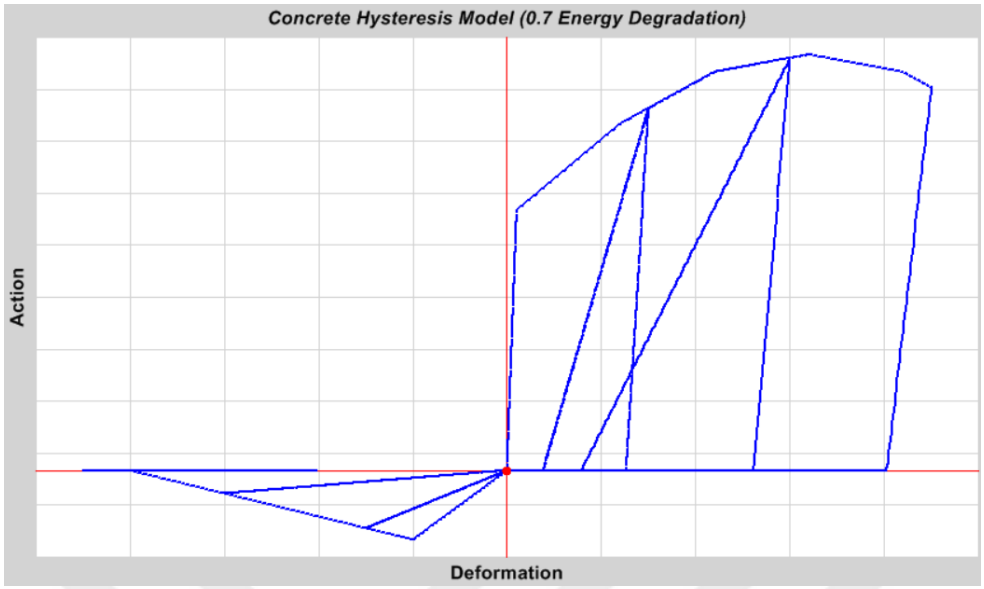


Figure A.1 Concrete Hysteresis Model (CSI, 2024)

For fiber elements representing reinforcing steel material in P-M2-M3 hinges assigned to columns and P-M3 hinges assigned to structural walls, Degrading Hysteresis Model is utilized. This model uses a degrading hysteretic curve that accounts for decreasing energy dissipation and unloading stiffness with increasing plastic deformation.

Two measures are used for plastic deformation:

- Maximum plastic deformation in positive and negative directions,
- Accumulated plastic deformation, which is the absolute sum of each increment of positive or negative plastic deformation. Plastic deformation is defined as the deformation that does not occur on the two elastic segments of the action-deformation curve.

For this model, the following parameters are required:

- Separately for positive and negative deformations
    - Initial energy factor at yield, *f0*, usually 1.0

    - Energy factor at moderate deformation, *f1*
    - Energy factor at maximum deformation, *f2*
    - Moderate deformation level, *x1*, as a multiple of the deformation scale factor
    - Maximum deformation level, *x2*, as a multiple of the deformation scale factor
    - Accumulated deformation weighting factor, *a*
- Stiffness degradation weighting factor, *s*
- Larger-smaller weighting factor, *w*, usually 0.0

Degrading Hysteresis Model and corresponding hysteresis parameters are provided in Figures A.2 and A.3, respectively. The hysteresis parameters, presented in Figure A.3, are identified as the values that best capture the pinching behavior observed in the validation studies of the RW2 specimen. The energy factors represent the area of a degraded hysteresis loop divided by the energy of the nondegraded loop. For example, an energy factor of 0.3 means that a full cycle of deformation would only dissipate 30% of the energy that the nondegraded material would. Reducing the energy factors toward 0 results in an artificially amplified pinching response extending closer to the origin, whereas increasing them toward 1 leads to an almost negligible pinching behavior.

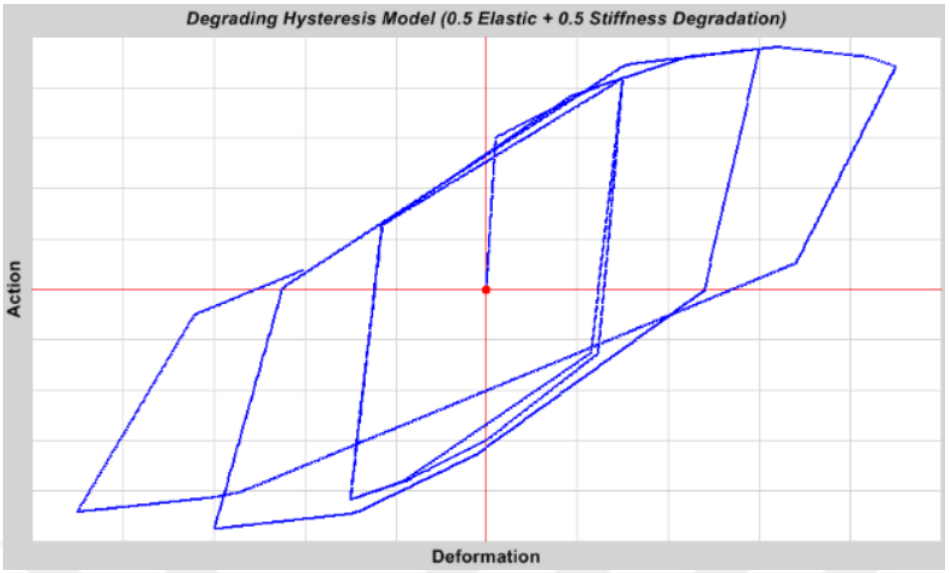


Figure A.2 Degrading Hysteresis Model (CSI, 2024)

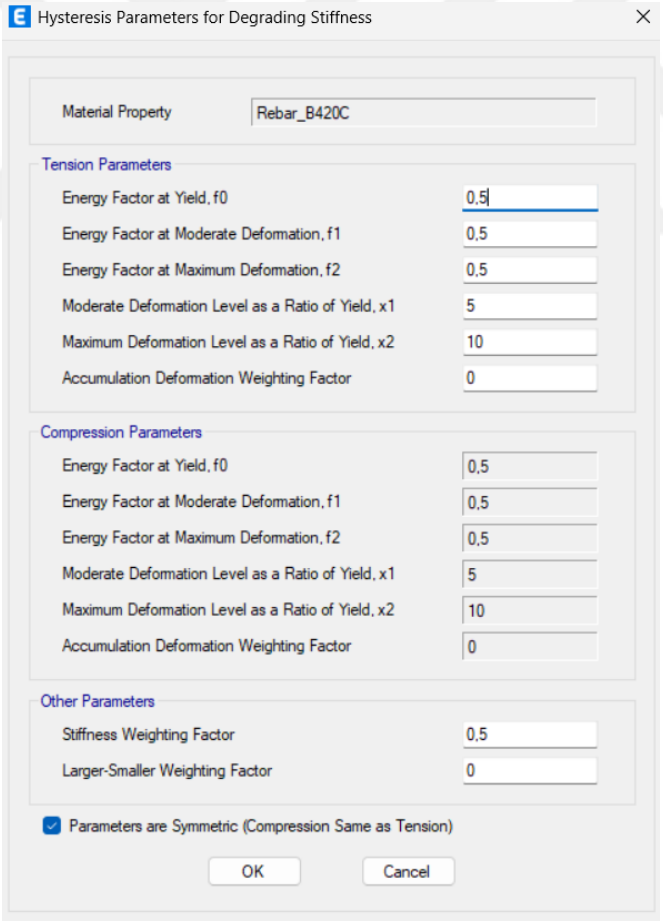


Figure A.3 Parameters for Degrading Stiffness Hysteresis

Pivot Hysteresis Model is utilized for the hysteretic behavior of M3 plastic hinges assigned to beams. It is particularly well suited for reinforced concrete members and is based on the observation that unloading and reverse loading tend to be directed toward specific points, called pivot points, in the action-deformation plane. The most common use of this model is for moment-rotation response of reinforced concrete members (Dowell, Seible, and Wilson (1998)) and not intended for unreinforced concrete (Computers and Structures, Inc. [CSI], 2024).

The following additional parameters are specified for the Pivot model:

a_1: locates the pivot point for unloading to zero from positive force. Unloading occurs toward a point on the extension of the positive elastic line, but at a negative force value of a_1 times the positive yield force.

a_2: locates the pivot point for unloading to zero from negative force. Unloading occurs toward a point on the extension of the negative elastic line, but at a positive force value of a_2 times the negative yield force.

b_1: locates the pivot point for reverse loading from zero toward positive force. Reloading occurs toward a point on the positive elastic line at a force value of b_1 times the positive yield force, where $0.0 < b_1 \leq 1.0$. Beyond that point, loading occurs along the secant to the point of maximum previous positive deformation on the backbone curve.

b_2: locates the pivot point for reverse loading from zero toward negative force. Reloading occurs toward a point on the positive elastic line at a force value of b_2 times the positive yield force, where $0.0 < b_2 < 1.0$. Beyond that point, loading occurs along the secant to the point of maximum previous negative deformation on the backbone curve.

h: determines the amount of degradation of the elastic slopes after plastic deformation, where $0.0 < h < 1.0$.

These parameters and the behavior are illustrated in Figures A.4 and A.5.

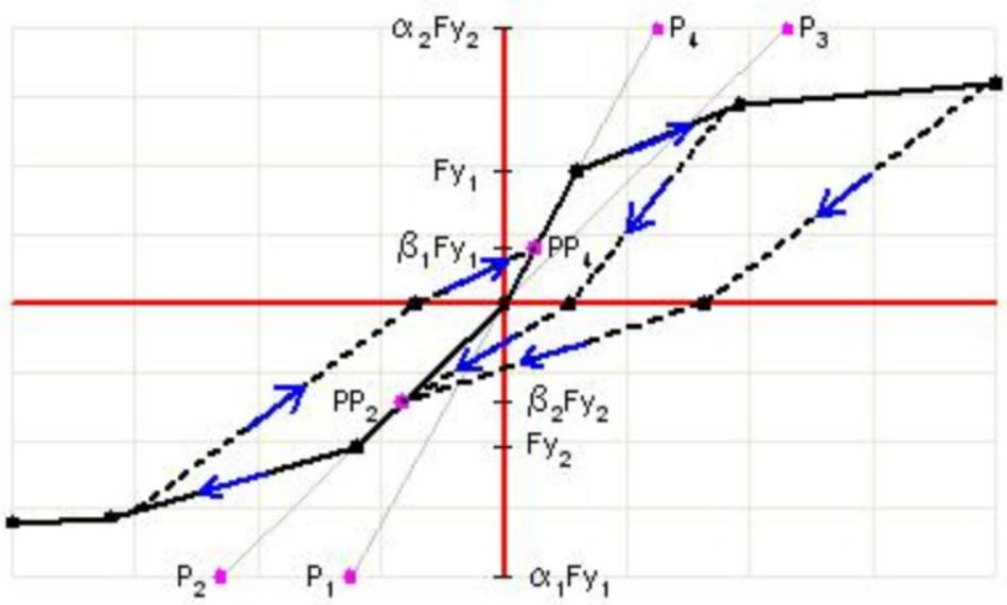


Figure A.4 Pivot Hysteresis parameters (CSI, 2024)

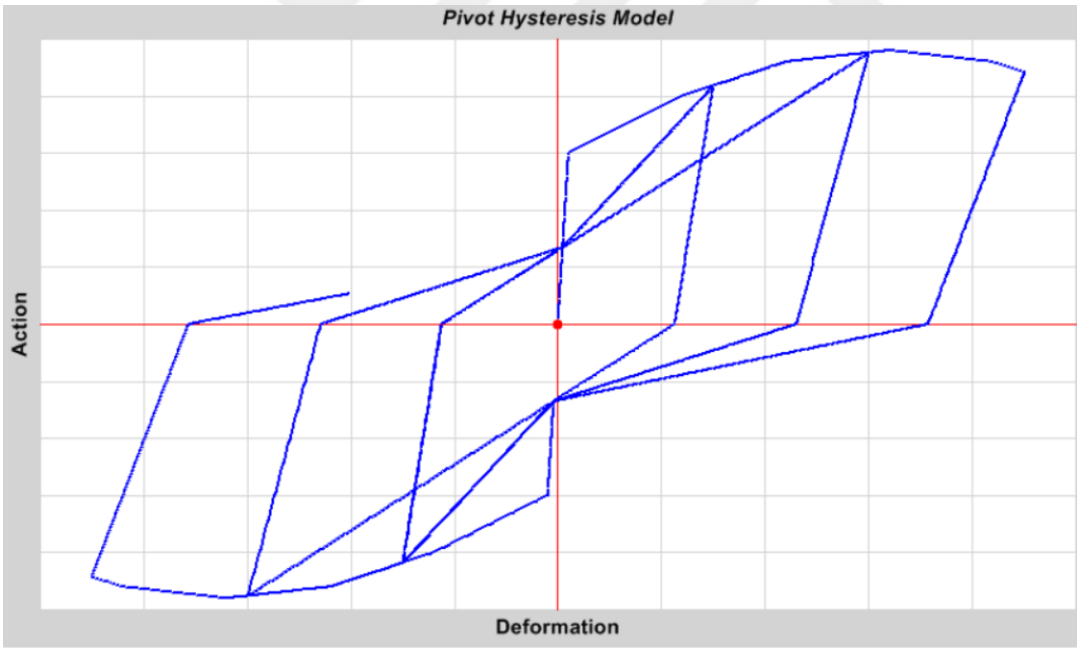


Figure A.5 Pivot Hysteresis Model (CSI, 2024)

The default Pivot Hysteresis parameters are found to adequately capture the stiffness degradation of beams and are therefore adopted in the nonlinear analyses. These parameters are provided in Figure A.6.

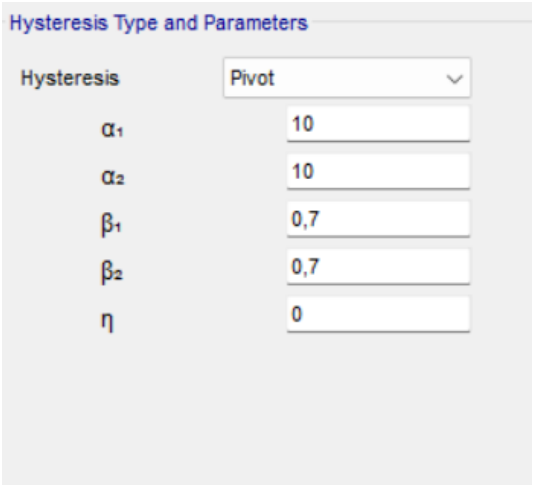


Figure A.6 Pivot Hysteresis parameters

B. Reinforcement Detailing of Seven Story Test Building

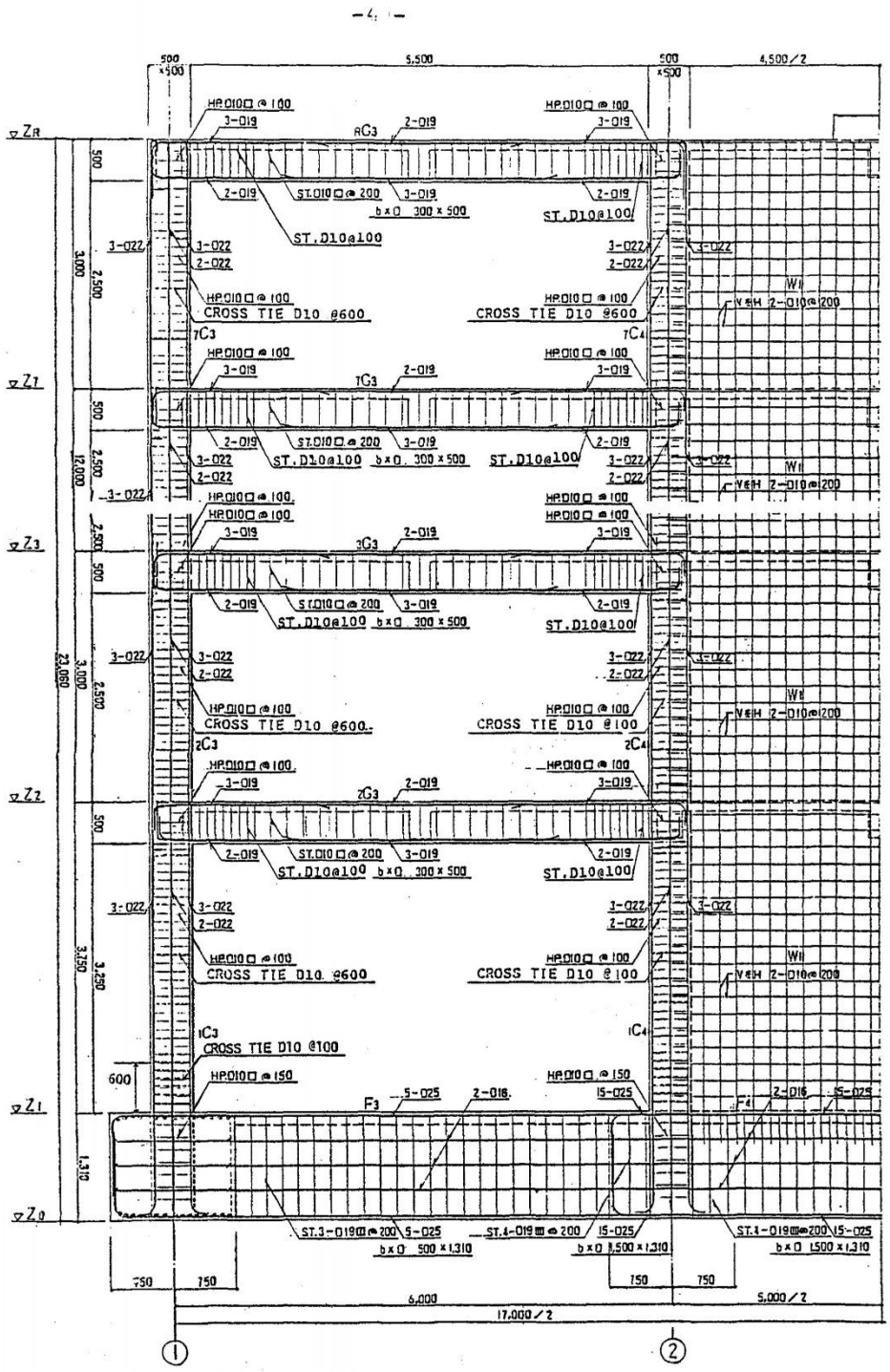
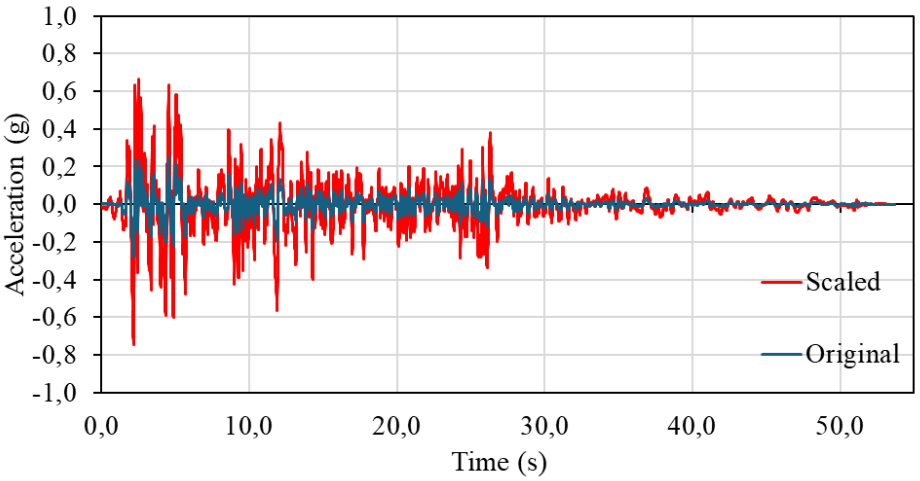
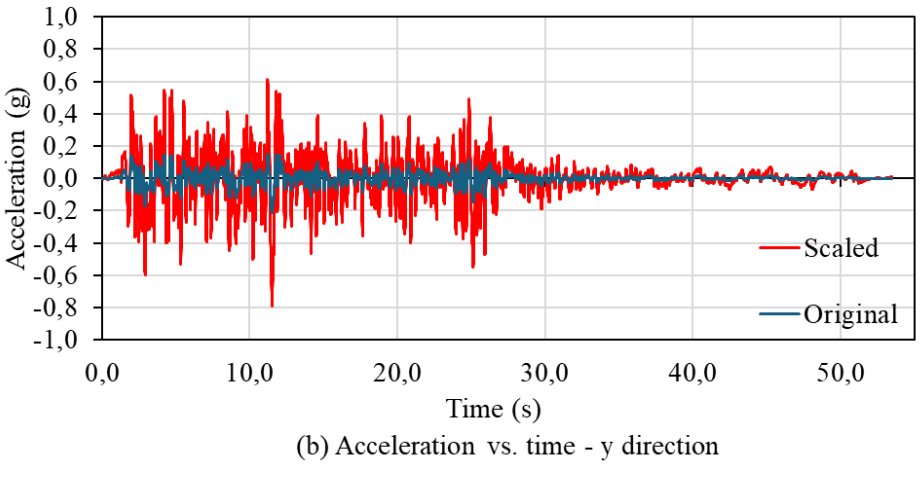


Figure B.1 Frame B reinforcement detailing of 7 story test building (Wight et al., 1995)

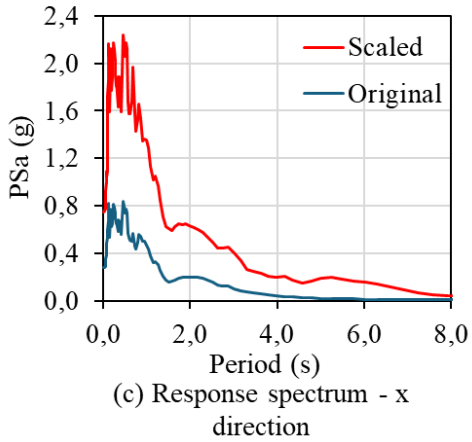
C. Spectral Matching of Time History Records



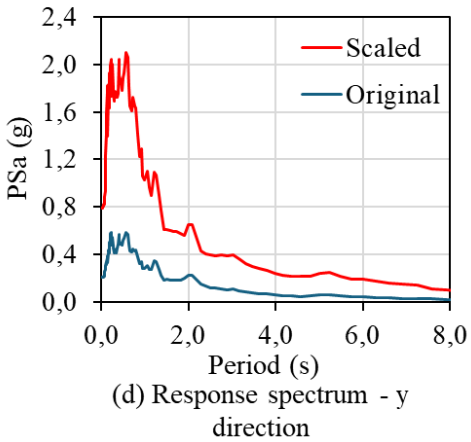
(a) Acceleration vs. time - x direction



(b) Acceleration vs. time - y direction

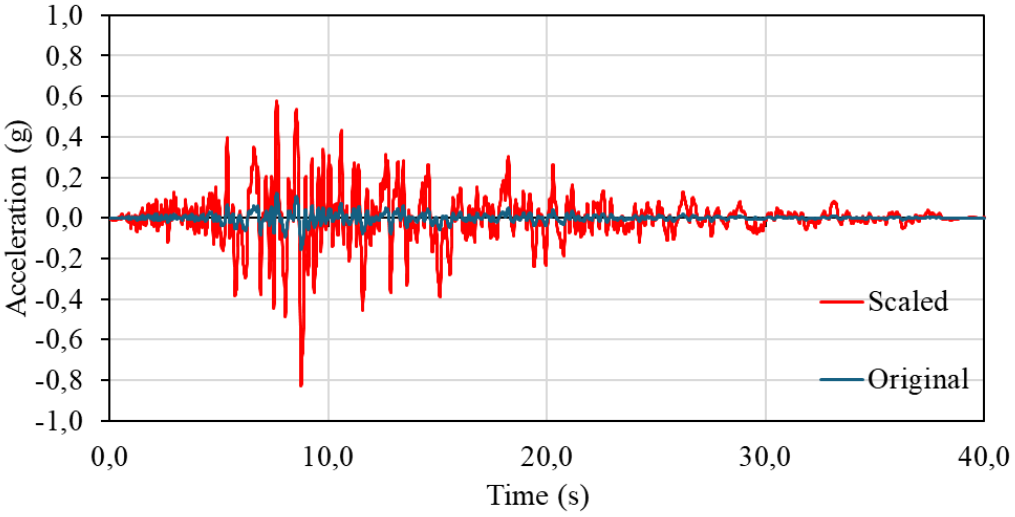


(c) Response spectrum - x direction

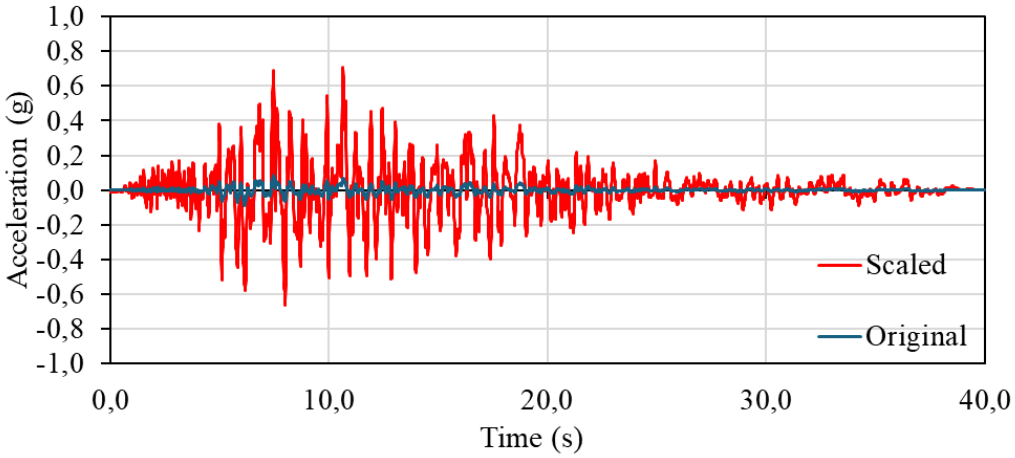


(d) Response spectrum - y direction

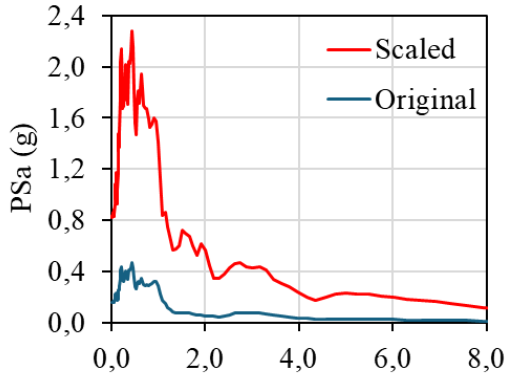
Figure C.1 Spectral matching of Imperial Valley Earthquake



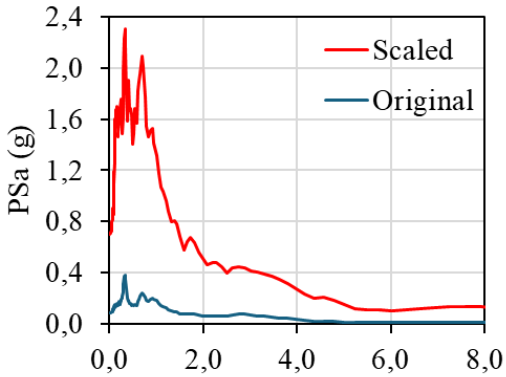
(a) Acceleration vs. time - x direction



(b) Acceleration vs. time - y direction

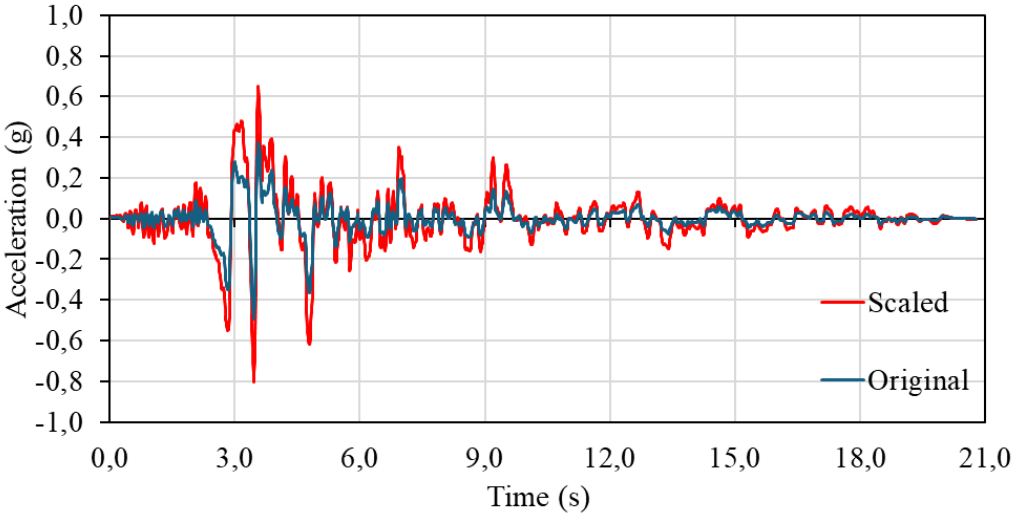


(c) Response spectrum - x direction

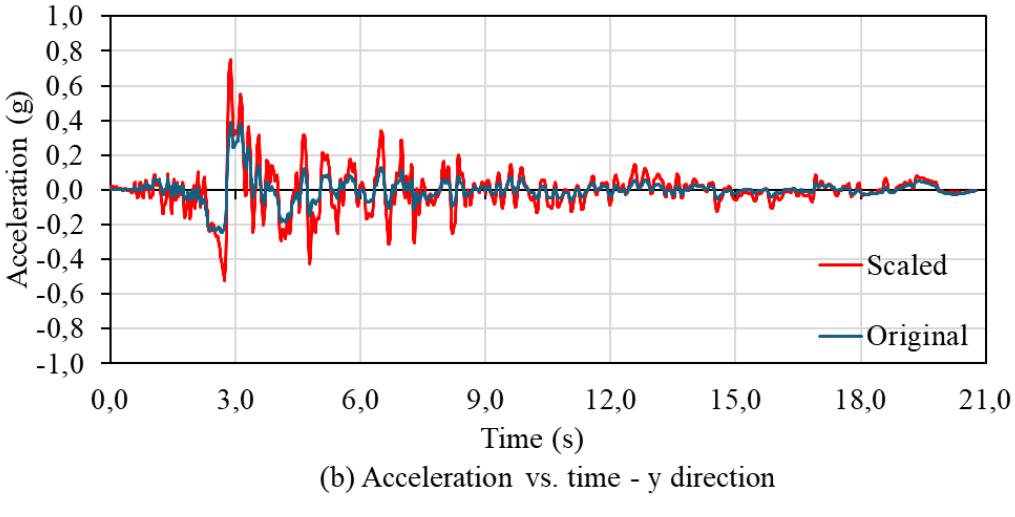


(d) Response spectrum - y direction

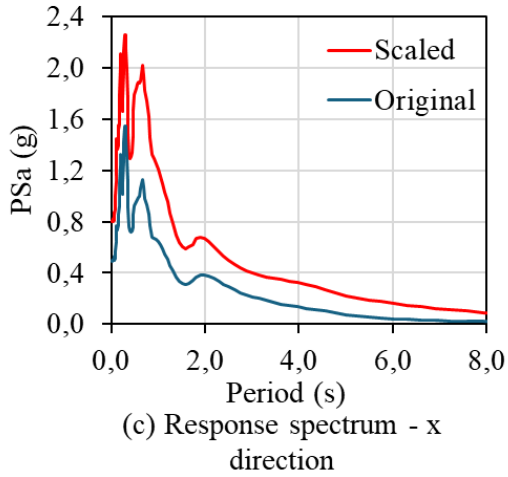
Figure C.2 Spectral matching of Loma Prieta Earthquake



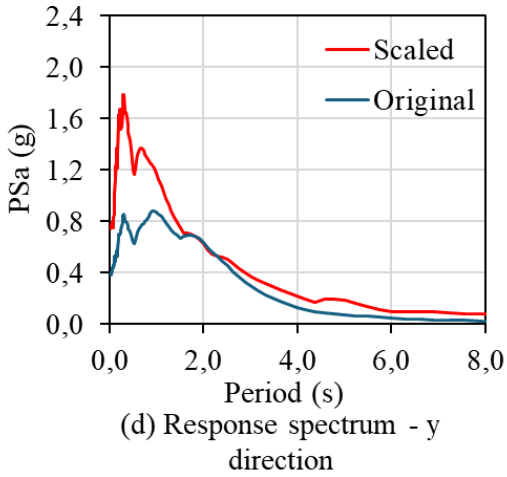
(a) Acceleration vs. time - x direction



(b) Acceleration vs. time - y direction

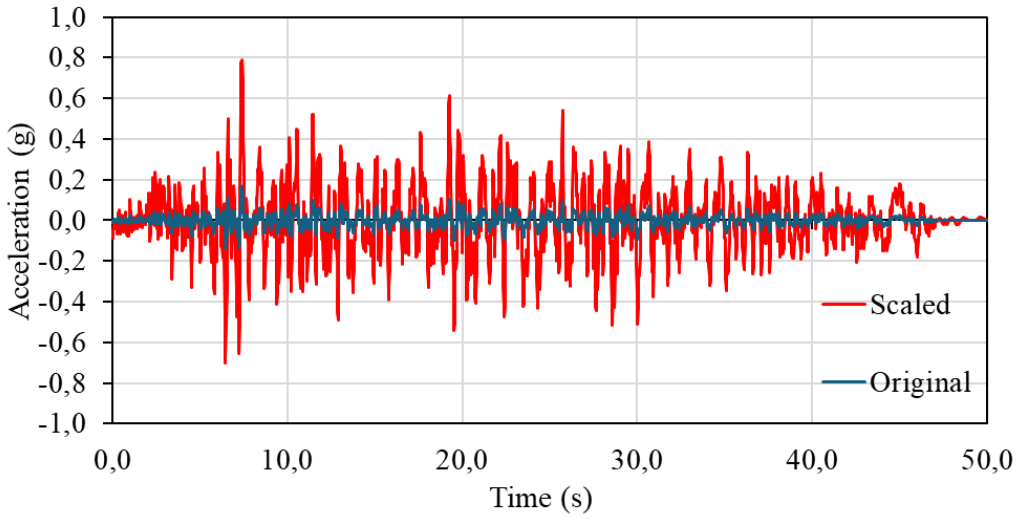


(c) Response spectrum - x direction

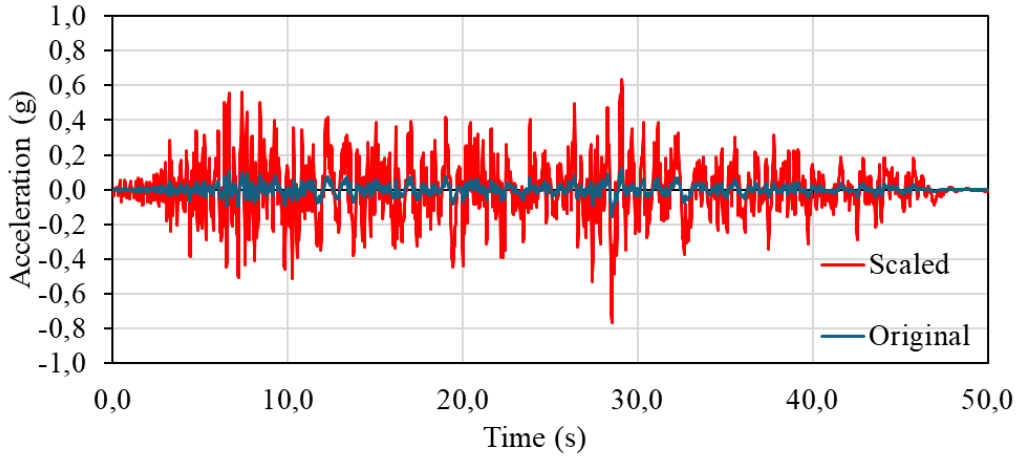


(d) Response spectrum - y direction

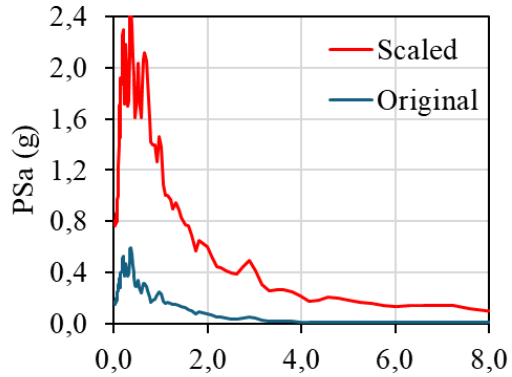
Figure C.3 Spectral matching of Erzincan Earthquake



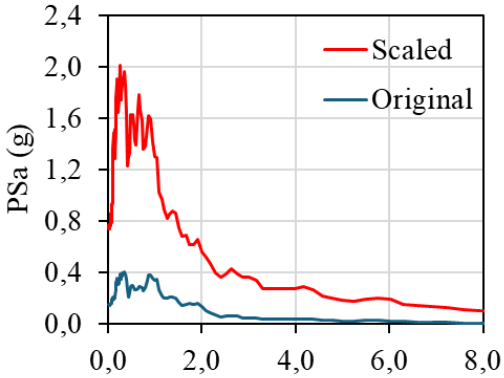
(a) Acceleration vs. time - x direction



(b) Acceleration vs. time - y direction

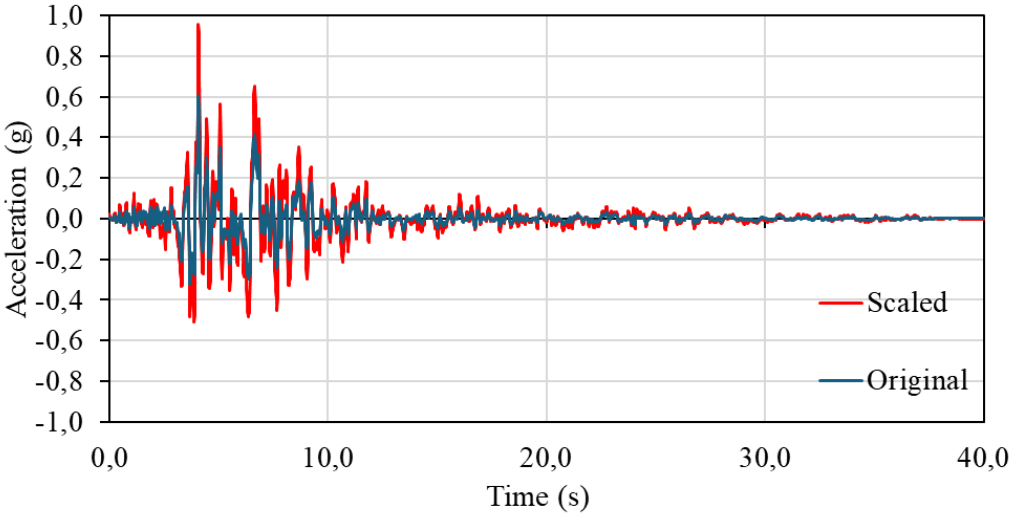


(c) Response spectrum - x direction

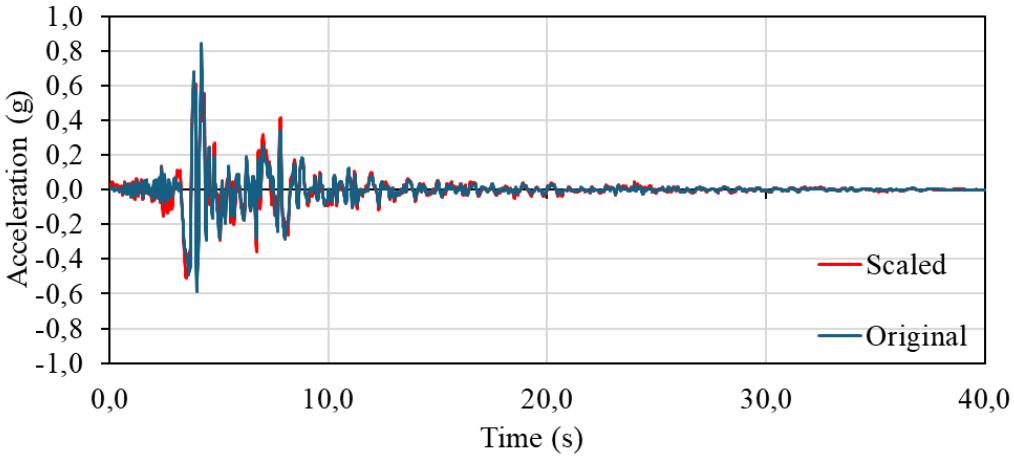


(d) Response spectrum - y direction

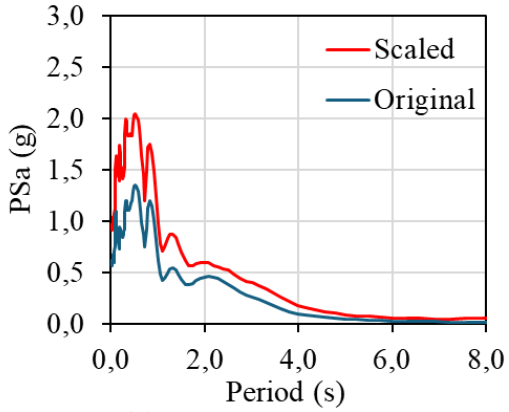
Figure C.4 Spectral matching of Landers Earthquake



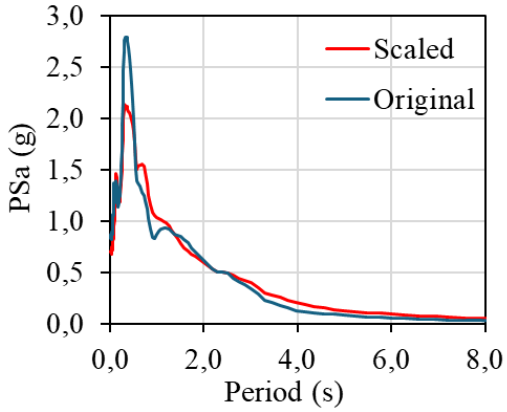
(a) Acceleration vs. time - x direction



(b) Acceleration vs. time - y direction

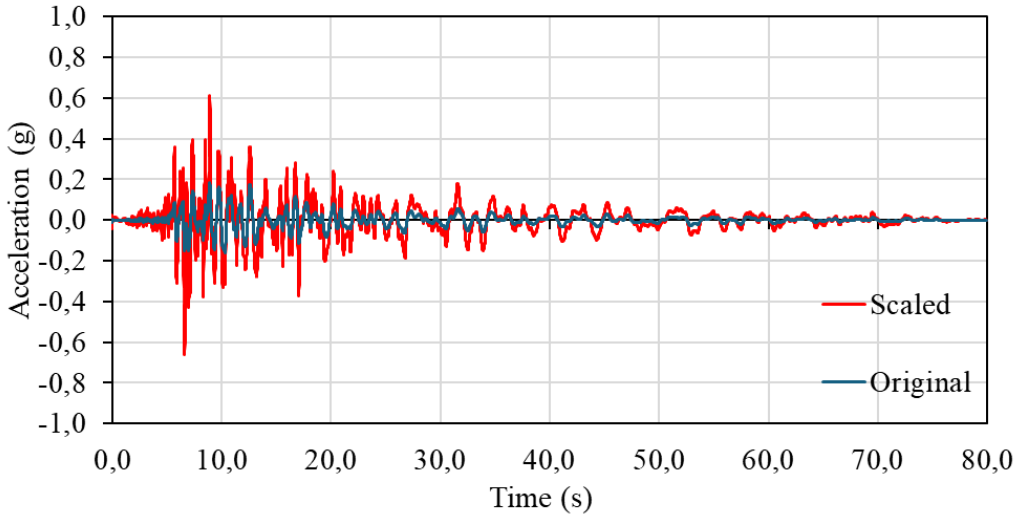


(c) Response spectrum - x direction

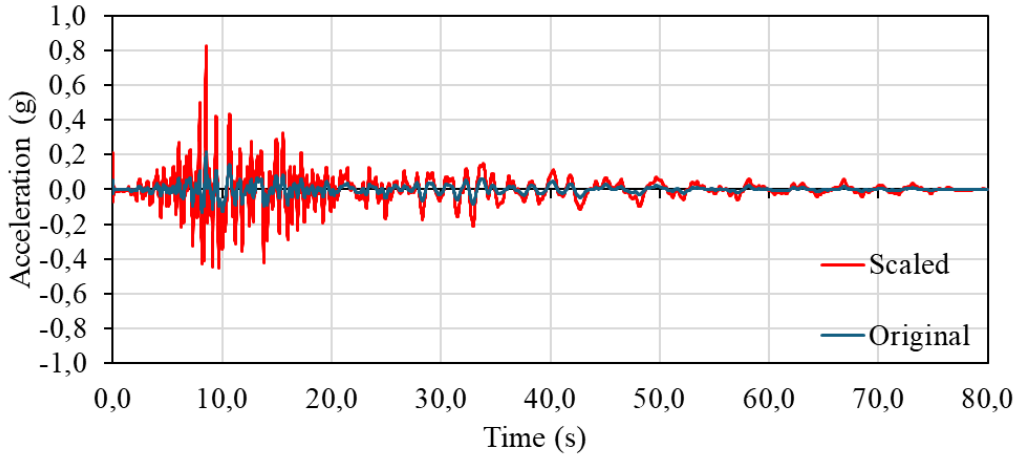


(d) Response spectrum - y direction

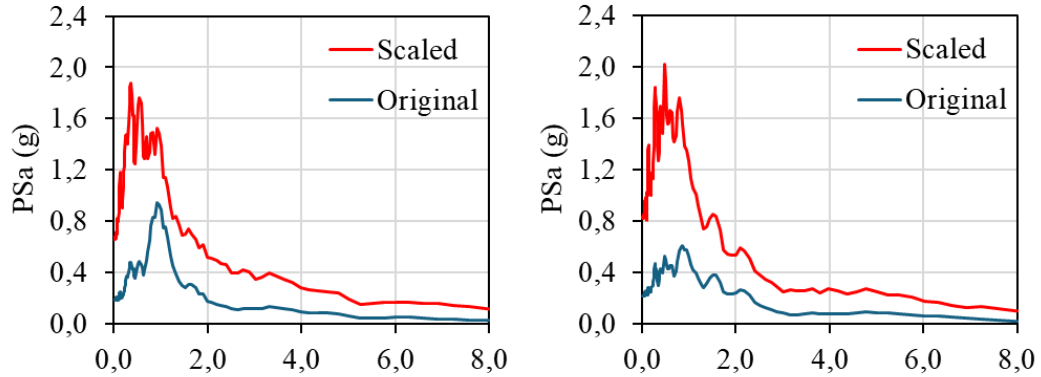
Figure C.5 Spectral matching of Northridge Earthquake



(a) Acceleration vs. time - x direction



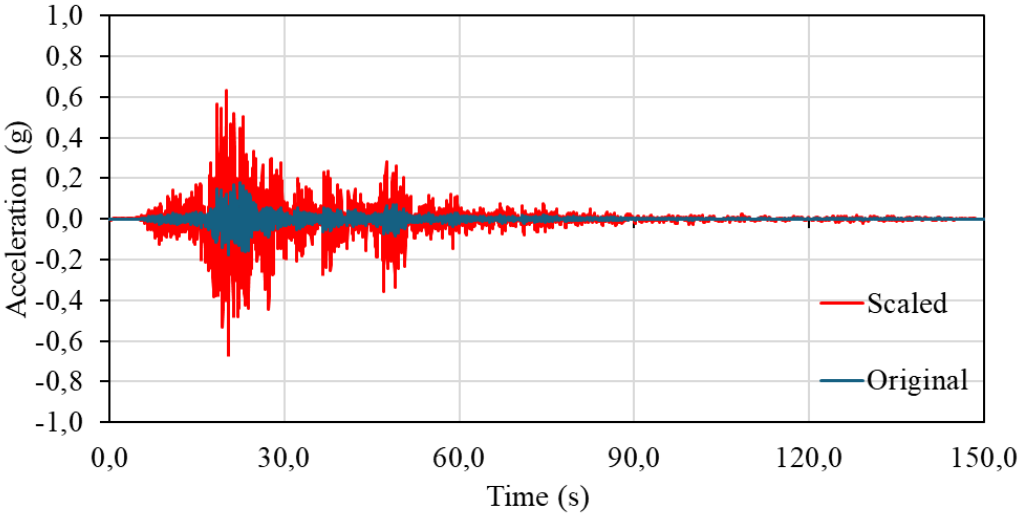
(b) Acceleration vs. time - y direction



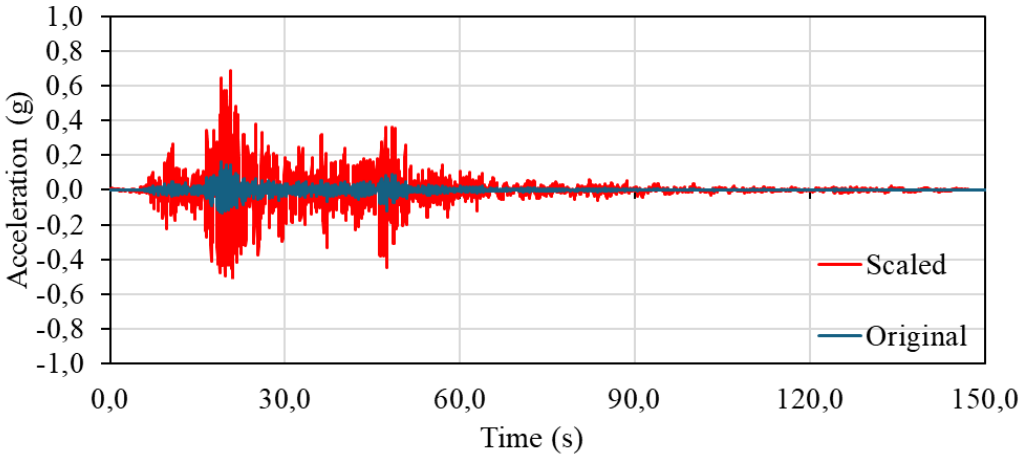
(c) Response spectrum - x direction

(d) Response spectrum - y direction

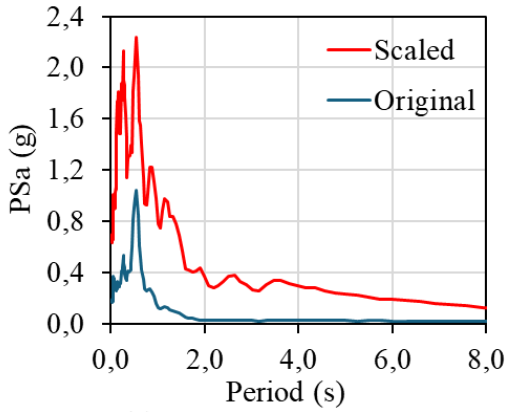
Figure C.6 Spectral matching of Kobe Earthquake



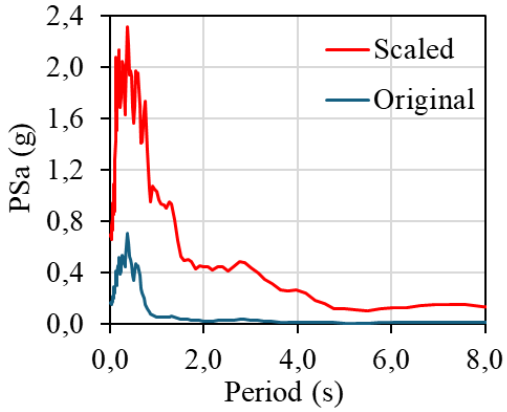
(a) Acceleration vs. time - x direction



(b) Acceleration vs. time - y direction

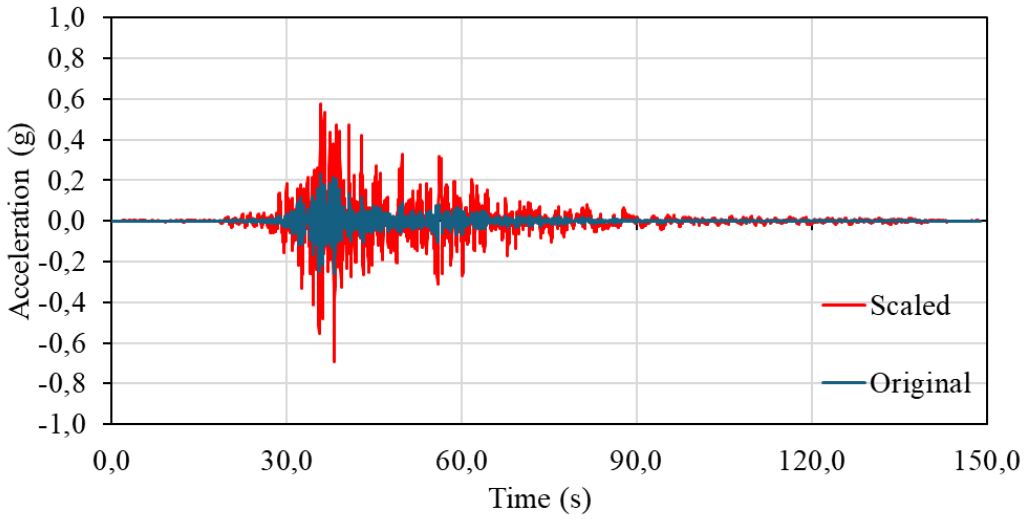


(c) Response spectrum - x direction

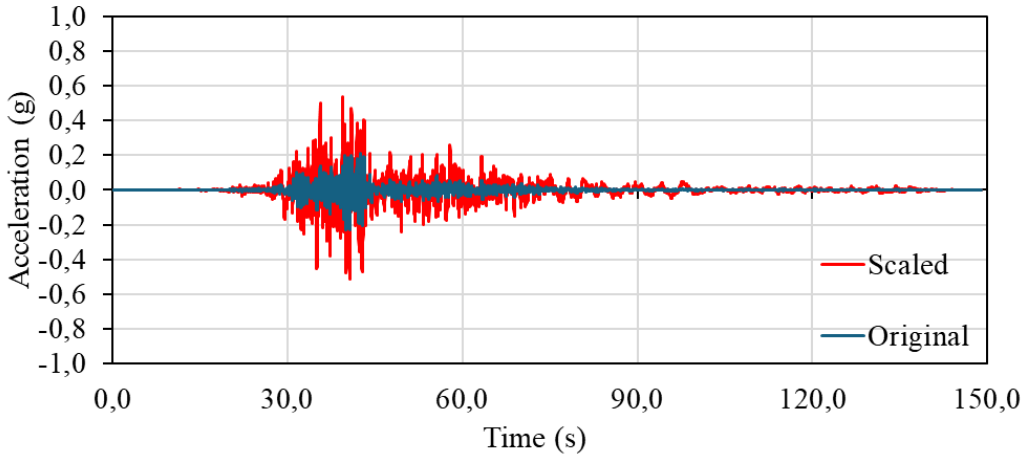


(d) Response spectrum - y direction

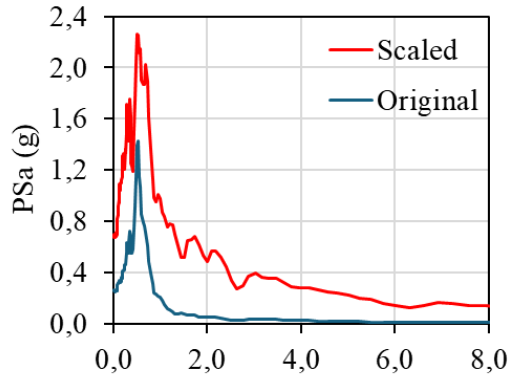
Figure C.7 Spectral matching of Kocaeli Earthquake



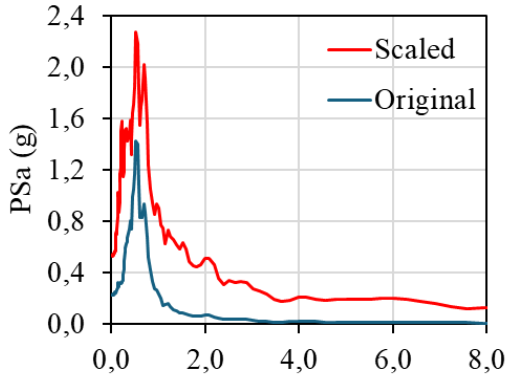
(a) Acceleration vs. time - x direction



(b) Acceleration vs. time - y direction

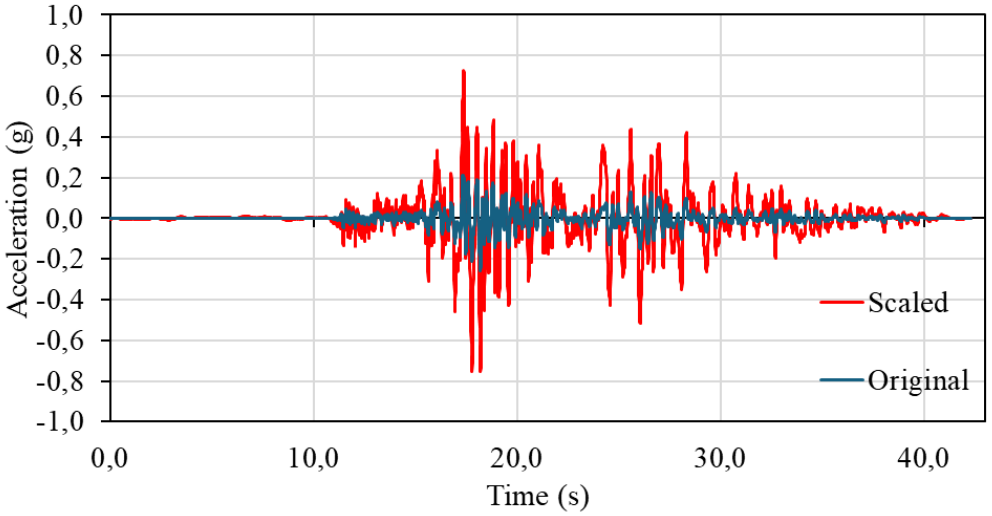


(c) Response spectrum - x direction

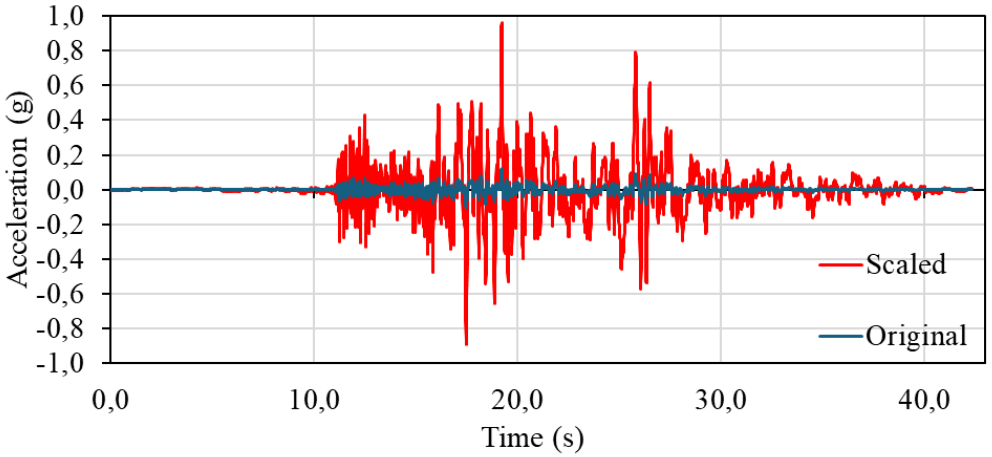


(d) Response spectrum - y direction

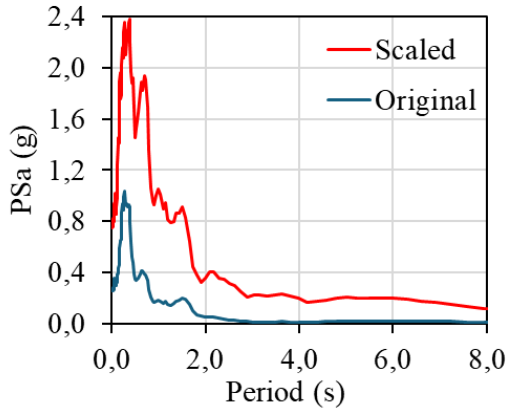
Figure C.8 Spectral matching of Chi Chi Earthquake



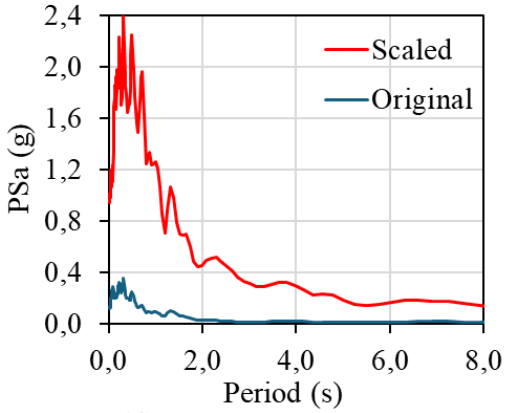
(a) Acceleration vs. time - x direction



(b) Acceleration vs. time - y direction

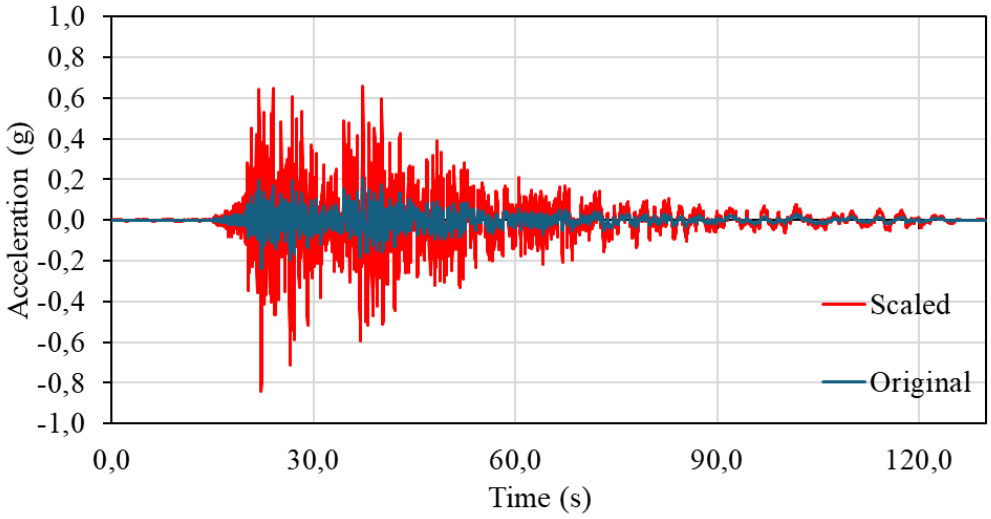


(c) Response spectrum - x direction

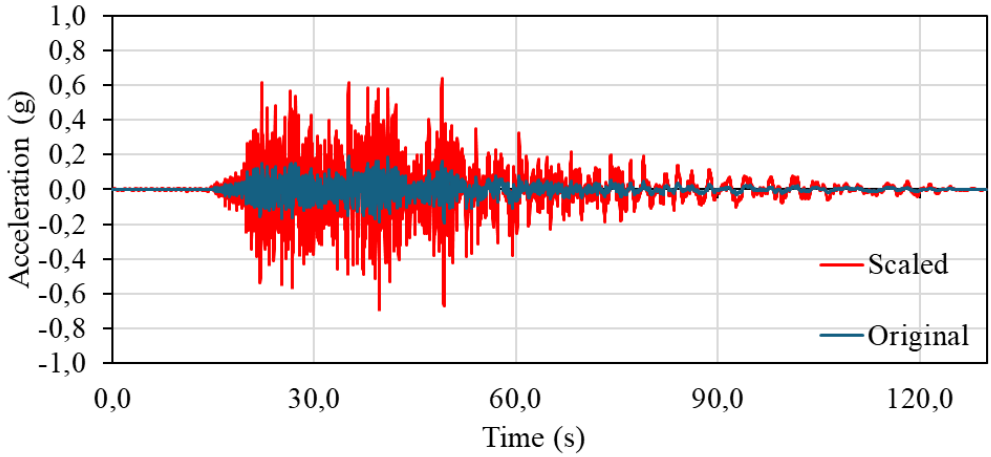


(d) Response spectrum - y direction

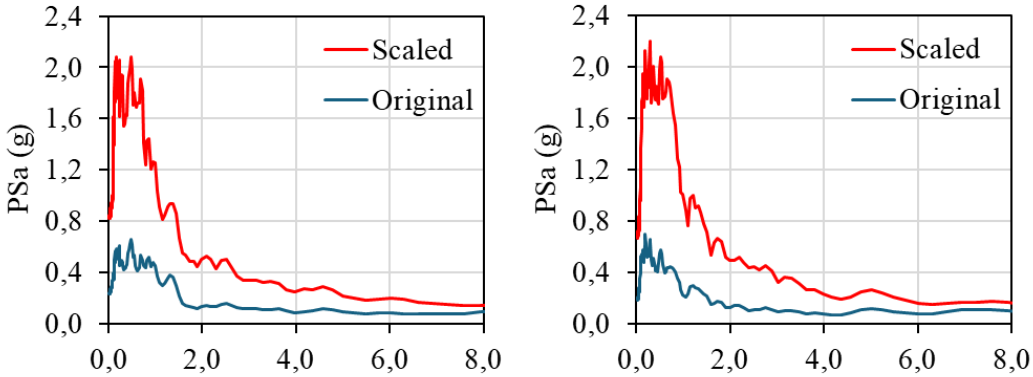
Figure C.9 Spectral matching of Duzce Earthquake



(a) Acceleration vs. time - x direction



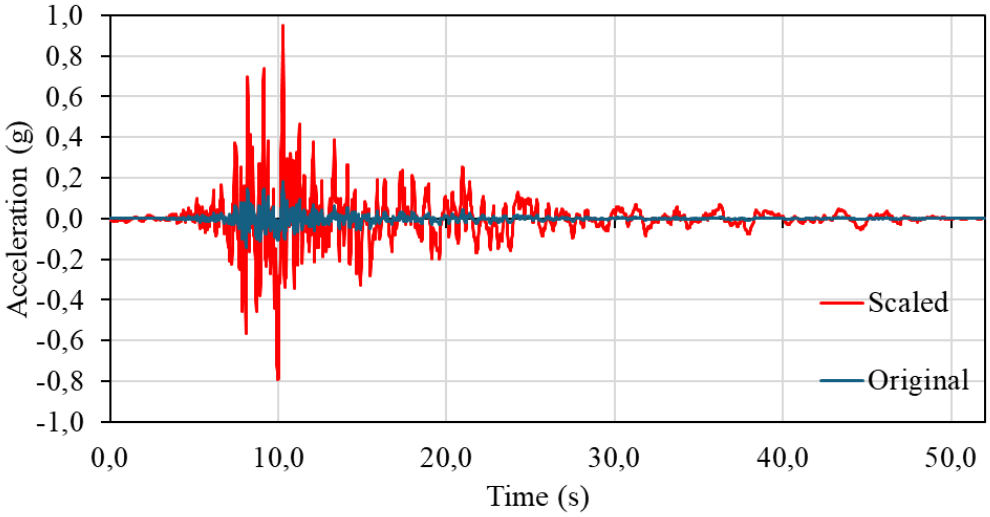
(b) Acceleration vs. time - y direction



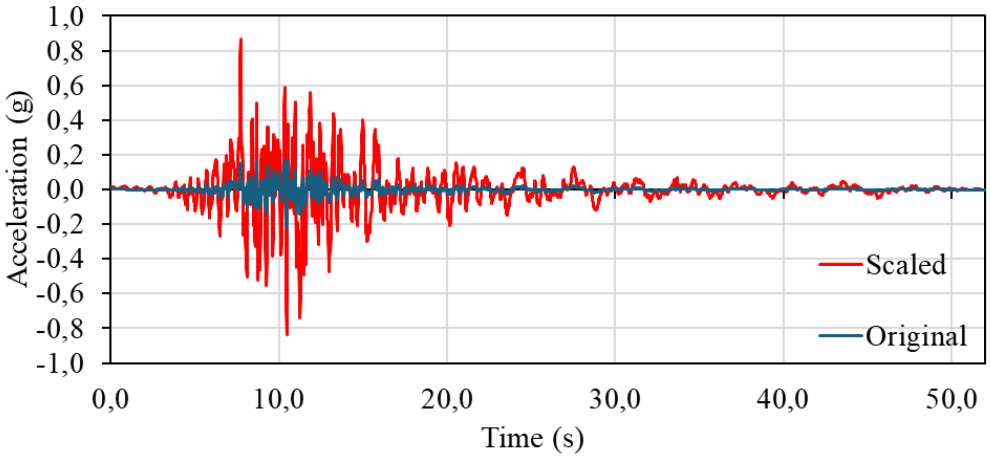
(c) Response spectrum - x direction

(d) Response spectrum - y direction

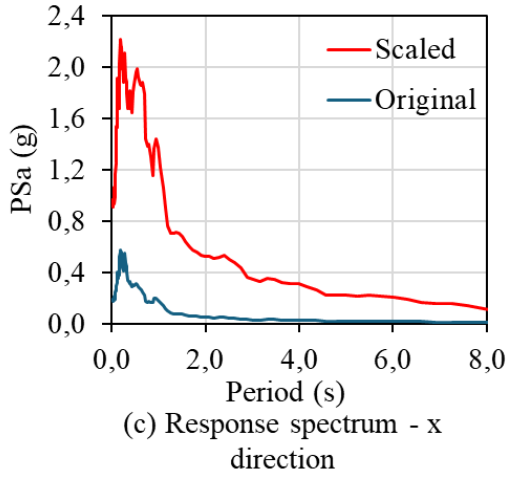
Figure C.10 Spectral matching of Sierramex Earthquake



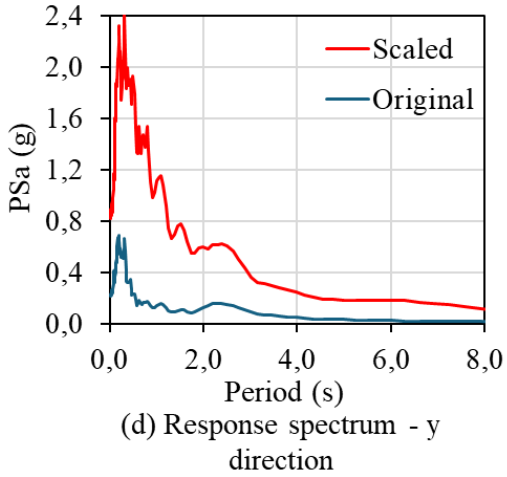
(a) Acceleration vs. time - x direction



(b) Acceleration vs. time - y direction



(c) Response spectrum - x direction



(d) Response spectrum - y direction

Figure C.11 Spectral matching of Christchurch Earthquake

D. Percentage of Members with Reinforcement Yielding

Table D.6.1 Percentage of members with reinforcement yielding - 7 story buildings

Model	Story	NOR			KOB			KOC			CHI			DUZ			SM			LOM			CC			ERZ			LAN			IMP		
		W	C	B	W	C	B	W	C	B	W	C	B	W	C	B	W	C	B	W	C	B	W	C	B	W	C	B	W	C	B	W	C	B
S07_R00	1	-	100	100	-	100	100	-	100	100	-	100	100	-	100	100	-	100	100	-	100	100	-	100	100	-	100	100	-	100	100	-	100	100
	2	-	31	100	-	6	100	-	28	100	-	31	100	-	42	100	-	50	100	-	25	100	-	3	100	-	81	100	-	44	100	-	31	100
	3	-	67	100	-	0	100	-	0	100	-	0	100	-	8	100	-	39	100	-	11	100	-	75	100	-	94	100	-	36	100	-	25	100
	4	-	81	100	-	0	100	-	0	100	-	0	100	-	0	100	-	67	100	-	8	100	-	69	100	-	97	100	-	58	100	-	58	100
	5	-	0	100	-	0	100	-	0	100	-	0	100	-	0	100	-	11	100	-	0	100	-	33	100	-	97	100	-	0	100	-	0	100
	6	-	0	100	-	0	100	-	0	95	-	0	98	-	0	100	-	0	100	-	0	100	-	0	100	-	0	93	-	0	100	-	0	100
	7	-	0	0	-	0	0	-	0	0	-	0	0	-	0	0	-	0	0	-	0	0	-	0	0	-	0	0	-	0	0	-	0	0
S07_R05	1	100	100	100	100	50	100	100	30	100	100	33	100	100	100	100	100	97	100	100	57	100	100	47	100	100	100	100	100	100	100	100	57	100
	2	100	53	100	25	10	100	50	10	100	75	7	100	50	40	100	100	33	100	25	13	100	100	17	100	0	100	100	50	80	100	100	43	100
	3	0	0	100	0	0	100	0	0	100	0	0	100	0	0	100	0	3	100	0	0	100	0	0	100	0	3	100	0	0	100	0	3	100
	4	0	0	100	0	0	100	0	0	100	0	0	100	0	0	100	0	0	100	0	0	100	0	0	100	0	13	100	0	0	100	0	3	100
	5	0	0	100	0	0	100	0	0	100	0	0	100	0	0	100	0	0	100	0	0	100	0	0	100	100	13	100	0	0	100	0	0	100
	6	0	0	100	0	0	100	0	0	100	0	0	100	0	0	100	0	0	100	0	0	100	0	0	100	100	3	100	0	0	100	0	0	100
	7	0	90	100	0	67	100	0	53	100	0	60	98	0	93	100	0	90	100	0	73	100	0	93	100	0	93	100	0	93	100	0	93	100

Table D.1 Percentage of members with reinforcement yielding - 7 story buildings (cont'd)

Model	Story	NOR			KOB			KOC			CHI			DUZ			SM			LOM			CC			ERZ			LAN			IMP		
		W	C	B	W	C	B	W	C	B	W	C	B	W	C	B	W	C	B	W	C	B	W	C	B	W	C	B	W	C	B	W	C	B
S07_R10	1	100	29	100	100	4	100	100	4	100	100	0	100	100	29	100	100	33	100	100	13	100	100	21	100	100	100	100	100	46	100	100	38	100
	2	50	17	100	38	0	100	13	0	100	25	0	100	88	25	100	75	21	100	50	13	100	50	4	100	25	58	100	63	21	100	100	33	100
	3	0	0	100	0	0	100	0	0	100	0	0	100	0	0	100	0	0	100	0	0	100	0	0	100	0	0	100	0	0	100	0	0	100
	4	0	0	100	0	0	100	0	0	100	0	0	100	0	0	100	0	0	100	0	0	100	0	0	100	0	0	100	0	0	100	0	0	100
	5	0	0	100	0	0	100	0	0	100	0	0	100	0	0	100	0	0	100	0	0	100	0	0	100	0	0	100	0	0	100	0	0	100
	6	0	0	100	0	0	100	0	0	100	0	0	100	0	0	100	0	0	100	0	0	100	0	0	100	0	0	100	0	0	100	0	0	100
	7	0	100	100	0	83	100	0	67	96	0	67	96	0	100	100	0	92	100	0	100	100	0	83	100	0	92	98	0	100	100	0	100	100
S07_R15	1	100	22	100	100	0	100	100	0	100	100	11	100	100	22	100	100	22	100	100	22	100	100	0	100	100	44	100	100	39	100	100	39	100
	2	17	11	100	8	0	100	0	0	100	17	6	100	42	11	100	75	17	100	17	17	100	17	0	100	17	17	100	33	22	100	17	22	100
	3	0	0	100	0	0	100	0	0	100	0	0	100	0	0	100	0	0	100	0	0	100	0	0	100	0	0	100	0	0	100	0	0	100
	4	0	0	100	0	0	100	0	0	100	0	0	100	0	0	100	0	0	100	0	0	100	0	0	100	0	0	100	0	0	100	0	0	100
	5	0	0	100	0	0	100	0	0	100	0	0	100	0	0	100	0	0	100	0	0	100	0	0	100	0	0	100	0	0	100	0	0	100
	6	0	0	100	0	0	100	0	0	100	0	0	100	0	0	100	0	0	100	0	0	100	0	0	100	0	0	100	0	0	100	0	0	100
	7	0	83	100	0	44	96	0	17	96	0	67	100	0	100	100	0	89	100	0	89	100	0	44	100	0	72	96	0	78	100	0	100	100

Table D.1 Percentage of members with reinforcement yielding - 7 story buildings (cont'd)

Model	Story	NOR			KOB			KOC			CHI			DUZ			SM			LOM			CC			ERZ			LAN			IMP		
		W	C	B	W	C	B	W	C	B	W	C	B	W	C	B	W	C	B	W	C	B	W	C	B	W	C	B	W	C	B	W	C	B
S07_R20	1	100	8	95	100	0	100	100	0	100	100	0	100	100	0	100	100	0	100	100	8	100	100	0	100	100	8	98	100	25	100	100	25	100
	2	13	0	100	13	0	100	0	0	100	0	0	100	6	0	100	25	0	100	13	0	100	13	0	100	0	0	100	25	25	100	13	8	100
	3	0	0	100	0	0	100	0	0	100	0	0	100	0	0	100	0	0	100	0	0	100	0	0	100	0	0	100	0	0	100	0	0	100
	4	0	0	100	0	0	100	0	0	100	0	0	100	0	0	100	0	0	100	0	0	100	0	0	100	0	0	100	0	0	100	0	0	100
	5	0	0	100	0	0	100	0	0	100	0	0	100	0	0	100	0	0	100	0	0	100	0	0	100	0	0	100	0	0	100	0	0	100
	6	0	0	100	0	0	100	0	0	100	0	0	100	0	0	100	0	0	100	0	0	100	0	0	100	0	0	100	0	0	100	0	0	100
	7	0	33	100	0	33	100	0	17	100	0	33	98	0	33	100	0	42	100	0	42	100	0	33	100	0	17	100	0	50	100	0	67	100
S07_R25	1	100	0	98	100	0	100	100	0	100	100	0	93	100	0	100	100	0	100	100	0	100	100	0	100	100	0	100	100	0	100	100	13	100
	2	10	0	100	0	0	100	0	0	100	0	0	100	0	0	100	10	0	100	0	0	100	0	0	100	0	0	100	0	0	100	0	0	100
	3	0	0	100	0	0	100	0	0	100	0	0	100	0	0	100	0	0	100	0	0	100	0	0	100	0	0	100	0	0	100	0	0	100
	4	0	0	100	0	0	100	0	0	100	0	0	100	0	0	100	0	0	100	0	0	100	0	0	100	0	0	100	0	0	100	0	0	100
	5	0	0	100	0	0	100	0	0	100	0	0	100	0	0	100	0	0	100	0	0	100	0	0	100	0	0	100	0	0	100	0	0	100
	6	0	0	100	0	0	100	0	0	100	0	0	100	0	0	100	0	0	100	0	0	100	0	0	100	0	0	100	0	0	100	0	0	100
	7	0	13	93	0	13	100	0	0	100	0	0	95	0	0	100	0	25	100	0	13	100	0	13	100	0	0	100	0	38	95	0	13	100

Table D.1 Percentage of members with reinforcement yielding- 7 story buildings (cont'd)

Model	Story	NOR			KOB			KOC			CHI			DUZ			SM			LOM			CC			ERZ			LAN			IMP		
		W	C	B	W	C	B	W	C	B	W	C	B	W	C	B	W	C	B	W	C	B	W	C	B	W	C	B	W	C	B	W	C	B
S07_R30	1	100	-	92	100	-	100	100	-	100	100	-	97	100	-	100	100	-	100	100	-	100	100	-	100	100	-	89	100	-	97	100	-	100
	2	0	-	97	0	-	100	0	-	100	0	-	100	0	-	100	0	-	100	0	-	100	0	-	100	0	-	100	0	-	100	0	-	100
	3	0	-	97	0	-	100	0	-	100	0	-	100	0	-	100	0	-	100	0	-	100	0	-	100	0	-	100	0	-	100	0	-	100
	4	0	-	100	0	-	100	0	-	100	0	-	100	0	-	100	0	-	100	0	-	100	0	-	100	0	-	100	0	-	100	0	-	100
	5	0	-	100	0	-	100	0	-	100	0	-	100	0	-	100	0	-	100	0	-	100	0	-	100	0	-	100	0	-	100	0	-	100
	6	0	-	100	0	-	100	0	-	100	0	-	100	0	-	100	0	-	100	0	-	100	0	-	100	0	-	100	0	-	100	0	-	100
	7	0	-	89	0	-	100	0	-	100	0	-	94	0	-	100	0	-	100	0	-	100	0	-	100	0	-	94	0	-	94	0	-	100

Note: NOR = Northridge; KOB = Kobe; KOC = Kocaeli; CHI = Chi Chi; DUZ = Duzce; SM = Sierramex; LOM = Loma prieta; CC = Christchurch; ERZ = Erzincan; LAN = Landers; IMP = Imperial Valley; W = Structural wall; C = Column; B = Beam

Table D.2 Percentage of members with reinforcement yielding - 10 story buildings

Model	Story	NOR			KOB			KOC			CHI			DUZ			SM			LOM			CC			ERZ			LAN			IMP		
		W	C	B	W	C	B	W	C	B	W	C	B	W	C	B	W	C	B	W	C	B	W	C	B	W	C	B	W	C	B	W	C	B
S10_R00	1	-	100	100	-	100	100	-	100	100	-	100	100	-	100	100	-	100	100	-	100	100	-	100	100	-	100	100	-	100	100	-	100	100
	2	-	67	100	-	22	100	-	8	100	-	19	100	-	31	100	-	31	100	-	33	100	-	86	100	-	92	100	-	56	100	-	33	100
	3	-	36	100	-	3	100	-	0	100	-	3	100	-	3	100	-	3	100	-	17	100	-	75	100	-	72	100	-	31	100	-	22	100
	4	-	36	100	-	0	100	-	0	100	-	0	100	-	3	100	-	0	100	-	14	100	-	78	100	-	81	100	-	17	100	-	22	100
	5	-	11	100	-	0	100	-	0	100	-	0	100	-	0	100	-	0	100	-	3	100	-	75	100	-	44	100	-	3	100	-	0	100
	6	-	0	100	-	0	100	-	0	100	-	0	100	-	0	100	-	0	100	-	0	100	-	19	100	-	17	100	-	0	100	-	0	100
	7	-	0	100	-	0	100	-	0	100	-	0	100	-	0	100	-	0	100	-	0	100	-	0	100	-	0	100	-	0	100	-	0	100
	8	-	0	100	-	0	100	-	0	100	-	0	100	-	0	100	-	0	100	-	0	100	-	0	100	-	0	100	-	0	100	-	0	100
	9	-	0	90	-	0	83	-	0	35	-	0	63	-	0	97	-	0	97	-	0	83	-	0	45	-	0	20	-	0	87	-	0	100
	10	-	0	0	-	0	0	-	0	0	-	0	0	-	0	0	-	0	0	-	0	0	-	0	0	-	0	0	-	0	0	-	0	0
S10_R05	1	100	100	100	100	63	100	100	23	100	100	30	100	100	40	100	100	50	100	100	63	100	100	73	100	100	100	100	100	50	100	100	37	100
	2	100	93	100	100	30	100	100	10	100	100	17	100	100	30	100	100	37	100	100	37	100	50	33	100	75	100	100	100	40	100	100	30	100
	3	0	10	100	0	0	100	0	3	100	0	3	100	0	0	100	25	17	100	0	0	100	0	7	100	25	10	100	0	10	100	25	7	100
	4	25	3	100	0	0	100	0	0	100	0	0	100	0	0	100	0	13	100	25	0	100	0	0	100	0	7	100	25	0	100	0	3	100
	5	50	3	100	0	0	100	0	0	100	0	0	100	0	0	100	0	3	100	25	0	100	0	0	100	25	13	100	25	0	100	0	0	100
	6	50	0	100	0	0	100	0	0	100	0	0	100	0	0	100	0	3	100	50	0	100	25	0	100	75	13	100	0	0	100	0	0	100
	7	50	0	100	0	0	100	0	0	100	0	0	100	0	0	100	0	0	100	0	0	100	50	0	100	100	17	100	0	0	100	25	0	100
	8	100	0	100	0	0	100	0	0	100	0	0	100	0	0	100	0	0	100	25	0	100	25	0	100	100	3	100	0	0	100	0	0	100
	9	0	0	100	0	0	100	0	0	100	0	0	100	0	0	100	0	0	100	0	0	100	0	0	100	0	0	100	0	0	100	0	0	100
	10	0	93	100	0	60	100	0	60	100	0	70	98	0	73	100	0	90	100	0	73	100	0	83	100	0	80	100	0	87	100	0	83	100

Table D.2 Percentage of members with reinforcement yielding- 10 story buildings (cont'd)

Model	Story	NOR			KOB			KOC			CHI			DUZ			SM			LOM			CC			ERZ			LAN			IMP		
		W	C	B	W	C	B	W	C	B	W	C	B	W	C	B	W	C	B	W	C	B	W	C	B	W	C	B	W	C	B	W	C	B
S10_R10	1	100	29	100	100	13	100	100	0	98	100	8	100	100	8	100	100	17	98	100	38	100	100	25	100	100	100	100	100	33	100	100	25	100
	2	100	29	100	88	13	100	63	4	100	88	8	100	100	21	100	100	25	100	88	21	100	100	21	100	100	92	100	100	29	100	100	25	100
	3	0	17	100	0	0	100	0	0	100	0	0	100	0	0	100	0	4	100	0	4	100	0	8	100	0	17	100	0	4	100	0	0	100
	4	0	0	100	0	0	100	0	0	100	0	0	100	0	0	100	0	0	100	0	0	100	0	0	100	0	8	100	0	0	100	0	0	100
	5	0	0	100	0	0	100	0	0	100	0	0	100	0	0	100	0	0	100	0	0	100	0	0	100	0	8	100	0	0	100	0	0	100
	6	0	0	100	0	0	100	0	0	100	0	0	100	0	0	100	0	0	100	0	0	100	0	0	100	0	4	100	0	0	100	0	0	100
	7	0	0	100	0	0	100	0	0	100	0	0	100	0	0	100	0	0	100	0	0	100	0	0	100	0	4	100	0	0	100	0	0	100
	8	0	0	100	0	0	100	0	0	100	0	0	100	0	0	100	0	0	100	0	0	100	0	0	100	0	4	100	0	0	100	0	0	100
	9	0	0	100	0	0	100	0	0	100	0	0	100	0	0	100	0	0	100	0	0	100	0	0	100	0	4	100	0	0	100	0	0	100
	10	0	96	100	0	100	100	0	88	98	0	92	98	0	100	100	0	92	100	0	96	100	0	96	100	0	96	98	0	100	100	0	100	100
S10_R15	1	100	33	100	100	0	100	100	11	100	100	0	100	100	11	100	100	22	100	100	22	100	100	28	100	100	89	100	100	28	100	100	17	100
	2	100	28	100	100	6	100	33	11	100	58	11	100	100	33	100	100	22	100	92	28	100	100	28	100	100	83	100	100	33	100	100	33	100
	3	0	22	100	0	0	100	0	6	100	0	6	100	0	6	100	0	22	100	0	0	100	0	0	100	0	11	100	0	0	100	0	11	100
	4	0	6	100	0	0	100	0	0	100	0	0	100	0	0	100	0	11	100	0	0	100	0	0	100	0	11	100	0	0	100	0	6	100
	5	0	0	100	0	0	100	0	0	100	0	0	100	0	0	100	0	6	100	0	0	100	0	0	100	0	6	100	0	0	100	0	0	100
	6	0	0	100	0	0	100	0	0	100	0	0	100	0	0	100	0	0	100	0	0	100	0	0	100	0	6	100	0	0	100	0	0	100
	7	0	0	100	0	0	100	0	0	100	0	0	100	0	0	100	0	0	100	0	0	100	0	0	100	0	6	100	0	0	100	0	0	100
	8	0	0	100	0	0	100	0	0	100	0	0	100	0	0	100	0	0	100	0	0	100	0	0	100	0	6	100	0	0	100	0	0	100
	9	0	0	100	0	0	100	0	0	100	0	0	100	0	0	100	0	0	100	0	0	100	0	0	100	0	0	100	0	0	100	0	0	100
	10	0	94	100	0	89	100	0	83	100	0	83	100	0	100	100	0	94	100	0	89	100	0	100	100	0	89	100	0	100	100	0	100	100

Table D.2 Percentage of members with reinforcement yielding- 10 story buildings (cont'd)

Model	Story	NOR			KOB			KOC			CHI			DUZ			SM			LOM			CC			ERZ			LAN			IMP		
		W	C	B	W	C	B	W	C	B	W	C	B	W	C	B	W	C	B	W	C	B	W	C	B	W	C	B	W	C	B	W	C	B
S10_R20	1	100	33	100	100	0	100	100	17	95	100	0	100	100	8	100	100	33	100	100	8	100	100	0	100	100	58	98	100	17	100	100	8	100
	2	75	33	100	75	17	100	25	17	100	31	8	100	81	33	100	81	33	100	88	17	100	69	42	100	69	58	100	100	25	100	100	58	100
	3	0	17	100	0	0	100	0	8	100	0	0	100	0	8	100	0	17	100	0	0	100	0	0	100	0	17	100	0	17	100	0	17	100
	4	0	0	100	0	0	100	0	0	100	0	0	100	0	0	100	0	8	100	0	0	100	0	0	100	0	17	100	0	8	100	0	8	100
	5	0	0	100	0	0	100	0	0	100	0	0	100	0	0	100	0	0	100	0	0	100	0	0	100	0	17	100	0	0	100	0	0	100
	6	0	0	100	0	0	100	0	0	100	0	0	100	0	0	100	0	0	100	0	0	100	0	0	100	0	17	100	0	0	100	0	0	100
	7	0	0	100	0	0	100	0	0	100	0	0	100	0	0	100	0	0	100	0	0	100	0	0	100	0	17	100	0	0	100	0	0	100
	8	0	0	100	0	0	100	0	0	100	0	0	100	0	0	100	0	0	100	0	0	100	0	0	100	0	8	100	0	0	100	0	0	100
	9	0	0	100	0	0	100	0	0	100	0	0	100	0	0	100	0	0	100	0	0	100	0	0	100	0	0	100	0	0	100	0	0	100
	10	0	75	100	0	83	100	0	33	100	0	42	100	0	83	100	0	67	100	0	75	100	0	67	100	0	83	100	0	100	100	0	100	100
S10_R25	1	100	25	100	100	0	100	100	0	95	100	0	100	100	13	100	100	25	100	100	0	100	100	0	100	100	38	100	100	25	100	100	0	100
	2	90	50	100	80	0	100	30	13	100	55	0	100	80	38	100	85	50	100	55	0	100	60	0	100	65	38	100	100	25	100	100	75	100
	3	0	0	100	0	0	100	0	0	100	0	0	100	0	13	100	0	13	100	0	0	100	0	0	100	0	25	100	0	13	100	0	25	100
	4	0	0	100	0	0	100	0	0	100	0	0	100	0	0	100	0	0	100	0	0	100	0	0	100	0	25	100	0	0	100	0	0	100
	5	0	0	100	0	0	100	0	0	100	0	0	100	0	0	100	0	0	100	0	0	100	0	0	100	0	13	100	0	0	100	0	0	100
	6	0	0	100	0	0	100	0	0	100	0	0	100	0	0	100	0	0	100	0	0	100	0	0	100	0	13	100	0	0	100	0	0	100
	7	0	0	100	0	0	100	0	0	100	0	0	100	0	0	100	0	0	100	0	0	100	0	0	100	0	13	100	0	0	100	0	0	100
	8	0	0	100	0	0	100	0	0	100	0	0	100	0	0	100	0	0	100	0	0	100	0	0	100	0	0	100	0	0	100	0	0	100
	9	0	0	100	0	0	100	0	0	100	0	0	100	0	0	100	0	0	100	0	0	100	0	0	100	0	0	100	0	0	100	0	0	100
	10	0	75	100	0	75	100	0	25	100	0	38	100	0	75	100	0	50	100	0	75	100	0	38	100	0	88	100	0	63	100	0	100	100

Table D.2 Percentage of members with reinforcement yielding- 10 story buildings (cont'd)

Model	Story	NOR			KOB			KOC			CHI			DUZ			SM			LOM			CC			ERZ			LAN			IMP		
		W	C	B	W	C	B	W	C	B	W	C	B	W	C	B	W	C	B	W	C	B	W	C	B	W	C	B	W	C	B	W	C	B
S10_R30	1	100	-	100	100	-	100	100	-	100	100	-	100	100	-	100	100	-	100	100	-	100	100	-	100	100	-	94	100	-	100	100	-	100
	2	83	-	100	67	-	100	21	-	100	21	-	100	67	-	100	67	-	100	46	-	100	46	-	100	38	-	100	67	-	100	92	-	100
	3	0	-	100	0	-	100	0	-	100	0	-	100	0	-	100	0	-	100	0	-	100	0	-	100	0	-	100	0	-	100	0	-	100
	4	0	-	100	0	-	100	0	-	100	0	-	100	0	-	100	0	-	100	0	-	100	0	-	100	0	-	100	0	-	100	0	-	100
	5	0	-	100	0	-	100	0	-	100	0	-	100	0	-	100	0	-	100	0	-	100	0	-	100	0	-	100	0	-	100	0	-	100
	6	0	-	100	0	-	100	0	-	100	0	-	100	0	-	100	0	-	100	0	-	100	0	-	100	0	-	100	0	-	100	0	-	100
	7	0	-	100	0	-	100	0	-	100	0	-	100	0	-	100	0	-	100	0	-	100	0	-	100	0	-	100	0	-	100	0	-	100
	8	0	-	100	0	-	100	0	-	100	0	-	100	0	-	100	0	-	100	0	-	100	0	-	100	0	-	100	0	-	100	0	-	100
	9	0	-	100	0	-	100	0	-	100	0	-	100	0	-	100	0	-	100	0	-	100	0	-	100	0	-	100	0	-	100	0	-	100
	10	0	-	100	0	-	100	0	-	100	0	-	100	0	-	100	0	-	100	0	-	100	0	-	100	0	-	100	0	-	100	0	-	100

Note: NOR = Northridge; KOB = Kobe; KOC = Kocaeli; CHI = Chi Chi; DUZ = Duzce; SM = Sierramex; LOM = Loma prieta; CC = Christchurch; ERZ = Erzincan; LAN = Landers; IMP = Imperial Valley; W = Structural wall; C = Column; B = Beam

Table D.3 Percentage of members with reinforcement yielding - 20 story buildings

Model	Story	NOR			KOB			KOC			CHI			DUZ			SM			LOM			CC			ERZ			LAN			IMP		
		W	C	B	W	C	B	W	C	B	W	C	B	W	C	B	W	C	B	W	C	B	W	C	B	W	C	B	W	C	B	W	C	B
S20_R00	1	-	100	100	-	100	100	-	100	100	-	100	100	-	100	100	-	100	100	-	100	100	-	100	100	-	100	100	-	100	100	-	100	100
	2	-	86	100	-	33	100	-	36	100	-	6	100	-	22	100	-	19	100	-	47	100	-	39	100	-	100	100	-	28	100	-	86	100
	3	-	42	100	-	14	100	-	11	100	-	3	100	-	8	100	-	11	100	-	31	100	-	17	100	-	69	100	-	8	100	-	33	100
	4	-	33	100	-	11	100	-	11	100	-	0	100	-	3	100	-	3	100	-	25	100	-	14	100	-	33	100	-	6	100	-	28	100
	5	-	25	100	-	8	100	-	8	100	-	0	100	-	0	100	-	0	100	-	17	100	-	14	100	-	25	100	-	3	100	-	28	100
	6	-	14	100	-	3	100	-	3	100	-	0	100	-	0	100	-	0	100	-	8	100	-	14	100	-	25	100	-	3	100	-	14	100
	7	-	6	100	-	3	100	-	0	100	-	0	100	-	0	100	-	0	100	-	6	100	-	6	100	-	19	100	-	0	100	-	8	100
	8	-	3	100	-	0	100	-	0	100	-	0	100	-	0	100	-	0	100	-	3	100	-	6	100	-	8	100	-	0	100	-	6	100
	9	-	0	100	-	0	100	-	0	100	-	0	100	-	0	100	-	0	100	-	0	100	-	0	100	-	0	100	-	0	100	-	3	100
	10	-	0	100	-	0	100	-	0	100	-	0	100	-	0	100	-	0	100	-	0	100	-	0	100	-	0	100	-	0	100	-	0	100
	11	-	0	100	-	0	100	-	0	100	-	0	100	-	0	100	-	0	100	-	0	100	-	0	100	-	0	100	-	0	100	-	0	100
	12	-	0	100	-	0	100	-	0	100	-	0	100	-	0	100	-	0	100	-	0	100	-	0	100	-	0	100	-	0	100	-	0	100
	13	-	0	100	-	0	100	-	0	100	-	0	100	-	0	100	-	0	100	-	0	100	-	0	100	-	0	100	-	0	100	-	0	100
	14	-	0	100	-	0	100	-	0	100	-	0	100	-	0	100	-	0	100	-	0	100	-	0	100	-	0	100	-	0	100	-	0	100
	15	-	0	100	-	0	100	-	0	100	-	0	100	-	0	100	-	0	100	-	0	100	-	0	100	-	0	100	-	0	100	-	0	100
	16	-	0	100	-	0	100	-	0	100	-	0	100	-	0	100	-	0	100	-	0	100	-	0	100	-	0	100	-	0	100	-	0	100
	17	-	0	100	-	0	100	-	0	100	-	0	100	-	0	100	-	0	100	-	0	100	-	0	100	-	0	100	-	0	100	-	0	100
	18	-	0	100	-	0	97	-	0	93	-	0	100	-	0	97	-	0	100	-	0	98	-	0	98	-	0	92	-	0	100	-	0	100
	19	-	0	43	-	0	0	-	0	0	-	0	3	-	0	23	-	0	35	-	0	47	-	0	50	-	0	15	-	0	18	-	0	72
	20	-	0	0	-	0	0	-	0	0	-	0	0	-	0	0	-	0	0	-	0	0	-	0	0	-	0	2	-	0	0	-	0	0

Table D.3 Percentage of members with reinforcement yielding - 20 story buildings (cont'd)

Model	Story	NOR			KOB			KOC			CHI			DUZ			SM			LOM			CC			ERZ			LAN			IMP		
		W	C	B	W	C	B	W	C	B	W	C	B	W	C	B	W	C	B	W	C	B	W	C	B	W	C	B	W	C	B	W	C	B
S20_R05	1	100	97	100	100	30	100	100	37	100	100	17	100	100	60	100	100	23	100	100	97	100	100	47	100	100	100	100	100	100	100	100	100	100
	2	100	97	100	100	30	100	100	37	100	100	7	100	100	23	100	100	23	100	100	97	100	100	47	100	100	100	100	100	33	100	100	50	100
	3	0	17	100	50	13	100	25	20	100	0	0	100	0	0	100	0	7	100	25	13	100	100	30	100	25	27	100	0	13	100	25	30	100
	4	0	13	100	0	7	100	0	17	100	0	0	100	0	0	100	0	7	100	0	7	100	25	30	100	0	17	100	0	13	100	0	27	100
	5	0	13	100	0	7	100	0	13	100	0	0	100	0	0	100	0	7	100	0	0	100	0	30	100	0	17	100	0	10	100	0	17	100
	6	0	7	100	0	0	100	0	10	100	0	0	100	0	0	100	0	3	100	0	0	100	0	30	100	25	20	100	0	7	100	0	13	100
	7	0	7	100	25	0	100	0	10	100	0	0	100	0	0	100	0	3	100	25	0	100	0	30	100	25	20	100	0	0	100	0	7	100
	8	25	7	100	25	0	100	0	3	100	0	0	100	25	0	100	0	3	100	50	0	100	0	33	100	25	10	100	0	0	100	0	7	100
	9	25	0	100	25	0	100	0	0	100	0	0	100	50	0	100	25	0	100	50	0	100	0	27	100	25	3	100	0	0	100	25	0	100
	10	25	0	100	0	0	100	0	0	100	50	0	100	50	0	100	50	0	100	50	0	100	25	27	100	25	3	100	0	0	100	50	0	100
	11	25	0	100	0	0	100	0	0	100	50	0	100	50	0	100	50	0	100	50	0	100	50	13	100	25	3	100	25	0	100	50	0	100
	12	25	0	100	25	0	100	0	0	100	25	0	100	50	0	100	50	0	100	0	0	100	25	7	100	25	7	100	25	0	100	75	0	100
	13	0	0	100	25	0	100	0	0	100	0	0	100	0	0	100	25	0	100	0	0	100	25	7	100	50	3	100	25	0	100	25	0	100
	14	0	0	100	25	0	100	0	0	100	0	0	100	0	0	100	0	0	100	25	0	100	0	7	100	50	0	100	25	0	100	25	0	100
	15	0	0	100	25	0	100	0	0	100	0	0	100	0	0	100	0	0	100	25	0	100	25	7	100	50	0	100	0	0	100	50	0	100
	16	0	0	100	0	0	100	0	0	100	0	0	100	0	0	100	0	0	100	25	0	100	50	3	100	50	0	100	0	0	100	50	0	100
	17	0	0	100	0	0	100	0	0	100	0	0	100	0	0	100	0	0	100	0	0	100	50	0	100	25	0	100	0	0	100	0	0	100
	18	0	0	100	0	0	100	0	0	100	0	0	100	0	0	100	0	0	100	0	0	100	0	0	100	0	0	100	0	0	100	0	0	100
	19	0	0	100	0	0	100	0	0	100	0	0	100	0	0	100	0	0	100	0	0	100	0	0	100	0	0	100	0	0	100	0	0	100
	20	0	17	93	0	23	98	0	47	100	0	60	96	0	23	100	0	67	100	0	23	100	0	83	98	0	50	100	0	63	100	0	80	100

Table D.3 Percentage of members with reinforcement yielding - 20 story buildings (cont'd)

Model	Story	NOR			KOB			KOC			CHI			DUZ			SM			LOM			CC			ERZ			LAN			IMP		
		W	C	B	W	C	B	W	C	B	W	C	B	W	C	B	W	C	B	W	C	B	W	C	B	W	C	B	W	C	B	W	C	B
S20_R10	1	100	38	98	100	17	100	100	13	100	100	0	100	100	4	100	100	8	100	100	38	100	100	29	100	100	100	100	100	17	100	100	29	100
	2	100	38	100	100	21	100	100	25	100	100	0	100	100	4	100	100	21	100	100	38	100	100	33	100	100	96	100	100	21	100	100	29	100
	3	25	21	100	13	17	100	0	8	100	0	0	100	0	0	100	0	4	100	38	21	100	38	21	100	38	21	100	0	8	100	13	17	100
	4	0	21	100	0	8	100	0	4	100	0	0	100	0	0	100	0	0	100	0	13	100	13	21	100	0	21	100	0	8	100	0	13	100
	5	0	21	100	0	4	100	0	4	100	0	0	100	0	0	100	0	0	100	0	13	100	0	21	100	0	21	100	0	4	100	0	13	100
	6	0	17	100	0	4	100	0	4	100	0	0	100	0	0	100	0	0	100	0	13	100	0	21	100	13	13	100	0	4	100	0	8	100
	7	13	13	100	0	4	100	0	0	100	0	0	100	0	0	100	0	0	100	0	8	100	0	21	100	13	13	100	0	4	100	0	4	100
	8	13	8	100	0	4	100	0	0	100	0	0	100	0	0	100	0	0	100	0	8	100	0	21	100	0	13	100	0	0	100	13	4	100
	9	13	4	100	0	4	100	0	0	100	0	0	100	0	0	100	0	0	100	0	8	100	0	17	100	0	8	100	0	0	100	13	4	100
	10	0	0	100	0	4	100	0	0	100	0	0	100	0	0	100	0	0	100	13	8	100	0	17	100	0	8	100	0	0	100	25	4	100
	11	0	0	100	0	0	100	0	0	100	0	0	100	0	0	100	0	0	100	0	8	100	0	13	100	0	8	100	0	0	100	25	4	100
	12	0	0	100	0	0	100	0	0	100	0	0	100	0	0	100	0	0	100	0	8	100	0	17	100	0	8	100	0	0	100	13	4	100
	13	0	0	100	0	0	100	0	0	100	0	0	100	0	0	100	0	0	100	0	4	100	0	13	100	0	8	100	0	0	100	0	4	100
	14	0	0	100	0	0	100	0	0	100	0	0	100	0	0	100	0	0	100	0	4	100	0	8	100	0	8	100	0	0	100	0	4	100
	15	0	0	100	0	0	100	0	0	100	0	0	100	0	0	100	0	0	100	0	4	100	0	4	100	0	8	100	0	0	100	0	4	100
	16	0	0	100	0	0	100	0	0	100	0	0	100	0	0	100	0	0	100	0	4	100	0	8	100	0	8	100	0	0	100	0	4	100
	17	0	0	100	0	0	100	0	0	100	0	0	100	0	0	100	0	0	100	0	4	100	0	17	100	0	8	100	0	0	100	0	4	100
	18	0	0	100	0	0	100	0	0	100	0	0	100	0	0	100	0	0	100	0	4	100	0	29	100	0	17	100	0	0	100	0	4	100
	19	0	0	100	0	0	100	0	0	100	0	0	100	0	0	100	0	0	100	0	0	100	0	21	100	0	13	100	0	0	100	0	0	100
	20	0	100	100	0	100	100	0	96	100	0	100	100	0	96	100	0	96	100	0	96	100	0	100	100	0	100	100	0	100	100	0	100	100

Table D.3 Percentage of members with reinforcement yielding - 20 story buildings (cont'd)

Model	Story	NOR			KOB			KOC			CHI			DUZ			SM			LOM			CC			ERZ			LAN			IMP		
		W	C	B	W	C	B	W	C	B	W	C	B	W	C	B	W	C	B	W	C	B	W	C	B	W	C	B	W	C	B	W	C	B
S20_R15	1	100	33	98	100	6	100	100	17	100	100	0	100	100	0	94	100	6	100	100	22	98	100	33	100	100	83	100	100	28	100	100	28	100
	2	100	39	100	100	33	100	92	22	100	92	6	100	75	0	100	100	33	100	92	33	100	100	44	100	100	83	100	100	33	100	100	33	100
	3	25	22	100	0	22	100	0	17	100	0	0	100	0	0	100	0	17	100	8	17	100	42	33	100	33	28	100	8	22	100	17	28	100
	4	0	22	100	0	6	100	0	6	100	0	0	100	0	0	100	0	6	100	0	11	100	0	33	100	0	28	100	0	22	100	0	17	100
	5	0	17	100	0	6	100	0	6	100	0	0	100	0	0	100	0	0	100	0	6	100	0	33	100	0	22	100	0	22	100	0	11	100
	6	0	17	100	0	6	100	0	6	100	0	0	100	0	0	100	0	0	100	0	6	100	0	33	100	8	22	100	0	17	100	0	11	100
	7	0	17	100	0	0	100	0	0	100	0	11	100	0	0	100	0	0	100	0	6	100	0	33	100	8	22	100	0	17	100	0	11	100
	8	0	17	100	0	0	100	0	0	100	0	11	100	0	0	100	0	0	100	0	6	100	0	33	100	0	22	100	0	17	100	0	11	100
	9	0	6	100	0	0	100	0	0	100	0	11	100	0	0	100	0	0	100	0	6	100	0	33	100	0	17	100	0	17	100	0	11	100
	10	8	0	100	0	0	100	0	0	100	0	11	100	0	0	100	0	0	100	0	0	100	0	28	100	0	17	100	0	11	100	0	11	100
	11	8	0	100	0	0	100	0	0	100	0	11	100	0	0	100	0	0	100	0	0	100	0	33	100	0	6	100	0	11	100	0	11	100
	12	8	0	100	0	0	100	0	0	100	0	11	100	0	0	100	0	0	100	0	0	100	0	33	100	0	6	100	0	6	100	0	17	100
	13	0	0	100	0	0	100	0	0	100	0	11	100	0	0	100	0	0	100	0	0	100	0	39	100	0	6	100	0	6	100	0	17	100
	14	0	0	100	0	0	100	0	0	100	0	11	100	0	0	100	0	0	100	0	6	100	0	39	100	0	6	100	0	6	100	0	17	100
	15	0	0	100	0	0	100	0	0	100	0	11	100	0	0	100	0	0	100	0	6	100	0	33	100	0	6	100	0	6	100	0	17	100
	16	0	0	100	0	0	100	0	0	100	0	11	100	0	0	100	0	0	100	0	6	100	0	39	100	0	6	100	0	6	100	0	28	100
	17	0	6	100	0	0	100	0	0	100	0	11	100	0	0	100	0	0	100	0	6	100	0	61	100	0	17	100	0	11	100	0	22	100
	18	0	6	100	0	0	100	0	0	100	0	11	100	0	0	100	0	0	100	0	17	100	0	67	100	0	22	100	0	11	100	0	22	100
	19	0	0	100	0	0	100	0	0	100	0	6	100	0	0	100	0	0	100	0	6	100	0	50	100	0	22	100	0	11	100	0	11	100
	20	0	100	100	0	100	100	0	100	100	0	100	100	0	100	100	0	94	100	0	100	100	0	100	100	0	100	100	0	100	100	0	100	100

Table D.3 Percentage of members with reinforcement yielding - 20 story buildings (cont'd)

Model	Story	NOR			KOB			KOC			CHI			DUZ			SM			LOM			CC			ERZ			LAN			IMP		
		W	C	B	W	C	B	W	C	B	W	C	B	W	C	B	W	C	B	W	C	B	W	C	B	W	C	B	W	C	B	W	C	B
S20_R20	1	100	42	100	100	8	100	100	8	100	100	0	98	100	0	95	100	0	100	100	17	100	100	33	100	100	42	100	100	25	98	100	42	100
	2	94	50	100	94	33	100	63	25	100	81	0	100	81	17	100	100	8	100	81	33	100	100	50	100	100	50	100	94	33	100	94	50	100
	3	31	42	100	0	8	100	0	8	100	0	0	100	13	17	100	0	8	100	0	25	100	31	42	100	38	50	100	13	33	100	25	42	100
	4	0	33	100	0	8	100	0	8	100	0	0	100	0	17	100	0	0	100	0	17	100	6	33	100	0	42	100	0	25	100	0	17	100
	5	0	33	100	0	8	100	0	0	100	0	0	100	0	17	100	0	0	100	0	17	100	6	33	100	0	33	100	0	25	100	0	17	100
	6	0	33	100	0	8	100	0	0	100	0	0	100	0	17	100	0	0	100	0	17	100	0	42	100	0	33	100	0	25	100	0	17	100
	7	0	33	100	0	8	100	0	0	100	0	17	100	0	17	100	0	0	100	0	17	100	0	42	100	0	33	100	0	25	100	0	17	100
	8	0	25	100	0	8	100	0	0	100	0	17	100	0	17	100	0	0	100	0	17	100	0	42	100	0	33	100	0	17	100	0	17	100
	9	0	25	100	0	0	100	0	0	100	0	17	100	0	17	100	0	0	100	0	17	100	0	42	100	0	33	100	0	17	100	0	8	100
	10	0	25	100	0	0	100	0	0	100	0	17	100	0	17	100	0	0	100	0	25	100	0	42	100	0	25	100	0	17	100	0	8	100
	11	0	17	100	0	0	100	0	0	100	0	17	100	0	17	100	0	0	100	0	25	100	0	33	100	0	25	100	0	17	100	0	8	100
	12	0	8	100	0	0	100	0	0	100	0	17	100	0	8	100	0	0	100	0	25	100	0	33	100	0	25	100	0	17	100	0	8	100
	13	0	8	100	0	0	100	0	0	100	0	17	100	0	0	100	0	0	100	0	25	100	0	33	100	0	25	100	0	8	100	0	8	100
	14	0	8	100	0	0	100	0	0	100	0	17	100	0	0	100	0	0	100	0	17	100	0	33	100	0	25	100	0	8	100	0	8	100
	15	0	8	100	0	0	100	0	0	100	0	17	100	0	0	100	0	0	100	0	17	100	0	25	100	0	17	100	0	8	100	0	8	100
	16	0	8	100	0	0	100	0	0	100	0	17	100	0	0	100	0	0	100	0	8	100	0	25	100	0	17	100	0	8	100	0	8	100
	17	0	8	100	0	0	100	0	0	100	0	8	100	0	0	100	0	0	100	0	8	100	0	25	100	0	17	100	0	0	100	0	8	100
	18	0	8	100	0	0	100	0	0	100	0	8	100	0	0	100	0	0	100	0	8	100	0	33	100	0	17	100	0	0	100	0	8	100
	19	0	8	100	0	0	100	0	0	100	0	0	100	0	0	100	0	0	100	0	0	100	0	17	100	0	8	100	0	0	100	0	8	100
	20	0	92	100	0	100	100	0	100	100	0	100	100	0	92	100	0	100	100	0	100	100	0	100	100	0	100	100	0	100	100	0	92	100

Table D.3 Percentage of members with reinforcement yielding - 20 story buildings (cont'd)

Model	Story	NOR			KOB			KOC			CHI			DUZ			SM			LOM			CC			ERZ			LAN			IMP		
		W	C	B	W	C	B	W	C	B	W	C	B	W	C	B	W	C	B	W	C	B	W	C	B	W	C	B	W	C	B	W	C	B
S20_R25	1	100	38	100	100	0	100	100	0	80	100	0	100	100	0	93	100	0	100	100	13	100	100	50	100	100	63	100	100	25	100	100	25	100
	2	95	75	100	95	25	100	60	0	100	65	0	100	75	25	100	95	0	100	90	25	100	100	75	100	100	75	100	95	50	100	100	50	100
	3	30	38	100	0	13	100	0	0	100	5	0	100	30	25	100	0	0	100	0	25	100	15	50	100	35	75	100	30	38	100	30	25	100
	4	0	50	100	0	13	100	0	0	100	0	0	100	0	25	100	0	0	100	0	13	100	0	50	100	0	50	100	0	25	100	0	25	100
	5	0	38	100	0	0	100	0	0	100	0	0	100	0	25	100	0	0	100	0	13	100	0	50	100	0	38	100	0	25	100	0	25	100
	6	0	38	100	0	0	100	0	0	100	0	13	100	0	25	100	0	0	100	0	0	100	0	50	100	0	38	100	0	25	100	0	25	100
	7	0	38	100	0	0	100	0	0	100	0	25	100	0	25	100	0	0	100	0	0	100	0	50	100	0	38	100	0	25	100	0	25	100
	8	0	38	100	0	0	100	0	0	100	0	25	100	0	25	100	0	0	100	0	0	100	0	50	100	0	38	100	0	25	100	0	25	100
	9	0	38	100	0	0	100	0	0	100	0	13	100	0	25	100	0	0	100	0	0	100	0	50	100	0	25	100	0	25	100	0	25	100
	10	0	38	100	0	0	100	0	0	100	0	13	100	0	25	100	0	0	100	0	0	100	0	50	100	0	25	100	0	25	100	0	13	100
	11	0	25	100	0	0	100	0	0	100	0	0	100	0	0	100	0	0	100	0	13	100	0	38	100	0	25	100	0	25	100	0	13	100
	12	0	25	100	0	0	100	0	0	100	0	0	100	0	0	100	0	0	100	0	13	100	0	38	100	0	13	100	0	25	100	0	13	100
	13	0	25	100	0	0	100	0	0	100	0	0	100	0	0	100	0	0	100	0	13	100	0	25	100	0	13	100	0	0	100	0	13	100
	14	0	25	100	0	0	100	0	0	100	0	0	100	0	0	100	0	0	100	0	13	100	0	25	100	0	13	100	0	0	100	0	13	100
	15	0	13	100	0	0	100	0	0	100	0	0	100	0	0	100	0	0	100	0	13	100	0	25	100	0	13	100	0	0	100	0	13	100
	16	0	13	100	0	0	100	0	0	100	0	0	100	0	0	100	0	0	100	0	13	100	0	25	100	0	13	100	0	0	100	0	13	100
	17	0	13	100	0	0	100	0	0	100	0	0	100	0	0	100	0	0	100	0	13	100	0	25	100	0	13	100	0	0	100	0	13	100
	18	0	13	100	0	0	100	0	0	100	0	0	100	0	0	100	0	0	100	0	13	100	0	13	100	0	13	100	0	0	100	0	13	100
	19	0	13	100	0	0	100	0	0	100	0	0	100	0	0	100	0	0	100	0	0	100	0	13	100	0	13	100	0	0	100	0	0	100
	20	0	100	100	0	100	100	0	75	100	0	100	100	0	100	100	0	100	100	0	100	100	0	100	100	0	100	100	0	100	100	0	100	100

Table D.3 Percentage of members with reinforcement yielding - 20 story buildings (cont'd)

Model	Story	NOR			KOB			KOC			CHI			DUZ			SM			LOM			CC			ERZ			LAN			IMP		
		W	C	B	W	C	B	W	C	B	W	C	B	W	C	B	W	C	B	W	C	B	W	C	B	W	C	B	W	C	B	W	C	B
S20_R30	1	100	-	94	100	-	100	100	-	83	100	-	100	100	-	92	100	-	100	100	-	100	100	-	92	100	-	100	100	-	100	100	-	100
	2	92	-	100	79	-	100	46	-	100	46	-	100	79	-	100	75	-	100	75	-	100	100	-	100	100	-	100	75	-	100	100	-	100
	3	25	-	100	0	-	100	0	-	100	13	-	100	21	-	100	0	-	100	0	-	100	13	-	100	25	-	100	25	-	100	25	-	100
	4	0	-	100	0	-	100	0	-	100	0	-	100	0	-	100	0	-	100	0	-	100	0	-	100	0	-	100	0	-	100	0	-	100
	5	0	-	100	0	-	100	0	-	100	0	-	100	0	-	100	0	-	100	0	-	100	0	-	100	0	-	100	0	-	100	0	-	100
	6	0	-	100	0	-	100	0	-	100	0	-	100	0	-	100	0	-	100	0	-	100	0	-	100	0	-	100	0	-	100	0	-	100
	7	0	-	100	0	-	100	0	-	100	0	-	100	0	-	100	0	-	100	0	-	100	0	-	100	0	-	100	0	-	100	0	-	100
	8	0	-	100	0	-	100	0	-	100	0	-	100	0	-	100	0	-	100	0	-	100	0	-	100	0	-	100	0	-	100	0	-	100
	9	0	-	100	0	-	100	0	-	100	0	-	100	0	-	100	0	-	100	0	-	100	0	-	100	0	-	100	0	-	100	0	-	100
	10	0	-	100	0	-	100	0	-	100	0	-	100	0	-	100	0	-	100	0	-	100	0	-	100	0	-	100	0	-	100	0	-	100
	11	0	-	100	0	-	100	0	-	100	0	-	100	0	-	100	0	-	100	0	-	100	0	-	100	0	-	100	0	-	100	0	-	100
	12	0	-	100	0	-	100	0	-	100	0	-	100	0	-	100	0	-	100	0	-	100	0	-	100	0	-	100	0	-	100	0	-	100
	13	0	-	100	0	-	100	0	-	100	0	-	100	0	-	100	0	-	100	0	-	100	0	-	100	0	-	100	0	-	100	0	-	100
	14	0	-	100	0	-	100	0	-	100	0	-	100	0	-	100	0	-	100	0	-	100	0	-	100	0	-	100	0	-	100	0	-	100
	15	0	-	100	0	-	100	0	-	100	0	-	100	0	-	100	0	-	100	0	-	100	0	-	100	0	-	100	0	-	100	0	-	100
	16	0	-	100	0	-	100	0	-	100	0	-	100	0	-	100	0	-	100	0	-	100	0	-	100	0	-	100	0	-	100	0	-	100
	17	0	-	100	0	-	100	0	-	100	0	-	100	0	-	100	0	-	100	0	-	100	0	-	100	0	-	100	0	-	100	0	-	100
	18	0	-	100	0	-	100	0	-	100	0	-	100	0	-	100	0	-	100	0	-	100	0	-	100	0	-	100	0	-	100	0	-	100
	19	0	-	100	0	-	100	0	-	100	0	-	100	0	-	100	0	-	100	0	-	100	0	-	100	0	-	100	0	-	100	0	-	100
	20	0	-	100	0	-	100	0	-	100	0	-	100	0	-	100	0	-	100	0	-	100	0	-	100	0	-	100	0	-	100	0	-	100

Note: NOR = Northridge; KOB = Kobe; KOC = Kocaeli; CHI = Chi Chi; DUZ = Duzce; SM = Sierramex; LOM = Loma prieta; CC = Christchurch; ERZ = Erzincan; LAN = Landers; IMP = Imperial Valley; W = Structural wall; C = Column; B = Beam

Table D.4 Percentage of members with reinforcement yielding - 30 story buildings

Model	Story	NOR			KOB			KOC			CHI			DUZ			SM			LOM			CC			ERZ			LAN			IMP		
		W	C	B	W	C	B	W	C	B	W	C	B	W	C	B	W	C	B	W	C	B	W	C	B	W	C	B	W	C	B	W	C	B
S30_R00	1	-	100	100	-	100	100	-	100	100	-	100	100	-	100	100	-	100	100	-	100	100	-	100	100	-	100	100	-	100	100	-	100	100
	2	-	83	100	-	11	100	-	19	100	-	25	100	-	69	100	-	50	100	-	58	100	-	61	100	-	100	100	-	58	100	-	81	100
	3	-	8	100	-	8	100	-	8	100	-	11	100	-	22	100	-	14	100	-	8	100	-	19	100	-	78	100	-	8	100	-	22	100
	4	-	8	100	-	8	100	-	8	100	-	6	100	-	11	100	-	11	100	-	6	100	-	17	100	-	64	100	-	8	100	-	19	100
	5	-	6	100	-	0	100	-	8	100	-	3	100	-	8	100	-	8	100	-	6	100	-	6	100	-	50	100	-	3	100	-	19	100
	6	-	6	100	-	0	100	-	3	100	-	3	100	-	6	100	-	3	100	-	6	100	-	6	100	-	22	100	-	0	100	-	19	100
	7	-	3	100	-	0	100	-	0	100	-	3	100	-	0	100	-	0	100	-	6	100	-	0	100	-	17	100	-	0	100	-	17	100
	8	-	3	100	-	0	100	-	0	100	-	0	100	-	0	100	-	0	100	-	0	100	-	0	100	-	17	100	-	0	100	-	11	100
	9	-	3	100	-	0	100	-	0	100	-	0	100	-	0	100	-	0	100	-	0	100	-	0	100	-	11	100	-	0	100	-	11	100
	10	-	0	100	-	0	100	-	0	100	-	0	100	-	0	100	-	0	100	-	0	100	-	0	100	-	11	100	-	0	100	-	8	100
	11	-	0	100	-	0	100	-	0	100	-	0	100	-	0	100	-	0	100	-	0	100	-	0	100	-	11	100	-	0	100	-	6	100
	12	-	0	100	-	0	100	-	0	100	-	0	100	-	0	100	-	0	100	-	0	100	-	0	100	-	8	100	-	0	100	-	0	100
	13	-	0	100	-	0	100	-	0	100	-	0	100	-	0	100	-	0	100	-	0	100	-	0	100	-	3	100	-	0	100	-	0	100
	14	-	0	100	-	0	100	-	0	100	-	0	100	-	0	100	-	0	100	-	0	100	-	0	100	-	0	100	-	0	100	-	0	100
	15	-	0	100	-	0	100	-	0	100	-	0	100	-	0	100	-	0	100	-	0	100	-	0	100	-	0	100	-	0	100	-	0	100

Table D.4 Percentage of members with reinforcement yielding - 30 story buildings (cont'd)

Model	Story	NOR			KOB			KOC			CHI			DUZ			SM			LOM			CC			ERZ			LAN			IMP		
		W	C	B	W	C	B	W	C	B	W	C	B	W	C	B	W	C	B	W	C	B	W	C	B	W	C	B	W	C	B	W	C	B
S30_R00	16	-	0	100	-	0	100	-	0	100	-	0	100	-	0	100	-	0	100	-	0	100	-	0	100	-	0	100	-	0	100	-	0	100
	17	-	0	100	-	0	100	-	0	100	-	0	100	-	0	100	-	0	100	-	0	100	-	0	100	-	0	100	-	0	100	-	0	100
	18	-	0	100	-	0	100	-	0	100	-	0	100	-	0	100	-	0	100	-	0	100	-	0	100	-	0	100	-	0	100	-	0	100
	19	-	0	100	-	0	100	-	0	100	-	0	100	-	0	100	-	0	100	-	0	100	-	0	100	-	0	100	-	0	100	-	0	100
	20	-	0	100	-	0	100	-	0	100	-	0	100	-	0	100	-	0	100	-	0	100	-	0	100	-	0	100	-	0	100	-	0	100
	21	-	0	100	-	0	100	-	0	100	-	0	100	-	0	100	-	0	100	-	0	100	-	0	100	-	0	100	-	0	100	-	0	100
	22	-	0	100	-	0	100	-	0	100	-	0	100	-	0	100	-	0	100	-	0	100	-	0	100	-	0	100	-	0	100	-	0	100
	23	-	0	100	-	0	100	-	0	100	-	0	100	-	0	100	-	0	100	-	0	100	-	0	100	-	0	100	-	0	100	-	0	100
	24	-	0	100	-	0	100	-	0	100	-	0	100	-	0	100	-	0	100	-	0	100	-	0	100	-	0	100	-	0	100	-	0	100
	25	-	0	100	-	0	100	-	0	100	-	0	100	-	0	100	-	0	100	-	0	100	-	0	100	-	0	100	-	0	100	-	0	100
	26	-	0	100	-	0	100	-	0	100	-	0	100	-	0	100	-	0	100	-	0	100	-	0	100	-	0	100	-	0	100	-	0	100
	27	-	0	100	-	0	100	-	0	93	-	0	97	-	0	100	-	0	100	-	0	100	-	0	100	-	0	100	-	0	100	-	0	100
	28	-	0	82	-	0	62	-	0	53	-	0	57	-	0	90	-	0	92	-	0	83	-	0	87	-	0	75	-	0	65	-	0	97
	29	-	0	3	-	0	0	-	0	0	-	0	0	-	0	2	-	0	5	-	0	13	-	0	20	-	0	25	-	0	5	-	0	27
	30	-	0	0	-	0	0	-	0	0	-	0	0	-	0	0	-	0	0	-	0	0	-	0	0	-	0	8	-	0	0	-	0	2

Table D.4 Percentage of members with reinforcement yielding - 30 story buildings (cont'd)

Model	Story	NOR			KOB			KOC			CHI			DUZ			SM			LOM			CC			ERZ			LAN			IMP		
		W	C	B	W	C	B	W	C	B	W	C	B	W	C	B	W	C	B	W	C	B	W	C	B	W	C	B	W	C	B	W	C	B
S30_R05	1	100	93	100	100	33	100	100	67	100	100	97	100	100	97	100	100	70	100	100	77	100	100	73	100	100	100	100	100	100	100	100	100	100
	2	100	53	100	100	7	100	100	23	100	100	37	100	100	27	100	100	27	100	100	27	100	100	20	100	100	97	100	100	83	100	100	97	100
	3	0	0	100	0	7	100	25	7	100	25	3	100	0	3	100	50	17	100	0	3	100	25	17	100	50	27	100	0	10	100	50	17	100
	4	0	0	100	0	7	100	0	7	100	0	3	100	0	3	100	0	17	100	0	0	100	0	17	100	0	17	100	0	7	100	25	17	100
	5	0	0	100	0	7	100	0	7	100	0	0	100	0	3	100	0	13	100	0	0	100	0	17	100	0	17	100	0	7	100	0	20	100
	6	0	0	100	0	3	100	0	7	100	0	0	100	0	3	100	0	10	100	0	0	100	0	13	100	0	17	100	0	3	100	0	20	100
	7	0	0	100	0	0	100	0	7	100	0	0	100	0	3	100	0	3	100	0	0	100	0	7	100	0	13	100	0	0	100	0	20	100
	8	0	0	100	0	0	100	0	3	100	0	0	100	0	3	100	0	3	100	0	0	100	0	3	100	0	10	100	0	0	100	0	20	100
	9	0	0	100	0	0	100	0	3	100	0	0	100	0	3	100	0	3	100	0	0	100	0	0	100	0	7	100	0	0	100	0	17	100
	10	0	0	100	0	0	100	0	0	100	0	0	100	0	3	100	0	0	100	0	0	100	0	0	100	0	3	100	0	0	100	0	13	100
	11	0	0	100	0	0	100	0	0	100	0	0	100	0	0	100	0	0	100	0	0	100	0	0	100	0	3	100	0	0	100	0	13	100
	12	0	0	100	0	0	100	0	0	100	0	0	100	0	0	100	0	0	100	0	0	100	0	0	100	0	3	100	0	0	100	0	13	100
	13	0	0	100	0	0	100	0	0	100	0	0	100	0	0	100	0	0	100	0	0	100	0	0	100	0	0	100	0	0	100	0	13	100
	14	0	0	100	0	0	100	0	0	100	0	0	100	0	0	100	0	0	100	0	0	100	0	0	100	0	0	100	0	0	100	0	10	100
	15	0	0	100	0	0	100	0	0	100	0	0	100	0	0	100	0	0	100	0	0	100	0	0	100	0	0	100	0	0	100	0	10	100

Table D.4 Percentage of members with reinforcement yielding - 30 story buildings (cont'd)

Model	Story	NOR			KOB			KOC			CHI			DUZ			SM			LOM			CC			ERZ			LAN			IMP		
		W	C	B	W	C	B	W	C	B	W	C	B	W	C	B	W	C	B	W	C	B	W	C	B	W	C	B	W	C	B	W	C	B
S30_R05	16	0	0	100	0	0	100	0	0	100	0	0	100	0	0	100	0	0	100	0	0	100	0	0	100	0	0	100	0	0	100	0	0	100
	17	0	0	100	0	0	100	0	0	100	0	0	100	0	0	100	0	0	100	0	0	100	25	0	100	0	0	100	0	0	100	0	0	100
	18	0	0	100	0	0	100	0	0	100	0	0	100	0	0	100	0	0	100	0	0	100	25	0	100	0	0	100	0	0	100	0	0	100
	19	0	0	100	0	0	100	0	0	100	0	0	100	25	0	100	0	0	100	0	0	100	25	0	100	0	0	100	0	0	100	0	0	100
	20	0	0	100	0	0	100	0	0	100	0	0	100	25	0	100	0	0	100	0	0	100	25	0	100	0	0	100	0	0	100	0	0	100
	21	0	0	100	0	0	100	0	0	100	0	0	100	0	0	100	0	0	100	0	0	100	0	0	100	0	0	100	0	0	100	0	0	100
	22	0	0	100	0	0	100	0	0	100	0	0	100	0	0	100	0	0	100	0	0	100	0	0	100	0	0	100	0	0	100	0	0	100
	23	0	0	100	0	0	100	0	0	100	0	0	100	0	0	100	0	0	100	0	0	100	0	0	100	0	0	100	0	0	100	0	0	100
	24	0	0	100	0	0	100	0	0	100	0	0	100	0	0	100	0	0	100	0	0	100	0	0	100	0	0	100	0	0	100	0	0	100
	25	0	0	100	0	0	100	0	0	100	0	0	100	0	0	100	0	0	100	0	0	100	0	0	100	0	0	100	0	0	100	0	0	100
	26	0	0	100	0	0	100	0	0	100	0	0	100	0	0	100	0	0	100	0	0	100	0	0	100	0	0	100	0	0	100	0	0	100
	27	0	0	100	0	0	100	0	0	100	0	0	100	0	0	100	0	0	100	0	0	100	0	0	100	0	0	100	0	0	100	0	0	100
	28	0	0	98	0	0	100	0	0	100	0	0	100	0	0	100	0	0	100	0	0	100	0	0	100	0	0	100	0	0	100	0	0	100
	29	0	0	95	0	0	100	0	0	100	0	0	100	0	0	100	0	0	100	0	0	100	0	0	100	0	0	100	0	0	100	0	0	98
	30	0	10	84	0	37	95	0	23	100	0	3	79	0	23	98	0	37	96	0	30	93	0	53	93	0	17	84	0	47	100	0	67	86

Table D.4 Percentage of members with reinforcement yielding - 30 story buildings (cont'd)

Model	Story	NOR			KOB			KOC			CHI			DUZ			SM			LOM			CC			ERZ			LAN			IMP		
		W	C	B	W	C	B	W	C	B	W	C	B	W	C	B	W	C	B	W	C	B	W	C	B	W	C	B	W	C	B	W	C	B
S30_R10	1	100	0	94	100	0	100	100	0	100	100	0	100	100	25	100	100	8	98	100	4	100	100	8	100	100	71	96	100	21	100	100	54	100
	2	88	8	98	100	0	100	100	0	100	100	8	100	100	25	100	100	13	100	100	13	100	100	8	100	100	88	100	100	25	100	100	33	100
	3	25	4	100	0	0	100	13	0	100	0	0	100	13	4	100	25	8	100	38	8	100	13	8	100	50	21	100	25	13	100	63	8	100
	4	0	4	100	0	0	100	0	0	100	0	0	100	0	4	100	0	8	100	0	4	100	0	8	100	25	21	100	0	8	100	13	8	100
	5	0	4	100	0	0	100	0	0	100	0	0	100	0	0	100	0	4	100	0	4	100	0	8	100	0	21	100	0	0	100	0	8	100
	6	0	4	100	0	0	100	0	0	100	0	0	100	0	0	100	0	4	100	0	4	100	0	8	100	0	21	100	0	0	100	0	8	100
	7	0	4	100	0	0	100	0	0	100	0	0	100	0	0	100	0	0	100	0	4	100	0	8	100	0	17	100	0	0	100	0	8	100
	8	0	4	100	0	0	100	0	0	100	0	0	100	0	0	100	0	0	100	0	4	100	0	8	100	0	17	100	0	0	100	0	8	100
	9	0	0	100	0	0	100	0	0	100	0	0	100	0	0	100	0	0	100	0	0	100	0	4	100	0	13	100	0	0	100	0	8	100
	10	0	0	100	0	0	100	0	0	100	0	0	100	0	0	100	0	0	100	0	0	100	0	0	100	0	13	100	0	0	100	0	8	100
	11	0	0	100	0	0	100	0	0	100	0	0	100	0	0	100	0	0	100	0	0	100	0	0	100	0	8	100	0	0	100	0	4	100
	12	0	0	100	0	0	100	0	0	100	0	0	100	0	0	100	0	0	100	0	0	100	0	0	100	0	8	100	0	0	100	0	0	100
	13	0	0	100	0	0	100	0	0	100	0	0	100	0	0	100	0	0	100	0	0	100	0	0	100	0	0	100	0	0	100	0	0	100
	14	0	0	100	0	0	100	0	0	100	0	0	100	0	0	100	0	0	100	0	0	100	0	0	100	0	0	100	0	0	100	0	0	100
	15	0	0	100	0	0	100	0	0	100	0	0	100	0	0	100	0	0	100	0	0	100	0	0	100	0	0	100	0	0	100	0	0	100

Table D.4 Percentage of members with reinforcement yielding - 30 story buildings (cont'd)

Model	Story	NOR			KOB			KOC			CHI			DUZ			SM			LOM			CC			ERZ			LAN			IMP		
		W	C	B	W	C	B	W	C	B	W	C	B	W	C	B	W	C	B	W	C	B	W	C	B	W	C	B	W	C	B	W	C	B
S30_R10	16	0	0	100	0	0	100	0	0	100	0	0	100	0	0	100	0	0	100	0	0	100	0	0	100	0	0	100	0	0	100	0	0	100
	17	0	0	100	0	0	100	0	0	100	0	0	100	0	0	100	0	0	100	0	0	100	0	0	100	0	0	100	0	0	100	0	0	100
	18	0	0	100	0	0	100	0	0	100	0	0	100	0	0	100	0	0	100	0	0	100	0	0	100	0	0	100	0	0	100	0	0	100
	19	0	0	100	0	0	100	0	0	100	0	0	100	0	0	100	0	0	100	0	0	100	0	0	100	0	0	100	0	0	100	0	0	100
	20	0	0	100	0	0	100	0	0	100	0	0	100	0	0	100	0	0	100	0	0	100	0	0	100	0	0	100	0	0	100	0	0	100
	21	0	0	100	0	0	100	0	0	100	0	0	100	0	0	100	0	0	100	0	0	100	0	0	100	0	0	100	0	0	100	0	0	100
	22	0	0	100	0	0	100	0	0	100	0	0	100	0	0	100	0	0	100	0	0	100	0	0	100	0	0	100	0	0	100	0	0	100
	23	0	0	100	0	0	100	0	0	100	0	0	100	0	0	100	0	0	100	0	0	100	0	0	100	0	0	100	0	0	100	0	0	100
	24	0	0	100	0	0	100	0	0	100	0	0	100	0	0	100	0	0	100	0	0	100	0	0	100	0	0	100	0	0	100	0	0	100
	25	0	0	100	0	0	100	0	0	100	0	0	100	0	0	100	0	0	100	0	0	100	0	4	100	0	0	100	0	0	100	0	0	100
	26	0	0	100	0	0	100	0	0	100	0	0	100	0	0	100	0	0	100	0	0	100	0	4	100	0	0	100	0	0	100	0	0	100
	27	0	0	100	0	0	100	0	0	100	0	0	100	0	0	100	0	0	100	0	0	100	0	8	100	0	0	100	0	0	100	0	0	100
	28	0	0	100	0	0	100	0	0	100	0	0	100	0	0	100	0	0	100	0	0	100	0	8	100	0	4	100	0	0	100	0	0	100
	29	0	0	100	0	0	100	0	0	100	0	0	100	0	0	100	0	0	100	0	0	100	0	8	100	0	0	100	0	0	100	0	0	100
	30	0	96	96	0	100	98	0	96	100	0	100	100	0	96	100	0	100	100	0	100	100	0	100	100	0	96	100	0	100	100	0	96	98

Table D.4 Percentage of members with reinforcement yielding - 30 story buildings (cont'd)

Model	Story	NOR			KOB			KOC			CHI			DUZ			SM			LOM			CC			ERZ			LAN			IMP		
		W	C	B	W	C	B	W	C	B	W	C	B	W	C	B	W	C	B	W	C	B	W	C	B	W	C	B	W	C	B	W	C	B
S30_R15	1	100	0	0	100	0	0	100	6	0	100	0	0	100	0	0	100	17	0	100	0	0	100	11	0	100	33	0	100	11	0	100	39	0
	2	67	6	0	100	0	0	100	22	0	92	6	0	92	6	0	100	17	0	92	11	0	100	22	0	92	61	0	100	33	0	92	22	0
	3	17	6	0	0	0	0	25	22	0	8	0	0	8	6	0	8	17	0	17	6	0	8	17	0	42	22	0	17	17	0	58	17	0
	4	0	6	0	0	0	0	0	22	0	0	0	0	0	0	0	0	11	0	0	0	0	0	11	0	25	22	0	0	17	0	8	17	0
	5	0	6	94	0	0	94	0	22	94	0	0	94	0	0	92	0	11	92	0	0	92	0	11	92	0	28	94	0	11	94	0	17	94
	6	0	6	100	0	0	100	0	22	100	0	0	100	0	0	100	0	6	100	0	0	100	0	6	100	0	28	100	0	6	100	0	17	100
	7	0	6	100	0	0	100	0	22	100	0	0	100	0	0	100	0	6	100	0	0	100	0	6	100	0	17	100	0	0	100	0	17	100
	8	0	6	100	0	0	100	0	17	100	0	0	100	0	0	100	0	6	100	0	0	100	0	0	100	0	17	100	0	0	100	0	17	100
	9	0	0	100	0	0	100	0	6	100	0	0	100	0	0	100	0	0	100	0	0	100	0	0	100	0	17	100	0	0	100	0	17	100
	10	0	0	100	0	0	100	0	0	100	0	0	100	0	0	100	0	0	100	0	0	100	0	0	100	0	17	100	0	0	100	0	17	100
	11	0	0	100	0	0	100	0	0	100	0	0	100	0	0	100	0	0	100	0	0	100	0	0	100	0	11	100	0	0	100	0	17	100
	12	0	0	100	0	0	100	0	0	100	0	0	100	0	6	100	0	0	100	0	0	100	0	0	100	0	6	100	0	0	100	0	17	100
	13	0	0	100	0	0	100	0	0	100	0	0	100	0	6	100	0	0	100	0	0	100	0	0	100	0	6	100	0	0	100	0	17	100
	14	0	0	100	0	0	100	0	6	100	0	0	100	0	6	100	0	0	100	0	0	100	0	6	100	0	0	100	0	0	100	0	17	100
	15	0	0	100	0	0	100	0	6	100	0	0	100	0	6	100	0	0	100	0	0	100	0	6	100	0	0	100	0	0	100	0	11	100

Table D.4 Percentage of members with reinforcement yielding - 30 story buildings (cont'd)

Model	Story	NOR			KOB			KOC			CHI			DUZ			SM			LOM			CC			ERZ			LAN			IMP		
		W	C	B	W	C	B	W	C	B	W	C	B	W	C	B	W	C	B	W	C	B	W	C	B	W	C	B	W	C	B	W	C	B
S30_R15	16	0	0	100	0	0	100	0	6	100	0	0	100	0	6	100	0	0	100	0	0	100	0	6	100	0	0	100	0	0	100	0	6	100
	17	0	0	100	0	0	100	0	6	100	0	0	100	0	0	100	0	6	100	0	0	100	0	6	100	0	0	100	0	0	100	0	6	100
	18	0	0	100	0	0	100	0	6	100	0	0	100	0	0	100	0	6	100	0	0	100	0	6	100	0	0	100	0	0	100	0	6	100
	19	0	0	100	0	0	100	0	6	100	0	0	100	0	0	100	0	11	100	0	0	100	0	6	100	0	0	100	0	0	100	0	6	100
	20	0	0	100	0	0	100	0	6	100	0	0	100	0	0	100	0	11	100	0	0	100	0	6	100	0	0	100	0	0	100	0	6	100
	21	0	0	100	0	0	100	0	6	100	0	0	100	0	0	100	0	11	100	0	0	100	0	6	100	0	0	100	0	0	100	0	6	100
	22	0	0	100	0	0	100	0	6	100	0	0	100	0	0	100	0	11	100	0	0	100	0	6	100	0	6	100	0	0	100	0	6	100
	23	0	0	100	0	0	100	0	6	100	0	0	100	0	0	100	0	11	100	0	0	100	0	11	100	0	6	100	0	0	100	0	6	100
	24	0	0	100	0	0	100	0	6	100	0	0	100	0	0	100	0	6	100	0	0	100	0	11	100	0	6	100	0	0	100	0	6	100
	25	0	0	100	0	0	100	0	6	100	0	0	100	0	0	100	0	6	100	0	0	100	0	22	100	0	6	100	0	0	100	0	6	100
	26	0	0	100	0	0	100	0	6	100	0	0	100	0	0	100	0	6	100	0	0	100	0	22	100	0	6	100	0	0	100	0	6	100
	27	0	0	100	0	0	100	0	0	100	0	0	100	0	0	100	0	11	100	0	0	100	0	28	100	0	6	100	0	0	100	0	6	100
	28	0	11	100	0	0	100	0	0	100	0	0	100	0	0	100	0	17	100	0	17	100	0	33	100	0	17	100	0	0	100	0	17	100
	29	0	0	100	0	0	100	0	0	100	0	0	100	0	0	100	0	6	100	0	6	100	0	28	100	0	6	100	0	0	100	0	6	100
	30	0	100	100	0	100	98	0	100	100	0	94	100	0	100	100	0	100	100	0	100	100	0	100	100	0	100	100	0	100	100	0	100	100

Table D.4 Percentage of members with reinforcement yielding - 30 story buildings (cont'd)

Model	Story	NOR			KOB			KOC			CHI			DUZ			SM			LOM			CC			ERZ			LAN			IMP		
		W	C	B	W	C	B	W	C	B	W	C	B	W	C	B	W	C	B	W	C	B	W	C	B	W	C	B	W	C	B	W	C	B
S30_R20	1	100	8	82	100	0	98	100	0	98	100	0	80	100	0	100	100	17	98	100	17	100	100	8	98	100	33	89	100	25	100	100	25	100
	2	75	17	100	94	0	100	88	33	100	69	8	100	81	17	100	100	33	100	88	33	100	100	25	100	100	42	100	100	33	100	94	33	100
	3	25	17	100	0	0	100	38	25	100	0	8	100	0	8	100	19	25	100	38	33	100	6	17	100	38	42	100	0	25	100	44	25	100
	4	0	17	100	0	0	100	0	17	100	0	0	100	0	8	100	0	8	100	0	33	100	0	17	100	13	42	100	0	17	100	6	25	100
	5	0	17	100	0	0	100	0	17	100	0	0	100	0	8	100	0	8	100	0	33	100	0	17	100	0	33	100	0	8	100	0	25	100
	6	0	17	100	0	0	100	0	8	100	0	0	100	0	0	100	0	8	100	0	33	100	0	8	100	0	33	100	0	0	100	0	25	100
	7	0	17	100	0	0	100	0	8	100	0	0	100	0	0	100	0	8	100	0	25	100	0	8	100	0	33	100	0	0	100	0	25	100
	8	0	17	100	0	0	100	0	0	100	0	0	100	0	0	100	0	0	100	0	25	100	0	0	100	0	25	100	0	0	100	0	25	100
	9	0	17	100	0	0	100	0	0	100	0	0	100	0	0	100	0	0	100	0	17	100	0	0	100	0	25	100	0	0	100	0	25	100
	10	0	17	100	0	0	100	0	0	100	0	0	100	0	0	100	0	0	100	0	8	100	0	0	100	0	25	100	0	0	100	0	25	100
	11	0	17	100	0	0	100	0	0	100	0	0	100	0	0	100	0	0	100	0	0	100	0	0	100	0	25	100	0	0	100	0	25	100
	12	0	8	100	0	0	100	0	0	100	0	0	100	0	0	100	0	0	100	0	0	100	0	0	100	0	25	100	0	0	100	0	8	100
	13	0	0	100	0	0	100	0	0	100	0	0	100	0	8	100	0	0	100	0	0	100	0	0	100	0	33	100	0	0	100	0	0	100
	14	0	0	100	0	0	100	0	0	100	0	0	100	0	8	100	0	0	100	0	0	100	0	0	100	0	33	100	0	0	100	0	0	100
	15	0	0	100	0	0	100	0	0	100	0	0	100	0	8	100	0	0	100	0	0	100	0	17	100	0	33	100	0	0	100	0	0	100

Table D.4 Percentage of members with reinforcement yielding - 30 story buildings (cont'd)

Model	Story	NOR			KOB			KOC			CHI			DUZ			SM			LOM			CC			ERZ			LAN			IMP		
		W	C	B	W	C	B	W	C	B	W	C	B	W	C	B	W	C	B	W	C	B	W	C	B	W	C	B	W	C	B	W	C	B
S30_R20	16	0	8	100	0	0	100	0	0	100	0	0	100	0	8	100	0	0	100	0	17	100	0	17	100	0	33	100	0	0	100	0	0	100
	17	0	8	100	0	0	100	0	0	100	0	0	100	0	8	100	0	8	100	0	17	100	0	17	100	0	42	100	0	17	100	0	0	100
	18	0	8	100	0	0	100	0	0	100	0	0	100	0	0	100	0	8	100	0	17	100	0	17	100	0	33	100	0	17	100	0	0	100
	19	0	8	100	0	0	100	0	8	100	0	0	100	0	0	100	0	8	100	0	17	100	0	8	100	0	33	100	0	17	100	0	0	100
	20	0	8	100	0	0	100	0	8	100	0	0	100	0	0	100	0	17	100	0	17	100	0	8	100	0	33	100	0	17	100	0	0	100
	21	0	8	100	0	0	100	0	8	100	0	0	100	0	0	100	0	17	100	0	17	100	0	17	100	0	33	100	0	17	100	0	0	100
	22	0	8	100	0	0	100	0	8	100	0	0	100	0	0	100	0	17	100	0	17	100	0	17	100	0	33	100	0	17	100	0	8	100
	23	0	17	100	0	0	100	0	8	100	0	0	100	0	0	100	0	17	100	0	17	100	0	17	100	0	42	100	0	17	100	0	8	100
	24	0	17	100	0	0	100	0	8	100	0	0	100	0	0	100	0	17	100	0	8	100	0	17	100	0	33	100	0	17	100	0	17	100
	25	0	17	100	0	0	100	0	8	100	0	0	100	0	0	100	0	8	100	0	8	100	0	17	100	0	25	100	0	17	100	0	17	100
	26	0	25	100	0	0	100	0	0	100	0	0	100	0	0	100	0	8	100	0	8	100	0	17	100	0	25	100	0	17	100	0	17	100
	27	0	33	100	0	0	100	0	0	100	0	0	100	0	0	100	0	8	100	0	8	100	0	17	100	0	25	100	0	8	100	0	17	100
	28	0	42	100	0	0	100	0	0	100	0	0	100	0	0	100	0	8	100	0	8	100	0	33	100	0	25	100	0	8	100	0	17	100
	29	0	8	100	0	0	100	0	0	100	0	0	100	0	0	100	0	8	100	0	8	100	0	8	100	0	8	100	0	0	100	0	8	100
	30	0	100	100	0	100	100	0	100	100	0	100	100	0	100	100	0	100	100	0	100	100	0	100	100	0	92	100	0	100	100	0	100	100

Table D.4 Percentage of members with reinforcement yielding - 30 story buildings (cont'd)

Model	Story	NOR			KOB			KOC			CHI			DUZ			SM			LOM			CC			ERZ			LAN			IMP		
		W	C	B	W	C	B	W	C	B	W	C	B	W	C	B	W	C	B	W	C	B	W	C	B	W	C	B	W	C	B	W	C	B
S30_R25	1	100	13	75	100	0	90	100	0	98	100	0	90	100	0	100	100	13	100	100	25	90	100	0	98	100	50	90	100	0	100	100	13	100
	2	80	25	93	90	0	100	90	50	100	80	0	100	85	13	100	95	25	100	90	50	100	100	25	100	100	63	100	90	13	100	100	38	100
	3	30	25	100	5	0	100	40	38	100	0	0	100	0	0	100	25	25	100	50	50	100	5	25	100	55	63	100	0	0	100	30	38	100
	4	0	25	100	0	0	100	0	25	100	0	0	100	0	0	100	0	13	100	0	50	100	0	13	100	20	38	100	0	0	100	5	38	100
	5	0	25	100	0	0	100	0	13	100	0	0	100	0	0	100	0	13	100	0	50	100	0	13	100	0	38	100	0	0	100	0	25	100
	6	0	25	100	0	0	100	0	13	100	0	0	100	0	0	100	0	0	100	0	38	100	0	0	100	0	38	100	0	0	100	0	25	100
	7	0	25	100	0	0	100	0	0	100	0	0	100	0	0	100	0	0	100	0	25	100	0	0	100	0	38	100	0	0	100	0	25	100
	8	0	25	100	0	0	100	0	0	100	0	0	100	0	0	100	0	0	100	0	25	100	0	0	100	0	38	100	0	0	100	0	25	100
	9	0	25	100	0	0	100	0	0	100	0	0	100	0	0	100	0	0	100	0	13	100	0	0	100	0	38	100	0	0	100	0	25	100
	10	0	25	100	0	0	100	0	0	100	0	0	100	0	0	100	0	0	100	0	13	100	0	0	100	0	38	100	0	0	100	0	25	100
	11	0	25	100	0	0	100	0	0	100	0	0	100	0	0	100	0	0	100	0	13	100	0	0	100	0	38	100	0	0	100	0	13	100
	12	0	13	100	0	0	100	0	0	100	0	0	100	0	0	100	0	0	100	0	0	100	0	0	100	0	38	100	0	0	100	0	13	100
	13	0	13	100	0	0	100	0	0	100	0	0	100	0	0	100	0	0	100	0	0	100	0	0	100	0	38	100	0	0	100	0	0	100
	14	0	0	100	0	0	100	0	0	100	0	0	100	0	0	100	0	0	100	0	0	100	0	13	100	0	38	100	0	0	100	0	0	100
	15	0	13	100	0	0	100	0	0	100	0	0	100	0	0	100	0	0	100	0	13	100	0	13	100	0	50	100	0	0	100	0	0	100

Table D.4 Percentage of members with reinforcement yielding - 30 story buildings (cont'd)

Model	Story	NOR			KOB			KOC			CHI			DUZ			SM			LOM			CC			ERZ			LAN			IMP		
		W	C	B	W	C	B	W	C	B	W	C	B	W	C	B	W	C	B	W	C	B	W	C	B	W	C	B	W	C	B	W	C	B
S30_R25	16	0	13	100	0	0	100	0	0	100	0	0	100	0	0	100	0	13	100	0	25	100	0	13	100	0	50	100	0	0	100	0	0	100
	17	0	13	100	0	0	100	0	0	100	0	0	100	0	0	100	0	13	100	0	25	100	0	13	100	0	50	100	0	0	100	0	0	100
	18	0	13	100	0	0	100	0	0	100	0	0	100	0	0	100	0	25	100	0	25	100	0	13	100	0	50	100	0	13	100	0	0	100
	19	0	13	100	0	0	100	0	0	100	0	0	100	0	0	100	0	25	100	0	25	100	0	13	100	0	50	100	0	25	100	0	0	100
	20	0	13	100	0	0	100	0	0	100	0	0	100	0	0	100	0	25	100	0	25	100	0	13	100	0	50	100	0	25	100	0	13	100
	21	0	13	100	0	0	100	0	0	100	0	0	100	0	0	100	0	25	100	0	25	100	0	13	100	0	50	100	0	25	100	0	0	100
	22	0	13	100	0	0	100	0	0	100	0	0	100	0	0	100	0	25	100	0	13	100	0	13	100	0	63	100	0	25	100	0	0	100
	23	0	13	100	0	0	100	0	0	100	0	0	100	0	0	100	0	25	100	0	13	100	0	13	100	0	63	100	0	13	100	0	0	100
	24	0	13	100	0	0	100	0	0	100	0	0	100	0	0	100	0	25	100	0	13	100	0	25	100	0	63	100	0	13	100	0	0	100
	25	0	13	100	0	0	100	0	0	100	0	0	100	0	0	100	0	25	100	0	13	100	0	25	100	0	63	100	0	13	100	0	0	100
	26	0	13	100	0	0	100	0	0	100	0	0	100	0	0	100	0	13	100	0	13	100	0	25	100	0	63	100	0	13	100	0	0	100
	27	0	13	100	0	0	100	0	0	100	0	0	100	0	0	100	0	13	100	0	13	100	0	25	100	0	63	100	0	13	100	0	0	100
	28	0	50	100	0	0	100	0	0	100	0	0	100	0	0	100	0	13	100	0	13	100	0	25	100	0	63	100	0	13	100	0	0	100
	29	0	13	100	0	0	100	0	0	100	0	0	100	0	0	100	0	13	100	0	13	100	0	25	100	0	13	100	0	0	100	0	0	100
	30	0	100	100	0	100	100	0	100	100	0	100	100	0	100	100	0	100	100	0	100	100	0	100	100	0	100	100	0	100	100	0	100	100

Table D.4 Percentage of members with reinforcement yielding - 30 story buildings (cont'd)

Model	Story	NOR			KOB			KOC			CHI			DUZ			SM			LOM			CC			ERZ			LAN			IMP		
		W	C	B	W	C	B	W	C	B	W	C	B	W	C	B	W	C	B	W	C	B	W	C	B	W	C	B	W	C	B	W	C	B
S30_R30	1	100	-	69	100	-	83	100	-	100	100	-	81	100	-	100	100	-	100	100	-	81	100	-	97	100	-	89	100	-	100	100	-	100
	2	71	-	81	63	-	100	75	-	100	58	-	100	63	-	100	88	-	100	83	-	100	79	-	100	100	-	100	75	-	100	92	-	100
	3	25	-	94	4	-	100	21	-	100	0	-	100	0	-	100	13	-	100	42	-	100	4	-	100	50	-	100	0	-	100	29	-	100
	4	0	-	100	0	-	100	0	-	100	0	-	100	0	-	100	0	-	100	0	-	100	0	-	100	8	-	100	0	-	100	0	-	100
	5	0	-	100	0	-	100	0	-	100	0	-	100	0	-	100	0	-	100	0	-	100	0	-	100	0	-	100	0	-	100	0	-	100
	6	0	-	100	0	-	100	0	-	100	0	-	100	0	-	100	0	-	100	0	-	100	0	-	100	0	-	100	0	-	100	0	-	100
	7	0	-	100	0	-	100	0	-	100	0	-	100	0	-	100	0	-	100	0	-	100	0	-	100	0	-	100	0	-	100	0	-	100
	8	0	-	100	0	-	100	0	-	100	0	-	100	0	-	100	0	-	100	0	-	100	0	-	100	0	-	100	0	-	100	0	-	100
	9	0	-	100	0	-	100	0	-	100	0	-	100	0	-	100	0	-	100	0	-	100	0	-	100	0	-	100	0	-	100	0	-	100
	10	0	-	100	0	-	100	0	-	100	0	-	100	0	-	100	0	-	100	0	-	100	0	-	100	0	-	100	0	-	100	0	-	100
	11	0	-	100	0	-	100	0	-	100	0	-	100	0	-	100	0	-	100	0	-	100	0	-	100	0	-	100	0	-	100	0	-	100
	12	0	-	100	0	-	100	0	-	100	0	-	100	0	-	100	0	-	100	0	-	100	0	-	100	0	-	100	0	-	100	0	-	100
	13	0	-	100	0	-	100	0	-	100	0	-	100	0	-	100	0	-	100	0	-	100	0	-	100	0	-	100	0	-	100	0	-	100
	14	0	-	100	0	-	100	0	-	100	0	-	100	0	-	100	0	-	100	0	-	100	0	-	100	0	-	100	0	-	100	0	-	100
	15	0	-	100	0	-	100	0	-	100	0	-	100	0	-	100	0	-	100	0	-	100	0	-	100	0	-	100	0	-	100	0	-	100

Table D.4 Percentage of members with reinforcement yielding - 30 story buildings (cont'd)

Model	Story	NOR			KOB			KOC			CHI			DUZ			SM			LOM			CC			ERZ			LAN			IMP		
		W	C	B	W	C	B	W	C	B	W	C	B	W	C	B	W	C	B	W	C	B	W	C	B	W	C	B	W	C	B	W	C	B
S30_R30	16	0	-	100	0	-	100	0	-	100	0	-	100	0	-	100	0	-	100	0	-	100	0	-	100	0	-	100	0	-	100	0	-	100
	17	0	-	100	0	-	100	0	-	100	0	-	100	0	-	100	0	-	100	0	-	100	0	-	100	0	-	100	0	-	100	0	-	100
	18	0	-	100	0	-	100	0	-	100	0	-	100	0	-	100	0	-	100	0	-	100	0	-	100	0	-	100	0	-	100	0	-	100
	19	0	-	100	0	-	100	0	-	100	0	-	100	0	-	100	0	-	100	0	-	100	0	-	100	0	-	100	0	-	100	0	-	100
	20	0	-	100	0	-	100	0	-	100	0	-	100	0	-	100	0	-	100	0	-	100	0	-	100	0	-	100	0	-	100	0	-	100
	21	0	-	100	0	-	100	0	-	100	0	-	100	0	-	100	0	-	100	0	-	100	0	-	100	0	-	100	0	-	100	0	-	100
	22	0	-	100	0	-	100	0	-	100	0	-	100	0	-	100	0	-	100	0	-	100	0	-	100	0	-	100	0	-	100	0	-	100
	23	0	-	100	0	-	100	0	-	100	0	-	100	0	-	100	0	-	100	0	-	100	0	-	100	0	-	100	0	-	100	0	-	100
	24	0	-	100	0	-	100	0	-	100	0	-	100	0	-	100	0	-	100	0	-	100	0	-	100	0	-	100	0	-	100	0	-	100
	25	0	-	100	0	-	100	0	-	100	0	-	100	0	-	100	0	-	100	0	-	100	0	-	100	0	-	100	0	-	100	0	-	100
	26	0	-	100	0	-	100	0	-	100	0	-	100	0	-	100	0	-	100	0	-	100	0	-	100	0	-	100	0	-	100	0	-	100
	27	0	-	100	0	-	100	0	-	100	0	-	100	0	-	100	0	-	100	0	-	100	0	-	100	0	-	100	0	-	100	0	-	100
	28	0	-	100	0	-	100	0	-	100	0	-	100	0	-	100	0	-	100	0	-	100	0	-	100	0	-	100	0	-	100	0	-	100
	29	0	-	100	0	-	100	0	-	100	0	-	100	0	-	100	0	-	100	0	-	100	0	-	100	0	-	100	0	-	100	0	-	100
	30	0	-	100	0	-	100	0	-	100	0	-	100	0	-	100	0	-	100	0	-	100	0	-	100	0	-	100	0	-	100	0	-	100

Note: NOR = Northridge; KOB = Kobe; KOC = Kocaeli; CHI = Chi Chi; DUZ = Duzce; SM = Sierramex; LOM = Loma prieta; CC = Christchurch; ERZ = Erzincan; LAN = Landers; IMP = Imperial Valley; W = Structural wall; C = Column; B = Beam